SEISMIC BEARING CAPACITY OF SURFICIAL STRIP FOOTINGS NEAR COHESIVE SLOPES

by

Anıl Erkli

B.S., Civil Engineering, Dokuz Eylül University, 2007

Submitted to the Institute for Graduate Studies in
Science and Engineering in partial fulfillment of
the requirements for the degree of
Master of Science

Graduate Program in Civil Engineering

Boğaziçi University

2015

SEISMIC BEARING CAPACITY OF SURFICIAL STRIP FOOTINGS NEAR COHESIVE SLOPES

APPROVED BY:

Assoc. Prof. Özer Çinicioğlu (Thesis Supervisor)	.....
Prof. Erol Güler	.....
Asst. Prof. Berrak Teymur	.....

DATE OF APPROVAL: 15.07.2015

To my daughter,

ACKNOWLEDGEMENTS

Even though no complete solution methodology has been developed so far, I would like to express my gratitude to all researchers who have made major or even minor contribution previously for the solution of the problem investigated in the scope of this thesis.

First and foremost, my sincere appreciation and gratitude goes to my thesis supervisor Assoc. Prof. Özer Çinicioğlu for his valuable help, sharing of his knowledge and engineering judgment, guiding me throughout the whole duration of the thesis. He always believed my ability and encouraged me as well since the beginning of this long journey. Furthermore, he supported me all the time even in challenging moments which I completely gave up to write down this thesis.

Also, I extend my sincere thanks to the members of my Master's thesis examination committee: Prof. Erol Güler and Asst. Prof. Berrak Teymur for their kind and supportive attitude towards me and in depth comments and advice.

My gratitude also goes to my colleagues with whom I have met since the beginning of my semi-student life at Boğaziçi University and during professional life pursued in İstanbul. Special thanks to Tufan Dalkıran, Ahmet Volkan Akkuzu and Sercan Gür for their kind assistance, our discussions on engineering or even sometimes simply daily life and sharing their own valuable experiences with me.

And finally, I would like to thank my wife Özlem Gündoğan Erkli for her endless love, moral support and great patience at all times. I am also very thankful to my parents Cumhur & Göksel Erkli and my sister Irmak Erkli since they have given me their support throughout the thesis, as always they do during my educational life.

ABSTRACT

SEISMIC BEARING CAPACITY OF SURFICIAL STRIP FOOTINGS NEAR COHESIVE SLOPES

Even if most foundation failures during earthquakes occur due to liquefaction phenomenon, failures due to reduction in bearing capacity have been typically observed. In order to avoid similar foundation failures due to reduction in bearing capacity, number of performed research studies on seismic bearing capacity has increased in the course of time. Thus, the seismic bearing capacity becomes one of significant issues in geotechnical earthquake engineering. In this study, in a similar manner to the previous attempts, it is aimed to determine all factors which influence seismic bearing capacity of surficial strip footings near cohesive slopes. It is a problem typically encountered in the design of certain type structural elements' footings (retaining walls, bridge abutments and etc.) which does not have an exact solution. Within the scope of this study, finite elements method was utilized to investigate the problem of seismic bearing capacity. Since finite elements method allows easy variation of geometry and parameters, the influence of different variables have been investigated. As a result, by evaluating more than one thousand numerical model outputs, five different factors (horizontal seismic acceleration coefficient, slope angle, footing distance from the slope edge, slope height, soil properties) which have an influence on seismic bearing capacity of surficial strip footings were detected. By compiling and interpreting the obtained results, an easily applied alternative solution method in which all factors identified to have an influence on seismic bearing capacity are taken into consideration was developed for geotechnical designers or practitioners.

ÖZET

KOHEZYONLU ŞEVLERİN ÜZERİNDEKİ YÜZEYSEL ŞERİT TEMELLERİN SİSMİK TAŞIMA GÜCÜ

Deprem sırasında gözlenen temel göçmelerinin büyük bir bölümü sıvılaşma nedeniyle oluşsa da taşıma gücünün azalması nedeniyle göçmenin meydana geldiği durumlar da sıklıkla gözlemlenmektedir. Taşıma gücü azalması nedeniyle meydana gelebilecek benzer göçmelerin önlenmesi için sismik taşıma gücü bahsi üzerine yapılan araştırma çalışmalarının sayısının zaman içerisinde artması bu konuyu geoteknik deprem mühendisliğinin önemli başlıklarından biri haline getirmiştir. Bu çalışmada, kohezyonlu şevlerin üzerindeki yüzeysel şerit temellerin sismik taşıma gücüne etki eden faktörlerin belirlenmesi amaçlanmıştır. Kohezyonlu şevlerin üzerindeki yüzeysel şerit temellerin sismik taşıma gücü, belirli tür yapı temellerinin (istinat duvarları, vb.) tasarımında sıklıkla karşılaşılan ve kesin çözümü olmayan bir problemdir. Bu çalışma kapsamında, sismik taşıma gücü probleminin incelenmesi için sonlu elemanlar metodu kullanılmıştır. Sonlu elemanlar metodu geometri ve parametrelerin kolaylıkla değişimine izin verdiğinden farklı değişkenlerin etkileri araştırılmıştır. Sismik taşıma gücü probleminde etkin parametrelerin bütünüyle değerlendirilmesi amacıyla yapılan 1000'den fazla model çözümü sonucunda, sismik taşıma gücü üzerinde etkisi olan 5 farklı faktör (yatay sismik ivme katsayısı, şev açısı, temelin şev köşesinden olan uzaklığı, şev yüksekliği, zemin özellikleri) belirlenmiştir. Elde edilen analiz sonuçları derlenerek ve değerlendirilerek tasarımda ya da uygulamada çalışan geoteknik mühendisleri için taşıma gücü üzerinde etkisi olduğu belirlenen tüm faktörleri göz önünde bulunduran kolay uygulanabilir alternatif bir çözüm yöntemi geliştirilmiştir.

TABLE OF CONTENTS

ACKNOWLEDGEMENTS iv
ABSTRACT v
ÖZET vi
LIST OF FIGURES ix
LIST OF TABLES xx
LIST OF SYMBOLS xxii
LIST OF ACRONYMS/ABBREVIATIONS xxiv
1. INTRODUCTION 1
2. LITERATURE REVIEW 5
2.1. Static Bearing Capacity of Strip Footings Located on or near Cohesive Slopes 5
2.2. Seismic Bearing Capacity of Footings Located near Cohesive Slopes 23
2.3. Stability of Cohesive Slopes in Static and Seismic Conditions 52
3. METHOD OF ANALYSIS 56
3.1. FEM in Geotechnical Engineering and Plaxis 2D 57
3.2. Definition and Assumptions of the Problem 58
3.3. Suggested Solution Method 59
3.4. Parametric Study 60
3.5. Data Input in Plaxis 2D 61
3.5.1. General Settings 61
3.5.2. Model geometry 64
3.5.3. Properties of Surficial Strip Footing 64
3.5.4. Boundary Conditions 65
3.5.5. Loads 65
3.5.6. Material Properties 67
3.5.7. Finite Element Mesh Generation 70
3.5.8. Generation of Initial Stresses 74
3.6. Solution of Finite Element Model and Determination of Seismic Bearing Capacity Factor (N_{cse}) by Calculations Module of Plaxis 2D 74
3.7. Evaluation of Plaxis 2D Outputs 78
3.8. Comparison of Numerical Model Results with Previous Researches 79

3.8.1. Comparisons Made for Static Condition....79
3.8.2. Comparisons Made for Seismic Conditions....81
3.8.3. Stability Assessment of Cohesive Slopes Both in Static and Seismic Condition....83
4. RESULTS AND DISCUSSIONS....90
4.1. Determination of Influential Parameters....91
4.1.1. Influence of Horizontal Seismic Acceleration Coefficient....91
4.1.2. Influence of Slope Angle....92
4.1.3. Influence of Normalized Footing Distance....92
4.1.4. Influence of Slope Height....93
4.1.5. Influence of Slope Soil Strength....94
4.2. Examination of Failure Mechanisms....95
4.3. Design Charts....101
4.4. Other Remarkable Results....108
4.5. Design Examples....109
4.5.1. Design Example 1....110
4.5.2. Design Example 2....112
4.5.3. Design Example 3....115
4.5.4. Design Example 4....118
4.5.5. Design Example 5....120
4.5.6. Design Example 6....123
5. CONCLUSIONS....125
APPENDIX A: STABILITY ASSESMENT of COHESIVE SLOPES in SEISMIC CONDITION by USING KOPPULA'S METHOD (1984).....128
APPENDIX B: LIST OF RESULTS OF FINITE ELEMENTS MODELS CREATED FOR STATIC CONDITION.....131
APPENDIX C: LIST OF RESULTS OF FINITE ELEMENTS MODELS CREATED FOR SEISMIC CONDITION.....136
REFERENCES....155

LIST OF FIGURES

Figure 1.1. Building toppled due to lack of seismic bearing capacity during Mexico City Earthquake- Mexico (1985) (Merlos and Romo, 2006). 1

Figure 1.2. Bridge abutment constructed on top of slope (Ziyaret Bridge, Adiyaman, Turkey). 2

Figure 2.1. Plastic zones near strip foundation on face of a slope (Meyerhof, 1957). 7

Figure 2.2. Bearing capacity factors for strip foundation on face of a purely cohesive slope (Meyerhof, 1957). 8

Figure 2.3. Plastic zones and slip surfaces near rough strip foundation on top of slope (Meyerhof, 1957). 9

Figure 2.4. Bearing capacity factors for strip foundation on top of purely cohesive slope (Meyerhof, 1957). 10

Figure 2.5. Footings on or adjacent to a slope (Bowles, 1997). 11

Figure 2.6. Failure surfaces and stress trajectories in the plastic zone beneath the footing (Bowles, 1997)..... 11

Figure 2.7. Failure mechanism adopted for the upper bound solution (Kusakabe *et al.*, 1981). 13

Figure 2.8. No.1 design chart presented to calculate dimensionless factor (μ) (Kusakabe *et al.*, 1981). 13

Figure 2.9. No.2 and No.3 design charts presented to calculate dimensionless factor (μ) (Kusakabe *et al.*, 1981). 14

Figure 2.10. Schematic representation of the problem (Georgiadis, 2010)..... 15

Figure 2.11. Failure modes (a) and (b) bearing capacity failure and (c) overall slope failure (Georgiadis, 2010). 16

Figure 2.12. Variation of failure mode and N_c with H/B for λ= 0 and β= 45° (Georgiadis, 2010)..... 17

Figure 2.13. Variation of N_c with λ for $c_u/\gamma B$= 0.5 (Georgiadis, 2010). 17

Figure 2.14. Variation of N_c with λ for $c_u/\gamma B$= 1 (Georgiadis, 2010). 18

Figure 2.15. Variation of N_c with λ for $c_u/\gamma B$= 1.5 (Georgiadis, 2010). 18

Figure 2.16. Variation of N_c with λ for $c_u/\gamma B$= 2, 2.5 and 5 (Georgiadis, 2010). 19

Figure 2.17. Variation of λ_o with β (Georgiadis, 2010). 20

Figure 2.18. Failure mechanism and applied forces adopted in the analysis (Castelli and Motta, 2010). 21

Figure 2.19. Variation of ground factors (N_c^*/N_c) in static condition with the footing distance from the edge of the slope (Castelli and Motta, 2010). 22

Figure 2.20. Log-spiral failure mechanism (Sawada *et al.*, 1994). 24

Figure 2.21. Failure mechanism and applied forces of foundation-soil system (Sarma and Chen, 1996)..... 26

Figure 2.22. Failure mechanism used in the analysis (Askari and Farzaneh, 2003). .. 31

Figure 2.23. Both sides failure mechanism used in the analysis (Kumar and Rao, 2003). 34

Figure 2.24. Single side failure mechanism used in the analysis (Kumar and Rao, 2003). 34

Figure 2.25. Variation of N_q with α_h for different values of Φ and β: (a) Φ= 10°; (b) Φ= 20°; (c) Φ= 30°; (d) Φ= 40°; (e) Φ= 50° (Kumar and Rao, 2003). .. 35

Figure 2.26. Variation of N_c with α_h for different values of Φ and β: (a) Φ= 0°; (b) Φ= 10°; (c) Φ= 20°; (d) Φ= 30°; (e) Φ= 40°; (f) Φ= 50° (Kumar and Rao, 2003). 36

Figure 2.27. Variation of N_γ with α_h for different values of Φ and β: (a) Φ= 10°; (b) Φ= 20°; (c) Φ= 30°; (d) Φ= 40°; (e) Φ= 50° (Kumar and Rao, 2003) ... 37

Figure 2.28. Graphical representation of the problem (Shiau *et al.*, 2006). 38

Figure 2.29. Effect of $tan\theta$ on $p/\gamma B$ for various Φ (Shiau *et al.*, 2006). 39

Figure 2.30. Comparison of upper bound velocity diagrams for the effect of inertia forces (Shiau *et al.*, 2006). 39

Figure 2.31. Effect of $q/\gamma B$ on $p/\gamma B$ for various β (Shiau *et al.*, 2006). 40

Figure 2.32. Effect of soil inertia k_h on $p/\gamma B$ (Shiau *et al.*, 2006). 40

Figure 2.33. Failure mechanism used in the analysis (Yamamoto, 2010). 42

Figure 2.34. Failure mechanisms for different values of Φ, β, α and K_h (Yamamoto, 2010). 44

Figure 2.35. Design charts for N_{ce} (Φ= 30°, 40°, D/B= 0, a= 0.0) (Yamamoto, 2010). 44

Figure 2.36. Design charts for N_{ce} (Φ= 30°, 40°, D/B= 1, a= 0.0) (Yamamoto, 2010). 45

Figure 2.37. Design charts for N_{ce} (Φ= 30°, 40°, D/B= 0, a= 0.5) (Yamamoto, 2010). 45

Figure 2.38. Design charts for $N_{\gamma e}$ (Φ= 30°, 40°, D/B= 0, a= 0.0) (Yamamoto, 2010). 45

Figure 2.39. Design charts for $N_{\gamma e}$ (Φ= 30°, 40°, D/B= 1, a= 0.0) (Yamamoto, 2010). 46

Figure 2.40. Design charts for $N_{\gamma e}$ (Φ= 30°, 40°, D/B= 0, a= 0.5) (Yamamoto, 2010). 46

Figure 2.41. N_c^*/N_c ratios as a function of the normalized d/B slope distance (Castelli and Motta, 2010)..... 47

Figure 2.42. Problem parameters (Farzaneh *et al.*, 2013). 49

Figure 2.43. Variation of seismic bearing capacity with a/B (Farzaneh *et al.*, 2013). 50

Figure 2.44. Variation of seismic bearing capacity $c_u/\gamma B$ (Farzaneh *et al.*, 2013). 50

Figure 2.45. Design charts for seismic bearing capacity of strip footings near cohesive slopes (Farzaneh *et al.*, 2013). 51

Figure 2.46. Definition of parameters for midpoint circle type of failure (Taylor, 1937) (Adapted from Das, 2009). 53

Figure 2.47. Plot of stability number (m) against slope angle (β) (Taylor, 1937) (Adapted from Das, 2009)..... 53

Figure 2.48. Variation of N_2 with k_h and β (Koppula, 1984) (Adapted from Das and Ramana, 2010). 55

Figure 2.49. Variation of N_2 with $\beta \geq 55$ and k_h (Koppula, 1984) (Adapted from Das and Ramana, 2010)..... 55

Figure 3.1. Graphical representation of the problem. 58

Figure 3.2. "Project" tab of "General settings" window. 62

Figure 3.3. "Dimensions" tab of "General settings" window..... 62

Figure 3.4. Position of nodes and stress points in soil elements (Brinkgreve *et al.*, 2006). 63

Figure 3.5. Schematic representation of created finite elements model. 64

Figure 3.6. Inclined load acting on the rigid footing and unit load definition (For k_h= 0.4) 66

Figure 3.7. Tresca yield surface in principal total stress space (Potts and Zdravkovic, 1999). 69

Figure 3.8. Mohr's circles of total stress (Potts and Zdravkovic, 1999). 69

Figure 3.9. Prandtl type failure mechanism (Prandtl, 1920) (Adapted from Potts and Zdravkovic, 2001). 71

Figure 3.10. Failure mechanism determined by Plaxis 2D at the ultimate state and its enlarged view. 72

Figure 3.11. Shear surfaces determined by Plaxis 2D at the ultimate state. 72

Figure 3.12. Typical connectivity plot obtained applying to developed mesh generation procedure (β= 15°, H= 8.0m; λ= 0.25). 73

Figure 3.13. Variation of N_{cse} with the number of triangular elements (β= 30°, H= 4.0m, λ= 0, c_u= 100kPa, k_h= 0.2)..... 74

Figure 3.14. Typical view of "Calculations Module" window..... 75

Figure 3.15. The load multiplier (*Σ-MloadA)* obtained by using Calculations module of Plaxis 2D for the ultimate limit state. 77

Figure 3.16. Failure mechanism obtained for the finite element model named as C_30_2_3_200_0.3_D and enlarged view of the failure mechanism. 78

Figure 3.17. Shear surfaces obtained for the finite element model named as C_30_2_3_200_0.3_D and enlarged view of the shear surfaces. 79

Figure 3.18. Variation of N_{cs} with β (For λ= 0, $c_u/\gamma B$= 5)..... 80

Figure 3.19. Variation of N_{cs} with λ (For β= 30°, $c_u/\gamma B$= 5). 81

Figure 3.20. Variation of N_{cse} with k_h for all slope angles (For λ= 0, $c_u/\gamma B$= 5). 82

Figure 3.21. Variation of N_{cse} with λ (For β= 30°, $c_u/\gamma B$= 5, k_h= 0.2)..... 83

Figure 3.22. Failure mechanism of unstable cohesive slope in static condition (β= 15°, H=8.0 m and c_u= 25 kPa). 85

Figure 3.23. Failure mechanism of unstable cohesive slope in static condition (β= 30°, H=8.0 m and c_u= 25 kPa). 85

Figure 3.24. Failure mechanism of unstable cohesive slope in static condition (β= 45°, H=8.0 m and c_u= 25 kPa). 86

Figure 3.25. Failure mechanism of unstable cohesive slope in seismic condition (β= 30°, H= 4.0 m, c_u= 50 kPa, k_h= 0.3). 88

Figure 3.26. Failure mechanism of unstable cohesive slope in seismic condition (β= 30°, H= 4.0 m, c_u= 50 kPa, k_h= 0.4). 88

Figure 3.27. Failure mechanism of unstable cohesive slope in seismic condition (β= 45°, H=4.0 m, c_u= 25 kPa, k_h= 0.1). 88

Figure 3.28. Failure mechanism of unstable cohesive slope in seismic condition (β= 45°, H=4.0 m, c_u= 25 kPa, k_h= 0.2). 89

Figure 3.29. Failure mechanism of unstable cohesive slope in seismic condition (β= 45°, H=4.0 m, c_u= 25 kPa, k_h= 0.3). 89

Figure 3.30. Failure mechanism of unstable cohesive slope in seismic condition (β= 45°, H=4.0 m, c_u= 25 kPa, k_h= 0.4). 89

Figure 4.1. Variation of N_{cse} with k_h for all λ values (β= 15°, $c_u/\gamma B$= 2.5). 91

Figure 4.2. Variation of N_{cse} with β for all λ values (k_h= 0.2, $c_u/\gamma B$= 5). 92

Figure 4.3. Variation of N_{cse} with λ for all k_h values (β= 45°, $c_u/\gamma B$= 2.5). 93

Figure 4.4. Variation of N_{cse} with $c_u/\gamma B$ for all k_h values (β= 30°, H/B= 1, λ= 0)..... 94

Figure 4.5. Base failure due to self-weight of cohesive slope (β= 45°, H/B= 4, $c_u/\gamma B$= 0.625). 95

Figure 4.6. Base failure due to earthquake inertia force (β= 30°, H/B= 2, $c_u/\gamma B$= 0.625, k_h= 0.2). 95

Figure 4.7. Typical "Foundation failure" modes for λ= 0 condition (a) β= 45°, H/B= 1, $c_u/\gamma B$= 1.25, k_h= 0.2; (b) β= 45°, H/B= 1, $c_u/\gamma B$= 0.625, k_h= 0.1. 96

Figure 4.8. Typical "Foundation failure" modes for λ> 0 condition (a) β= 45°, H/B= 4, $c_u/\gamma B$= 2.5, k_h= 0.3; (b) β= 45°, H/B= 4, $c_u/\gamma B$= 2.5, k_h= 0.1; (c) β= 45°, H/B= 4, $c_u/\gamma B$= 1.25, k_h= 0.1. 96

Figure 4.9. Typical view of "Foundation sliding" failure mode (β= 45°, H/B= 4, λ= 2, $c_u/\gamma B$= 2.5, k_h= 0.4)..... 97

Figure 4.10. Variation of N_{ce} with k_h (β= 0°)..... 99

Figure 4.11. Variation of failure modes with influential parameters (λ< 0.25 or 0.5). 100

Figure 4.12. Variation of failure modes with influential parameters ($\lambda \geq$ 0.25 or 0.5). 100

Figure 4.13. Design chart for seismic bearing capacity factor of surficial strip footings near cohesive slopes (β= 15°, $c_u/\gamma B$= 5, H/B= 1, 2, 4). 102

Figure 4.14. Design chart for seismic bearing capacity factor of surficial strip footings near cohesive slopes (β= 15°, $c_u/\gamma B$= 2.5, H/B= 1, 2, 4). 102

Figure 4.15. Design chart for seismic bearing capacity factor of surficial strip footings near cohesive slopes (β= 15°, $c_u/\gamma B$= 1.25, H/B= 1, 2, 4). 103

Figure 4.16. Design chart for seismic bearing capacity factor of surficial strip footings near cohesive slopes (β= 15°, $c_u/\gamma B$= 0.625, H/B= 1, 2, 4). 103

Figure 4.17. Design chart for seismic bearing capacity factor of surficial strip footings near cohesive slopes (β= 30°, $c_u/\gamma B$= 5, H/B= 1, 2, 4). 104

Figure 4.18. Design chart for seismic bearing capacity factor of surficial strip footings near cohesive slopes (β= 30°, $c_u/\gamma B$= 2.5, H/B= 1, 2, 4). 104

Figure 4.19. Design chart for seismic bearing capacity factor of surficial strip footings near cohesive slopes (β= 30°, $c_u/\gamma B$= 1.25, H/B= 1, 2, 4). 105

Figure 4.20. Design chart for seismic bearing capacity factor of surficial strip footings near cohesive slopes (β= 30°, $c_u/\gamma B$= 0.625, H/B= 1, 2, 4). 105

Figure 4.21. Design chart for seismic bearing capacity factor of surficial strip footings near cohesive slopes (β= 45°, $c_u/\gamma B$= 5, H/B= 1, 2, 4). 106

Figure 4.22. Design chart for seismic bearing capacity factor of surficial strip footings near cohesive slopes (β= 45°, $c_u/\gamma B$= 2.5, H/B= 1, 2, 4). 106

Figure 4.23. Design chart for seismic bearing capacity factor of surficial strip footings near cohesive slopes (β= 45°, $c_u/\gamma B$= 1.25, H/B= 1, 2, 4). 107

Figure 4.24. Design chart for seismic bearing capacity factor of surficial strip footings near cohesive slopes (β= 45°, $c_u/\gamma B$= 0.625, H/B= 1, 2, 4). 107

Figure 4.25. Geometry of failure mechanisms obtained at the ultimate state for all k_h values. 109

Figure 4.26. Schematic representation of the design example 1. 110

Figure 4.27. Estimation of the failure mode for the design example 1. 111

Figure 4.28. N_{cse} values to be used in linear interpolation for the design example 1. . 111

Figure 4.29. Load multiplier (*Σ-MloadA*) and the failure mechanism obtained by Plaxis 2D for the design example 1..... 112

Figure 4.30. Schematic representation of the design example 2. 112

Figure 4.31. Estimation of the failure mode for the design example 2. 113

Figure 4.32. The first N_{cse} value to be used in linear interpolation for the design example 2. 114

Figure 4.33. The second N_{cse} value to be used in linear interpolation for the design example 2. 114

Figure 4.34. Load multiplier (*Σ-MloadA*) and the failure mechanism obtained by Plaxis 2D for the design example 2..... 115

Figure 4.35. Schematic representation of the design example 3. 115

Figure 4.36. Estimation of the failure mode for the design example 3. 116

Figure 4.37. The first N_{cse} value to be used in linear interpolation for the design example 3. 117

Figure 4.38. The second N_{cse} value to be used in linear interpolation for the design example 3. 117

Figure 4.39. Load multiplier (*Σ-MloadA*) and the failure mechanism obtained by Plaxis 2D for the design example 3..... 118

Figure 4.40. Schematic representation of the design example 4. 118

Figure 4.41. Linear relationship between $N_{cse} - \beta$. 119

Figure 4.42. Load multiplier (*Σ-MloadA*) and the failure mechanism obtained by Plaxis 2D for the design example 4..... 120

Figure 4.43. Schematic representation of the design example 5. 121

Figure 4.44. Estimation of the failure mode for the design example 5. 121

Figure 4.45. View of "Calculations Module" window for the design example 5. 122

Figure 4.46. Failure mechanism obtained by Plaxis 2D for the design example 5. 122

Figure 4.47. Schematic representation of the design example 5 123

Figure 4.48. Estimation of the failure mode for the design example 6. 124

Figure 4.49. Load multiplier (*Σ-MloadA*) and the failure mechanism obtained by Plaxis 2D for the design example 6..... 124

LIST OF TABLES

Table 2.1. Bearing capacity factors Nc' ve Nq' for footings on or adjacent to a slope (Bowles, 1997). 12

Table 2.2. Variation in seismic bearing capacity with earthquake acceleration factor, K for the case of submerged slope (β= 20°, b/B_l= 2.0, B_l= 10 m, Φ=30°, c=9.8 kPa, x=1.0) (Sawada *et al.*, 1994). 25

Table 2.3. Variation in seismic bearing capacity with b/B_l ratio and γ (gf/cm^3) (K= 0.5, β= 20°, Φ= 30°, c= 9.8 kPa, B_l= 10 m, x= 1.0) (Sawada *et al.*, 1994). 25

Table 2.4. N_γ expressed in terms of slope angle, $logN\gamma = a\ tan2\beta + b\ tan\beta + c$, with respect to friction angle (Φ in degrees) and ground acceleration (kg) (Sarma and Chen, 1996). 28

Table 2.5. N_q expressed in terms of slope angle, $logNq = a\ tan2\beta + b\ tan\beta + c$, with respect to friction angle (Φ in degrees) and ground acceleration (kg) (Sarma and Chen, 1996). 29

Table 2.6. N_c expressed in terms of slope angle, $logNc = a\ \beta 2 + b\beta + c$, with respect to friction angle (Φ in degrees) and ground acceleration (kg) (Sarma and Chen, 1996). 30

Table 2.7. Normalized seismic limit pressure (q/c) for $\gamma b/c$= 0.25, 0.5, 1 and 2, Φ= 15°, 30° and 45°, $K_{cl} = K_{ce} = K_c$= 0.15 and 0.3 and β= 15°, 30° and 45° (Askari and Farzaneh, 2003) 33

Table 3.1. Physical and elastic properties of rigid plate element. 65

Table 3.2. Properties of the cohesive slope soils considered in this study. 70

Table 3.3. In “Parameters” and “Multipliers” tabs adjustments to be made in each calculation stage. 76

Table 3.4. H_{cr} values calculations and stability assessment of cohesive slopes in static condition by using Taylor's method. 84

Table 3.5. H_{cr} values calculations and stability assessment of cohesive slopes in seismic condition using Koppula's method. 86

Table 4.1. Variation of N_{ce} with k_h (β= 0°). 98

Table 4.2. Range of threshold distance varied with horizontal seismic acceleration coefficient. 108

Table A.1. H_{cr} values calculations and stability assessment of cohesive slopes in seismic condition using Koppula's method. 128

Table B.1. List of results of finite elements models created for static condition. 132

Table C.1. List of results of finite elements models created for seismic condition (β= 15°). 137

Table C.2. List of results of finite elements models created for seismic condition (β= 30°). 143

Table C.3. List of results of finite elements models created for seismic condition (β= 45°). 149

LIST OF SYMBOLS

B	Footing width
c_u	Undrained shear strength of cohesive slope soil
d_{eq}	Equivalent plate thickness
D_f	Depth of footing
EA	Axial stiffness of the plate element
EI	Flexural stiffness of the plate element
E_u	Undrained elasticity modulus of cohesive soil
$F(\{\boldsymbol{\sigma}\}, \{\mathbf{k}\})$	Yield function of Tresca model
g	Gravitational acceleration
q_f	Seismic bearing capacity of surficial strip footings near cohesive slopes
q_{fh}	Magnitude of horizontal component of inclined load imposed on the footing
H	Slope height
k_h	Horizontal seismic acceleration coefficient
k_x	Permeability in horizontal direction (x axis)
k_v	Vertical seismic acceleration coefficient
k_y	Permeability in vertical direction (y axis)
N_{ce}	Seismic bearing capacity factor for surficial strip footings on level ground
N_{cs}	Static bearing capacity factor for surficial strip footings near cohesive slopes
N_{cse}	Seismic bearing capacity factor of surficial strip footings near cohesive slopes
$P(\{\boldsymbol{\sigma}\}, \{\mathbf{m}\})$	Plastic potential of Tresca model
R_{inter}	Interface strength reduction factor
R^2	Corelation coefficient
u_x	Nodal displacement in horizontal direction (x axis)
u_y	Nodal displacement in vertical direction (y axis)
w	Weight of the plate element

β	Slope angle
γ_{sat}	Soil unit weight below phreatic level (Saturated)
γ_{unsat}	Soil unit weight above phreatic level (Wet)
λ	Normalized footing distance from the slope edge
λ_0	Threshold value of normalized footing distance
v	Poisson ratio of the plate element
v_u	Undrained Poisson ratio of soil
σ_1	Major principal total stress
σ_3	Minor principal total stress
Σ-Maccel	Load multiplier which controls the magnitude of the pseudo-static force
Σ-MloadA	Load factor which controls the magnitude of load system A
Σ-Mweight	Load multiplier which controls the proportion of standard gravity applied in the analysis
Φ_u	Undrained angle of internal friction
ψ_u	Undrained dilation angle of soil

LIST OF ACRONYMS/ABBREVIATIONS

FEM	Finite Elements Method
UU	Unconsolidated-Undrained

1. INTRODUCTION

Structures constructed on clays and dense sands for which liquefaction is unlikely to occur had been damaged with undesirable rotation and excessive settlement by the influence of strong or even moderate earthquake. When foundation soil does not have sufficient capacity to resist seismic loads transmitted by structure during an earthquake, seismic bearing capacity failure occurs. Examples of such failures have been observed during powerful earthquakes such as Naigata-Japan (1964), Mexico City-Mexico (1985), Izmit-Turkey (1999) (Day, 2002; Merlos and Romo, 2006). Building toppled due to degradation of soil bearing capacity during Mexico City Earthquake - Mexico (1985) is shown in Figure 1.1 (Merlos and Romo, 2006). Making similar observations to the case presented in Figure 1.1 after destructive earthquakes encourages researchers about evaluating this phenomenon in a much more detailed way. In order to comprehend likely reasons of the phenomenon and prevent catastrophic effects on buildings, numerous research studies were conducted especially in the last two decades.



Figure 1.1. Building toppled due to lack of seismic bearing capacity during Mexico City Earthquake- Mexico (1985) (Merlos and Romo, 2006).

Bridge abutments, energy transmission towers, retaining walls and etc. are commonly constructed at nearby positions to natural or man-made slopes due to existing terrain conditions. Therefore, in order to avoid presence of structures exposed to rotation

and excessive settlement due to earthquake impact, determination of seismic bearing capacity for these indispensable structural elements which are integral parts of engineering structures such as highway bridge, energy transmission line and etc. is of great importance. For instance, the abutment of Ziyaret Bridge (Adiyaman, Turkey) which was constructed at a nearby position to the top of the slope is presented in Figure 1.2.



Figure 1.2. Bridge abutment constructed on top of slope (Ziyaret Bridge, Adiyaman, Turkey).

Seismic bearing capacity is a significant and wide-ranging topic within the study area of geotechnical earthquake engineering. In this study, seismic bearing capacity of surficial foundations near cohesive slopes which is a specific subheading of “seismic bearing capacity” topic had been discussed and major factors which have an influence on seismic bearing capacity of such foundations were investigated.

As it is known, the first condition -necessary but not only the sufficient condition- which should be satisfied to achieve any successful foundation design is that there should be adequate safety factor against general or local shear failure of underlying soil (Skempton, 1951). The criterion is entirely valid for foundations constructed at nearby positions on top of slopes as well. However, unless there is a design method that enables the calculation of bearing capacity of foundations near slopes for both static and seismic cases, it is impossible to check whether the stated condition is fulfilled.

Static bearing capacity of surficial foundations on top of slopes or located near slopes has been studied by several researchers since the middle of 50s. As a result, various empirical equations and design charts have been developed so far. One of these research studies (Meyerhof, 1957) was even published in several well-accepted technical specifications and design manuals such as American Association of State Highway Transportation Officials (AASHTO, 1996) Standard Specification of Highway Bridges, Washington State of Transportation Department (WSDOT, 2005) Geotechnical Design Manual and etc. On the contrary, it is also seen that published research studies about seismic bearing capacity generally considers foundations on level ground. Furthermore, research studies about seismic bearing capacity of foundations near cohesive slopes are seldomly found in geotechnical earthquake engineering literature. It should also be mentioned that limited number of research studies on seismic bearing capacity of foundations located near cohesive slopes were conducted in the last decade.

In this study, as being different than analysis methods previously used (method of stress characteristics, limit equilibrium) numerical methods was utilized. Firstly, influential parameters were determined via a parametric study. Then, seismic bearing capacity coefficient, denoted by N_{cse}, was defined as a function of several independent variables. Finally, by evaluating and interpreting obtained results, an easily-applied alternative solution method was developed for geotechnical practitioners. Proposed solution method allows the consideration of the influences of all the variables that affect the problem under investigation. As it can be seen in the following sections, various noteworthy outcomes have been obtained by interpreting analysis results. For instance, for models with identical geometries and soil properties, failure surface passes through a shallower depth for the model with the greater coefficient of horizontal seismic acceleration. Furthermore, the distance from the edge of the slope at which the effects of slope disappears (the threshold distance) is dependent on the horizontal seismic acceleration coefficient.

Content of the remaining part of the thesis can be briefly summarized as follows; In "Literature Review" chapter, research studies regarding to static bearing capacity of surficial strip foundations near cohesive slopes will be the primary focus since studies on seismic conditions will be dealt with in the "Method of Analysis" chapter. Then, details of various research studies that had been performed so far to propose alternative

methodologies for the determination of seismic bearing capacity of foundations near slopes will be presented. On the other hand, depending on the geometrical properties of slope and strength characteristics of slope soil, the slope can lose its stability by the influence of even gravity in static condition or by the inertia force in seismic condition. Since this situation was observed in some of numerical model outputs, research studies regarding to stability of cohesive slopes in both static and seismic conditions will also be given briefly to check whether the results of numerical model are consistent with previous researches.

"Method of Analysis" chapter includes important details regarding to development of the numerical model for determination of seismic bearing capacity of foundations near cohesive slopes. Model geometry, constitutive modelling of slope soil, mesh generation, loading and boundary conditions and etc. will be studied in detail in this chapter. As stated in the above paragraph, validation check of developed numerical model will be performed separately for both static and seismic cases at this stage.

In "Results and Discussions" chapter, firstly, it will be determined that which variables are influential onto the seismic bearing capacity factor (N_{cse}). Thus, independent variables of the function defined for the seismic bearing capacity factor would be clarified. Another objective of the thesis is to propose alternative methodology for the determination of seismic bearing capacity of surficial foundations located near cohesive slopes. Therefore, design charts which were prepared to establish an easily-applied methodology, for the use of geotechnical designers and practitioners, will be introduced. Additionally, evaluations will be made regarding to how failure mode varies as the foundation reaches its seismic bearing capacity by interpreting outputs of developed numerical model. Finally, several design examples will be presented in order to demonstrate the practical use of suggested methodology.

In "Conclusions" chapter, results obtained in this study will be briefly summarized.

2. LITERATURE REVIEW

As mentioned in the "Introduction" chapter of the thesis, "Literature Review" chapter is basically divided into three parts. Firstly, research studies related to static bearing capacity of strip footings located on or near cohesive slopes will be referred. Main reason of addressing these researches is that the accuracy of developed numerical model is investigated by comparing numerical model results with those obtained by previous researchers presented in Chapter 2.1.

Secondly, research studies related to seismic bearing capacity of footings located near slopes which have been performed so far will be referred. Some of the results of those researches given in Chapter 2.2 are utilized to investigate the reliability of numerical model results. Thus, this step to be performed in the subsequent chapter of the thesis can be considered as second phase verification of the solution method developed.

Lastly, some model results reveal that under certain circumstances, the slope cannot maintain its stability under the influence of gravity for static conditions and under the action of inertia forces during seismic events. Therefore, research studies investigating stability of cohesive slopes (excluding footing pressure on slope) for both static and seismic condition will also be mentioned later for the purposes of making comparison with numerical model results.

2.1. Static Bearing Capacity of Strip Footings Located on or near Cohesive Slopes

Several researchers have developed numerous calculation techniques since the middle of 50s for determination of ultimate bearing capacity of strip footings located on or near cohesive slopes in static conditions. Those calculation methods developed have been presented together with several empirical equations and design charts.

Ultimate bearing capacity of a surficial strip footing on horizontal level ground under concentric load action is basically calculated by using Equation 2.1. (Prandtl, 1920; Skempton, 1951).

$$q_u = c_u N_c \tag{2.1}$$

Besides that, owing to sloping ground surface, Hansen (1961) and Vesic (1975) had presented correction factors to modify the ultimate bearing capacity equation given in Equation 2.1. Correction factors presented by Hansen (1961) and Vesic (1975) are given in Equation 2.2 and 2.3 respectively.

$$N_c = 5.14\left(1-\frac{2\beta}{\pi+2}\right) \tag{2.2}$$

$$N_c = 5.14\left(1-\frac{2\beta}{\pi+2}\right) - \frac{\gamma B}{c_u}\sin\beta \tag{2.3}$$

where q_u is the ultimate bearing capacity of strip footing; N_c is the bearing capacity factor; β is the slope angle (in radian); B is the footing width; γ is the saturated unit weight of soil; c_u is the undrained shear strength of soil.

Equation 2.2 and 2.3 are valid for the cases in which the footing is located on a slope surface or on top edge of a slope. While Hansen's correction factor for sloping ground does not involve any physical and strength properties of cohesive soil, neither Hansen nor Vesic considers the influence of slope height on correction factor for sloping ground.

Meyerhof (1957) is the prominent research study which has been adopted by well-known design manuals such as American Association of State Highway Transportation Officials (AASHTO, 1996) “Standard Specification of Highway Bridges”, Washington State Department of Transportation (WSDOT, 2005) “Geotechnical Design Manual”. For the purposes of determination of static ultimate bearing capacity of a footing located on or near cohesive and granular slopes, a methodology had been introduced combining bearing capacity theory proposed for footings on level ground with slope stability theory.

Meyerhof (1957) stated that as a footing located on face of a slope is loaded until failure, failure surfaces in soil develop on side of the slope and length of the failure surfaces are much shorter than those of an identical foundation on level ground. Therefore,

the author had concluded that static bearing capacity of a footing located on face of the slope is less than that of the identical footing on level ground. Failure surfaces assumed by Meyerhof (1957) are shown in Figure 2.1.

Static ultimate bearing capacity of the surficial strip footing on the slope is calculated in general by using formula given in Equation 2.4 (Meyerhof, 1957).

$$q_u = cN_{cq} + \frac{1}{2}\gamma B N_{\gamma q} \tag{2.4}$$

where q_u is the ultimate bearing capacity of strip footing; c is the cohesion; N_{cq} and $N_{\gamma q}$ are the bearing capacity factors determined depending on slope angle (β), angle of internal friction (Φ) and ratio of depth of footing to footing width (D/B), γ is the unit weight of soil; B is the footing width.

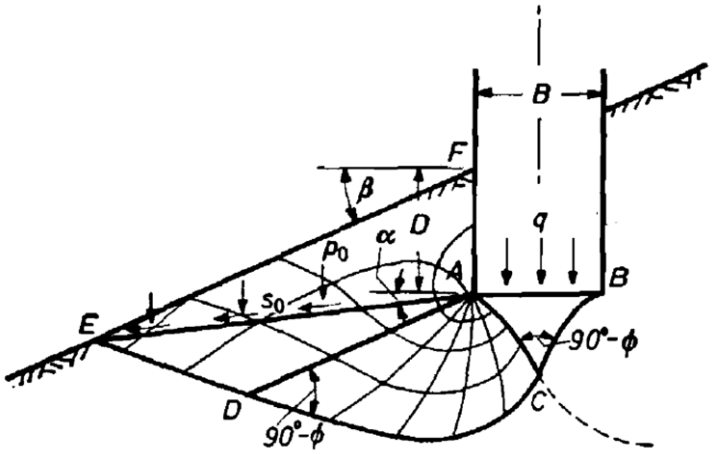


Figure 2.1. Plastic zones near strip foundation on face of a slope (Meyerhof, 1957).

Static ultimate bearing capacity of the surficial strip footing on cohesive slope is estimated by using formula given in Equation 2.5.

$$q_u = c_u N_{cq} \tag{2.5}$$

where q_u is the ultimate bearing capacity of strip footing; c_u is the undrained shear strength; N_{cq} is the bearing capacity factor determined depending on slope angle (β); ratio of depth

of footing to footing width (D/B) and slope stability number ($N_s = \gamma H / c_u$); γ the is unit weight of soil; B is the footing width; D is the depth of footing. Bearing capacity factor (N_{cq}) given in Equation 2.5 is determined by using design charts shown in Figure 2.2.

As the design chart shown in Figure 2.2 is examined, it is seen that the bearing capacity factor decreases with the increase of slope angle. The author had also stated that decrease in ultimate bearing capacity observed for cohesive soils is less than that of granular soils for slope angles used in practice (β<30°).

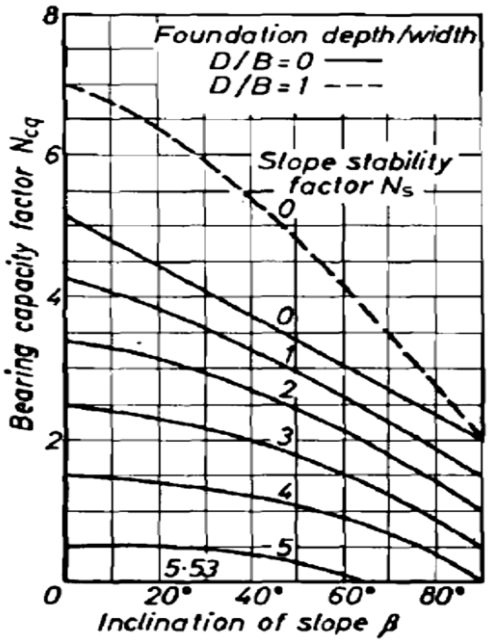


Figure 2.2. Bearing capacity factors for strip foundation on face of a purely cohesive slope (Meyerhof, 1957).

Static ultimate bearing capacity of a surficial strip footing on cohesive slope may be limited in some cases depending on the overall stability of slope. Meyerhof (1957) postulated that when a footing located on a cohesive slope reaches to its ultimate bearing capacity, three different failure modes can be observed. First failure mode is “foundation failure” for which failure surface intersects with slope surface above slope toe level. Remaining two failure modes are named as "slope failure". While toe failure surface passes from the toe of the slope, base failure surface passes below the toe level as footing reaches its bearing capacity. Different failure modes mentioned in the above are shown in Figure 2.3.

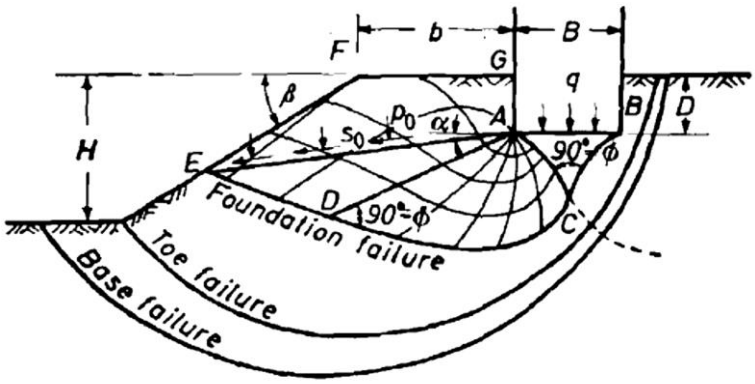


Figure 2.3. Plastic zones and slip surfaces near rough strip foundation on top of slope (Meyerhof, 1957).

Static ultimate bearing capacity of a surficial footing located at a certain distance from the edge of slope can be estimated by using Equation 2.5. In this case, bearing capacity coefficient (N_{cq}) given in Equation 2.5 is determined by using design chart presented in Figure 2.4. Bearing capacity coefficient (N_{cq}) is a function of slope angle (β), ratio of depth of footing to footing width (D/B), slope stability number ($N_s = \gamma H / c_u$) and ratio of distance between footing and slope edge to slope height (b/H). As seen in Figure 2.4, slope stability number has more decisive effect than that of slope angle on bearing capacity of footing in static conditions. It can also be seen that bearing capacity coefficient increases with the increase of distance between footing and slope edge. It is concluded that when a footing is 2-4 times of slope height away from the slope edge, static ultimate bearing capacity of a footing is independent of slope angle.

Bowles (1997) had used a compiled computer code to calculate static ultimate bearing capacity of a footing located on face of a slope or on a slope and the design table presented in Table 2.1 was developed. In this calculation method, after failure surface is defined using mathematical expressions presented in Figure 2.5, modified bearing capacity coefficient is calculated by following the methodology mentioned below. It should also be noted that failure surfaces developed beneath an identical footing located on level ground (refer to Figure 2.6) are taken into account.

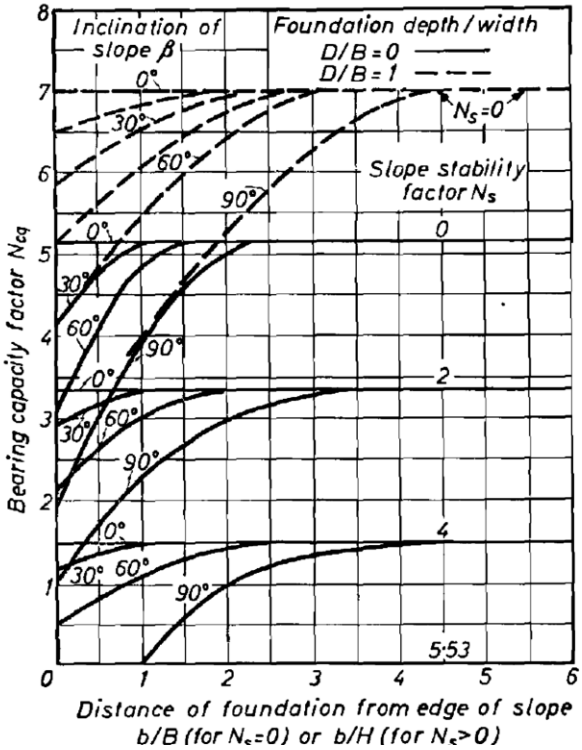


Figure 2.4. Bearing capacity factors for strip foundation on top of purely cohesive slope (Meyerhof, 1957).

- Compute a reduced bearing capacity factor (N_c) based on the failure surface ade = L_0 of Figure 2.6 and the failure surface adE = L_1 of Figure 2.5 to obtain

$$N_c' = N_c \frac{L_1}{L_0} \tag{2.6}$$

- Compute a reduced N_q based on the ratio of area ecfg (A_0) of Figure 2.6 to the equivalent area Efg = A_1 (footings on slope) or Efgh = A_1 (footings adjacent to slope) of Figure 2.5 to obtain the following:

$$N_q' = N_q \frac{A_1}{A_0} \tag{2.7}$$

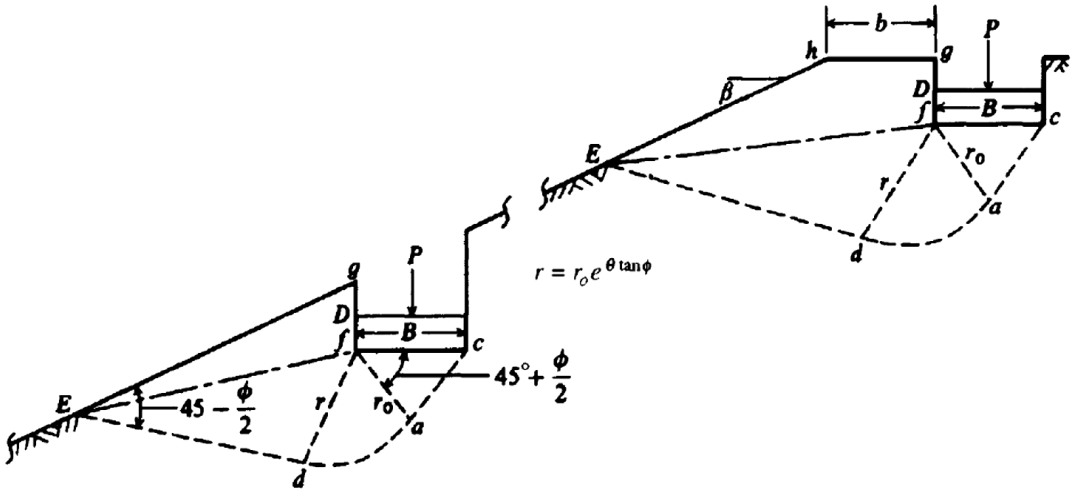


Figure 2.5. Footings on or adjacent to a slope (Bowles, 1997).

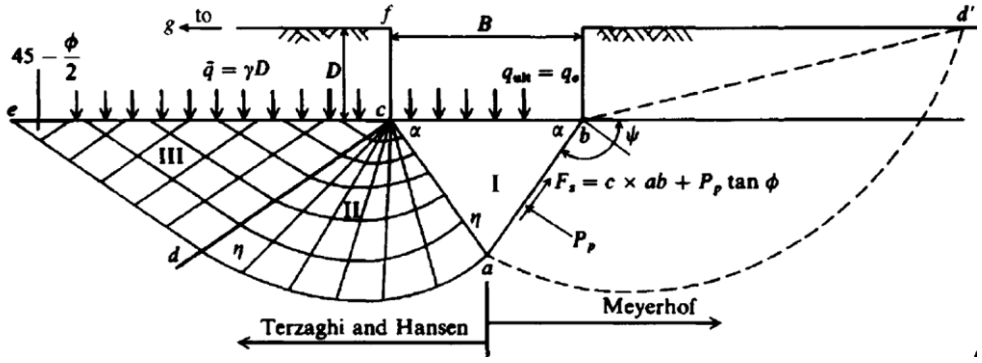


Figure 2.6. Failure surfaces and stress trajectories in the plastic zone beneath the footing (Bowles, 1997).

In order to calculate static bearing capacity of surficial footings located adjacent to cohesive slopes, the author proposed that Hansen's bearing capacity equation should be used together with coefficients determined by using design table presented in Table 2.1. As the design table given in Table 2.1 is examined, it is seen that bearing capacity coefficients $\left(N_c^{'} \text{ and } N_q^{'}\right)$ are function of slope angle (β), ratio of depth of footing to footing width (D/B), ratio of distance between the footing and slope edge to footing width (b/B) and angle of internal friction (Φ_u= 0°). According to the proposed calculation method, as the area ratio defined in Equation 2.7 equals to unity or the ratio of (b/B) varies between 1.5 and 2, reducing effect due to presence of slope on bearing capacity coefficients disappears.

Table 2.1. Bearing capacity factors $\left(N_c^{'} \text{ ve } N_q^{'}\right)$ for footings on or adjacent to a slope (Bowles, 1997).

$\beta \downarrow$		***D*/*B* = 0**			***b*/*B* = 0**		***D*/*B* = 0.75**			***b*/*B* = 0**		***D*/*B* = 1.50**			***b*/*B* = 0**	
	$\Phi \rightarrow$	0	10	20	30	40	0	10	20	30	40	0	10	20	30	40
0°	N'_c=	5.14	8.35	14.83	30.14	75.31	5.14	8.35	14.83	30.14	75.31	5.14	8.25	14.83	30.14	75.31
	N'_q=	1.03	2.47	6.40	18.40	64.20	1.03	2.47	6.40	18.40	64.20	1.03	2.47	6.40	18.40	64.20
10°		4.89	7.80	13.37	26.80	64.42	5.14	8.35	14.83	30.14	75.31	5.14	8.35	14.83	30.14	75.31
		1.03	2.47	6.40	18.40	64.20	0.92	1.95	4.43	11.16	33.94	1.03	2.47	5.85	14.13	40.81
20°		4.63	7.28	12.39	23.78	55.01	5.14	8.35	14.83	30.14	66.81	5.14	8.35	14.83	30.14	75.31
		1.03	2.47	6.40	18.40	64.20	0.94	1.90	4.11	9.84	28.21	1.03	2.47	5.65	12.93	35.14
25°		4.51	7.02	11.82	22.38	50.80	5.14	8.35	14.83	28.76	62.18	5.14	8.35	14.83	30.14	73.57
		1.03	2.47	6.40	18.40	64.20	0.92	1.82	3.85	9.00	25.09	1.03	2.47	5.39	12.04	31.80
30°		4.38	6.77	11.28	21.05	46.88	5.14	8.35	14.83	27.14	57.76	5.14	8.35	14.83	30.14	68.64
		1.03	2.47	6.40	18.40	64.20	0.88	1.71	3.54	8.08	21.91	1.03	2.47	5.04	10.99	28.33
60°		3.62	5.33	8.33	14.34	28.56	4.70	6.83	10.55	17.85	34.84	5.14	8.34	12.76	21.37	41.12
		1.03	2.47	6.40	18.40	64.20	0.37	0.63	1.17	2.36	5.52	0.62	1.04	1.83	3.52	7.80

Kusakabe *et al.* (1981) proposed a method to calculate static ultimate bearing capacity of a footing located near slope using upper bound plasticity theorem together with failure mechanism shown in Figure 2.7. Assumed failure mechanism consists of CDE active wedge, BCE log-spiral region and AB straight line which connects log spiral region to slope face. It is assumed that failure surface intersects slope face only above slope toe level. In this study, failure surface passing below slope toe level is not considered. Bearing capacity of foundations on slopes is determined by using formula given in Equation 2.8.

$$q_s = \mu \, q_L \tag{2.8}$$

q_s is the ultimate bearing capacity of a footing near slope; q_L is the ultimate bearing capacity of footing on level ground; μ is the dimensionless factor (Function of Φ, $c/\gamma B$, β, H); Φ is the angle of internal friction (for undrained conditions, $\Phi_u = 0°$); c is the cohesion; γ is the unit weight of soil; B is the footing width; β is the slope angle; H is the slope height.

To calculate dimensionless factor, design charts presented in Figure 2.8 and Figure 2.9 are used.

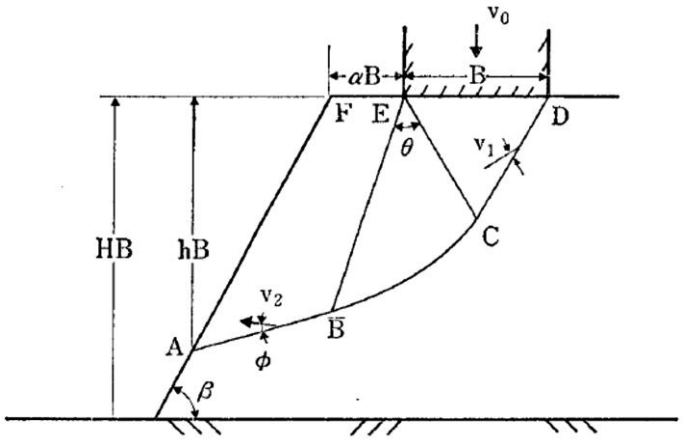


Figure 2.7. Failure mechanism adopted for the upper bound solution (Kusakabe *et al.*, 1981).

Authors compared the results of proposed calculation method with those of previous research studies and concluded that results were in good agreement with previous findings. Moreover, he mentioned that $c/\gamma B$ parameter (defined as 0.5, 1 and 5) has decisive effect on bearing capacity factor (N_c). It was stated that model tests, in which Kanto loam was used, can be considered undrained due to rapid loading capacity of the test apparatus. Mechanical and physical properties of material used during model tests and properties of the test apparatus can be found in detail in the related reference (Kusakabe *et al.*, 1981).

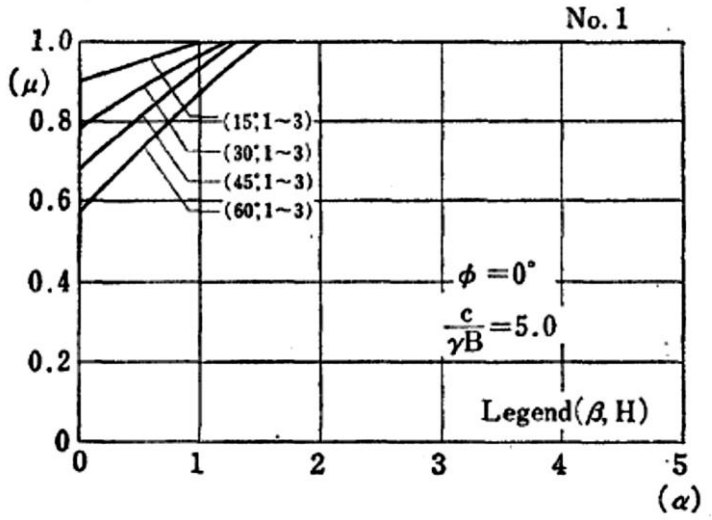


Figure 2.8. No.1 design chart presented to calculate dimensionless factor (μ) (Kusakabe *et al.*, 1981).

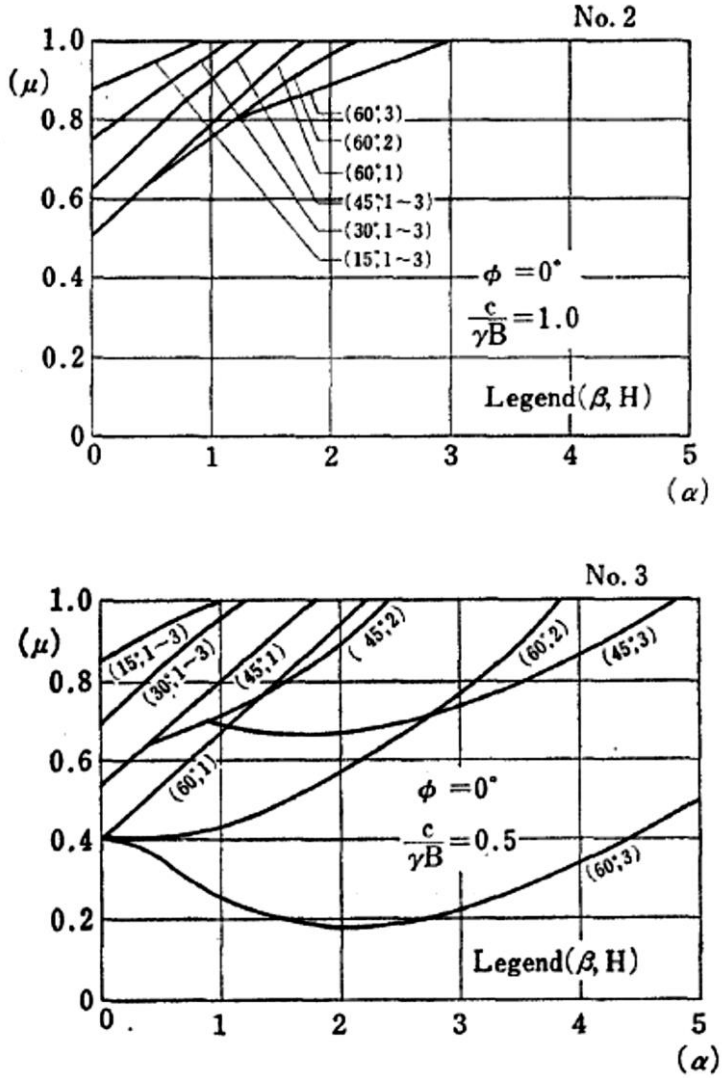


Figure 2.9. No.2 and No.3 design charts presented to calculate dimensionless factor (μ) (Kusakabe *et al.*, 1981).

Unconfined compression strengths of consolidated samples were measured in this study (Kusakabe *et al.*, 1981). While ultimate bearing capacity values obtained by using the proposed calculation technique are usually less than values determined during model tests, failure surfaces observed during the model tests were in good agreement with assumed failure surfaces. Calculated ultimate bearing capacity values using proposed theory are less than that observed in the experiments. This is mainly attributed to the influence of the side friction in the test apparatus. Additionally, variation in stress states between those established in model tests and those assumed in the proposed methodology can be considered as secondary reason.

Georgiadis (2010) used finite element method to determine all influential parameters on undrained bearing capacity of surficial strip footings located near slopes. According to this study, static ultimate bearing capacity of a surficial strip footing located near slope can be calculated by using formula given in Equation 2.9.

$$q_u = \frac{V_u}{B} = c_u N_c \tag{2.9}$$

q_u is the undrained bearing capacity of a footing located near slope; V_u is the ultimate vertical load; B is the footing width; c_u is the undrained shear strength; N_c is the undrained bearing capacity factor for sloping ground.

To define the problem, graphical representation presented by the author is shown in Figure 2.10. In this study, three different footing widths (1, 2 and 4 m) and three slope angles (15, 30 and 45) were considered. Additionally, several slope heights (H) and normalized footing distances (λ) were used to indicate influences of those variables onto ultimate bearing capacity. Slope soil material was described by elastic-perfectly plastic Mohr-Coulomb constitutive model. Accordingly, undrained total stress parameters were used. Undrained elasticity modulus (E_u), saturated unit weight (γ_{sat}) and undrained Poisson's ratio (v_u) was defined constant as 30 MPa, 20 kN/m^3 and 0.49 respectively. In order to reveal the influence of undrained shear strength (c_u) (20, 40, 100, 150, 200, 300 and 1000 kPa) onto the ultimate bearing capacity, seven different undrained shear strength were used in the analyses. Footing which has 1.0m thickness was modelled using beam element. "Rough footing" assumption was made in all analyses.

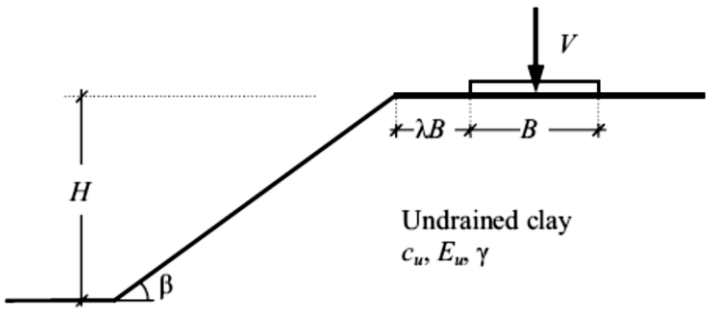


Figure 2.10. Schematic representation of the problem (Georgiadis, 2010).

The author compared the results of developed numerical model with those of calculation techniques presented by previous researchers so far. As a result of the comparisons, the author concluded that results of the proposed method obtained for certain soil and geometrical combinations shows a good agreement with those presented by the previous researchers. However, differences between results of the various calculation methods were also detected for certain cases. The fact that previous studies failed is not to consider all the influential variables was presented as the main reason of stated differences. The author determined three different failure modes shown in Figure 2.11 that might occur as a footing approaches to its ultimate capacity for all soil and geometrical combinations.

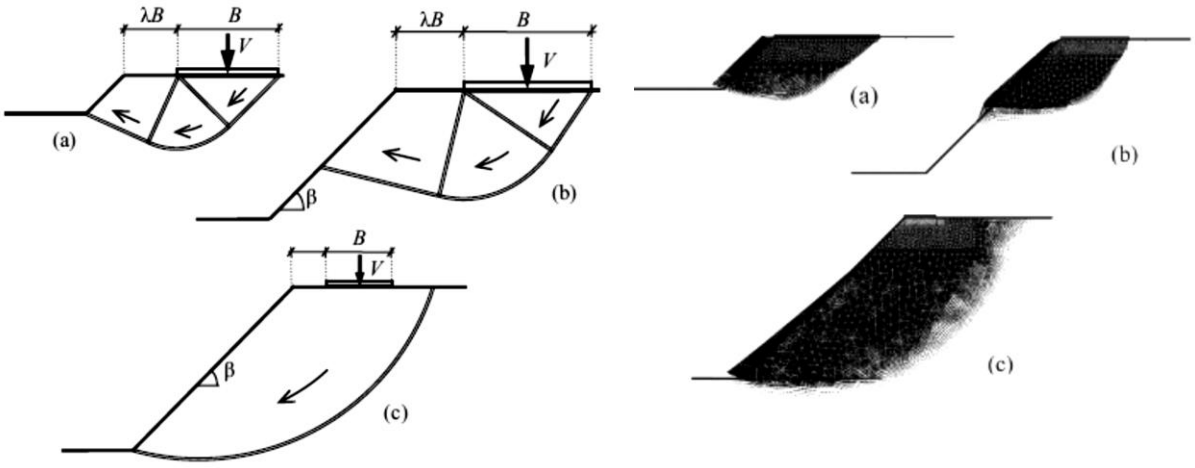


Figure 2.11. Failure modes (a) and (b) bearing capacity failure and (c) overall slope failure (Georgiadis, 2010).

The author had concluded that failure mode varies depending on the ratio of slope height to footing width (H/B). It is also shown in the diagram presented in Figure 2.12. In failure mode 1, a sudden fall from the value obtained for level ground is observed. Then, while bearing capacity coefficient (N_c) is constant for failure mode 2, calculated value for failure mode 3 diminishes to zero rapidly. While failure mode 1 and 2 are described as bearing capacity failure, failure mode 3 is described as overall slope failure. As seen in Figure 2.12, aforementioned variation is not valid for the case $c_u/\gamma B$= 0.5. Moreover, it is observed that failure mode 2 is more dominant as $c_u/\gamma B$ ratio increases.

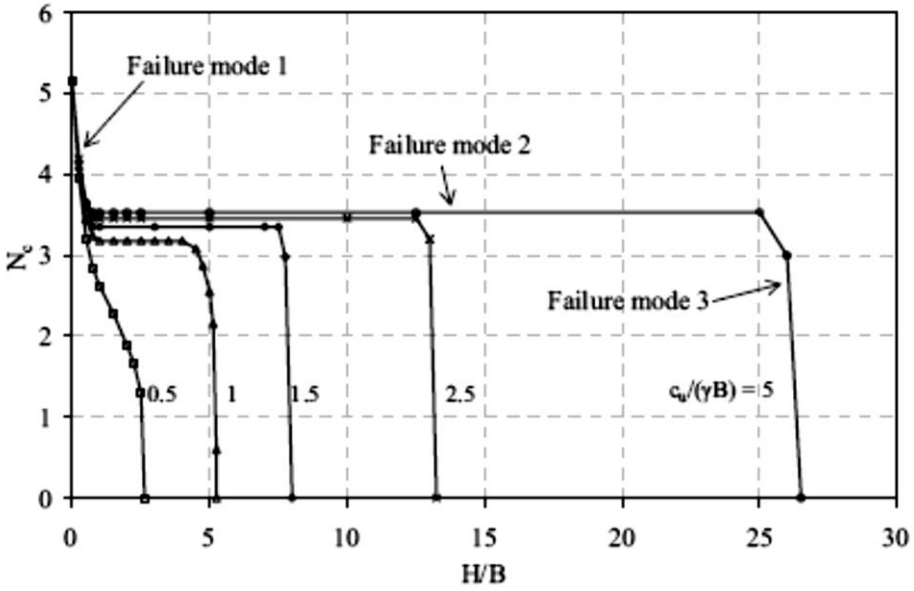


Figure 2.12. Variation of failure mode and N_c with H/B for λ= 0 and β= 45° (Georgiadis, 2010).

Variation in bearing capacity factor (N_c) with normalized λ parameter and ratio of $c_u/\gamma B$ is shown in Figure 2.13, 2.14, 2.15 and 2.16. Presented design charts are drawn for slope angles (β) of 0°, 15°, 30° and 45° and several H/B ratios.

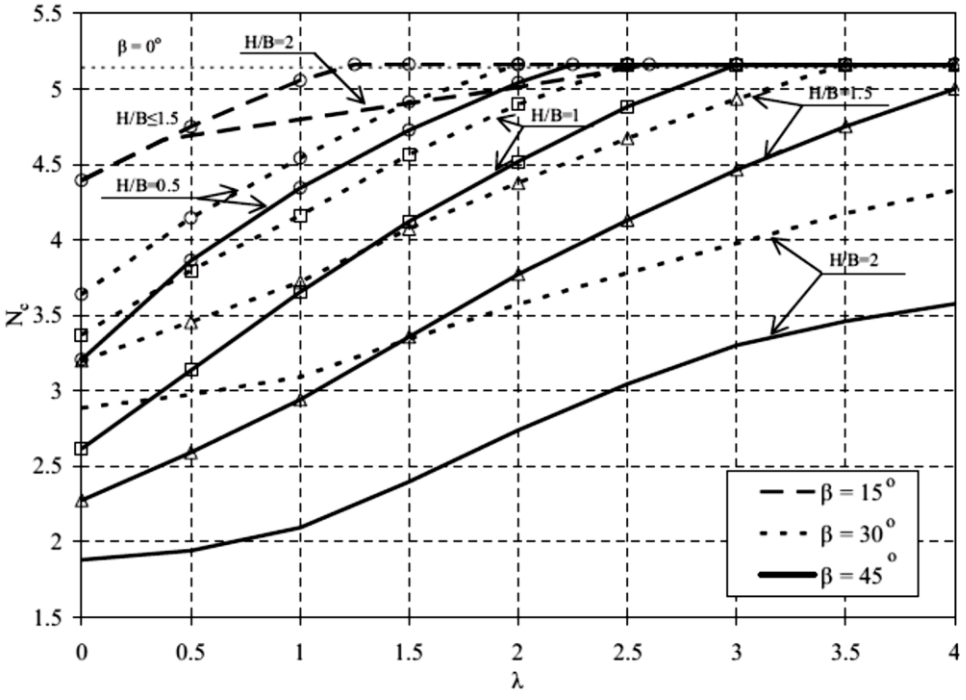


Figure 2.13. Variation of N_c with λ for $c_u/\gamma B$= 0.5 (Georgiadis, 2010).

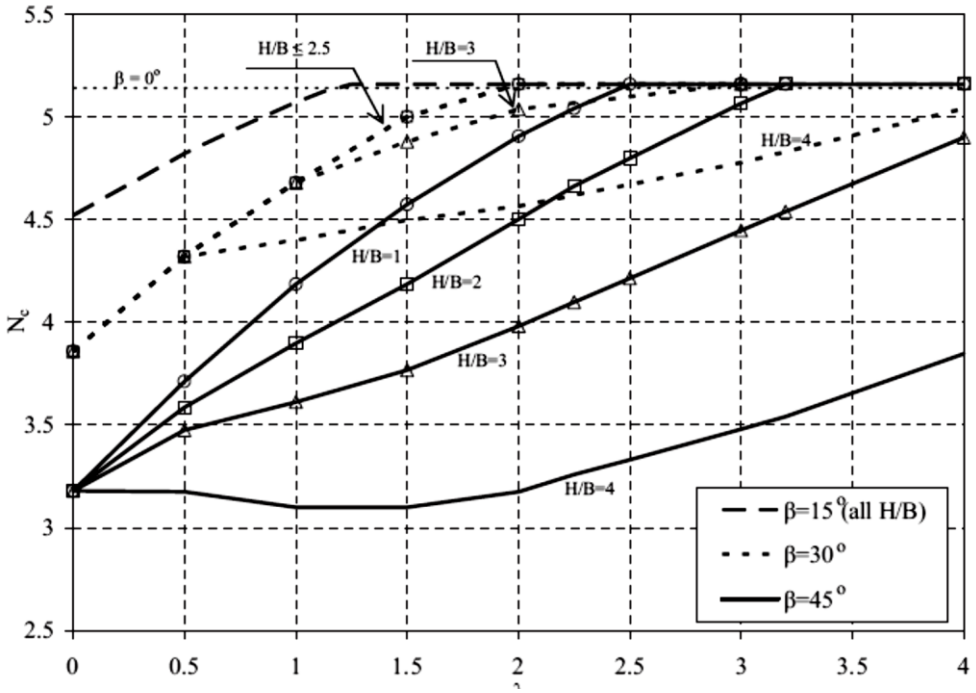


Figure 2.14. Variation of N_c with λ for $c_u/\gamma B$= 1 (Georgiadis, 2010).

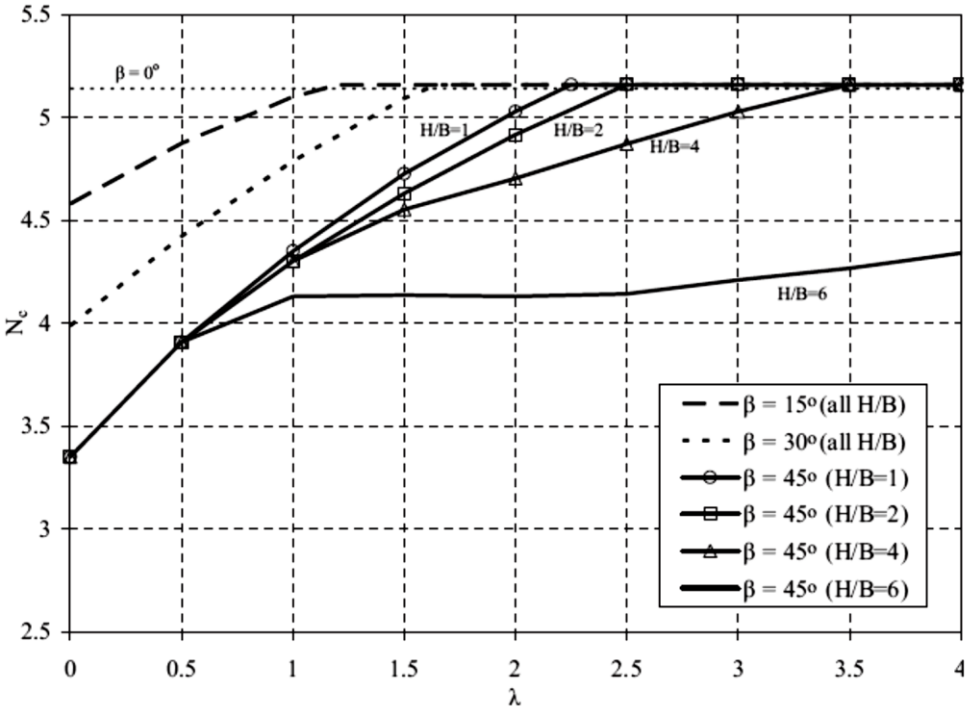


Figure 2.15. Variation of N_c with λ for $c_u/\gamma B$= 1.5 (Georgiadis, 2010).

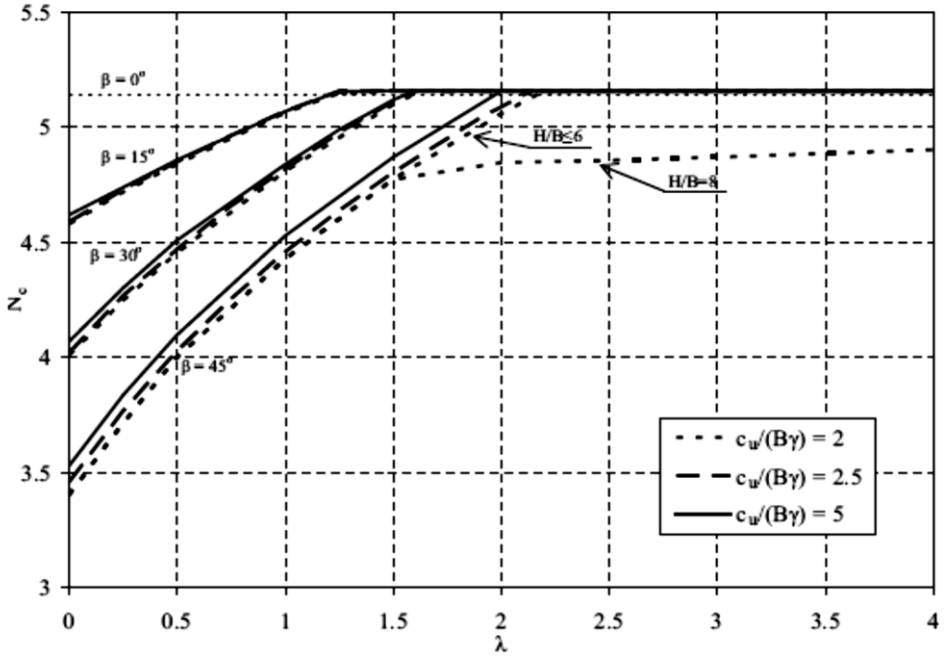


Figure 2.16. Variation of N_c with λ for $c_u/\gamma B$= 2, 2.5 and 5 (Georgiadis, 2010).

As expected, bearing capacity coefficient (N_c) increases with the increase of $c_u/\gamma B$ ratio. Since failure mode 3 is observed for lower values of $c_u/\gamma B$ ratio and greater values of λ and β, bearing capacity coefficient (N_c) is dependent on H/B ratio in general. For greater values of $c_u/\gamma B$ ratio, bearing capacity coefficient is independent of H/B ratio and failure mode 2 is observed for those cases.

Bearing capacity coefficient (N_c) increases with the increase of distance between footing and slope edge. The increase in (N_c) value continues until reaching a specific location which footing is at the critical normalized distance (λ_0) away from the slope edge where bearing capacity of footing is equal to that of footing located on level ground. Variation of critical values of normalized distance (λ_0) is presented in Figure 2.17 depending on slope angle (β) and $c_u/\gamma B$ ratio (shown for values as 2, 2.5, 3.75, 5 and 7.5). The critical value of normalized distance can be calculated by using Equation 2.10.

$$\lambda_0 = \left(\frac{5.14}{2}\right)^{\beta} \tag{2.10}$$

where β is slope angle (in radian).

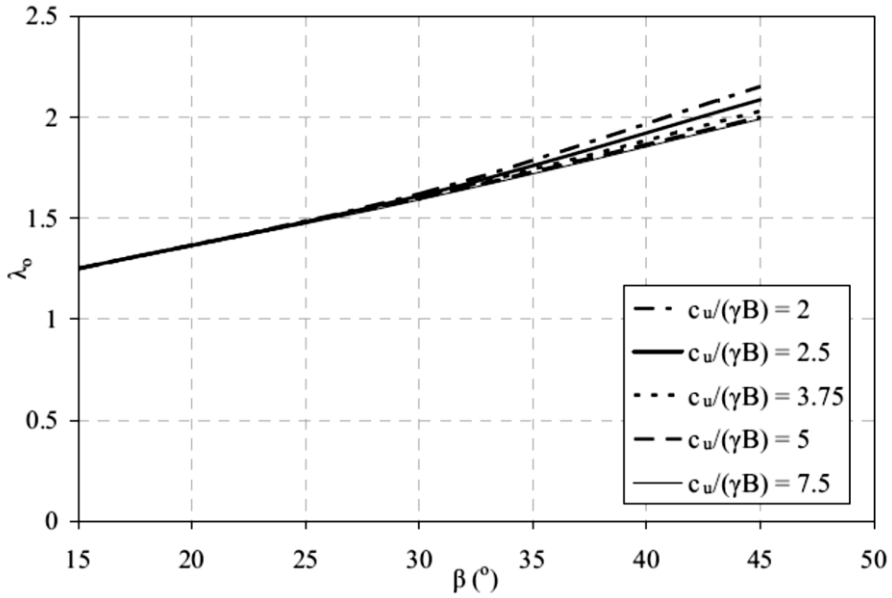


Figure 2.17. Variation of λ_o with β (Georgiadis, 2010).

As seen in Figure 2.17, slope angle (β) has decisive influence on critical value of normalized distance (λ_0) and it varies between 1.25 and 2.25 approximately.

As a result of analyses performed, the author concluded that four factors (λ, β, H/B and $c_u/\gamma B$) have decisive influences on the bearing capacity coefficient (N_c). According to the presented methodology, bearing capacity coefficient (N_c) can be calculated by using linear interpolation between values obtained from design charts given in Figure 2.13 - Figure 2.16 for all combinations of $c_u/\gamma B$ ratio and slope angle (β).

Castelli and Motta (2010) used limit equilibrium method of slices to determine bearing capacity coefficients of strip footings located near granular and cohesive slopes. In the calculation model developed within the scope of this study, circular failure surface starts propagation from footing edge then continues its relative movement until reaching sloping ground surface. Assumed failure mechanism and forces taken into account in the calculation model are shown in Figure 2.18. In the proposed method, the limit base pressure can be calculated for an arbitrary circular failure surface based on principle of moment equilibrium ($\sum M_{mobilizing} = \sum M_{resisting}$). Accordingly, failure surface for which minimum base pressure is calculated is the most critical surface among all possible circular surfaces whose centers and radii are different. Thus, the value of minimum base pressure

(q_{lim}) determined for the critical circular failure surface corresponds to the ultimate bearing capacity of shallow footing.

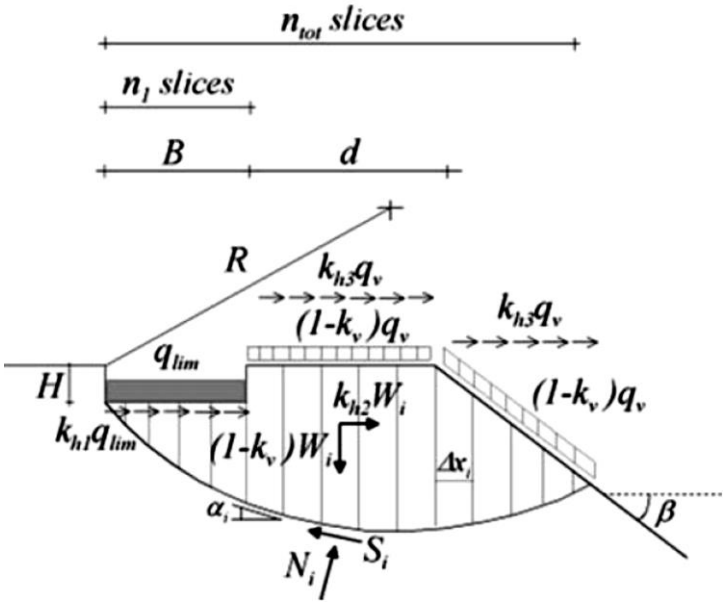


Figure 2.18. Failure mechanism and applied forces adopted in the analysis (Castelli and Motta, 2010).

In performed static analyses (for static condition $k_{h1}= k_{h2}= k_{h3}= k_v= 0$), the distance between footing and slope edge varies between 0 and 6*B* considering greater values of internal friction angle. Similarly, slope angle (β) and internal friction angle (Φ) vary in between 5° - 35° and 0° - 40° respectively.

Consequently, the ratio of bearing capacity coefficients (N_c^*/N_c) in static conditions was presented as a function of the internal friction angle (Φ), the slope angle (β), the ratio of distance between footing and slope edge to footing width (*d/B*) and depth of footing (*H*).

For undrained conditions ($\Phi= \Phi_u= 0°$), the ratio of bearing capacity coefficients (N_c^*/N_c) varies with the slope angle (β), the normalized distance between footing and slope edge (*d/B*) and normalized embedment depth of footing (*H/B*). Accordingly, the ratio of bearing capacity coefficients is calculated by using design charts given in Figure 2.19.

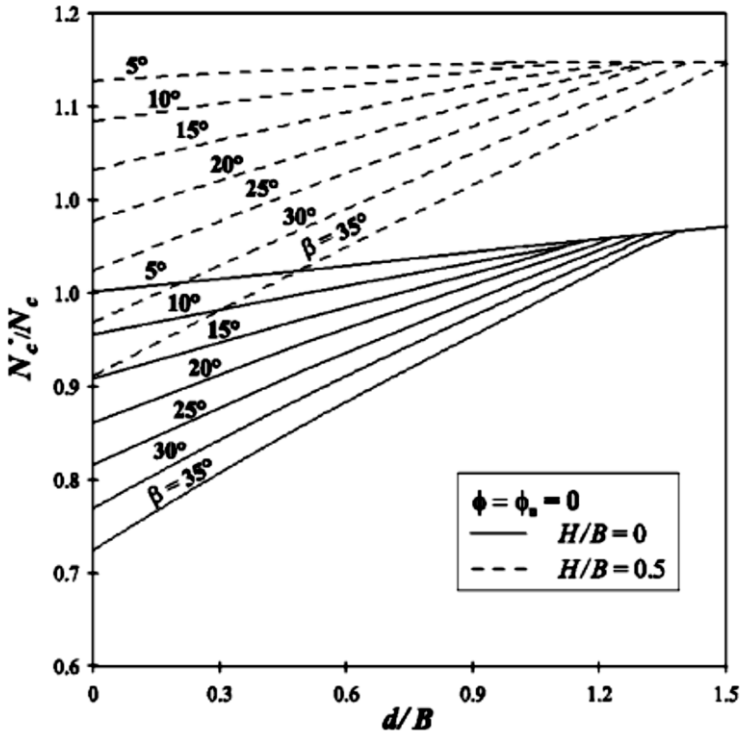


Figure 2.19. Variation of ground factors (N_c*/N_c) in static condition with the footing distance from the edge of the slope (Castelli and Motta, 2010).

When the footing is located at the top edge of slope, reduction in the bearing capacity arises at most. Additionally, it is determined that when the distance between footing and slope edge increases, the ratio of bearing capacity coefficients (N_c*/N_c) approaches to unity for the surficial strip footing. On the other hand, embedment effect increases the ultimate load capacity of footing and may result in calculation of the ratio of bearing capacity coefficients (N_c*/N_c) as greater than one which is also shown in Figure 2.19. The authors had also defined the threshold distances (denoted by d_t) from the slope edge at which reducing effect on the bearing capacity vanishes due to sloping ground. In undrained analyses, these critical distances normalized with footing width mostly vary between 1 and 1.4 depending on slope angle (β). As stated above, the embedment factor has no influence on the threshold distances (d_t). In fact, the increase in footing depth only leads to an increase in the calculated bearing capacity values.

2.2. Seismic Bearing Capacity of Footings Located near Cohesive Slopes

Research studies given in the literature of geotechnical engineering relating to the thesis subject will be referred in this chapter. As stated earlier, there is a limited number of research studies towards the determination of seismic bearing capacity of surficial footings near cohesive slopes. Essentially, only three studies (Kumar and Rao, 2003; Castelli and Motta, 2010; Farzaneh *et al.*, 2013) suggested a solution method to determine the seismic bearing capacity of such footings within the eight researches that will be referred in this chapter. On the other hand, reason for referring other five research studies is to give brief descriptions about their solution procedures and their assumptions. Following, the results obtained in each study will be summarized.

As solution tools which have been used so far are investigated, it is seen that the upper bound limit analysis (Sawada *et al.*, 1994; Askari and Farzaneh, 2003; Yamamoto, 2010) is the most preferred tool by the researchers within the existing alternatives. Besides that, another solution tool which has been frequently used is limit equilibrium method (Sarma and Chen, 1996; Castelli and Motta, 2010). Moreover, method of stress characteristics (Kumar and Rao, 2003), upper and lower bound finite element method (Shiau *et al.*, 2006; Farzaneh *et al.*, 2013) are the other alternative solution tools which were used by the researchers especially in the last decade.

Sawada *et al.* (1994) developed a solution methodology based on upper bound technique of limit analysis for the determination of seismic ultimate bearing capacity of shallow footings located near slopes. Assumed failure mechanism shown in Figure 2.20 initiates its relative movement from footing edge which is located farther from top edge of the slope then continues its rotational movement around center point “O” by following the log-spiral curve path.

In accordance with material assumptions of limit analysis, c-Φ soil is rigid-perfectly plastic material and obeys associated flow rule. Seismic effect determined by pseudo-static approach consists of a horizontal shear force acting on the footing at the footing base level and an inertia force of the sliding soil mass. The inertia force of the sliding soil mass also acts at its center of gravity. In this study, horizontal seismic acceleration coefficient (K)

which was used to calculate the inertia force of structure and of the sliding soil mass was assumed to be equal.

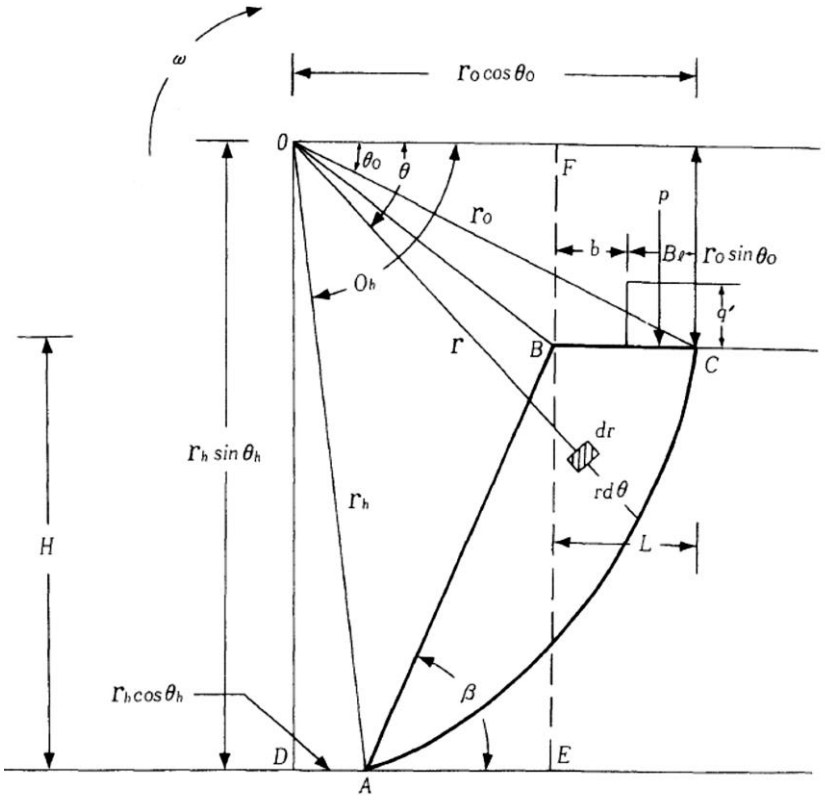


Figure 2.20. Log-spiral failure mechanism (Sawada *et al.*, 1994).

Energy balance, known as the main principle of upper bound limit analysis, enables the derivation of various equations for determining the ultimate bearing capacity of footing under both static and seismic cases. Accordingly, static ultimate bearing capacity (K= 0) of such a footing is the solution of the optimization function given in Equation 2.11.

$$p(\theta_0,\theta_h)= \frac{cf_c - \gamma r_0 (f_1 - f_2 - f_3)}{f_p} \tag{2.11}$$

On the other hand, under seismic conditions (K> 0), the objective function was rearranged in such a manner that it includes inertia terms. As the conditions given in Equation 2.13 are satisfied, objective function given in Equation 2.12 takes its minimum value. Thus, seismic ultimate bearing capacity defined herein as the minimum value of the

objective function was determined. Explanations about mathematical expressions given in Equation 2.11 and 2.12 are not covered in the thesis and mathematical expressions for objective functions are purely given for the informative purposes.

$$p(\theta_0,\theta_h)= \frac{cf_c\text{-}\gamma r_0(f_1\text{-}f_2\text{-}f_3)\text{-}K\gamma r_0(f_4\text{-}f_5\text{-}f_6)}{f_p+xKf_q} \tag{2.12}$$

$$\frac{\partial p}{\partial \theta_0}=0, \qquad \frac{\partial p}{\partial \theta_h}=0 \tag{2.13}$$

Although numerous tables had presented in this study to indicate the influence of various parameters on seismic ultimate bearing capacity, seismic ultimate bearing capacity values given in the following tables (Table 2.2 and Table 2.3) are sufficient to summarize the significant results of the study. As seen in Table 2.2, seismic ultimate bearing capacity decreases considerably with the increase of inertia forces. Additionally, as the footing approaches to the top edge of slope, seismic ultimate bearing capacity values decrease again dramatically (Table 2.3). Moreover, seismic ultimate bearing capacity increases with the increase of soil unit weight.

Table 2.2. Variation in seismic bearing capacity with earthquake acceleration factor, *K* for the case of submerged slope (β= 20°, b/B_l= 2.0, B_l= 10 m, Φ=30°, c=9.8 kPa, x=1.0) (Sawada *et al.*, 1994).

Bearing Capacity	***K***						
	0.10	0.15	0.20	0.25	0.35	0.40	0.45
***q* (kPa)**	226.93	203.68	182.60	163.67	131.61	118.27	106.60

Table 2.3. Variation in seismic bearing capacity with b/B_l ratio and γ (gf/cm^3) (K= 0.5, β= 20°, Φ= 30°, c= 9.8 kPa, B_l= 10 m, x= 1.0) (Sawada *et al.*, 1994).

***b*/*B*$_l$**	***q* (kPa)**					
	γ; 0.0	**0.5**	**1.0**	**1.5**	**2.0**	**2.5**
0.0	74.63	280.86	487.10	693.44	899.67	1106.01
1.0	93.56	351.37	609.38	867.50	1125.51	1383.63
2.0	110.82	417.09	723.37	1029.74	1336.01	1642.39
3.0	127.09	478.35	829.61	1180.87	1532.23	1883.50
4.0	142.49	536.32	930.15	1323.99	1717.82	2111.75
5.0	158.97	598.31	1037.76	1477.11	1916.56	2355.91

Sarma and Chen (1996) had derived bearing capacity factors given in Equation 2.14 for strip footings located near slopes through a solution technique developed by using limit equilibrium method. In fact, Sarma and Chen's study (1996) is the updated solution obtained by incorporating inertia forces into the existing technique developed previously by Sarma and Iossifelis (1990) for the determination of seismic bearing capacity factors of footings resting on horizontal level ground.

Assumed failure mechanism shown in Figure 2.21 consists of an active wedge, a passive wedge and a sheared transition zone between the two wedges. The sheared transition zone, defined by a log-spiral curve, initiates its own propagation from the top edge of the slope. As shown in Figure 2.21, this point also coincides with one of the footing edges. To define the soil strength, Mohr-Coulomb failure criteria was used in this study. However, excess pore water pressures generated due to cyclic loading and the static pore water pressures were not taken into account in performed analyses. Horizontal seismic acceleration coefficient (*k*) which was used to calculate the inertia force of structure and of the sliding soil mass was assumed to be equal. Additionally, the effect of seismic vertical acceleration was neglected.

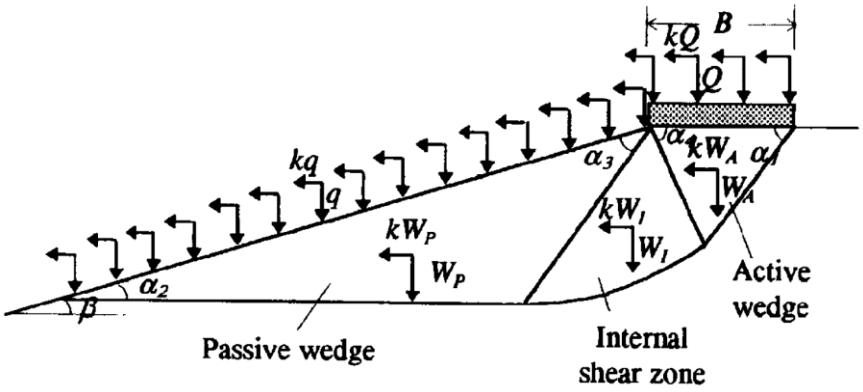


Figure 2.21. Failure mechanism and applied forces of foundation-soil system (Sarma and Chen, 1996).

In seismic case, the ultimate bearing capacity of strip footings located near slopes was expressed as a linear combination of the three bearing capacity factors shown in Equation 2.14.

$$Q = q\,N_q + c\,N_c + 0.5\,\gamma\,B\,N_\gamma \tag{2.14}$$

where Q is the ultimate bearing capacity of footing in seismic case; q is the surcharge pressure; c is the soil cohesion; γ is the unit weight of soil and B is the footing width.

Consequently, it was understood that N_c, N_q and N_γ seismic bearing capacity factors of such footings vary with the internal friction angle of soil (Φ), the seismic acceleration (kg) and the slope angle (β). Furthermore, it was concluded that seismic bearing capacity factors can be determined using various quadratic functions. For instance, seismic bearing capacity factor (N_c) can be calculated using quadratic function given in Equation 2.15 which purely depends on the slope angle (β). For the remaining two factors (N_q and N_γ), another quadratic function which depends on the tangent of slope angle ($tan\beta$) given in Equation 2.16 can be used as well.

$$log(N_c) = a\,\beta^2 + b\beta + c \tag{2.15}$$

$$log(N_\gamma \text{ or } N_q) = a\,tan^2(\beta) + b\,tan(\beta) + c \tag{2.16}$$

Constants of the each quadratic function given in the above are determined by using tables given as Table 2.4, 2.5 and 2.6. By substituting determined constants into the quadratic functions, seismic bearing capacity factors (N_γ, N_q and N_c), and hence seismic ultimate bearing capacity of strip footings can be calculated. The errors associated with using the quadratic functions are less than 4% compared to the calculated values.

Although constants of the quadratic functions are determined for the case that the footing is at the slope edge, seismic bearing capacity factors can also be calculated using the same constants through a geometrical conversion for the cases that the footing is far away from the slope edge.

Table 2.4. N_γ expressed in terms of slope angle, $log(N_\gamma) = a\ tan^2(\beta) + b\ tan(\beta) + c$, with respect to friction angle (Φ in degrees) and ground acceleration (kg) (Sarma and Chen, 1996).

k \ Φ	10	15	20	25	30	35	40	45	50
0.0	-6.492 -0.595 0.085	-3.923 -0.483 0.435	-2.479 -0.550 0.759	-1.755 0.634 1.075	-1.205 -0.780 1.402	-0.830 -0.940 1.750	-0.545 -1.130 2.130	-0.252 -1.380 2.564	-0.006 -1.680 3.068
0.1		-10.440 -0.680 0.166	-4.234 -0.740 0.535	-2.600 -0.790 0.875	-1.724 -0.894 1.212	-1.177 -1.035 1.561	-0.796 -1.210 1.940	-0.436 -1.440 2.364	-0.157 -1.720 2.853
0.2			-12.415 -0.880 0.215	-4.895 -0.930 0.614	-2.742 -1.020 0.979	-1.786 -1.130 1.342	-1.139 -1.290 1.723	-0.699 -1.500 2.141	-0.369 -1.770 2.625
0.3				-14.210 -1.060 0.262	-5.370 -1.130 0.692	-2.960 -1.230 1.087	-1.796 -1.370 1.482	-1.131 -1.570 1.907	-0.693 -1.810 2.379
0.4					-14.880 -1.240 -0.326	-5.638 -1.330 0.786	-3.030 -1.450 1.212	-1.776 -1.635 1.646	-1.138 -1.860 2.120
0.5						-15.115 -1.420 0.422	-5.544 -1.530 0.907	-3.008 -1.700 1.368	-1.789 -1.895 1.845
0.6							-13.830 -1.610 0.557	-5.331 -1.760 1.066	-2.970 -1.935 1.565
0.7								-12.394 -1.820 0.747	-5.530 -1.980 1.282
0.8	* Note: 1.The values listed above, from top to bottom, are the coefficients a, b & c respectively. 2.The coefficients are valid for $(i+\beta)<\Phi$ only, outside this region, N_γ drops to zero.								-9.560 -2.020 0.964

The authors had also developed a simplified method of which intermediate steps are given in detail in related reference (Sarma and Chen, 1996) then proved that the presence of ground water has reducing effect on the seismic bearing capacity factor (N_γ), and hence seismic ultimate bearing capacity of footings. It should also be noted that the water table is at the surface level and any water pressures due to seepage are not taken into account.

Table 2.5. N_q expressed in terms of slope angle, $log(N_q) = a\ tan^2(\beta) + b\ tan(\beta) + c$, with respect to friction angle (Φ in degrees) and ground acceleration (kg) (Sarma and Chen, 1996).

k \ Φ	10	15	20	25	30	35	40	45	50
0.0	-3.530 -0.363 0.393	-2.825 -0.328 0.594	-2.119 -0.370 0.802	-1.638 -0.431 1.020	-1.282 -0.519 1.255	-0.899 -0.677 1.513	-0.638 -0.828 1.799	-0.382 -1.030 2.125	-0.187 -1.243 2.502
0.1		-4.383 -0.586 0.486	-2.819 -0.573 0.699	-2.069 -0.595 0.918	-1.575 -0.652 1.151	-1.200 -0.742 1.402	-0.892 -0.867 1.680	-0.624 -1.027 1.994	-0.384 -1.230 2.359
0.2			-5.105 -0.802 0.559	-2.932 -0.788 0.789	-2.130 -0.788 1.025	-1.616 -0.834 1.276	-1.227 -0.924 1.549	-0.905 -1.058 1.855	-0.622 -1.239 2.208
0.3				-6.694 -0.925 0.625	-3.583 -0.910 0.876	-2.514 -0.905 1.132	-1.868 -0.957 1.404	-1.397 -1.062 1.705	-1.015 -1.223 2.048
0.4					-7.756 -1.060 0.696	-4.012 -1.049 0.970	-2.769 -1.046 1.248	-2.033 -1.110 1.549	-1.503 -1.239 1.885
0.5						-7.562 -1.259 0.781	-3.998 -1.232 1.079	-2.771 -1.235 1.385	-2.032 -1.318 1.720
0.6							-7.968 -1.359 0.889	-4.602 -1.294 1.211	-3.143 -1.335 1.550
0.7							-59.079 1.142 0.663	-12.959 -0.839 1.023	-7.959 -0.900 1.371
0.8	* Note: 1.The values listed above, from top to bottom, are the coefficients a, b & c respectively. 2.The coefficients are valid for $(i+\beta)<\Phi$ only, outside this region, N_q drops to zero.								-5.779 -1.766 -1.199

Askari and Farzaneh (2003) had developed a solution method based on upper bound technique of limit analysis for the determination of seismic ultimate bearing capacity of shallow footings located near slopes. The authors mentioned that the stated problem can be solved with a sufficient accuracy using finite elements and boundary element method with elasto-plastic constitutive models. Thus, load carrying capacity of such footings located near slopes is readily estimated. However, since aforementioned solution tools are very complicated in general and involve a lot of numerical calculations, they stated that the development of simplistic models based on limit analysis methods in such a manner that they involve inertia forces in seismic conditions is essential for practical applications. In this context, a computer program named as "TRASS" prepared by the authors for three dimensional analysis of locally loaded slopes were used to solve this two-dimensional special problem.

Table 2.6. N_c expressed in terms of slope angle, $log(N_c) = a\,\beta^2 + b\beta + c$, with respect to friction angle (Φ in degrees) and ground acceleration (kg) (Sarma and Chen, 1996).

k \ ***Φ***	**5**	**10**	**15**	**20**	**25**	**30**	**35**	**40**	**45**	**50**
0	-2.2E-05	-2.2E-05	-2.2E-05	-2.1E-05	-2.0E-05	-1.8E-05	-1.7E-05	-1.5E-05	-1.3E-05	-1.1E-05
(*β*≤90)	-3.1E-03	-3.9E-03	-4.9E-03	-6.0E-03	-7.2E-03	-8.7E-03	-1.0E-02	-1.2E-02	-1.5E-02	-1.8E-02
	0.8080	0.9173	1.0363	1.1670	1.3121	1.4749	1.6597	1.8728	2.1228	2.4227
0.1	-2.0E-05	-2.0E-05	-1.9E-05	-1.8E-05	-1.7E-05	-1.5E-05	-1.3E-05	-1.2E-05	-9.7E-06	-7.7E-06
(*β*≤80)	-3.2E-03	-4.0E-03	-5.0E-03	-6.1E-03	-7.4E-03	-8.9E-03	-1.1E-02	-1.3E-02	-1.5E-02	-1.8E-02
	0.7543	0.8598	0.9746	1.1004	1.2398	1.3959	1.5728	1.7765	2.0150	2.3006
0.2	-1.9E-05	-1.9E-05	-1.7E-05	-1.6E-05	-1.5E-05	-1.3E-05	-1.1E-05	-9.2E-06	-7.2E-06	-5.3E-06
(*β*≤75)	-3.0E-03	-3.9E-03	-4.9E-03	-6.1E-03	-7.4E-03	-8.9E-03	-1.1E-02	-1.3E-02	-1.5E-02	-1.8E-02
	0.6837	0.7869	0.8985	1.0205	1.1551	1.3053	1.4751	1.6700	1.8978	2.1699
0.3	-2.1E-05	-1.9E-05	-1.7E-05	-1.5E-05	-1.3E-05	-1.1E-05	-8.3E-06	-6.1E-06	-3.9E-06	-1.9E-06
(*β*≤70)	-2.5E-03	-3.5E-03	-4.6E-03	-5.8E-03	-7.2E-03	-8.8E-03	-1.1E-02	-1.3E-02	-1.5E-02	-1.8E-02
	0.5980	0.7002	0.8101	0.9293	1.0601	1.2055	1.3692	1.5564	1.7743	2.0339
0.4	-2.6E-05	-2.2E-05	-1.8E-05	-1.5E-05	-1.1E-05	-8.3E-06	-5.4E-06	-2.6E-06	6.7E-08	2.4E-06
(*β*≤65)	-1.5E-03	-2.7E-03	-4.0E-03	-5.4E-03	-6.9E-03	-8.5E-03	-1.0E-02	-1.3E-02	-1.5E-02	-1.8E-02
	0.4977	0.6008	0.7103	0.8282	0.9565	1.0982	1.2568	1.4373	1.6466	1.8948
0.5	-3.5E-05	-3.1E-05	-2.4E-05	-1.8E-05	-1.2E-05	-7.3E-06	-2.9E-06	1.0E-06	4.5E-06	7.4E-06
(*β*≤60)	-1.1E-04	-1.3E-03	-2.9E-03	-4.5E-03	-6.2E-03	-8.1E-03	-1.0E-02	1.2E-02	-1.5E-02	-1.8E-02
	0.3892	0.4892	0.6003	0.7183	0.8457	0.9849	1.1398	1.3148	1.5167	1.7549
0.6	-4.3E-05	-3.9E-05	-3.5E-05	-2.6E-05	-1.7E-05	-9.0E-06	-1.8E-06	4.0E-06	9.0E-06	1.3E-05
(*β*≤55)	1.2E-03	-6.5E-06	-1.4E-03	-3.2E-03	-5.2E-03	-7.3E-03	-9.5E-03	-1.2E-02	-1.5E-02	-1.8E-02
	0.2843	0.3797	0.4837	0.6011	0.7287	0.8671	1.0194	1.1904	1.3862	1.6159
0.7	-4.6E-05	-4.8E-05	-4.3E-05	-3.9E-05	-2.8E-05	-1.5E-05	-4.2E-06	5.6E-06	1.3E-05	1.9E-05
(*β*≤55)	2.1E-03	1.4E-03	3.6E-06	-1.5E-03	-3.6E-03	-6.0E-03	-8.6E-03	-1.1E-02	-1.4E-02	-1.8E-02
	0.1905	0.2724	0.3728	0.4813	0.6067	0.7455	0.8969	1.0653	1.2563	1.4790
0.8	-5.6E-05	-5.5E-05	-4.9E-05	-4.9E-05	-4.3E-05	-2.8E-05	-1.1E-05	3.7E-06	1.5E-05	2.4E-05
(*β*≤50)	3.4E-03	2.5E-03	1.1E-03	-3.9E-05	-1.8E-03	-4.4E-03	-7.3E-03	-1.0E-02	-1.4E-02	-1.7E-02
	0.0941	0.1770	0.2733	0.3703	0.4852	0.6213	0.7731	0.9403	1.1279	1.3450
0.9		-5.3E-05	-6.1E-05	-6.0E-05	-5.3E-05	-5.3E-05	-2.5E-05	-2.5E-06	1.4E-05	2.8E-05
(*β*≤45)		2.9E-03	2.6E-03	1.5E-03	-3.1E-04	-2.0E-03	-5.5E-03	-9.1E-03	-1.3E-02	-1.7E-02
		0.1025	0.1726	0.2650	0.3757	0.4942	0.6485	0.8162	1.0017	1.2146
1			-6.2E-05	-6.4E-05	-6.1E-05	-5.9E-05	-4.8E-05	-1.7E-05	8.6E-06	2.9E-05
(*β*≤45)			3.2E-03	2.4E-03	9.7E-04	-6.7E-04	-3.2E-03	-7.3E-03	-1.1E-02	-1.6E-02
			0.0950	0.1762	0.2755	0.3869	0.5240	0.6920	0.8776	1.0876
1.1				-7.4E-05	-6.9E-05	-7.5E-05	-7.2E-05	-4.2E-05	-3.1E-06	2.6E-05
(*β*≤40)				3.7E-03	2.2E-03	1.1E-03	-9.8E-04	-4.9E-03	-9.7E-03	-1.5E-02
				0.0888	0.1842	0.2821	0.4068	0.5689	0.7557	0.9646
1.2						-9.0E-05	-8.2E-05	-6.6E-05	-2.6E-05	1.9E-05
(*β*≤35)						2.6E-03	3.7E-04	-2.8E-03	-7.5E-03	-1.3E-02
						0.1883	0.3095	0.4552	0.6358	0.8453
1.3						-8.9E-05	-8.5E-05	-8.1E-05	-6.0E-05	1.7E-06
(*β*≤35)						3.2E-03	1.3E-03	-1.0E-03	-4.9E-03	-1.1E-02
						0.1137	0.2237	0.3527	0.5174	0.7282
1.4							-9.3E-05	-1.1E-04	-7.9E-05	-2.3E-05
(*β*≤35)							2.5E-03	1.3E-03	-2.9E-03	-8.9E-03
							0.1422	0.2500	0.4127	0.6142
1.5								-1.3E-04	-9.9E-05	-6.6E-05
(*β*≤30)								3.2E-03	-1.1E-03	-6.1E-03
								0.1615	0.3178	0.5033

* Note:

1.The values listed above, from top to bottom, are the coefficients *a*, *b* & *c* respectively.

2.β and Φ are in degrees.

Assumed failure mechanism shown in Figure 2.22 consists of an active wedge, a passive wedge and a shear transition zone between the two wedges. The radial shear zone is composed of a sequence of n rigid triangles. In accordance with material assumptions of limit analysis, *c*-*Φ* soil is rigid-perfectly plastic material and obeys associated flow rule. Seismic effect determined by pseudo-static approach consists of a horizontal shear force acting on the footing as well as the inertia force of the sliding soil mass. While seismic coefficients used for calculating the inertia force of the structure and of the sliding soil mass (denoted as K_{cl} and K_{ce} respectively) are assumed to be equal (K_{cl}= K_{ce}= K_c), the effect of vertical acceleration on seismic bearing capacity is neglected.

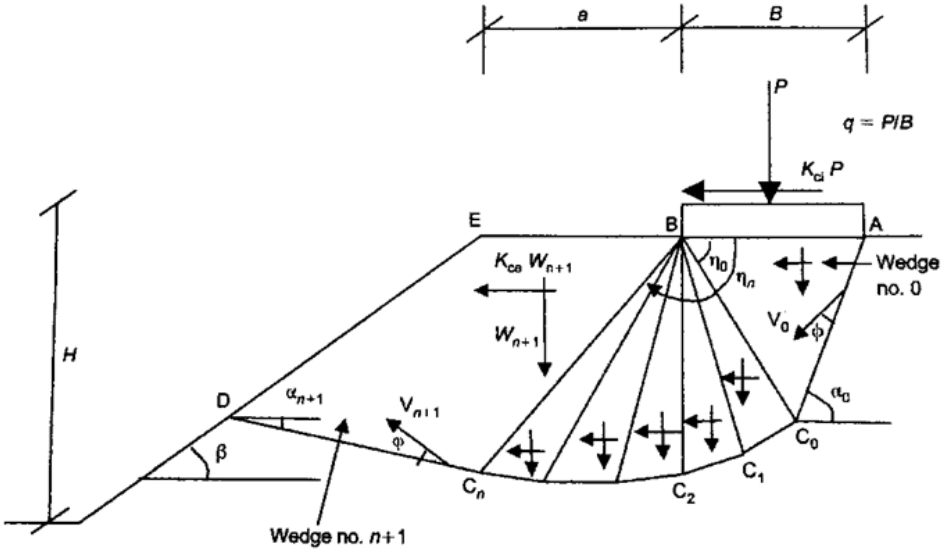


Figure 2.22. Failure mechanism used in the analysis (Askari and Farzaneh, 2003).

Limit load by upper bound limit analysis is obtained by equating the work rate of external forces (denoted as *E*) to the rate of energy dissipation (denoted as *I*) within the *c*-*Φ* soil. Accordingly, equations used for the calculation of "*E*" and "*I*" are given in Equation 2.17 and Equation 2.18 respectively.

$$E = P\,V_{0V} + K_{cl}\,P\,V_{0H} + \gamma \sum_{k=0}^{n+1} S_k\,V_{kV} + \gamma \sum_{k=0}^{n+1} K_{ce} S_k\,V_{kH} \tag{2.17}$$

where *P* is the limit load; K_{cl}= K_{ce}= K_c is the seismic coefficient; V_{0H} and V_{0V} are the magnitudes of the horizontal and vertical components of foundation velocity respectively;

V_{kH} and V_{kV} are the magnitudes of the horizontal and vertical components of block k velocity (k= 0 to n+1) respectively; S_k is of the kth block.

$$I = c\,cos\emptyset \sum_{k=0}^{n+1} L_k V_k + c\,cos\emptyset \sum_{k=0}^{n} L_k^{'} V_k^{'} \tag{2.18}$$

where c is the cohesion; Φ is the internal friction angle; L_k is the length of the velocity discontinuity in the base of the kth wedge; L'_k is the length of velocity discontinuity between wedges k and k+1; V_k is the velocity of wedge k; V'_k is the relative velocity between blocks k and k+1.

The objective of this method is to find the lowest upper bound load by using E= I principle and corresponding set of α_k & η_k parameter defining the geometry of failure mechanism. Therefore, a numerical approach had been developed and was used for the determination of aforementioned geometrical parameters in this study. However, the numerical approach will not be described herein and the intermediate steps of the numerical approach can be found in detail in the reference (Askari and Farzaneh, 2003).

Verification of suggested solutions was made by the authors in both static and seismic condition comparing the analysis results with those obtained previously in several researches. As a result, it is determined that seismic bearing capacity values obtained by presented method is less than those given in several researches in general and provides a better upper bound for the problem at hand. Furthermore, normalized seismic limit pressure was calculated depending on a/B ratio, $\gamma B/c$ ratio, internal friction angle (Φ), seismic acceleration coefficient (K_c) and slope angle (β). Calculated normalized seismic limit pressures are given in Table 2.6. As the normalized limit pressure values given in Table 2.7 are examined, it is seen that while normalized limit pressure increases with the increase of a/B ratio and internal friction angle (Φ), it decreases with increase of the seismic coefficient (K_c) and slope angle (β).

Table 2.7. Normalized seismic limit pressure (q/c) for $\gamma b/c$= 0.25, 0.5, 1 and 2, Φ= 15°, 30° and 45°, $K_{cl}= K_{ce}= K_c$= 0.15 and 0.3 and β= 15°, 30° and 45° (Askari and Farzaneh, 2003)

***a/B* = 0**						***a/B* = 0.5**					
K	***Φ*: degrees**	***γB/c***	***β*: degrees**			***K***	***Φ*: degrees**	***γB/c***	***β*: degrees**		
			15	**30**	**45**				**15**	**30**	**45**
0.15	15	0.25	7.28	5.87	4.66	0.15	15	0.25	7.83	6.73	5.68
		0.50	7.32	5.82	4.55			0.50	7.93	6.73	5.55
		1.00	7.39	5.71	-			1.00	8.11	6.70	-
		2.00	7.52	-	-			2.00	8.44	-	-
	30	0.25	17.30	12.05	8.35		30	0.25	18.56	13.77	10.13
		0.50	18.04	12.24	8.26			0.50	19.55	14.18	10.11
		1.00	19.44	12.57	8.04			1.00	21.46	14.94	9.94
		2.00	22.08	13.15	7.40			2.00	25.06	16.24	-
	45	0.25	63.95	34.56	18.96		45	0.25	68.34	39.06	22.71
		0.50	72.35	37.04	19.32			0.50	78.35	42.77	23.57
		1.00	88.35	41.75	19.93			1.00	97.49	49.83	25.05
		2.00	118.90	50.60	20.85			2.00	134.30	63.15	27.17
0.30	15	0.25	5.44	4.48	3.62	0.30	15	0.25	5.96	5.28	4.55
		0.50	5.42	4.41	3.52			0.50	5.96	5.22	4.41
		1.00	5.38	-	-			1.00	5.97	-	-
		2.00	-	-	-			2.00	-	-	-
	30	0.25	12.08	8.57	6.05		30	0.25	13.13	10.02	7.57
		0.50	12.33	8.56	5.92			0.50	13.52	10.12	7.42
		1.00	12.81	8.53	5.62			1.00	14.28	10.27	6.99
		2.00	13.68	-	-			2.00	15.68	-	-
	45	0.25	39.38	21.80	12.26		45	0.25	42.38	25.08	15.10
		0.50	42.87	22.58	12.18			0.50	46.76	26.48	15.17
		1.00	49.32	24.06	11.97			1.00	54.87	29.07	15.10
		2.00	62.00	26.72	-			2.00	70.68	33.73	-

Kumar and Rao (2003) had used the method of stress characteristics for the determination of seismic bearing capacity of footings placed horizontally on semi-infinite slopes. As seen in Figure 2.23 and Figure 2.24, this study is quite different from other researches given in Chapter 2.2 because of the "semi-infinite slope" assumption. However, the main reason of referring to this study in Chapter 2.2 is that it is one of the rare studies that describes the variation of undrained N_c bearing capacity factor (Φ_u= 0°) with respect to the seismic acceleration coefficient (α_h) and the slope angle (β). Furthermore, due to the assumption mentioned in above, solutions presented in this study would be taken into account for the purposes of comparison to be given in the subsequent chapter of the thesis only for the special case that the footing is at the slope edge (λ= 0).

Two failure mechanisms shown in Figure 2.23 and Figure 2.24 were taken into account in this study. The variation in seismic bearing capacity coefficients was

investigated with respect to the internal friction angle (Φ), the horizontal seismic acceleration coefficient (α_h) and the slope angle (β) using failure mechanisms named as single side and both sides. While slope soil material obeys Mohr-Coulomb failure criterion, internal friction angle (Φ) used in analyses varies in between 0° and 50°. The influence of slope angle (β) on seismic bearing capacity factors was also investigated using various slope angles.

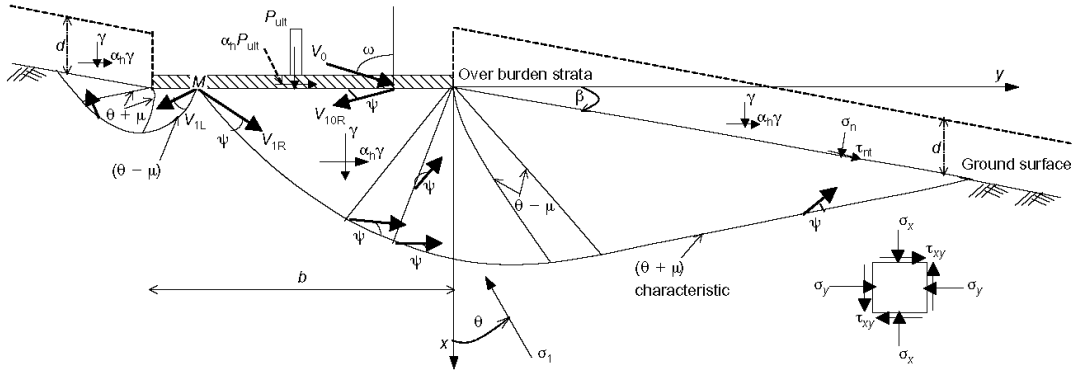


Figure 2.23. Both sides failure mechanism used in the analysis (Kumar and Rao, 2003).

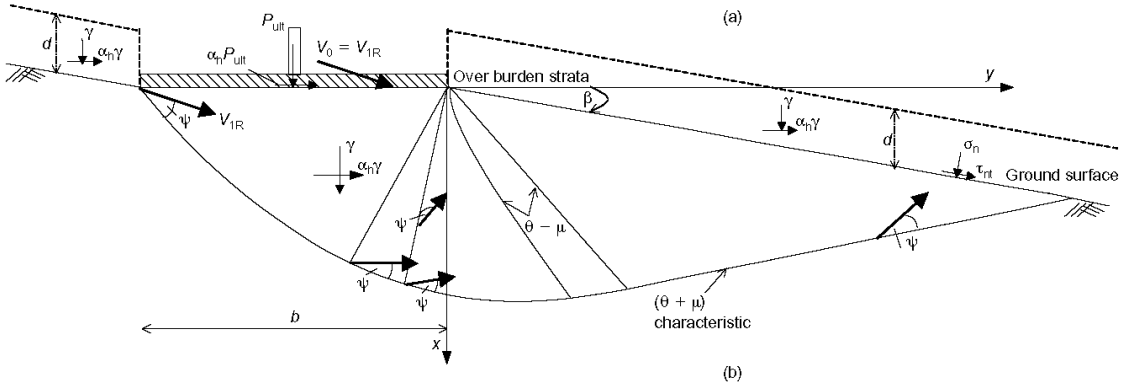


Figure 2.24. Single side failure mechanism used in the analysis (Kumar and Rao, 2003).

Consequently, for smaller values of the seismic acceleration coefficient (α_h) and the slope angle (β), values of N_γ bearing capacity factor determined by using both sides failure mechanism are less than those determined by using single side failure mechanism. However, both sides failure mechanism is no longer kinematically inadmissible for many situations in which the internal friction angle takes greater values. On the contrary, for the

other bearing capacity factors (N_c and N_q), it is determined that single side failure mechanism is only statically admissible.

In this study, it is expressed that the seismic ultimate bearing capacity of footings on slopes can be calculated using the well-known equation presented by Terzaghi (1943). Accordingly, bearing capacity factors shown in the mentioned equation will be determined by design charts shown in Figure 2.25, Figure 2.26 and Figure 2.27 for the cases in which $\alpha_h \geq 0$ and $\beta \geq 0$. Since two different failure mechanisms were taken into account separately for the assessment of N_γ bearing capacity factor, two different curves were drawn in the presented design graphs to represent the variation of N_γ factor corresponding to each failure mechanism considered. As stated in the above paragraph, it is also seen from the presented design graphs that both sides failure mechanism gives more conservative results for smaller values of the seismic acceleration coefficient (α_h) and the slope angle (β). The authors concluded that all bearing capacity factors decreases considerably with the increase of seismic acceleration coefficient (α_h). Moreover, it is stated that any increment in slope angle results in decrease in the values of seismic bearing capacity factors.

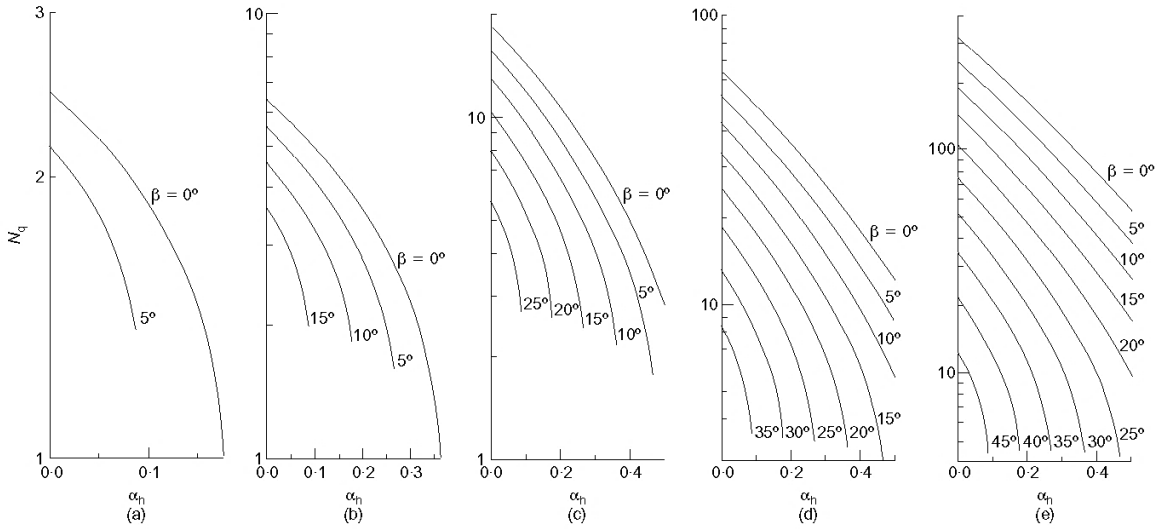


Figure 2.25. Variation of N_q with α_h for different values of Φ and β: (a) Φ= 10°; (b) Φ= 20°; (c) Φ= 30°; (d) Φ= 40°; (e) Φ= 50° (Kumar and Rao, 2003).

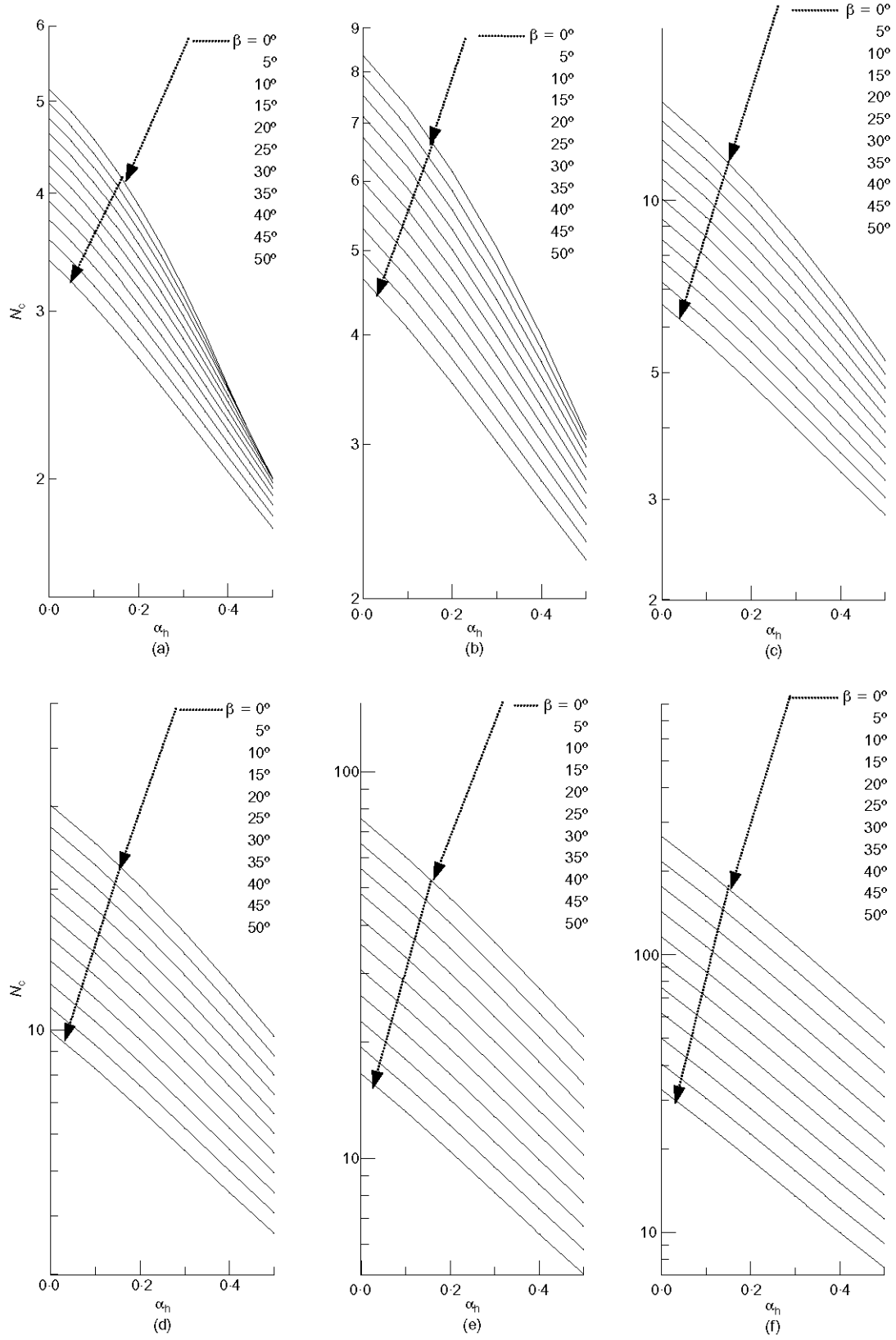


Figure 2.26. Variation of N_c with α_h for different values of Φ and β: (a) Φ= 0°; (b) Φ= 10°; (c) Φ= 20°; (d) Φ= 30°; (e) Φ= 40°; (f) Φ= 50° (Kumar and Rao, 2003).

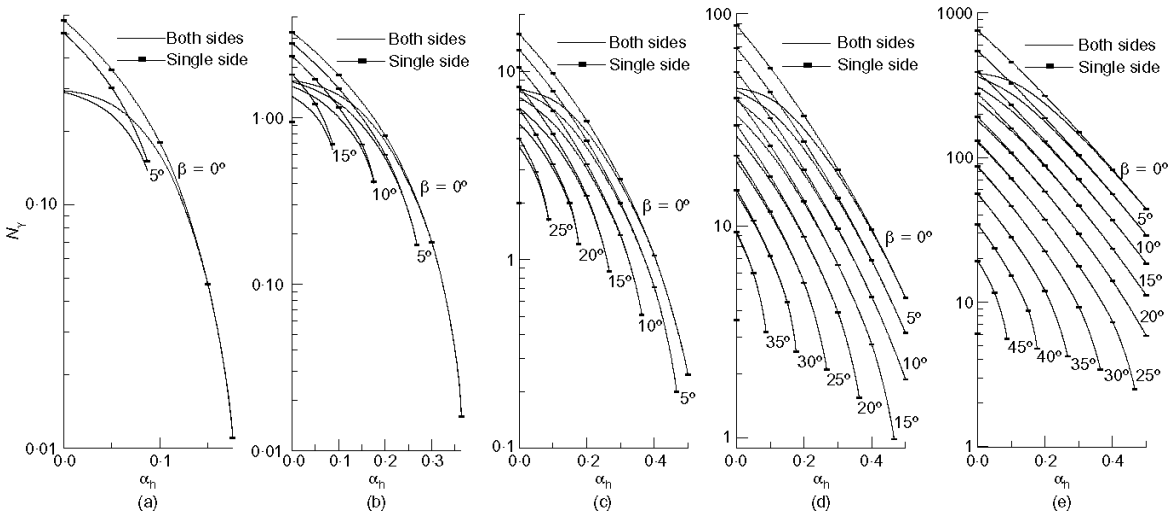


Figure 2.27. Variation of N_γ with α_h for different values of Φ and β: (a) Φ= 10°; (b) Φ= 20°; (c) Φ= 30°; (d) Φ= 40°; (e) Φ= 50° (Kumar and Rao, 2003)

Shiau *et al.* (2006) stated that the limit equilibrium method and upper bound limit analysis in conjunction with pseudo-static approach used for the stability analysis of geotechnical structures have own limitations in general. These limitations were described as being the need to define the overall shape of the failure surface in advance for the limit equilibrium method and giving greater results than exact limit loads and thus being non-conservative for the upper bound limit analysis. Therefore, the authors expressed that upper and lower bound finite element methods are more attractive solution tools comparing to the aforementioned methods in the above. Briefly, these methods enable to bound the exact limit load from above and below and hence give a reliable load interval to the design engineers for the exact limit load. Accordingly, the main goal of this study was to incorporate the pseudo-static approach into the numerical methods developed previously at the University of Newcastle based on the upper and lower bound finite element methods. To verify the results of updated numerical methods, "determination of seismic bearing capacity of rigid footings on homogenous slopes" was one of the benchmark exercises chosen in this context.

Graphical representation of the problem is presented in Figure 2.28. Homogenous slope material obeys the Mohr-Coulomb failure criterion with shear strength parameters cohesion (c) and internal friction angle (Φ). It is also assumed that the shear strength of

slope material does not vary with time and is not affected by complex, transient and dynamic earthquake loading. Moreover, the influence of pore water pressure is not taken into account. On the other hand, as shown in Figure 2.28, the horizontal and vertical acceleration coefficient had been chosen to be equal for slope, structure and surcharge load. Additionally, it is assumed that the inertia force of the structure acts at the base level of the footing and the overturning moment due to the inertia of the structure is neglected.

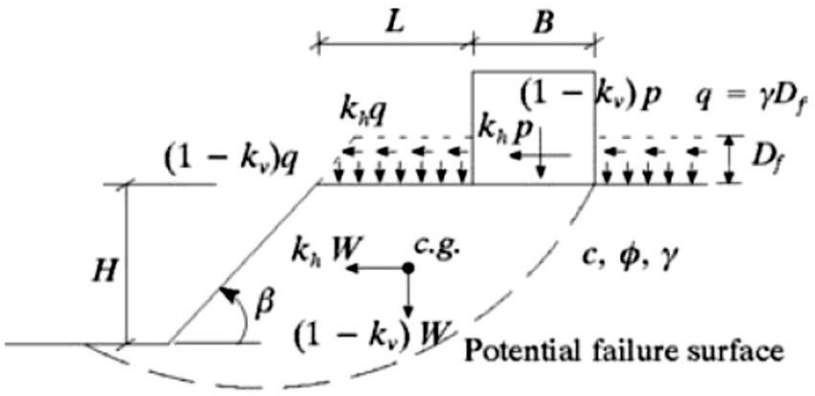


Figure 2.28. Graphical representation of the problem (Shiau *et al.*, 2006).

According to this study, normalized seismic bearing capacity of rigid footings located near slopes can be expressed as a function of independent variables given in Equation 2.19.

$$\frac{p}{\gamma B}=f\left(\beta,\ \frac{L}{B},\ \frac{c}{\gamma B},\ \frac{q}{\gamma B},\ \Phi,\ tan\theta\right) \tag{2.19}$$

where p is the average limit pressure under the footing, γ is the soil unit weight, B is the footing width, β is the slope angle, L is the distance from the edge of the slope to the footing edge, c is the cohesion, q is the surcharge load, Φ is the internal friction angle of slope soil and $tan\theta= k_h/(1-k_v)$.

As a result of made assessments, it is concluded that the issues given in the following have great importance. Accordingly;

Seismic bearing capacity of such footings decreases with the increase of earthquake inertia forces (with the increase of *tanθ* value). The zone, named as range of true solutions (shaded area in Figure 2.29), enclosed with upper and lower bound curve obtained by numerical methods which correct limit load falls into is determined. As shown in Figure 2.29, lower and upper bound curves approaches to each other with the increase of *tanθ* value and hence the accuracy of bounding solutions increases.

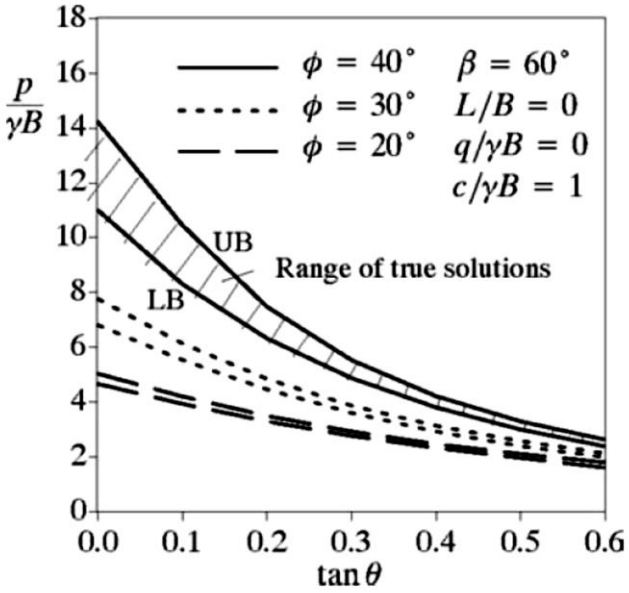


Figure 2.29. Effect of *tanθ* on *p/γB* for various *Φ* (Shiau *et al.*, 2006).

Upper bound velocity diagrams and normalized seismic bearing capacity values determined for different values of *tanθ* are shown in Figure 2.30. Deformed area and the proportion of the velocity field diminish with the increase of horizontal inertia force.

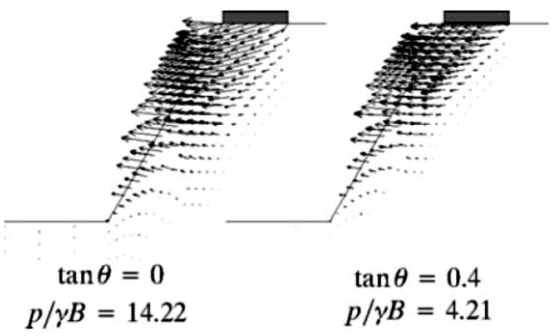


Figure 2.30. Comparison of upper bound velocity diagrams for the effect of inertia forces (Shiau *et al.*, 2006).

Presence of surcharge load on slopes may either decrease, increase or has no effect on the seismic bearing capacity of footings depending on β, L/B and $q/\gamma B$ parameters. As shown in the graph given Figure 2.31, reduction in seismic bearing capacity is only valid for the case of vertical slope. The influence of surcharge load on the seismic bearing capacity is considerably small for the smaller slope angles. Therefore even if $q/\gamma B$ ratio increases, $p/\gamma B$ ratio is constant.

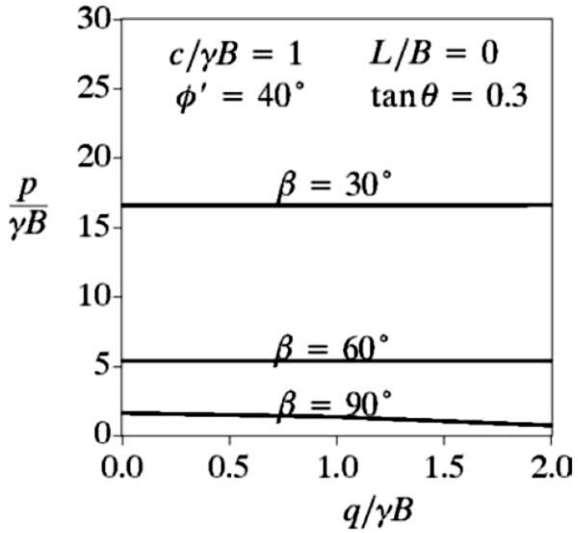


Figure 2.31. Effect of $q/\gamma B$ on $p/\gamma B$ for various β (Shiau *et al.*, 2006).

As the inertia force of slope is neglected, it is concluded that the seismic bearing capacity values obtained are not on the safe side anymore for all values of the slope angle. This result can easily be seen in Figure 2.32.

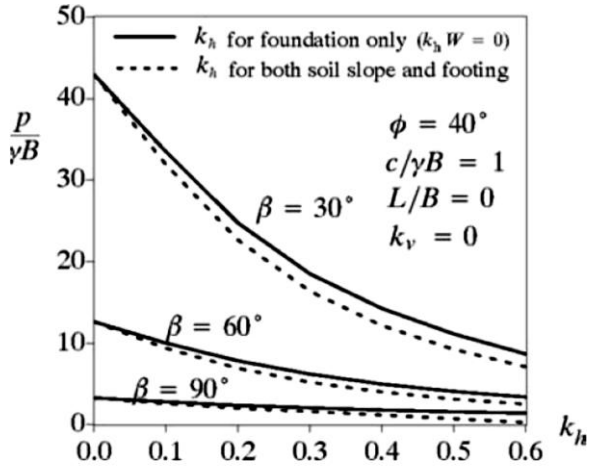


Figure 2.32. Effect of soil inertia k_h on $p/\gamma B$ (Shiau *et al.*, 2006).

The authors had reported that numerical upper and lower bounds mostly bracket the true solution within %10 or better. Based on the associated flow rule, it is expected that solutions based on any available method should yield results that are located between upper and lower bounds.

Yamamoto (2010) had expressed that it is obligatory to build structural foundations located on or near slopes for many cases in Japan. Additionally, he reported that although the damage of buildings was not considerably severe, it was much observed that the bearing stratum underneath the buildings had collapsed and sunk in the following earthquakes occurred in Japan in the last decade. Therefore, the author concluded that the evaluation of seismic bearing capacity in the design of such footings is of great importance and should be taken into account besides the allowable bearing capacity of such footings in static condition.

In this study, a solution method based on the upper bound theorem of limit analysis was developed for the determination of seismic bearing capacity of such footings located near slopes. Non-symmetrical failure mechanism shown in Figure 2.33 consists of triangular active wedge, log-spiral shear zone and passive wedge. Essentially, the author stated that the seismic bearing capacity equations can be derived using only two angular parameters (the variables denoted as ξ and η in Figure 2.33) without the need of a complex model. Moreover, the author particularly emphasized that the developed model can be used for the practical applications of geotechnical engineering.

In accordance with material assumptions of limit analysis, c-Φ soil is rigid-perfectly plastic material and obeys associated flow rule. Seismic effect determined by pseudo-static approach consists of a horizontal shear force acting on the footing at the base level of footing and an inertia force of the sliding soil mass. In this study, horizontal seismic acceleration coefficient (K_h) was assumed to be equal to calculate inertia force of structure acting on the footing and of the sliding soil mass. The effect of vertical acceleration onto the seismic bearing capacity was neglected.

Shear transfer coefficient (*f*) was also introduced to consider variable shear force transfer at the base level of footing due to inertia force of the structure. The effect of embedment onto the seismic bearing capacity was investigated as well.

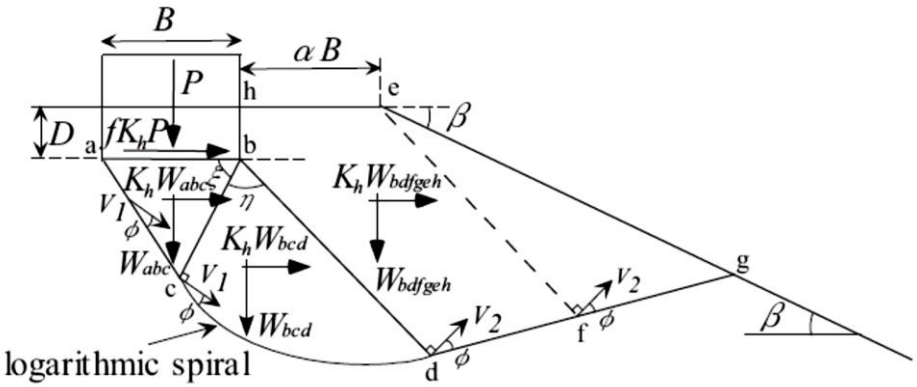


Figure 2.33. Failure mechanism used in the analysis (Yamamoto, 2010).

Through the solution of energy balance equation that establishes a basis of upper bound limit analysis, the upper limit of seismic bearing capacity is obtained by the formula given in Equation 2.20.

$$q_b = cN_{ce} + \frac{1}{2}\gamma B N_{\gamma e} \tag{2.20}$$

where c is the cohesion, B is the footing width, γ is the unit weight of the soil, N_{ce} and $N_{\gamma e}$ are the seismic bearing capacity factor.

N_{ce} and $N_{\gamma e}$ seismic bearing capacity factors given in Equation 2.20 are calculated by the equations given in Equation 2.21 and Equation 2.22 respectively.

$$N_{ce} = \frac{1}{\cos\xi + f K_h \sin\xi}\left(f_7 + f_8 + 2f_9\right) \tag{2.21}$$

$$N_{\gamma e} = \frac{1}{\cos\xi + f K_h \sin\xi}\left(f_1 + f_3 + f_5\right) + K_h\left(f_2 + f_4 + f_6\right) \tag{2.22}$$

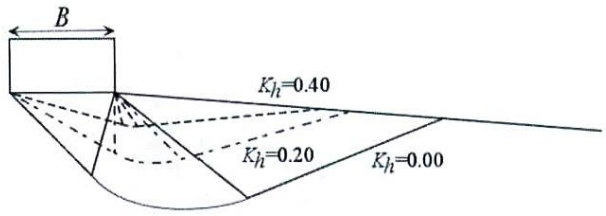
where ξ is the angle which defines the geometry of active wedge beneath the footing, f is the shear transfer coefficient, K_h is the horizontal seismic coefficient and f_i (i= 1 to 9) are the functions of which independent variables are ξ, η, β, αB, D/B and Φ. Since seismic bearing capacity factors obtained in this study are represented by design charts, the expanded forms of f_i function (i= 1 to 9) will not be given in detail. Related formulas can also be found in the reference (Yamamoto, 2010).

In order to take the minimum value of two factors (N_{ce} and $N_{\gamma e}$) independently of each other, all possible combinations of ξ and η variables satisfying a kinematically admissible velocity field were taken into account in this study. Thus, the use of superposition principle is in fact on the safe side.

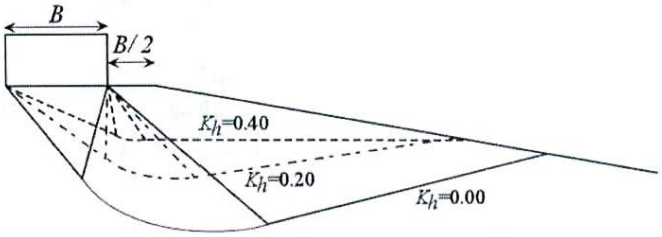
Results of developed method were compared with those presented by previous researchers then the accuracy of the method was verified for several cases. Outcomes of parametric study performed by using this method are summarized in the following:

- Seismic bearing capacity decreases with the increase of shear transfer coefficient (f).
- Seismic bearing capacity factors increase with the increase of D/B ratio and of the distance αB.
- Seismic bearing capacity factors decrease with the increase of K_h and of β.
- As shown in Figure 2.34, as K_h increases, the angle of active wedge increases and the angle of log-spiral zone decreases. Additionally, overall dimensions of failure mechanism become smaller with the increase of K_h.

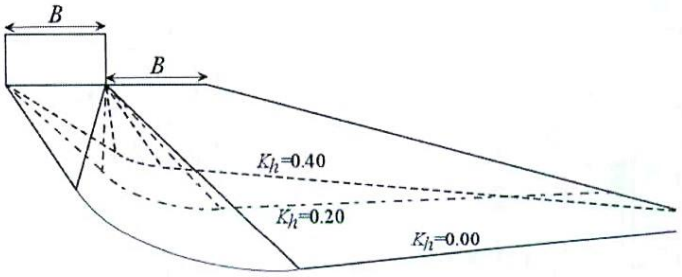
Design charts for the bearing capacity factor obtained N_{ce} and $N_{\gamma e}$ with K_h for different values of β are shown in Figure 2.35 to 2.40 (Φ= 30, 40, D/B= 0.0 and 1.0, α= 0.0 and 0.5).



(a) ϕ=30°, β=5°, α=0.0, K_h=0.00, 0.20 and 0.40.



(b) ϕ=35°, β=10°, α=0.5, K_h=0.00, 0.20 and 0.40.



(c) ϕ=40°, β=15°, α=1.0, K_h=0.00, 0.20 and 0.40.

Figure 2.34. Failure mechanisms for different values of Φ, β, α and K_h (Yamamoto, 2010).

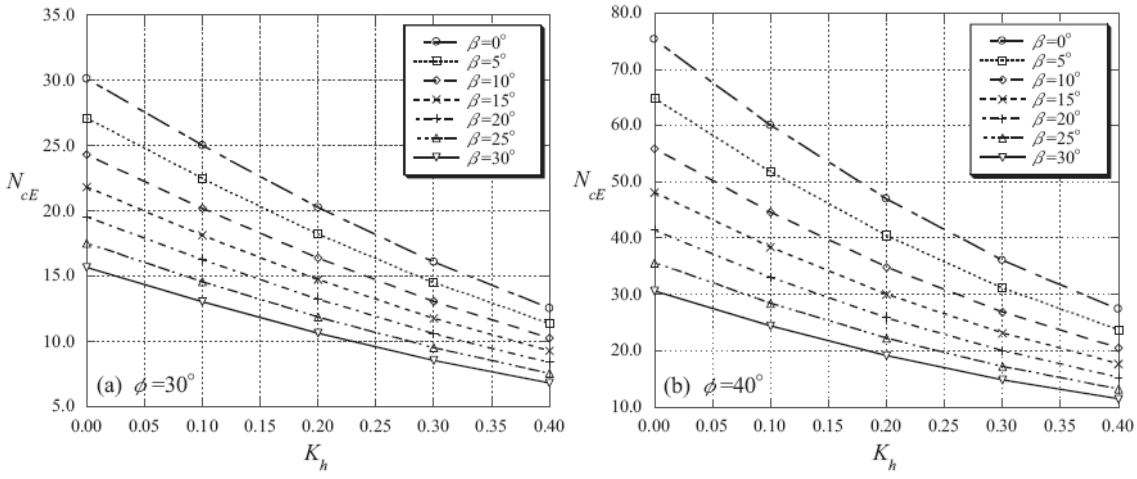


Figure 2.35. Design charts for N_{ce} (Φ= 30°, 40°, D/B= 0, a= 0.0) (Yamamoto, 2010).

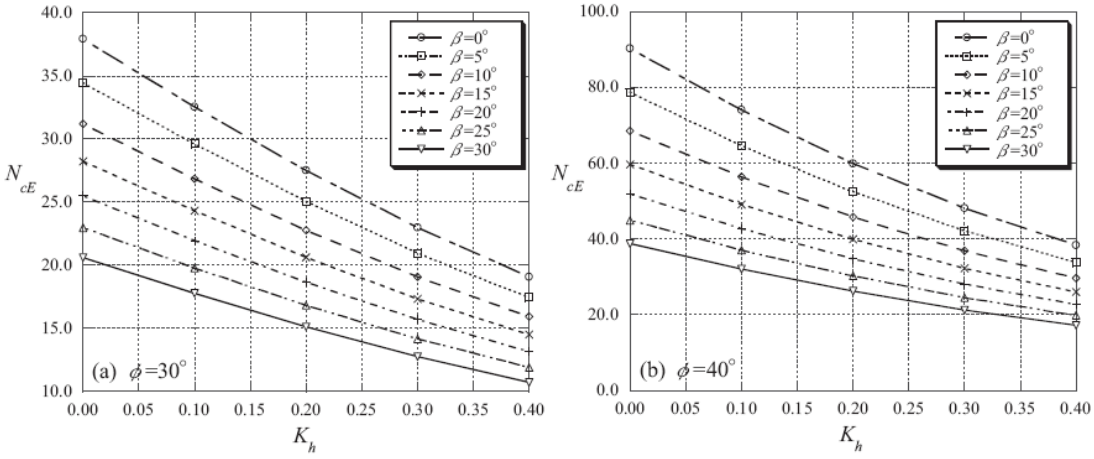


Figure 2.36. Design charts for N_{ce} (Φ= 30°, 40°, D/B= 1, a= 0.0) (Yamamoto, 2010).

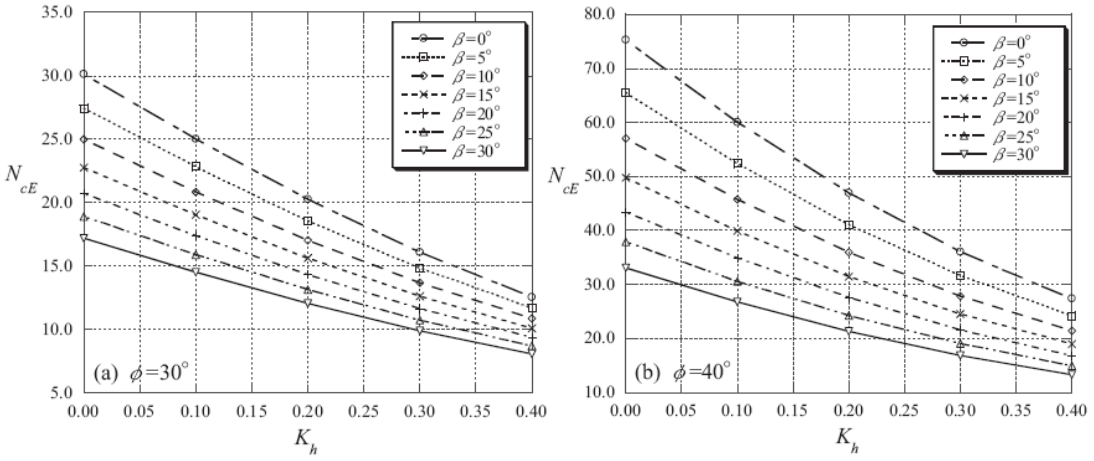


Figure 2.37. Design charts for N_{ce} (Φ= 30°, 40°, D/B= 0, a= 0.5) (Yamamoto, 2010).

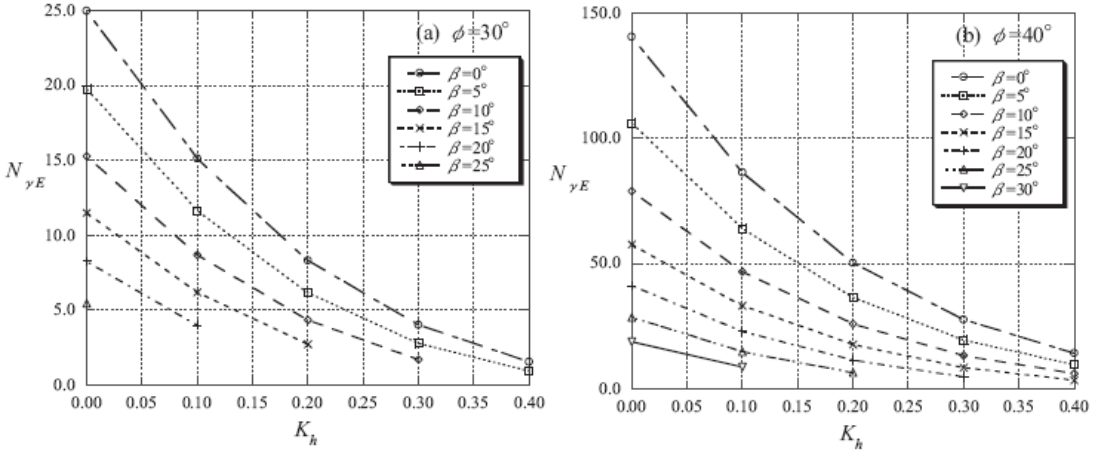


Figure 2.38. Design charts for $N_{\gamma e}$ (Φ= 30°, 40°, D/B= 0, a= 0.0) (Yamamoto, 2010).

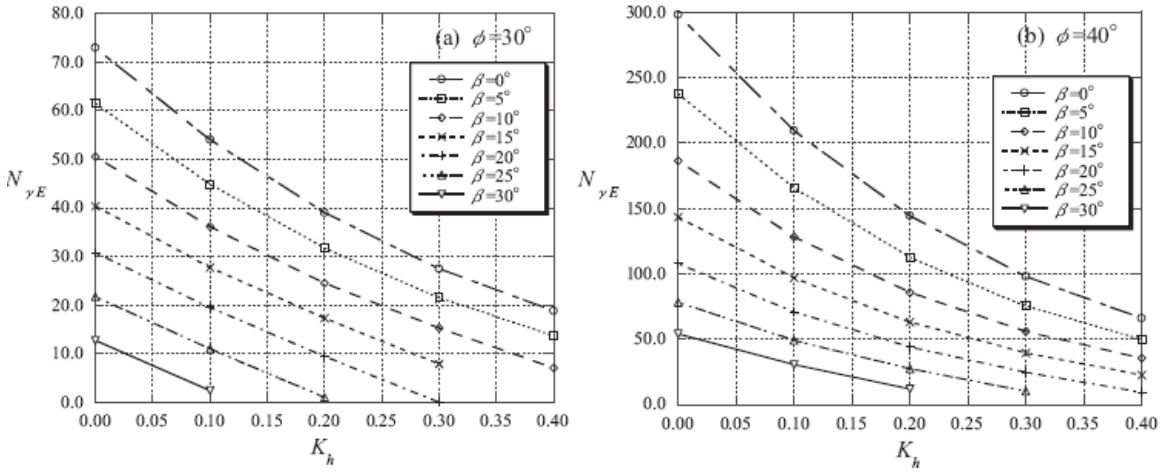


Figure 2.39. Design charts for $N_{\gamma e}$ (Φ= 30°, 40°, D/B= 1, a= 0.0) (Yamamoto, 2010).

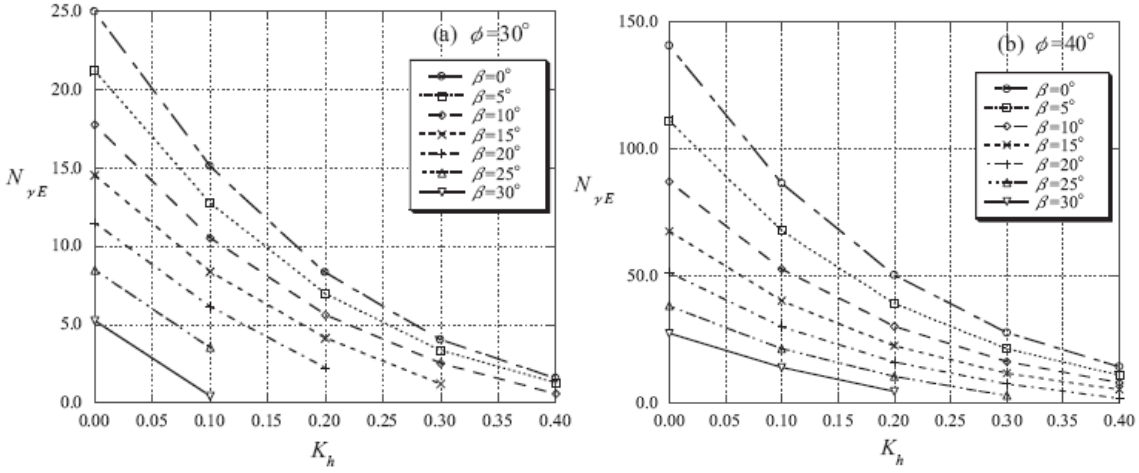


Figure 2.40. Design charts for $N_{\gamma e}$ (Φ= 30°, 40°, D/B= 0, a= 0.5) (Yamamoto, 2010).

Pseudo-static approach was used for the determination of seismic bearing capacity factors in the study of which the solution methodology is described in detail in Chapter 2.1. (Castelli and Motta, 2010). According to this approach, earthquake forces consist of the inertia forces acting on structure, sliding soil mass and surcharge. Two of them, defined as inertia force of the structure and of the surcharge were calculated using equal seismic acceleration coefficients (k_{h1}= k_{h3}) to each other. However, the seismic acceleration coefficient (k_{h2}) used for calculating inertia force of the soil mass was chosen greater than that of the structure. The reason of this choice is that Eurocode 8 allows reducing seismic effect on structures in the conditions which ductile structural behavior is ensured.

Therefore, while k_{h1} and k_{h3} takes the value of 0.1 and 0.2, k_{h2} takes the value of 0.2 and 0.4 in performed analysis.

The authors stated that despite of the simplistic failure mechanism assumption made in the presented calculation method, analysis results that were obtained in both static and seismic condition using proposed method show a good agreement with those obtained using calculation techniques developed by previous researchers. It is also concluded that the ratio of bearing capacity coefficients in seismic conditions (N_c*/N_c) varies with *d/B* ratio, slope angle (β), *H/B* ratio as well as internal friction angle (Φ) and seismic acceleration coefficients (k_{h1}, k_{h2} ve k_{h3}). Additionally, it was reported that *d/B* ratio, slope angle (β), *H/B* ratio and k_{h1} seismic acceleration coefficient are influential parameters on the N_c*/N_c ratio in undrained conditions (Φ= Φ_u= 0°). The variation in N_c*/N_c ratio with the stated variables is presented in Figure 2.41. As shown in the presented design charts, since the reduction in seismic bearing capacity due to inertia force of the structure is more decisive, k_{h1} coefficient only takes greater values than zero.

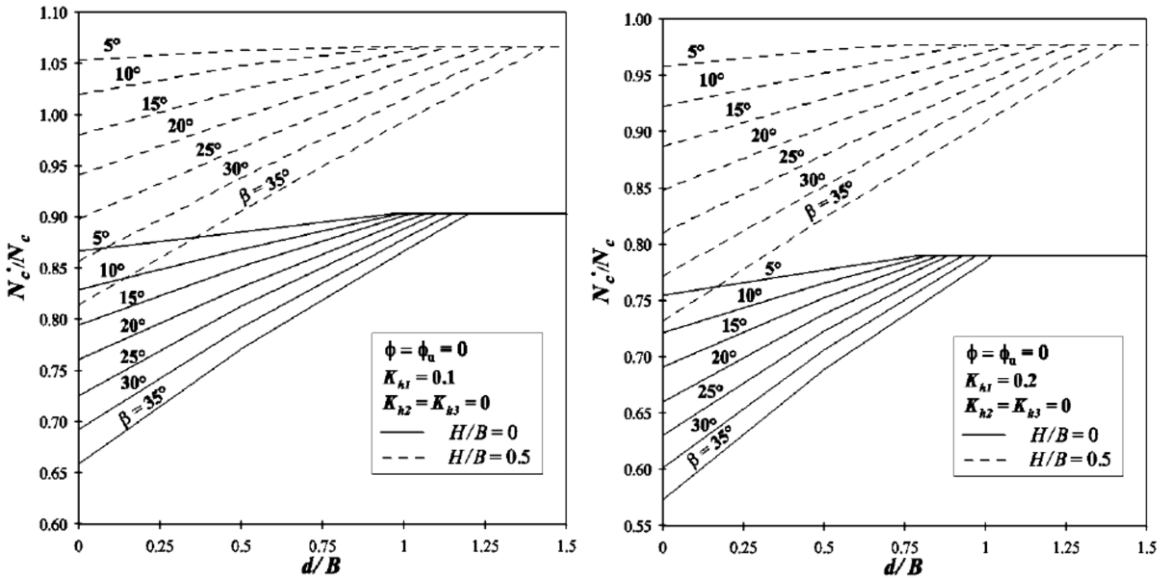


Figure 2.41. N_c*/N_c ratios as a function of the normalized *d*/*B* slope distance (Castelli and Motta, 2010).

Similar to the results obtained in static condition, severe reduction in the ratio of bearing capacity coefficients is observed when the footing is at the slope edge. Firstly, the ratio of bearing capacity coefficients increases with the increase of the footing distance

from the slope edge. Then, as the footing reaches to a certain distance from the slope edge defined herein as threshold distance, the presence of slope will not affect the failure mechanism. Thus, the ratio no longer takes constant value that is diminished by the influence of inertia forces only. As shown in Figure 2.41, the threshold distance varies in between 0.75*B* and 1.5*B*. Moreover, this distance increases with the increase of k_{h1} seismic acceleration coefficient. Besides, it is reported that the threshold distance is not changed by considering either inertia of the structure and of the sliding soil mass separately.

Farzaneh *et al.* (2013) had used the finite element lower bound method together with linear programming technique for the determination of seismic bearing capacity of strip footings located near slopes. The main reason of developing a solution based on lower bound method were described as that the limit load determined by this method is less than true limit load and thus always being on the safe side. Furthermore, the absence of any lower bound solution presented so far in the literature was given as secondary reason.

Three noded linear finite elements (also means the use of linear shape functions) were used in all finite element models prepared within the context of this study. It was assumed that the each shared edge of adjacent elements is a statically admissible stress discontinuity. Detailed explanations about the lower bound finite element method can be found in the related reference (Sloan, 1988).

Graphical representation of the problem is presented in Figure 2.42. For the slope angle (β), the values of 30°, 60° and 90° were chosen. Furthermore, several normalized distances (*a/B*) were used to indicate the effect of the footing distance from the slope edge. However, *H/B* ratio was assumed as a constant value. Accordingly, the value of *H/B* ratio was four in all analyses. The reason of the use of constant H/B ratio in all analyses will be clarified in later.

It is assumed that the soil material obeys associated flow rule and its undrained behavior can be modelled by Tresca failure criterion in seismic condition. Similar to *a/B* ratio, different values of $c_u/\gamma B$ ratio were used in the analysis. The base of the footing is also assumed rough. Earthquake forces determined by pseudo-static approach consist of the inertia force of the structure and of the sliding soil mass. To calculate the earthquake

forces, horizontal seismic acceleration coefficients (k_h) were chosen as 0, 0.1, 0.15, 0.2, 0.25 and 0.30. Vertical acceleration of the earthquake was neglected in the analyses.

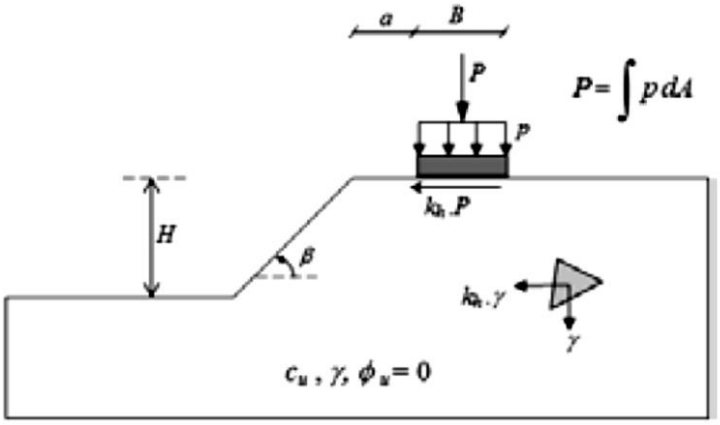


Figure 2.42. Problem parameters (Farzaneh *et al.*, 2013).

In essence, the approach adopted in this study is to express the normalized seismic limit pressure as a function of influential variables. Consequently, the functional expression of normalized seismic bearing capacity ($p/\gamma B$) and its influential parameters are given explicitly in Equation 2.23.

$$\frac{p}{\gamma B} = f\left(\beta, \frac{a}{B}, \frac{H}{B}, \frac{c_u}{\gamma B}, k_h\right) \tag{2.23}$$

The strip footing located near slopes reaches to its ultimate capacity in seismic condition by either foundation bearing capacity or overall stability of the slope. However, only foundation bearing capacity mode was investigated in this study. As mentioned earlier, *H/B* ratio was chosen as constant. According to results, the value of *H/B*= 4 insures that the bearing capacity mode will only occur for all values of k_h mentioned above.

Three main results obtained at the end of the study are summarized in the following:

- Seismic bearing capacity decreases with the increase of horizontal acceleration.
- As shown in Figure 2.43, the bearing capacity increases when footing distance from the slope edge increases and from a definite value of *a/B* the bearing capacity remains

constant. It can also be observed that the footing which rests on a slope with lower angle reaches to this constant value more rapidly.

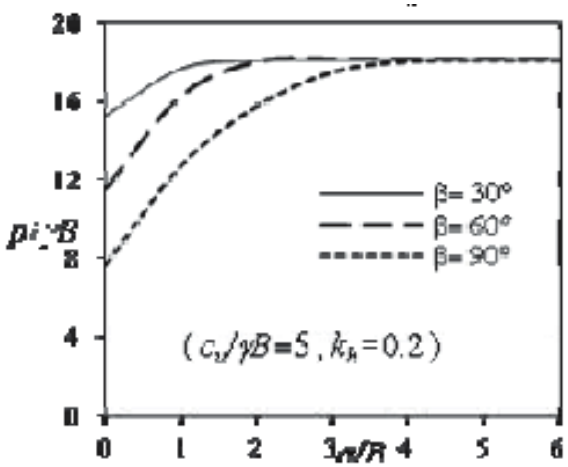


Figure 2.43. Variation of seismic bearing capacity with *a*/*B* (Farzaneh *et al.*, 2013).

- As shown in Figure 2.44, the variation in normalized seismic bearing capacity ($p/\gamma B$) with $c_u/\gamma B$ ratio is linear in the definite range of $c_u/\gamma B$ ratio. However, for the smaller values of $c_u/\gamma B$ ratio, the stability of slope decreases rapidly and reaches to its ultimate capacity by overall slope failure Due to this fact, the relationship between these two parameters is non-linear.

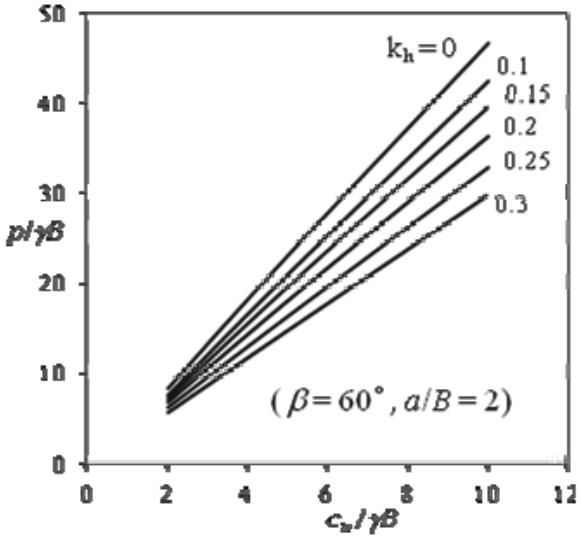


Figure 2.44. Variation of seismic bearing capacity $c_u/\gamma B$ (Farzaneh *et al.*, 2013).

As a result of the study, design charts shown in Figure 2.45 were presented to estimate seismic bearing capacity of strip footings located near slopes. Presented design charts were prepared considering only bearing capacity failure mode. Therefore, non-linear portion of the curves were not shown in the design charts.

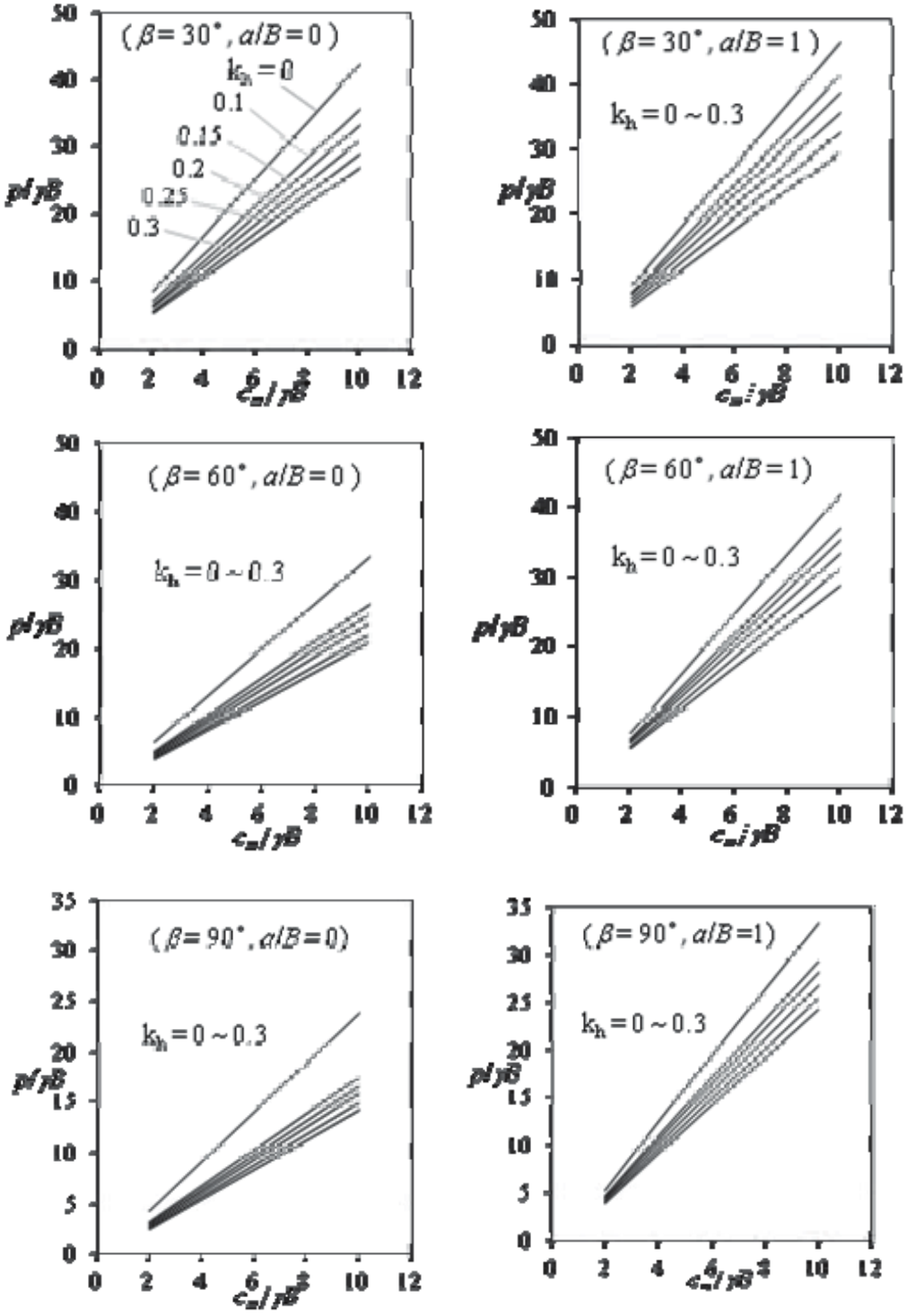


Figure 2.45. Design charts for seismic bearing capacity of strip footings near cohesive slopes (Farzaneh *et al.*, 2013).

2.3. Stability of Cohesive Slopes in Static and Seismic Conditions

Depending on geometrical properties and strength characteristics of slope soil, the slope can lose its overall stability under static conditions or by the inertia force during seismic events. Since this situation was observed in some of the numerical model outputs, research studies regarding to stability of cohesive slopes in both static and seismic conditions (without any footing pressure near the slope) will also be given briefly to check whether the results of numerical models are consistent with previous findings. For this purpose, Taylor (1937) and Koppula (1984) were chosen to evaluate the numerical model results for static and seismic conditions, respectively. Brief description for each study is presented in the following.

Taylor (1937) has solved analytically the stability problem of saturated cohesive slopes under undrained static conditions. According to this study, for the case of critical circles, mobilized cohesion (c_d) along sliding surface to maintain the equilibrium of slope is calculated using the formula given in Equation 2.24.

$$c_d = m\gamma H \tag{2.24}$$

where m is the stability number, γ is the saturated unit weight of soil and H is the slope height.

By substituting mobilized cohesion (c_d) with undrained shear strength (c_u) into Equation 2.24, the maximum height of which the slope can stand on without any stability loss is obtained by the formula given in the following. Stability number (m) given in the following formula can be determined using descriptions and the design chart given in Figure 2.46 and Figure 2.47 respectively.

$$H_{cr} = \frac{c_u}{\gamma m} \tag{2.25}$$

The following issues relating to the design chart presented in Figure 2.47 should be kept in mind.

- For a slope angle (β) greater than 53°, the critical circle is always toe circle.
- For β<53°, the critical circle may be a toe, slope or midpoint circle depending on the location of the firm base under the slope.

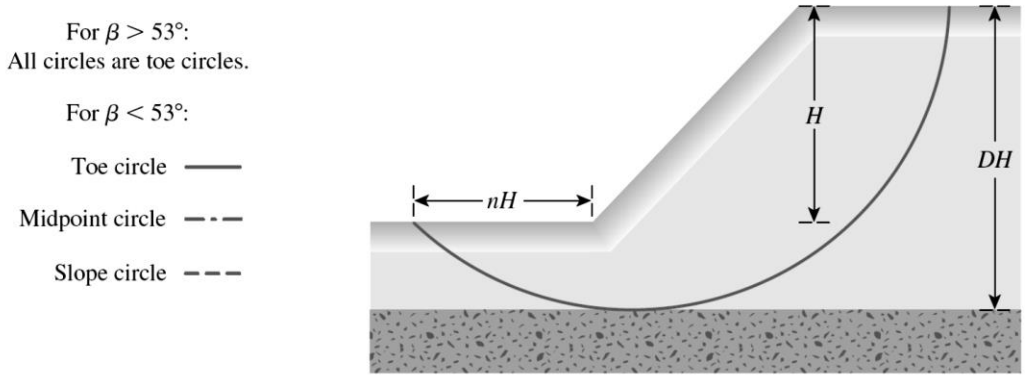


Figure 2.46. Definition of parameters for midpoint circle type of failure (Taylor, 1937) (Adapted from Das, 2009).

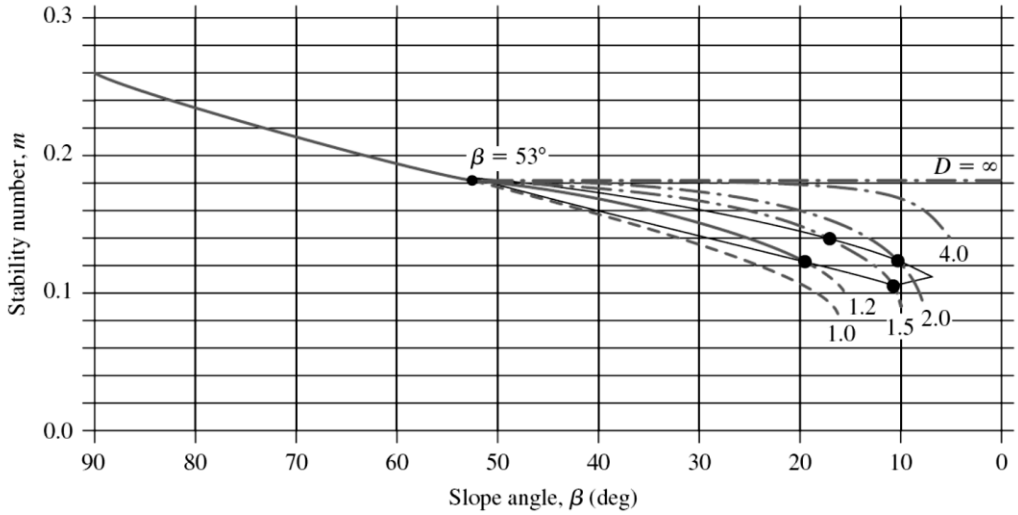


Figure 2.47. Plot of stability number (m) against slope angle (β) (Taylor, 1937) (Adapted from Das, 2009).

Stability analysis of cohesive slopes in seismic condition is in fact similar to the solution developed for static condition. Principally, the goal is to find the critical circular surface of which factor of safety against sliding is the lowest among all possible circular surfaces. However, the horizontal inertia force which acts outwards of the slope and also

generates a reducing effect onto its stability should be incorporated into the developed solution.

Koppula (1984) has produced a solution relating to the seismic stability of cohesive slopes in undrained conditions which has been adopted so far by the authors of numerous reference textbooks. This solution also considers the situation in which undrained shear strength of soil increases with depth. According to this study, minimum factor of safety can be calculated by the following formula.

$$F_s = \frac{a_0}{\gamma} N_1 + \frac{c_0}{\gamma H} N_2 \tag{2.26}$$

where N_1 and N_2 are stability numbers, a_0 is the variation in undrained shear strength with unit depth (constant), γ is the saturated unit weight of soil, H is the slope height and c_0 is the undrained shear strength at the top of slope.

Since undrained shear strength of soil does not vary with depth in finite elements models developed within the context of the thesis, it is not necessary to consider the first term in given formula and thus the maximum height (H_{cr}) of which the slope can stand on is calculated (by substituting c_0 with c_u and taking F_s as 1) by the formula given in Equation 2.27.

$$H_{cr} = \frac{c_u}{\gamma} N_2 \tag{2.27}$$

If slope angle (β) is less than 53°, the stability number N_2 is a function of slope angle (β), horizontal seismic acceleration coefficient (k_h) and depth factor (D). For that case, the value of N_2 is determined by the graph given in Figure 2.48. If slope angle (β) is greater than 53°, the critical surface passes from the toe of the slope and. For that case, N_2 is a function of slope angle (β), horizontal seismic acceleration coefficient (k_h) and is determined by the graph given in Figure 2.49.

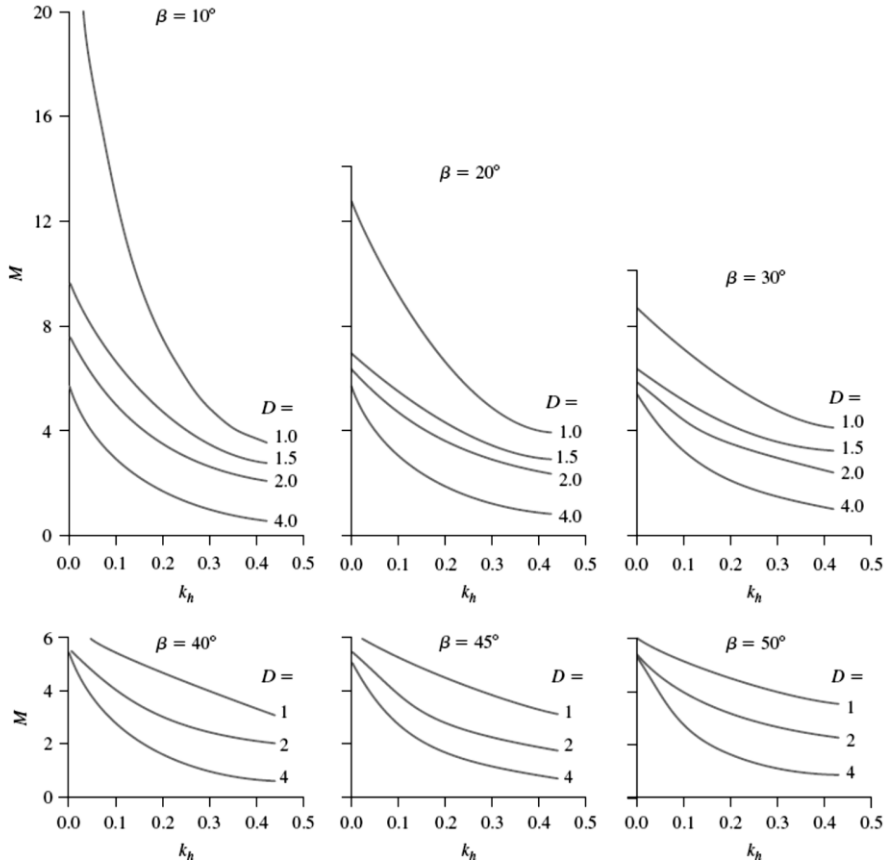


Figure 2.48. Variation of N_2 with k_h and β (Koppula, 1984) (Adapted from Das and Ramana, 2010).

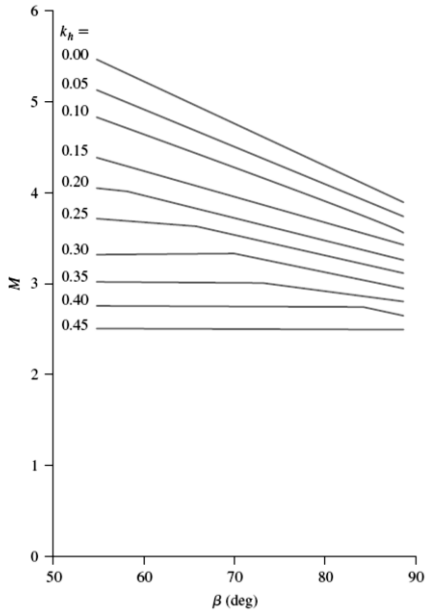


Figure 2.49. Variation of N_2 with $\beta \geq 55$ and k_h (Koppula, 1984) (Adapted from Das and Ramana, 2010).

3. METHOD OF ANALYSIS

In this chapter, the development and the use of the numerical model will be described in detail. The numerical approach adopted is the finite element method and a commercial FEM software Plaxis 2D is used.

Firstly, brief explanations related to applications of FEM in geotechnical engineering and FEM software Plaxis 2D will be presented. Secondly, the definition and basic assumptions of the problem will be given respectively. Then, the solution expressed by a simplified formula and the steps of the parametric study will be described. Thirdly, steps to be followed for making necessary operations within three submodules of Plaxis 2D (called as Input, Calculations and Output) will be addressed in detail.

The last part of this chapter is devoted to validation of results obtained. This verification will be performed for three different cases. Static bearing capacity coefficients obtained by previous researchers for strip footings located near cohesive slopes in undrained conditions will be compared at first with those obtained by Plaxis 2D. This comparison will be made for two conditions in which the footing is on the slope edge (λ= 0) and far away from the slope edge (λ> 0). Research studies of which the results are used to compare with Plaxis 2D outputs are those given in Chapter 2.1. Then, seismic bearing capacity coefficients obtained by previous researchers for such footings in undrained conditions will be compared with those obtained by Plaxis 2D. As in the first comparison, it will be made once again for two conditions (λ= 0 and λ> 0). As mentioned earlier, all research results given in Chapter 2.2 cannot be used for the comparison. Only three of them (Kumar and Rao, 2003; Castelli and Motta, 2010; Farzaneh *et al.*, 2013) suggested a solution for the problem at hand, and hence their results will be taken into account for the second comparison. Furthermore, results of numerical models in which overall slope failure was determined in either static or seismic condition prior to the application of footing pressure will be compared with findings of previous studies given in Chapter 2.3.

3.1. FEM in Geotechnical Engineering and Plaxis 2D

FEM is a numerical technique which can be used to solve problems in geotechnical engineering. Computer codes based on FEM have been developed to solve problems involving soil-structure interaction, embankment construction, seepage, and soil dynamics.

Traditional methods of analysis often use techniques that are based on assumptions that oversimplify the problem at hand. These methods lack the ability to account for all of the factors and variables the design engineer faces and may severely limit the accuracy of the solution. FEM can overcome many of these shortcomings, thereby offering many advantages over the conventional approaches (USACE, 1995). Their ability to accurately reflect field conditions essentially depends on the ability of the constitutive model to represent real soil behavior and correctness of the boundary conditions imposed. The user has only to define the appropriate geometry, construction procedure, soil parameters and boundary conditions. Structural members may be added and withdrawn during the numerical simulation to model field conditions. Retaining structures composed of several retaining walls, interconnected by structural components, can be considered and, because the soil mass is modelled in the analysis, the complex interaction between raking struts or ground anchors and the soil can be accounted for. The effect of time on the development of pore water pressures can also be simulated by including coupled consolidation. No postulated failure mechanism or mode of behavior of the problem is required, as these are predicted by the analysis. The analysis allows the complete history of the boundary value problem to be predicted and a single analysis can provide information on all design requirements (Potts *et al.*, 2002)

PLAXIS 2D is a special purpose two dimensional finite element computer program used to perform deformation and stability analyses for various types of geotechnical applications. Real situations may be modelled either by a plane strain or an axisymmetric model. The program uses a convenient graphical user interface that enables users to quickly generate a geometry model and finite element mesh based on a representative vertical cross-section of the situation at hand. The enhanced output facilities also provide a detailed presentation of computational results. The calculation itself is fully automated and based on robust numerical procedures (Brinkgreve *et al.*, 2006)

3.2. Definition and Assumptions of the Problem

Graphical representation of the problem is presented in Figure 3.1. The objective is to determine seismic bearing capacity (q_f) of surficial footings (D_f= 0) located near cohesive slopes under undrained conditions using pseudo-static approach.

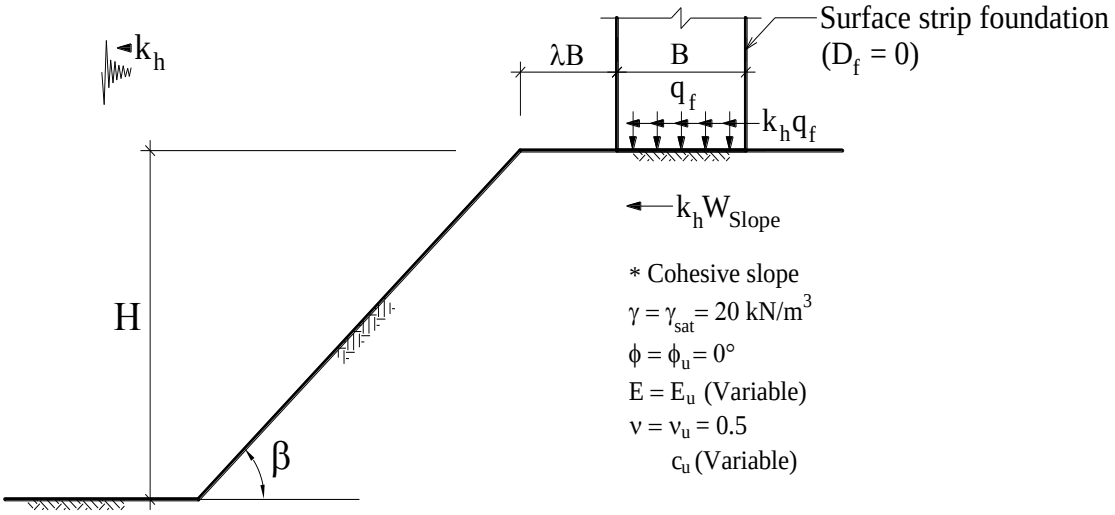


Figure 3.1. Graphical representation of the problem.

Assumptions made for the solution of the problem shown in Figure 3.1 are summarized below. If required, detailed explanations regarding the assumptions mentioned below will be given later. Accordingly;

- Slope geometry does not change along the z-axis directed perpendicular to the cross section (Plane strain condition).
- The footing is surficial strip footing. Therefore, the effect of embedment depth onto seismic bearing capacity of such footings will not be investigated in this study.
- The footing is represented by a rigid plate element and the interface is assumed to be rough.
- Seismic bearing capacity of such footings is determined by using pseudo-static approach. It is assumed that inertia force of structure acts at the base level of footing. Overturning moment due to the inertia force acting on structure is neglected as well.
- Horizontal seismic acceleration coefficients used for calculating the inertia force of structure and of slope soil are chosen to be equal (k_h).

- Effect of vertical component of earthquake acceleration onto seismic bearing capacity is neglected (k_v= 0).
- Mohr-Coulomb constitutive model is used to define soil behavior.
- Undrained shear strength of soil does not vary due to complex, temporary and dynamic earthquake loading.
- Slope soil is uniform and undrained shear strength of soil does not vary with depth as well.

3.3. Suggested Solution Method

In accordance with the assumptions mentioned in Chapter 3.2., seismic bearing capacity of such footings can be determined using Plaxis 2D. To do so, firstly, necessary data input should be completed within Input module of the software. Then, Calculation module of the software should be run to analyze the problem at hand. Furthermore, as the footing reaches to the seismic bearing capacity failure, failure mechanism formed at the ultimate limit state can be readily viewed within Output module of the software.

However, a convenient mathematical expression by which relationship between seismic bearing capacity (q_f) and undrained shear strength of cohesive slope soil (c_u) may be defined is investigated in this study. By taking the form of equation defined by Skempton (1951) as reference, it is suggested that seismic bearing capacity of such footings can be calculated using the formula given in Equation 3.1.

$$q_f = c_u \, N_{cse} \tag{3.1}$$

where q_f is the seismic bearing capacity of surficial strip footings near cohesive slopes, c_u is the undrained shear strength of cohesive slope soil and N_{cse} is the seismic bearing capacity factor of surficial strip footings near cohesive slopes.

Undrained shear strength of cohesive soils can be determined via several laboratory tests (UU triaxial compression test, unconfined compression test and etc.) or can be estimated with sufficient accuracy using correlations developed for in-situ tests such as standard penetration test (SPT), cone penetration test (CPT) and etc. Therefore,

determination of seismic bearing capacity factor is sufficient to obtain the ultimate footing pressure according to the methodology presented herein. This fact also demonstrates that the methodology is well-simplified as much as that can be used even in routine applications of geotechnical engineering. After that, the only thing that should be done is to find influential parameters onto the seismic bearing capacity factor, and then, if possible, to prepare design charts or to derive equations for the determination of seismic bearing capacity factor. To do so, parametric study of which the details are given in Chapter 3.4 has been done.

3.4. Parametric Study

As previously mentioned, it is required to make a parametric study to establish a complete methodology and to determine all influential parameters onto seismic bearing capacity factor. Accordingly, factors that are defined as variables can be categorized into three groups.

First group is mainly associated with factors that define the geometry of slope. In essence, knowing slope height (H) and slope angle (β) is sufficient to define the geometry of slope which footing is located near. Several arbitrarily selected magnitudes of these variables are selected for the parametric study: Considered magnitudes for slope height (H) are 2, 4 and 8m; slope angle (β) is chosen as 15°, 30° and 45°. Moreover, (λ) factor which defines footing distance from the slope edge is normalized with footing width (B). The normalized footing distance (λ) from the slope edge essentially takes the values of 0, 0.5, 1 and 2. In order to reveal the relationship between seismic bearing capacity factor (N_{cse}) and normalized footing distance (λ) shown in design graphs (will be presented in the subsequent chapter of the thesis) and to determine threshold distance (the distance at which the influence of the slope diminishes) values as accurate as possible for various cases, mostly, additional analyses were performed by using different normalized footing distance values.

Second group is associated with the strength of slope soil. Since the soil strength is represented by undrained shear strength according to the material model chosen, only this

parameter is considered as variable. Undrained shear strength of cohesive slope soil (c_u) is 25, 50, 100, 200 kPa.

Last group is associated with the earthquake effect. As it is known, in pseudo-static approach, earthquake effect is defined by horizontal seismic acceleration coefficient (k_h). In this study, horizontal seismic acceleration coefficient (k_h) varies in between 0.1 and 0.4.

3.5. Data Input in Plaxis 2D

It was already mentioned that chosen problem in the scope of this study can be analyzed by Plaxis 2D software and thus, seismic bearing capacity of a surficial strip footing located near a cohesive slope can be determined for a set of geometric, strength and seismic parameters. To solve the problem, issues related to the necessary operations within Input module of the software are divided into eight subheadings in this chapter. Significant aspects of developed numerical model will be fully described in each subheading.

3.5.1. General Settings

There are two tabs named as “Project” and “Dimensions” in “General settings” window of Plaxis 2D software. In “Project” tab, firstly, model and element type selections are made. If created model uses pseudo-static approach, magnitude of accelerations imposed along x and y axes should also be defined in terms of gravitational acceleration (g). Furthermore, as seen in Figure 3.2, the magnitude of gravitational acceleration whose direction is pre-defined can be adjusted by the user via “Acceleration” input box. On the other hand, basic units (force, length and time) are shown under “Dimensions” tab. Besides, there are four input data boxes in the same tab that enable the definition of outer boundaries of the drawing area into which the numerical model geometry fits (Refer to Figure 3.3).

Owing to the fact that slope geometry and footing properties do not vary along the axis directed perpendicular to the cross section at hand, model type is selected as plane strain. Accordingly, displacements and strains along this axis (z axis) are assumed to be

zero. However, normal stresses in *z* direction are taken into account (Brinkgreve *et al.*, 2006).

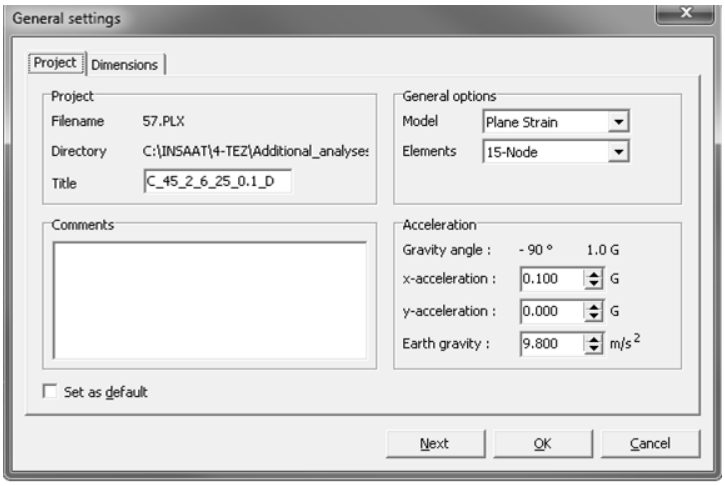


Figure 3.2. "Project" tab of "General settings" window.

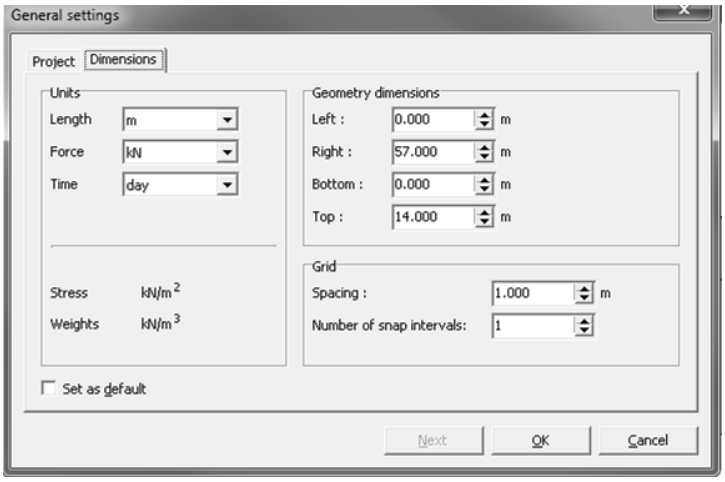


Figure 3.3. "Dimensions" tab of "General settings" window.

As shown in Figure 3.4, Plaxis 2D software offers two alternatives for the element type: 6-node triangular element and 15-node triangular element. Even though the use of 15-node triangular element consumes relatively much more computer memory and leads to the longer computational time than that of 6-node triangular element, it is expressed that the use of 15-node triangular element is more convenient particularly for the solution of difficult problems such as calculation of failure load for incompressible soils. Additionally, it is reported that failure loads in bearing capacity calculations are generally overestimated

using 6-node elements. (Brinkgreve *et al.*, 2006). Therefore, 15-node triangular element was used in all analyses performed in this study.

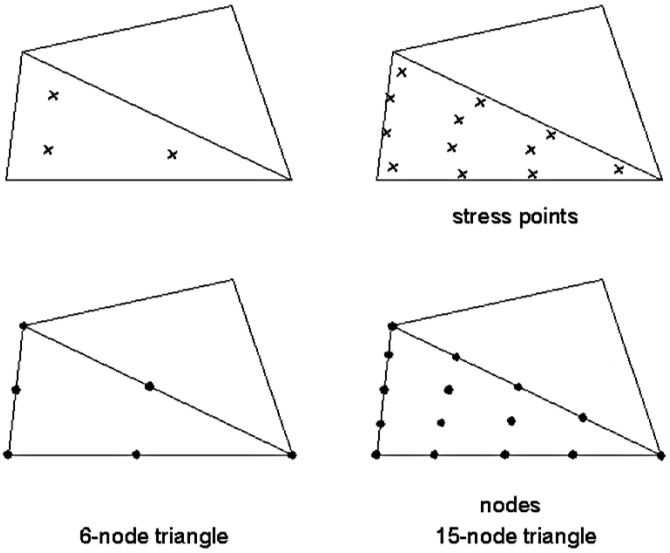


Figure 3.4. Position of nodes and stress points in soil elements (Brinkgreve *et al.*, 2006).

Since the influence of vertical component of earthquake acceleration is neglected, defining the magnitude of pseudo-static acceleration imposed parallel to x axis in "Project" tab of "General settings" window in terms of the gravitational acceleration is sufficient to model dynamic earthquake forces. Meanwhile, since dynamic earthquake forces are activated in Calculations module of the software, this issue will be discussed again later. As slope geometries created in this study and sign convention of Plaxis 2D software are considered together, defining the magnitude of pseudo-static acceleration imposed along x axis by a positive value ensures that slope inertia force directs outwards from the slope. Thus, the orientation of slope inertia force reduces the slope safety against sliding.

Basic units (force, length and time) used in the analysis are shown under the "Dimensions" tab of the "General Settings" window. The unit system used in models is the default unit system of the software. Moreover, numerical values shown in the frame of "geometry dimensions" which define outer boundaries of drawing area are determined automatically by the procedure developed for creating model geometry. Details of geometry creation procedure are given in Section 3.5.2.

3.5.2. Model geometry

During the creation of a finite elements model, how outer boundaries of the model are determined along both principal directions is one of the critical issues. Accordingly, it is aimed to determine a convenient procedure for the creation of outer boundaries that can be applied to all numerical models created in this study. While developing the procedure, the basic principle that should always be kept in mind is that outer boundaries' positions should not affect footing failure loads calculated by the software. For this purpose, definite model geometry was determined by trial and error method. As a result, it is concluded that the model geometry presented in Figure 3.5 is appropriate and applicable for all numerical models created in this study. As Figure 3.5 is examined, it is seen that horizontal distance between right footing edge and right vertical boundary varies with footing width (8*B*). However, remaining two distances were chosen as constants. These distances are the horizontal distance between bottom edge of slope and left vertical boundary and the vertical distance between bottom edge of slope and horizontal bottom boundary, and take the value of 25m and 12m respectively.

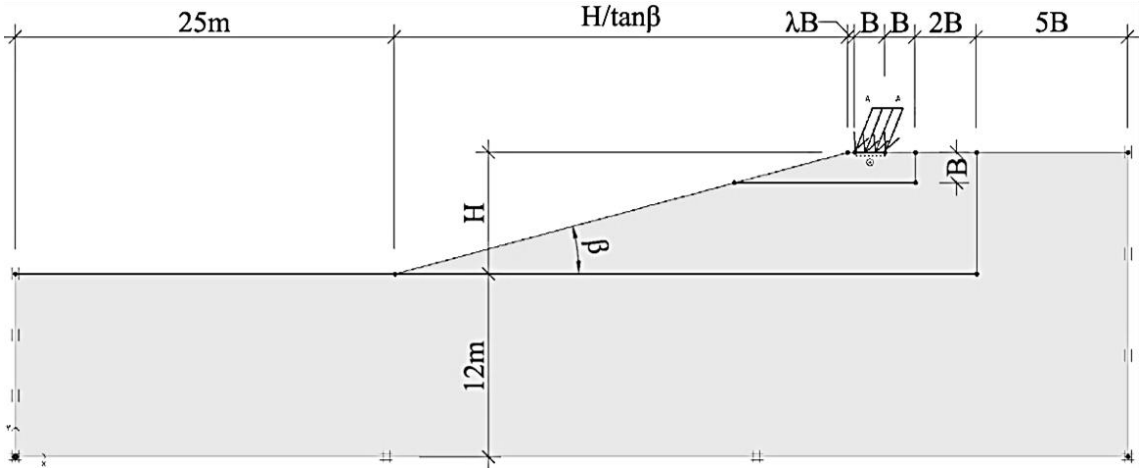


Figure 3.5. Schematic representation of created finite elements model.

3.5.3. Properties of Surficial Strip Footing

Surficial strip footing represented by a rigid plate element in finite element models is 2.0 m wide. The plate element is assumed to be weightless and elastic material type is assigned to it. Typical stiffness parameters of the plate element and equivalent plate

thickness (d_{eq}) values used in all models are presented in Table 3.1. Moreover, it was already mentioned that surficial strip footing is assumed to be "fully rough". To model this assumption in Plaxis 2D software, an interface was drawn below the footing plate and interface strength reduction factor (R_{inter}) was specified as one in four different soil data sets used in this study (Brinkgreve *et al.*, 2006; Georgiadis, 2010).

Table 3.1. Physical and elastic properties of rigid plate element.

Material Type	**Axial stiffness, EA (kN/m)**	**Flexural stiffness, *EI* (kNm^2/m)**	***d*$_{eq}$ (m)**	**Weight, *w* (kN/m/m)**	**Poisson ratio, *ν* (Unitless)**
Elastic	$3x10^7$	$2.5x10^6$	1.00	0	0.2

3.5.4. Boundary Conditions

"Standard fixities" boundary condition which is suitable for most of geotechnical problems is used in all prepared finite elements models. This option can be selected very quickly with a shortcut given on Input menu of the software. Accordingly, while horizontal fixity (u_x= 0) is defined across two geometry lines whose x coordinates are minimum and maximum, full fixity (u_x= u_y= 0) is specified across horizontal geometry line located at the bottom of model whose y coordinate is minimum (Refer to Figure 3.5).

3.5.5. Loads

As shown in Figure 3.6, rigid footing undergoes the action of an inclined load in seismic condition. In such a case, while vertical component of inclined load corresponds to the seismic bearing capacity (q_f) of footing-on-slope system at the ultimate state, horizontal component of inclined load corresponds to inertia force acting on structure ($k_h \times q_f$) in case of an earthquake. In order to determine the seismic bearing capacity of footing-on-slope system, firstly, a unit load, whose magnitude is small enough so as to not affect overall stability of slope in seismic condition, is defined after generating initial stresses. Then, slope inertia force imposed along x axis should be adjusted in a manner that acts outwards from the slope. To do so, an appropriate positive acceleration value should be initially entered inside "x acceleration" data box in "General settings" window of the software. After that, in the third calculation stage within Calculation module, *Σ-Maccel* value should be adjusted as one to activate the inertia force acting on the slope. At the final calculation

stage, the magnitude of inclined unit load shown as “load system A” in Figure 3.6 is increased by a load factor (*Σ-MloadA*) until reaching failure at ultimate state. Details regarding the calculation procedure will be addressed again in Chapter 3.6.

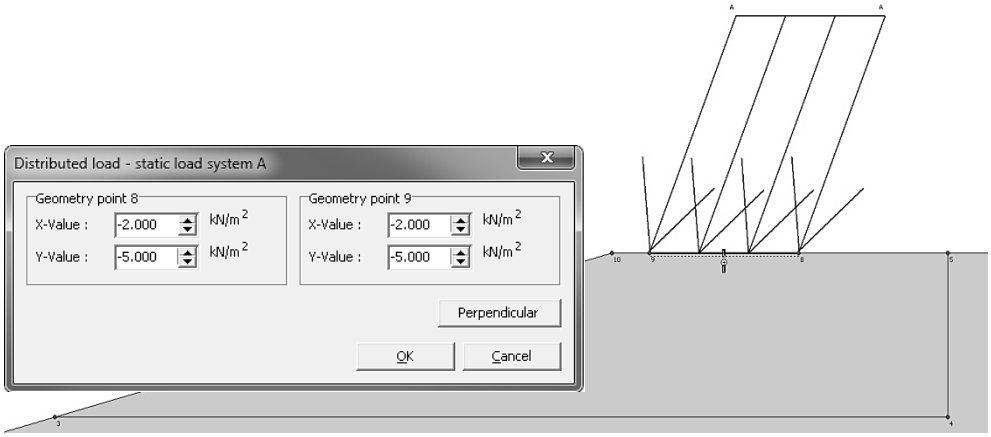


Figure 3.6. Inclined load acting on the rigid footing and unit load definition (For k_h= 0.4)

Another important issue which should be addressed is that why vertical component of the earthquake acceleration is neglected. As it is remembered, only one work in the literature took the effect of vertical earthquake acceleration into account. Shiau *et al.* (2006) incorporated the effect of horizontal and vertical earthquake acceleration ($tan\theta= k_h/1-k_v$) as explained in Chapter 2.2. Obviously, general trend in research studies given in Chapter 2.2 is towards neglecting the effect of vertical earthquake acceleration onto seismic bearing capacity of such footings. Additionally, Kramer (1996) mentioned that vertical pseudo-static force can reduce or increase at the same time both driving and resisting forces depending on its direction. For this reason, he concluded that the influence of vertical pseudo-static force is insignificant compared to the influence of horizontal pseudo-static force. That is why vertical pseudo-static force is frequently neglected in studies in which pseudo-static approach is used. In this study, the effect of vertical component of earthquake acceleration is neglected because of the explanations given in above.

3.5.6. Material Properties

Earthquake loading is described as complex, transient and most importantly high frequency loading. On the other hand, cohesive soils have low permeability. Due to these principal factors, it can be readily said that undrained conditions are valid for seismic bearing capacity problem of footings located near cohesive slopes and govern slope soil behavior utterly in case of an earthquake. Therefore, it was initially examined how to model undrained behavior properly for cohesive soils in Plaxis 2D software. As a result, it is understood that Plaxis 2D software offers three different options to the user in order to perform an undrained analysis (Brinkgreve *et al.*, 2006). These alternatives are,

- Undrained analysis with effective stiffness and strength parameters
- Undrained analysis with effective stiffness and undrained strength parameters
- Undrained analysis with undrained stiffness and strength parameters (total stress analysis)

As mentioned in Chapter 3.2, behavior of cohesive slopes is described by Mohr-Coulomb material model under seismic conditions. Although it is possible to use each alternative given above in conjunction with Mohr-Coulomb model, the third alternative called “total stress analysis with undrained stiffness and strength parameters” was preferred. When this modelling option is used, the number of stiffness and strength parameters that are needed to model undrained soil behaviour by Mohr-Coulomb material model would be two in total. These parameters are simply undrained elasticity modulus (E_u) and undrained shear strength (c_u). Besides that, undrained elasticity modulus was defined depending on undrained shear strength of soil ($E_u = 200c_u$) and for each cohesive soil stiffness considered in this study, a constant value was assigned to undrained elasticity modulus. As it is known, Mohr-Coulomb model needs five stiffness and strength parameters totally. However, by using the third undrained modelling alternative and aforementioned assumption related to undrained elasticity modulus, the number of stiffness and strength parameters required to define Mohr-Coulomb model was reduced and only undrained shear strength of cohesive soil (c_u) is sufficient to describe soil behaviour during a seismic event. This simplification is also very helpful to observe the influence of material properties on seismic bearing capacity.

It was also verified by several finite elements analyses that undrained elasticity modulus, being a deformation parameter, does not have any effect on seismic bearing capacity factor. Accordingly, the variation in undrained elasticity modulus could only lead to changes in calculated deformation values. However, since deformation is not a decisive criterion taken into consideration for the calculation of failure loads, undrained shear strength of cohesive soil (c_u) emerges as the only soil parameter that influences the seismic bearing capacity factor.

When undrained behavior of cohesive soils under seismic conditions is modelled by using undrained stiffness and strength parameters, Mohr-Coulomb material model turns into Tresca model. For this reason, general properties of Tresca model will be addressed briefly in following. Tresca model is a simple constitutive model regularly used in geotechnical engineering for calculating failure loads of cohesive soils under undrained conditions (Taiebat and Carter, 2007). Yield function $F(\{\boldsymbol{\sigma}\}, \{\mathbf{k}\})$ of this model presented in Equation 3.2 plots as a regular hexagonal cylinder in principal total stress space. Soil behaves purely elastic for total stress states inside the yield surface and perfectly plastic for total stress states on the yield surface. Thus, it is not likely to be strain hardening and/or softening for Tresca model. Additionally, Tresca model obeys “associated flow rule” and satisfies “normality condition” as well. Accordingly, yield function given in Equation 3.2 is also adopted as plastic potential $P(\{\boldsymbol{\sigma}\}, \{\mathbf{m}\})$. Moreover, satisfying "normality condition" means that incremental plastic strain vector is vertical (normal to the yield surface) at the limit state. This case is shown in Figure 3.8 and volumetric plastic strain rate is zero as expected (Potts and Zdravkovic 1999).

$$F(\{\boldsymbol{\sigma}\}, \{\mathbf{k}\}) = \sigma_1 - \sigma_3 - 2c_u = 0 \tag{3.2}$$

where σ_1 and σ_3 are the major and minor principal total stresses, respectively, among all three principal stresses for general stress states; c_u is the undrained shear strength of cohesive soil.

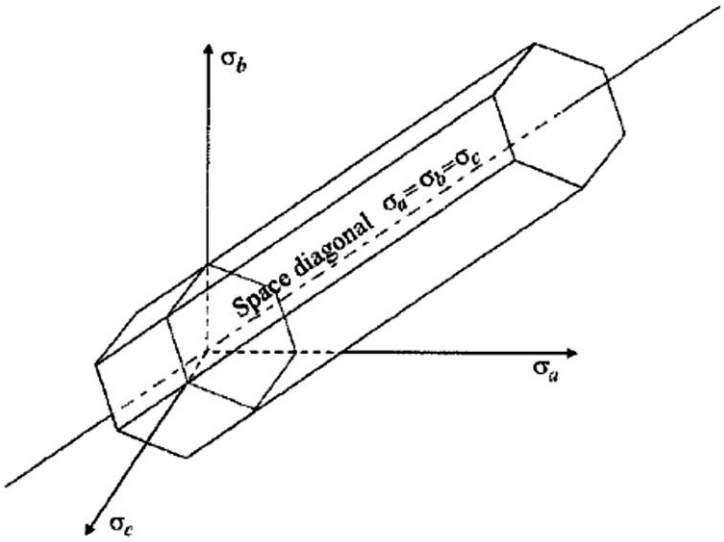


Figure 3.7. Tresca yield surface in principal total stress space (Potts and Zdravkovic, 1999).

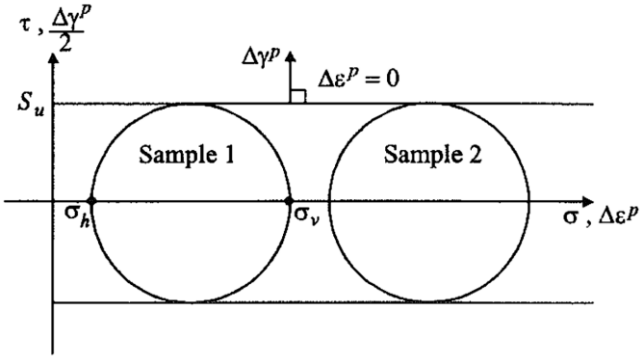


Figure 3.8. Mohr's circles of total stress (Potts and Zdravkovic, 1999).

To define Tresca model, necessary stiffness and strength parameters are essentially undrained elasticity modulus (E_u), undrained Poisson ratio (ν_u) and undrained shear strength of cohesive soil (c_u). Besides, undrained internal friction angle (Φ_u) and undrained dilation angle (ψ_u) should be defined as zero. In order to avoid volume change in undrained conditions, theoretically, undrained poisson ratio should take the value of 0.5. However, since this value leads to the singularity in stiffness matrix, it is reported that defining a value between 0.495 and 0.499 is more convenient (Brinkgreve *et al.*, 2006). Therefore, undrained Poisson ratio was chosen as 0.495 in all performed finite elements analyses.

Four soil data sets were used in the parametric study. Each soil data set corresponds to different cohesive soil stiffness (soft, medium, stiff, hard). Soil data sets and their stiffness and strength parameters are presented in Table 3.2. Additionally, saturated unit weight of soil (γ_{sat}) was defined as constant (20 kN/m^3) for all soil data sets. Since γ_{sat} data box is deactivated automatically by Plaxis 2D as the type of material behavior is chosen as "non-porous", the constant value of γ_{sat} is input in γ_{unsat} data box. It should be noted that there is no disagreement between selected value of γ_{sat} and data input in Plaxis 2D. As mentioned in Chapter 3.5.3, interface strength reduction factor (R_{inter}) was defined as one for all soil data sets because of the rough footing assumption.

Table 3.2. Properties of the cohesive slope soils considered in this study.

Parameter			**Cohesive Soil Stiffness**			
			Soft	**Medium**	**Stiff**	**Hard**
	Name	Unit	Value	Value	Value	Value
Material model	Model	-	MC	MC	MC	MC
Type of material behavior	Type	-	Non-porous	Non-porous	Non-porous	Non-porous
Soil unit weight above phreatic level	γ_{unsat}	kN/m^3	20	20	20	20
Soil unit weight below phreatic level	γ_{sat}	kN/m^3	-	-	-	-
Permeability in horizontal direction	k_x	m/day	-	-	-	-
Permeability in vertical direction	k_y	m/day	-	-	-	-
Undrained elasticity modulus	E_u	kN/m^2	5000	10000	20000	40000
Undrained Poisson ratio	ν_u	-	0.495	0.495	0.495	0.495
Undrained shear strength	c_u	kN/m^2	25	50	100	200
Undrained friction angle	Φ_u	°	0	0	0	0
Undrained dilatancy angle	Ψ_u	°	0	0	0	0
Interface strength reduction factor	R_{inter}	-	1	1	1	1

3.5.7. Finite Element Mesh Generation

During modelling studies, investigations have been also made to find an optimum finite element mesh creation procedure that enables solving the problem with sufficient accuracy. The main goal of determining an optimum mesh generation procedure was to keep the use of computer memory and computational time at an acceptable level. As the total number of numerical models created in this study in order to establish a complete methodology is considered, making such an effort is definitely essential.

Though researchers who have made an effort to find a better solution has used various calculation techniques, they mostly focused on "bearing capacity failure mode" in their study. Moreover, Yamamoto (2010) reported that failure surface passes through shallower depths below the ground surface with the increase of horizontal acceleration coefficient (K_h). Therefore, the first phase of these investigations was to determine boundaries of the specific zone beneath the footing where high stress and strain concentration was observed. In consequence, it was considered that choosing static bearing capacity problem of strip footings on level ground as benchmark exercise, and accordingly, determination of the specific zone boundaries beneath the footing where mesh refinement has to be applied is quite reasonable approach. Besides that, another significant reason of choosing this problem is that exact solution is available in the literature of geotechnical engineering (Prandtl, 1920).

Prandtl (1920) expressed that bearing capacity of rough strip footings on level ground can be calculated by the formula given in Equation 2.1 and the exact value of bearing capacity factor (N_c) given in this formula is 5.14 (π+2). Furthermore, Prandtl type failure mechanism formed at the ultimate state is presented in Figure 3.9.

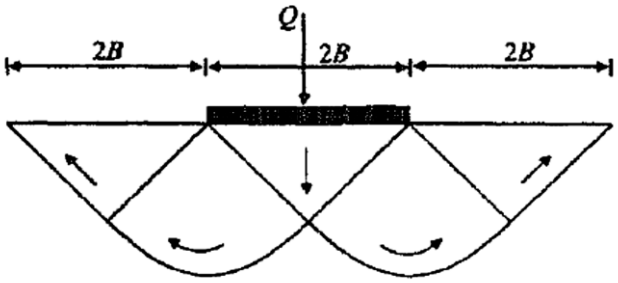


Figure 3.9. Prandtl type failure mechanism (Prandtl, 1920) (Adapted from Potts and Zdravkovic, 2001).

Various mesh creation procedures were applied to several selected finite element models and a great deal of effort has been spent to find out a suitable procedure whose result is converged to the exact value of bearing capacity factor at most. Consequently, the best result obtained is 5.16 and this value is only %0.4 greater than the exact value of bearing capacity factor (π+2= 5.14). Furthermore, failure mechanism and shear surfaces formed at the ultimate state beneath the footing are shown in Figure 3.10 and Figure 3.11

respectively. As Figure 3.10 is examined, it is seen that failure mechanism obtained by Plaxis 2D is the same with that presented by Prandtl (1920). It should also be noted that due to the symmetry condition, only right half of the footing was modelled and then analyzed.

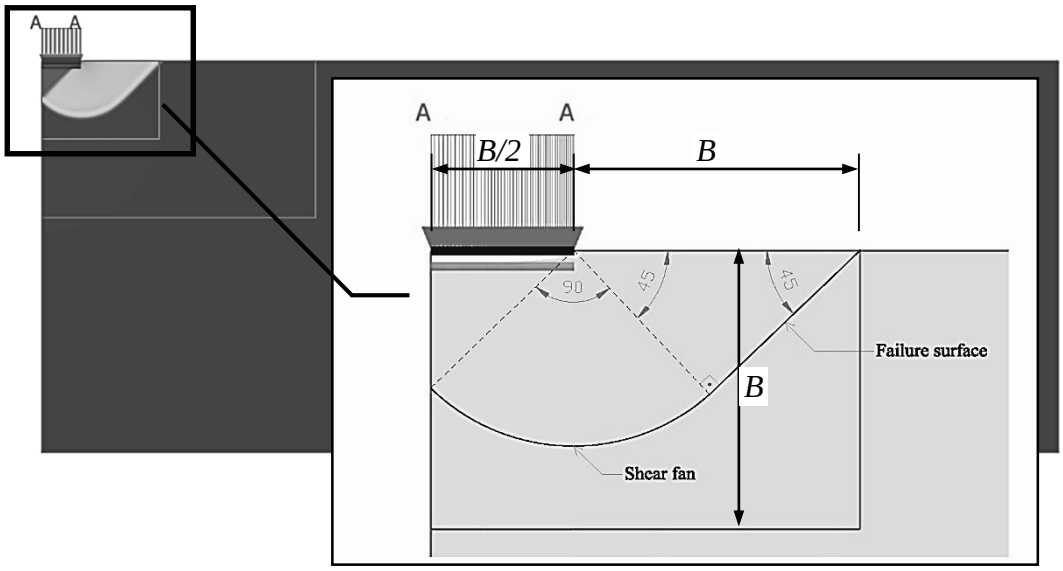


Figure 3.10. Failure mechanism determined by Plaxis 2D at the ultimate state and its enlarged view.



Figure 3.11. Shear surfaces determined by Plaxis 2D at the ultimate state.

The specific zone beneath the footing where mesh refinement should be applied was determined by detailed studies as stated in above. However, as seen in Figure 3.5, this zone where high stress and strain concentrations are observed corresponds to the small part of the whole model. Thus, it still remains as a question how to generate finite elements mesh

for the whole model by developing a definite mesh creation procedure that can be applied to all numerical models created in this study.

For this reason, various mesh creation procedures were tried. Consequently, the optimum mesh generation procedure which yields results with sufficient accuracy while keeping computational time at an acceptable level has been found. This procedure comprises of four steps. Description of each step is given in the following. Typical connectivity plot obtained as a result of the application of this procedure is shown in Figure 3.12.

- Set “fine” the global coarseness of the mesh initially and generate the mesh.
- Refine No.2 and No.3 clusters shown in Figure 3.12 simultaneously.
- Refine No.3 cluster again.
- Refine the mesh around both edges of the footing.

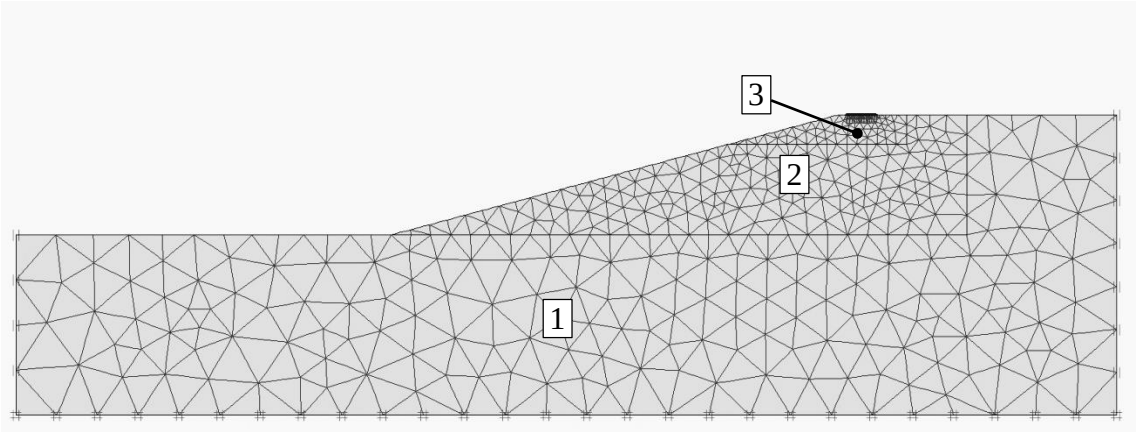


Figure 3.12. Typical connectivity plot obtained applying to developed mesh generation procedure (β= 15°, H= 8.0m; λ= 0.25).

A sample problem was chosen to evaluate whether mesh creation procedure is efficient and the variation of seismic bearing capacity factor (N_{cse}) with the number of triangular elements used in the model was investigated. As shown in Figure 3.13, for a selected set of parameters, calculated seismic bearing capacity factor has converged quite well to its limit value by following the mesh generation procedure. Furthermore, it can also be concluded that the same value of seismic bearing capacity factor was approximately found by using the number of elements that is equal to one-fourth of that used for its limit

value. Essentially, these facts indicate that the developed mesh generation procedure is quite reasonable according to the criteria expressed earlier.

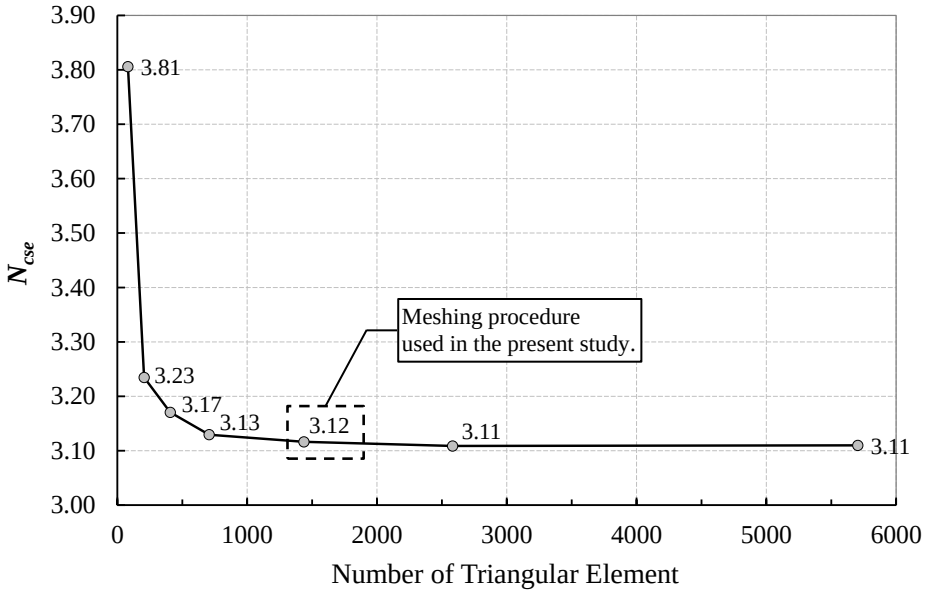


Figure 3.13. Variation of N_{cse} with the number of triangular elements (β= 30°, H= 4.0m, λ= 0, c_u= 100kPa, k_h= 0.2).

3.5.8. Generation of Initial Stresses

The first stage in the solution of geotechnical engineering problems by FEM is always to generate initial stresses within undisturbed soil material mobilized due to the gravity. To do so, Plaxis 2D software has two options called as "K_0 procedure" and Gravity loading". As a rule, one should only use "K_0 procedure" in cases with a horizontal surface with any soil layers and phreatic lines parallel to the surface. For all other cases one should use "Gravity loading" (Brinkgreve *et al.*, 2006). Since created finite elements models do not involve a horizontal ground surface, initial stresses were generated in the first calculation stage using "Gravity loading" option.

3.6. Solution of Finite Element Model and Determination of Seismic Bearing Capacity Factor (N_{cse}) by Calculations Module of Plaxis 2D

In order to determine seismic bearing capacity, and accordingly, seismic bearing capacity factor, an input file should be created in accordance with the principles given in

Chapter 3.5 and be analyzed in Calculations module of the software by defining related calculation stages. Four calculation stages, needed to be defined for the solution of the problem, are given in the following. Accordingly, these calculation stages are,

- Generation of initial stresses using “Gravity loading” option.
- Activation of footing, interface and unit load (load system A).
- Activation of inertia force acting on soil clusters.
- Increasing the unit load by the load factor (*Σ-MloadA*) until reaching failure condition.

Typical view of Calculations module of Plaxis 2D software in which related calculation stages were already defined is presented in Figure 3.14.

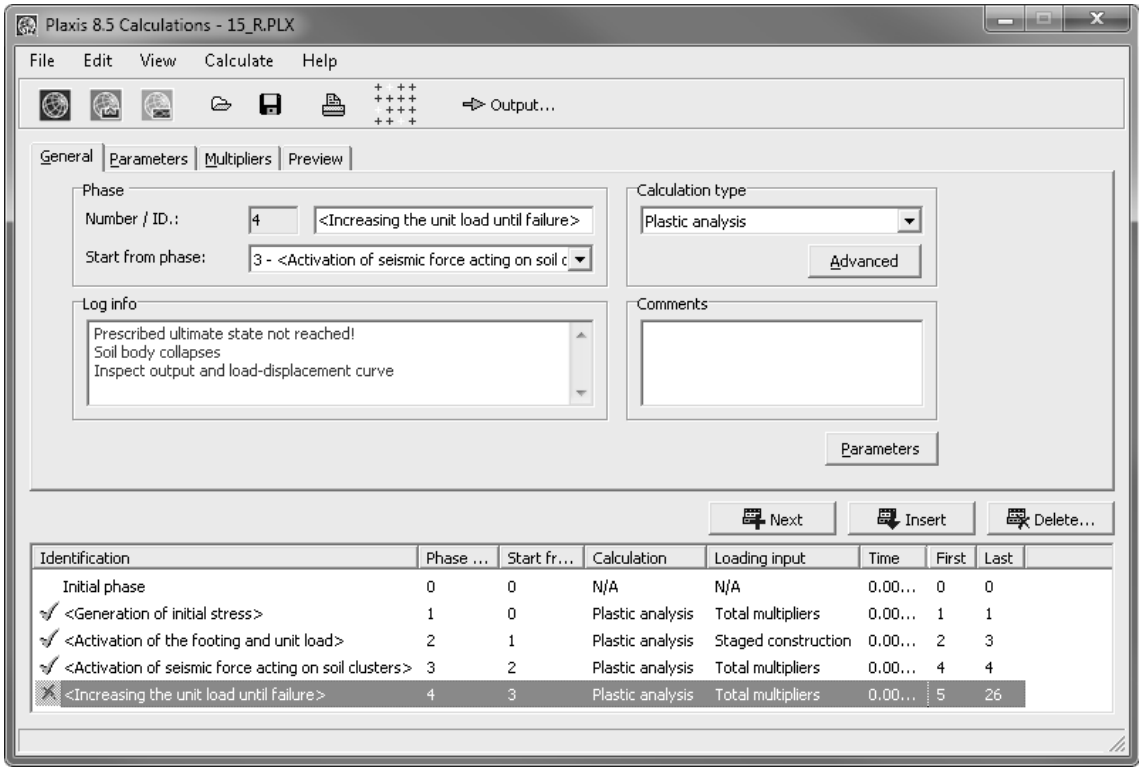
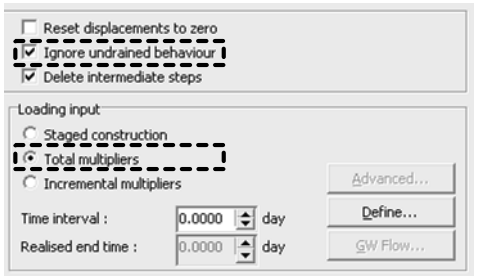
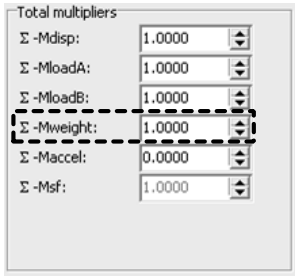
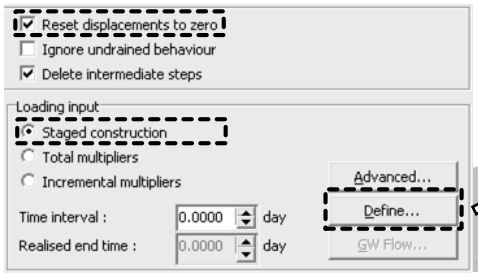
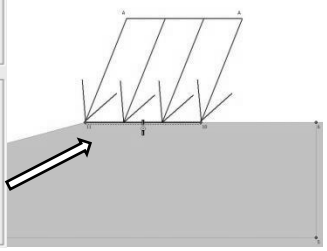
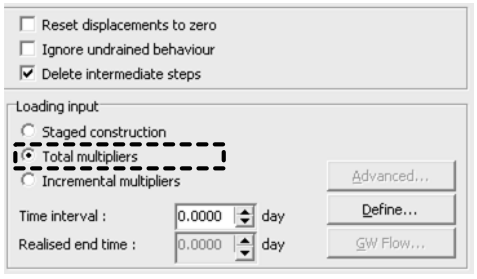
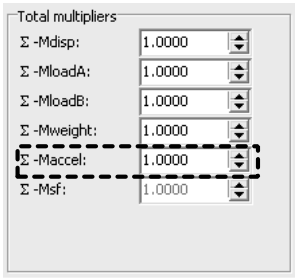
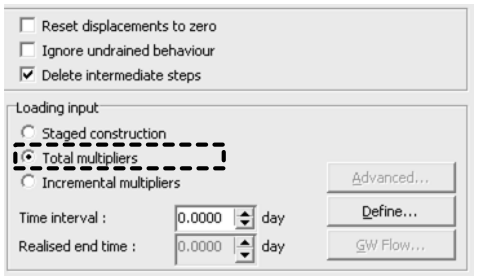
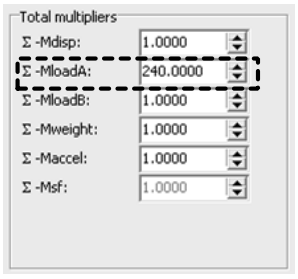


Figure 3.14. Typical view of “Calculations Module” window.

Additionally, adjustments to be made in each calculation stage are shown in detailed in Table 3.3 by means of graphical illustrations taken from Calculations module of the software.

Table 3.3. In “Parameters” and “Multipliers” tabs adjustments to be made in each calculation stage.

Phase Number	Identification	Parameters Tab Settings	Multipliers Tab Settings
1	Generation of initial stresses.		
2	Activation of surficial strip footing, interface and unit load.		
3	Activation of inertia force acting on soil clusters.		
4	Increasing the unit load until failure.		

After all calculation stages are defined as given in Table 3.3, the analysis of each calculation stage is performed separately. It should also be expressed that “standard setting” option of the software was used for the “iterative procedure” in all finite elements models created.

Failure was observed either at the first, the third or the fourth calculation stage in all numerical models created in this study. Accordingly, observation of soil failure at the end of the first calculation stage simply indicates that cohesive slope cannot maintain its stability under the influence of only gravity. Similarly, observation of soil failure at the end of the third calculation stage indicates that cohesive slope loses its stability by the influence of inertia force acting on slope soil as a result of seismic event. Finally, observation of the failure at the end of the fourth calculation stage indicates that footing-on-slope system reaches its ultimate seismic bearing capacity with various failure mechanisms. Therefore, seismic bearing capacity factor was only calculated for numerical models in which failure was observed at the end of the fourth calculation stage.

Seismic bearing capacity factor (N_{cse}) is determined by means of the load factor (*Σ-MloadA)* calculated by Plaxis 2D. For instance, as shown in Figure 3.15, the value of calculated load factor at the end of the fourth calculation phase is 128.11 for the numerical model whose model code is C_30_2_3_200_0.3_D (β= 30°, H= 2.0m, λ=3, c_u= 200 kPa, k_h= 0.3).

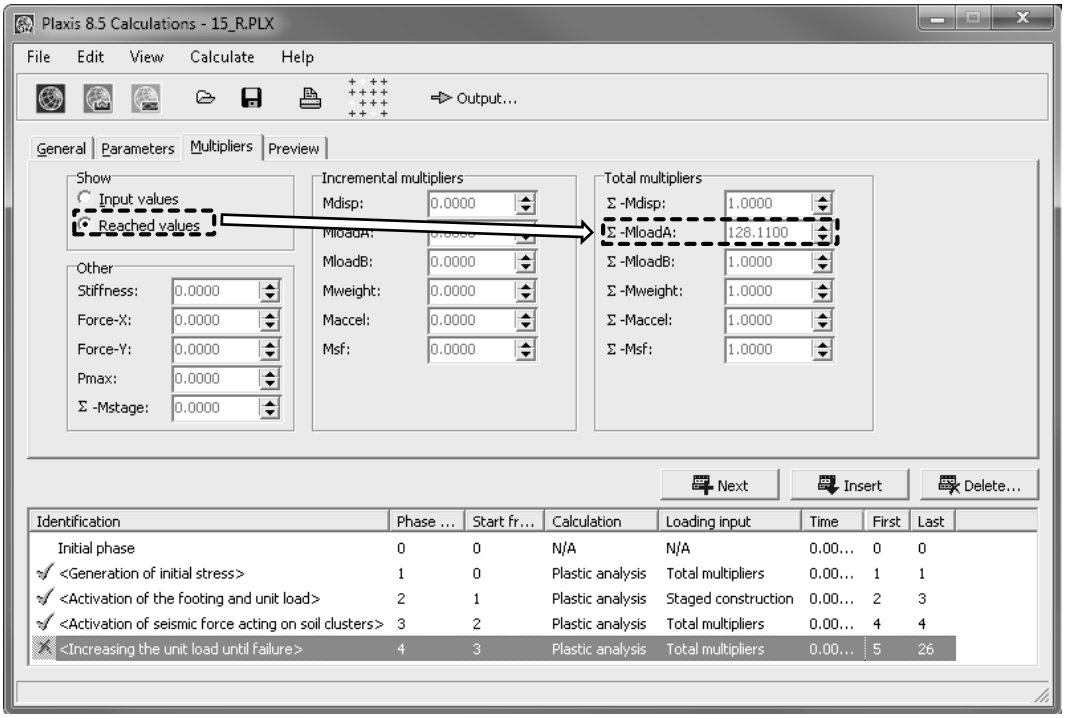


Figure 3.15. The load multiplier (*Σ-MloadA)* obtained by using Calculations module of Plaxis 2D for the ultimate limit state.

In this case, seismic bearing capacity of footing-on-slope system (q_f),

$$q_f \text{ (kPa)} = \text{Magnitude of vertical component of unit load (kPa)} \times \Sigma\text{-}MloadA$$

$$q_f = 5 \times 128.11 = 641 \text{ kPa} \tag{3.3}$$

Based Equation 3.1, seismic bearing capacity factor (N_{cse}),

$$N_{cse} = \frac{q_f}{c_u} = \frac{641}{200} = 3.21 \tag{3.4}$$

3.7. Evaluation of Plaxis 2D Outputs

As mentioned in Chapter 3.6, seismic ultimate bearing capacity and seismic bearing capacity factor can be determined by the load factor calculated using Calculations module of the software. However, failure mechanism and shear surfaces formed beneath the footing are other significant issues that should be taken into consideration. Both failure mechanism and shear surfaces formed beneath the footing can be readily seen by using Outputs module of the software. To do so, while "Total increments" option should be used to view failure mechanism obtained, "Incremental shear strain" option should be used to view shear surfaces formed beneath the footing. For instance, for the finite elements model whose model name is C_30_2_3_200_0.3_D (β= 30°, H= 2.0m, λ=3, c_u= 200 kPa, k_h= 0.3), the failure mechanism and shear surfaces obtained at the ultimate state is presented in Figure 3.16 and Figure 3.17 respectively.

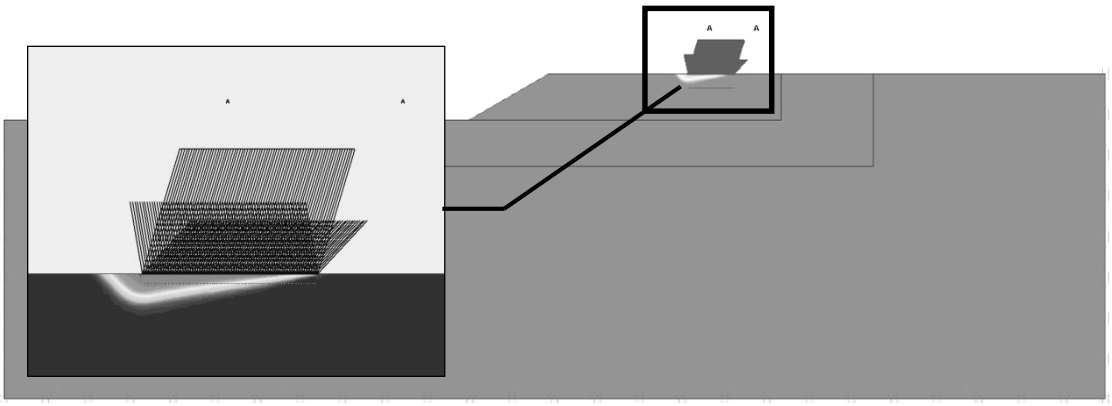


Figure 3.16. Failure mechanism obtained for the finite element model named as C_30_2_3_200_0.3_D and enlarged view of the failure mechanism.

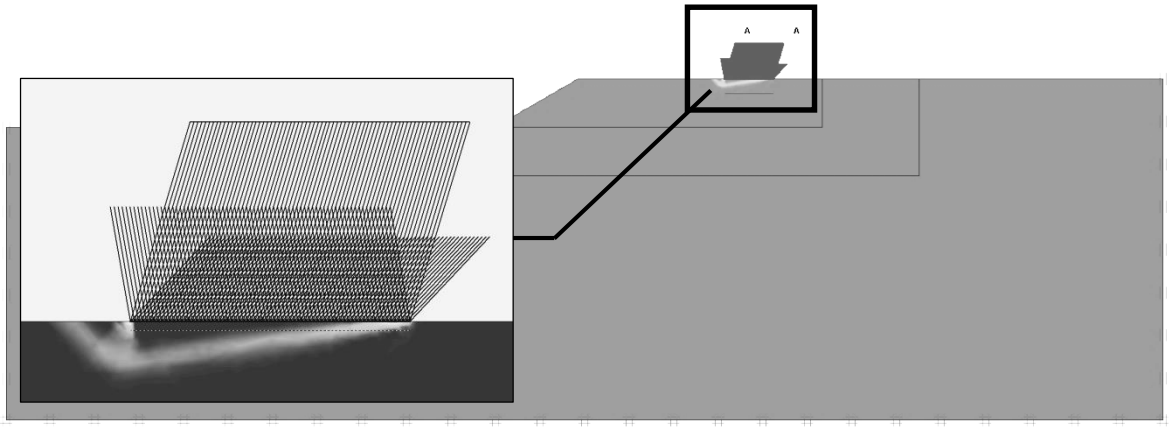


Figure 3.17. Shear surfaces obtained for the finite element model named as C_30_2_3_200_0.3_D and enlarged view of the shear surfaces.

3.8. Comparison of Numerical Model Results with Previous Researches

In this chapter of the thesis, results determined by Plaxis 2D will be compared with those of the results of previous researchers who worked on the same problem. Accuracy of the numerical model created in this study will be verified based on these comparisons. As stated in Chapter 3, a verification procedure that comprises of three stages totally will be applied to results obtained by FEM. In the first two stage of the verification procedure, static and seismic bearing capacity factors of footing-on-slope system determined by Plaxis 2D will be compared to those presented previously by other researchers. Then, it will be discussed that whether results of FEM are consistent with previous findings. In the final stage, results of numerical models in which overall slope failure was determined in either static or seismic condition prior to the application of footing pressure will be compared with findings of previous researches.

3.8.1. Comparisons Made for Static Condition

The first comparison for the static condition was made for the specific case that the footing is on the edge of the slope (λ= 0). The variation of static bearing capacity factor (N_{cs}) with slope angle (β) is investigated and results of the present study and the results of all previous studies given in Chapter 2.1, are compared. Consequently, it is obviously seen

in the chart presented in Figure 3.18 that static bearing capacity factor decreases with the increase of slope angle. Bowles (1997) overestimated the values of seismic bearing capacity factor for all slope angles. While Castelli and Motta (2010) estimated greater values than results presented by other researchers for small slope angles ($\beta \leq 15°$), seismic bearing capacity factor took smaller values than general distribution shown on the chart with the increase of slope angle. Results of FEM indicate perfect agreement with all studies, except that of Bowles (1997) and Castelli and Motta (2010).

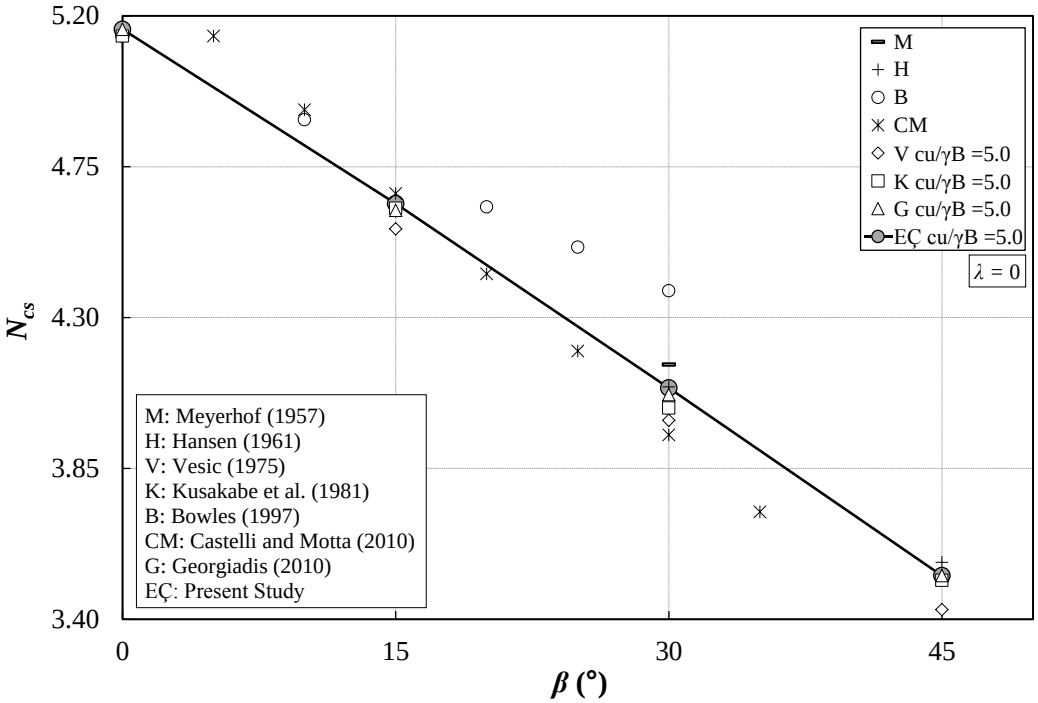


Figure 3.18. Variation of N_{cs} with β (For λ= 0, $c_u/\gamma B$= 5).

The second comparison of static condition was made for a relatively more common case for which the footing is far away from the slope edge (λ> 0). The variation of static bearing capacity factor (N_{cs}) with normalized footing distance (λ) was investigated and results of the thesis study and of five previous studies given in Chapter 2.1 were compared. Consequently, it is seen in the chart presented in Figure 3.19 that static bearing capacity factor increases with the increase in the normalized footing distance. This increase continues until the threshold value of the normalized footing distance. Beyond the threshold value of the normalized footing distance, the value of static bearing capacity factor does not vary and it is constant. Results found for all normalized footing distances indicate a good agreement with those of Kusakabe *et al.* (1981) and Georgiadis (2010).

However, the results of remaining three research studies are different than those obtained by FEM. In this context, the maximum difference between the results of FEM and those presented by other researchers is %6.3.

As a result of the two comparisons made, it can be said that the results of finite elements model have sufficient accuracy for both cases in static condition.

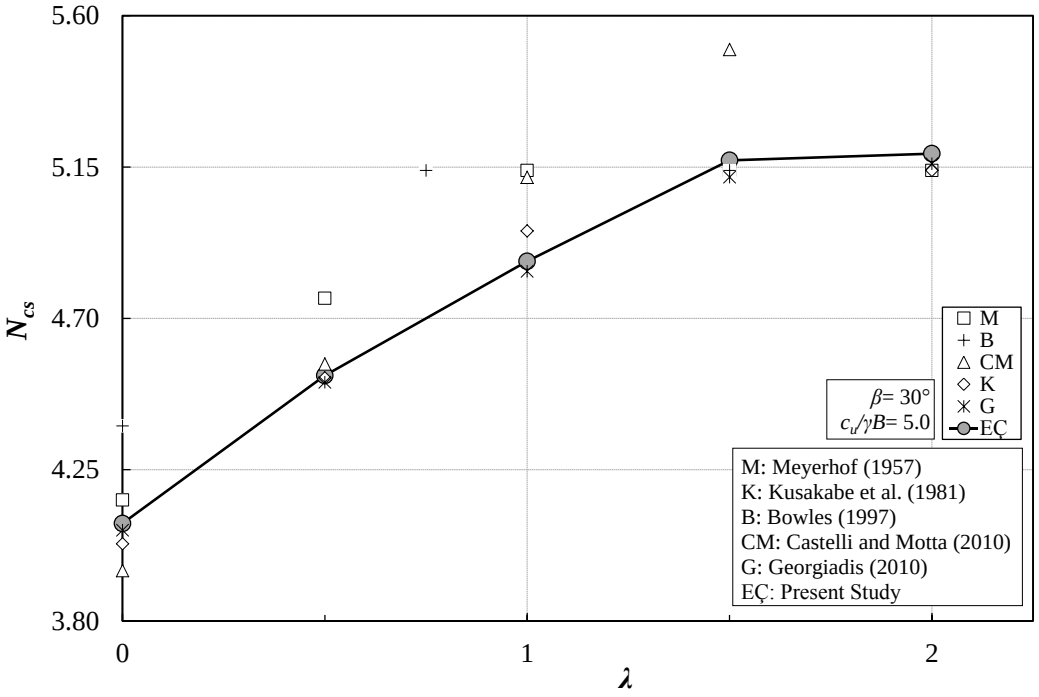


Figure 3.19. Variation of N_{cs} with λ (For β= 30°, $c_u/\gamma B$= 5).

3.8.2. Comparisons Made for Seismic Conditions

As being similar to the evaluations performed for static condition, the first comparison of seismic condition was also made for the case that the footing is on the edge of the slope (λ= 0). The variation of seismic bearing capacity factor (N_{cse}) with horizontal seismic acceleration coefficient (k_h) was investigated and results of the thesis study and of three previous studies (Kumar and Rao, 2003; Castelli and Motta, 2010; Farzaneh *et al.*, 2013) referred to in Chapter 2.2 were compared. As shown in the chart presented in Figure 3.20, seismic bearing capacity factor decreases considerably with the increase in horizontal earthquake acceleration coefficient. Results of FEM indicate a perfect agreement with other values given in literature for the slope angle values of 15 and 45. However, Castelli and Motta (2010) and Farzaneh *et al.* (2013) estimated smaller values in general than those

obtained by FEM for the slope angle of 30 degrees. The maximum difference between the results of FEM and those of other researches is only %4.2.

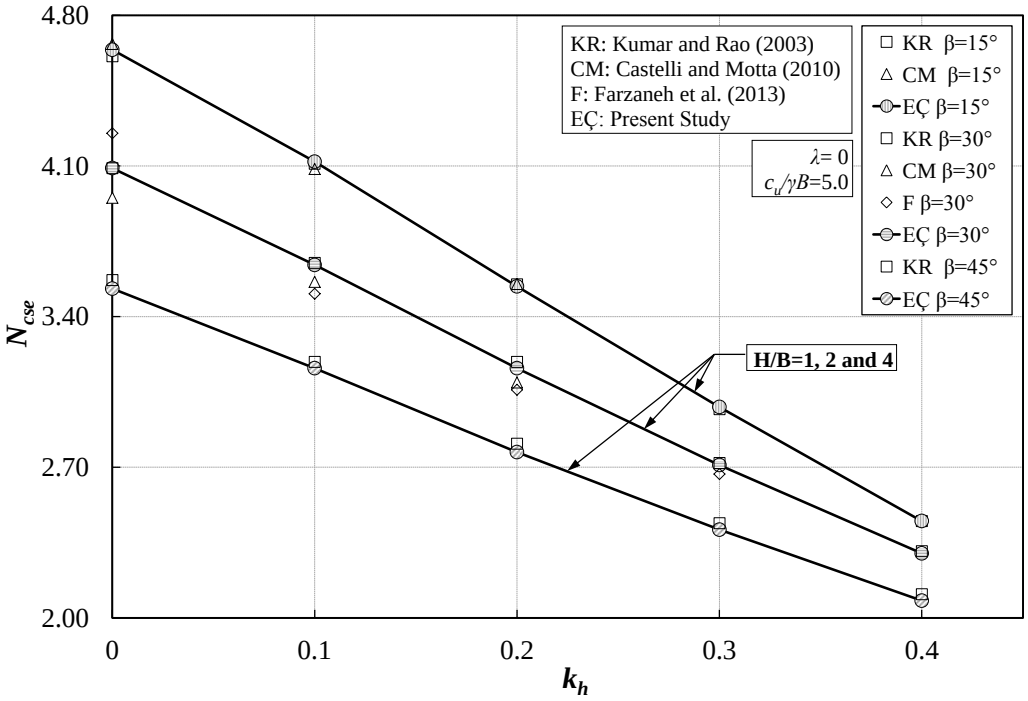


Figure 3.20. Variation of N_{cse} with k_h for all slope angles (For λ= 0, $c_u/\gamma B$= 5).

The second comparison of seismic condition was made for a more common case relatively for which the footing is far away from the slope edge (λ> 0). The variation of seismic bearing capacity factor (N_{cse}) with normalized footing distance (λ) was investigated and results of the thesis study and of two researches given in Chapter 2.2 were compared. Consequently, as being similar to the static condition results, it is seen in the chart presented in Figure 3.21 that seismic bearing capacity factor increases with the increase of the normalized footing distance until reaching to the threshold value of the normalized footing distance. Though seismic bearing capacity factors calculated for the normalized footing distances beyond threshold value are different, it can be said that the results of finite elements method are very close to the values given by Castelli and Motta (2010). Moreover, it is considered that Farzaneh *et al.* (2013) which is in fact a lower bound solution is too conservative indeed particularly for normalized footing distances greater than zero. The maximum difference between the results of FEM and those of other researches is %12.2. Even though the difference between obtained seismic bearing capacity factors reaches to considerable values, developed numerical model is quite

promising about convergence to the exact solution since the results of this study take place between the results of other two researches. Therefore, it is concluded that created numerical model has sufficient accuracy in seismic condition as well.

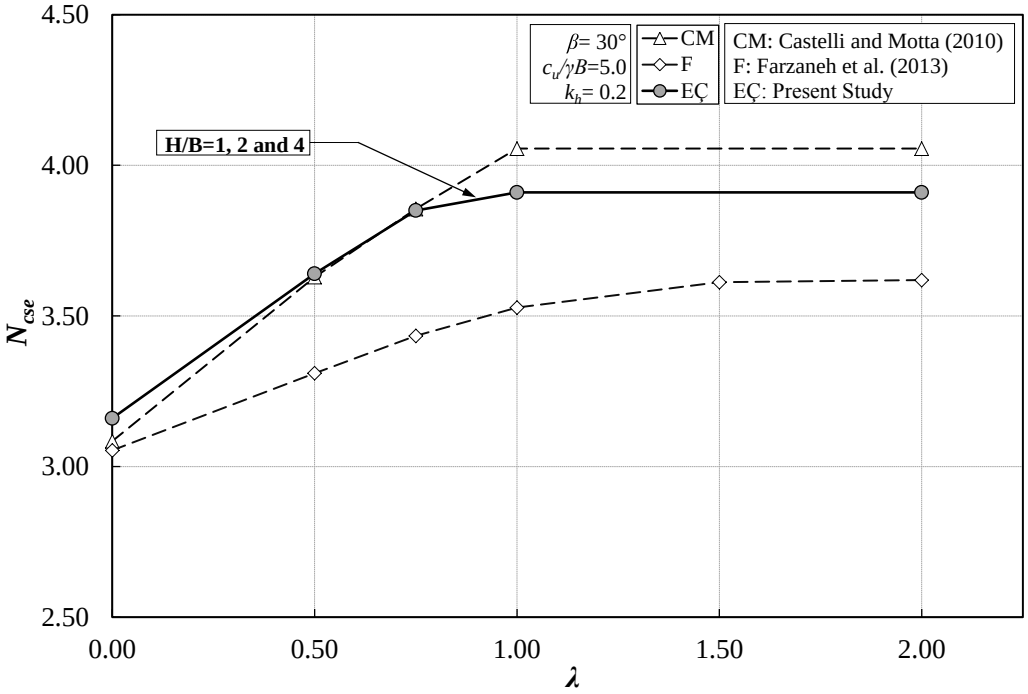


Figure 3.21. Variation of N_{cse} with λ (For β= 30°, $c_u/\gamma B$= 5, k_h= 0.2).

3.8.3. Stability Assessment of Cohesive Slopes Both in Static and Seismic Condition

When the results of finite elements models are examined, it is understood that there are numerous cases in which the cohesive slope loses its overall stability by the influence of self-weight in static condition or by the influence of inertia force in seismic condition prior to the application of ultimate seismic base pressure. Accordingly, determination of failure at the end of the first calculation stage means that the slope loses its stability in static condition. Similarly, determination of failure at the end of the third calculation stage means that the slope loses its stability in seismic condition. It will be discussed in this chapter that whether the results obtained by the developed numerical model are consistent with those presented previously. Evaluations will be performed separately for static and seismic conditions.

Depending on slope geometry and soil strength, the maximum height (H_{cr}) which a cohesive slope can stand without any stability loss can be determined by Taylor (1937). Accordingly, geometric and strength properties of cohesive slopes which are unstable by the influence of self-weight are given in Table 3.4.

Table 3.4. H_{cr} values calculations and stability assessment of cohesive slopes in static condition by using Taylor's method.

H **(m)**	***D***	***β*** **(°)**	***m***	***γ*** **(kN/m^3)**	c_u **(kPa)**	H_{cr} **(m)**	**Stability Check**
2	7	15	0.182	20	200	54.9	Stable
4	4	15	0.176	20	200	56.8	Stable
8	2.5	15	0.154	20	200	64.9	Stable
2	7	30	0.182	20	200	54.9	Stable
4	4	30	0.180	20	200	55.6	Stable
8	2.5	30	0.175	20	200	57.1	Stable
2	7	45	0.182	20	200	54.9	Stable
4	4	45	0.180	20	200	55.6	Stable
8	2.5	45	0.180	20	200	55.6	Stable
2	7	15	0.182	20	100	27.5	Stable
4	4	15	0.176	20	100	28.4	Stable
8	2.5	15	0.154	20	100	32.5	Stable
2	7	30	0.182	20	100	27.5	Stable
4	4	30	0.180	20	100	27.8	Stable
8	2.5	30	0.175	20	100	28.6	Stable
2	7	45	0.182	20	100	27.5	Stable
4	4	45	0.180	20	100	27.8	Stable
8	2.5	45	0.180	20	100	27.8	Stable
2	7	15	0.182	20	50	13.7	Stable
4	4	15	0.176	20	50	14.2	Stable
8	2.5	15	0.154	20	50	16.2	Stable
2	7	30	0.182	20	50	13.7	Stable
4	4	30	0.180	20	50	13.9	Stable
8	2.5	30	0.175	20	50	14.3	Stable
2	7	45	0.182	20	50	13.7	Stable
4	4	45	0.180	20	50	13.9	Stable
8	2.5	45	0.180	20	50	13.9	Stable
2	7	15	0.182	20	25	6.9	Stable
4	4	15	0.176	20	25	7.1	Stable
8	2.5	**15**	0.154	20	**25**	**8.1**	**Unstable**
2	7	30	0.182	20	25	6.9	Stable
4	4	30	0.180	20	25	6.9	Stable
8	2.5	**30**	0.175	20	**25**	**7.1**	**Unstable**
2	7	45	0.182	20	25	6.9	Stable
4	4	45	0.180	20	25	6.9	Stable
8	2.5	**45**	0.180	20	**25**	**6.9**	**Unstable**

When Table 3.4 is examined, it is readily seen that if c_u and H take the values of 25 kPa and 8.0 m respectively, cohesive slopes are unstable for all slope angles considered in this study. Though H_{cr} was calculated as 8.1 m for a certain set of parameters (β= 15°, c_u= 25 kPa and H=8.0 m), difference between height values (H and H_{cr}) is extremely small. Also, base failure was determined in the corresponding numerical model (shown in Figure 3.22). In static condition, numerical model results are fully consistent with the previous findings of Taylor (1937). For three sets of parameters defined as "Unstable" in Table 3.4, failure mechanisms obtained by Plaxis 2D are shown in Figure 3.22, Figure 3.23 and Figure 3.24.

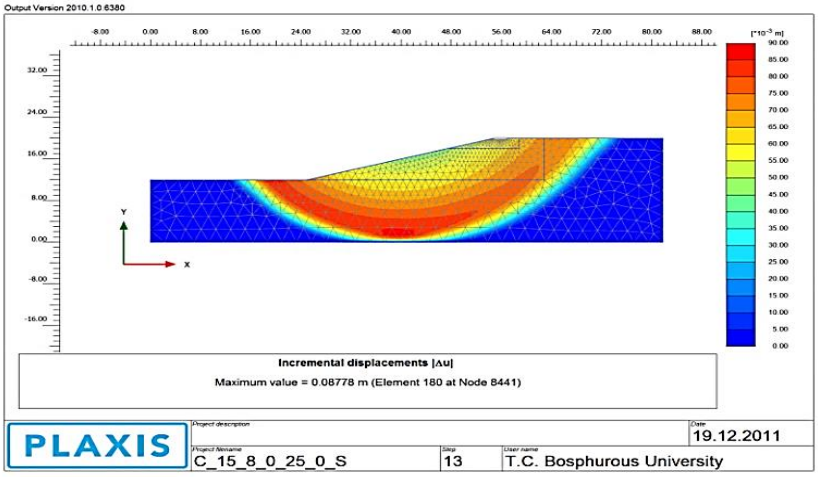


Figure 3.22. Failure mechanism of unstable cohesive slope in static condition (β= 15°, H=8.0 m and c_u= 25 kPa).

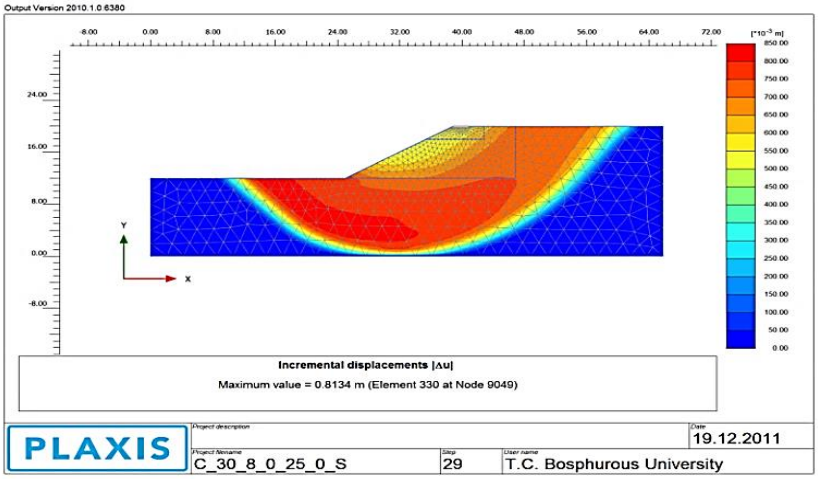


Figure 3.23. Failure mechanism of unstable cohesive slope in static condition (β= 30°, H=8.0 m and c_u= 25 kPa).

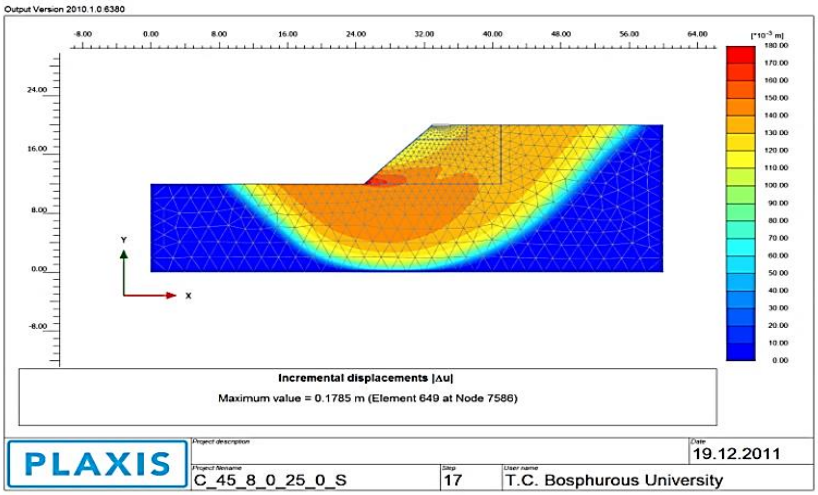


Figure 3.24. Failure mechanism of unstable cohesive slope in static condition (β= 45°, H=8.0 m and c_u= 25 kPa).

Depending on slope geometry, soil strength and seismic effect, the maximum height (H_{cr}) which a cohesive slope can withstand without any stability loss can be determined by Koppula (1984) for seismic conditions. However, since there is an ample number of influential parameters, number of combinations increases considerably for seismic conditions. For this reason, a small part of the entire table (H= 4 m) is presented in Table 3.5. The table, in its entirety, is given in Appendix-A.

Table 3.5. H_{cr} values calculations and stability assessment of cohesive slopes in seismic condition using Koppula's method.

***H* (m)**	***D***	***β* (°)**	***k_h***	***N_2***	***γ* (kN/m³)**	***c_u* (kPa)**	***H_cr* (m)**	**Stability Check**
4	4	30	0.1	3.24	20	200	32.4	Stable
4	4	30	0.2	2.11	20	200	21.1	Stable
4	4	30	0.3	1.49	20	200	14.9	Stable
4	4	30	0.4	1.08	20	200	10.8	Stable
4	4	30	0.1	3.24	20	100	16.2	Stable
4	4	30	0.2	2.11	20	100	10.5	Stable
4	4	30	0.3	1.49	20	100	7.4	Stable
4	4	30	0.4	1.08	20	100	5.4	Stable
4	4	30	0.1	3.24	20	50	8.1	Stable
4	4	30	0.2	2.11	20	50	5.3	Stable
4	4	**30**	**0.3**	1.49	20	**50**	**3.7**	**Unstable**
4	4	**30**	**0.4**	1.08	20	**50**	**2.7**	**Unstable**
4	4	**30**	**0.1**	3.24	20	**25**	**4.0**	**Unstable**
4	4	**30**	**0.2**	2.11	20	**25**	**2.6**	**Unstable**
4	4	**30**	**0.3**	1.49	20	**25**	**1.9**	**Unstable**
4	4	**30**	**0.4**	1.08	20	**25**	**1.3**	**Unstable**

Table 3.5. H_{cr} values calculations and stability assessment of cohesive slopes in seismic condition using Koppula's method (Cont.).

H **(m)**	***D***	***β*** **(°)**	k_h	N_2	***γ*** **(kN/m³)**	c_u **(kPa)**	H_{cr} **(m)**	**Stability Check**
4	4	45	0.1	2.73	20	200	27.3	Stable
4	4	45	0.2	1.68	20	200	16.8	Stable
4	4	45	0.3	1.15	20	200	11.5	Stable
4	4	45	0.4	0.81	20	200	8.1	Stable
4	4	45	0.1	2.73	20	100	13.7	Stable
4	4	45	0.2	1.68	20	100	8.4	Stable
4	4	45	0.3	1.15	20	100	5.8	Stable
4	4	45	0.4	0.81	20	100	4.0	Stable
4	4	45	0.1	2.73	20	50	6.8	Stable
4	4	45	0.2	1.68	20	50	4.2	Stable
4	4	**45**	**0.3**	1.15	20	**50**	**2.9**	**Unstable**
4	4	**45**	**0.4**	0.81	20	**50**	**2.0**	**Unstable**
4	4	**45**	**0.1**	2.73	20	**25**	**3.4**	**Unstable**
4	4	**45**	**0.2**	1.68	20	**25**	**2.1**	**Unstable**
4	4	**45**	**0.3**	1.15	20	**25**	**1.4**	**Unstable**
4	4	**45**	**0.4**	0.81	20	**25**	**1.0**	**Unstable**

When Table 3.5 is examined, it is readily seen that if H, β and c_u take the values of 4 m, 30° or 45° and 25 kPa respectively, cohesive slopes are unstable for all horizontal seismic acceleration coefficients considered in this study. Similarly, if c_u is 50 kPa, cohesive slopes are still unstable for the values of 0.3 and 0.4 of horizontal seismic acceleration coefficient. For some of the sets of parameters defined as "Unstable" in Table 3.5, failure mechanisms obtained by Plaxis 2D are shown in between Figure 3.25 and Figure 3.30. Although graphical outputs given for the base failure mode in seismic conditions seem like unrealistic, results of the stability evaluations performed by Plaxis 2D are fully consistent with those determined by Koppula (1984). Essentially, prior to the application of a base pressure near any cohesive slope, the engineer should have an idea about the stability condition of the slope in seismic conditions. Since both of these methods give the same answer to this critical question, that is clearly the stability loss by the influence of design earthquake, likely reasons of obtaining unrealistic failure mechanisms in seismic conditions were not examined in detail.

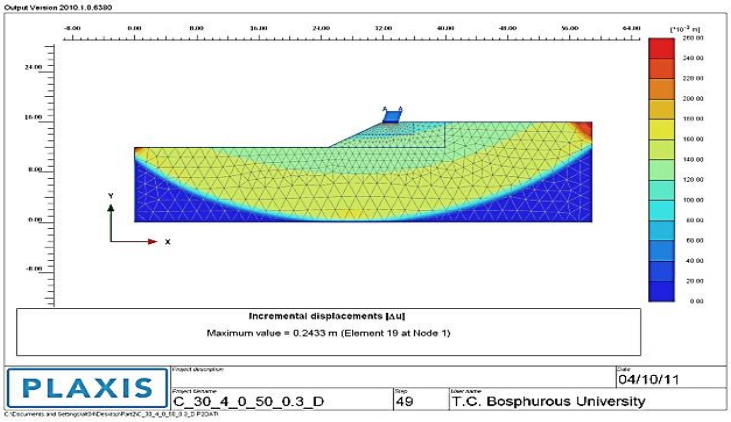


Figure 3.25. Failure mechanism of unstable cohesive slope in seismic condition (β= 30°, H= 4.0 m, c_u= 50 kPa, k_h= 0.3).

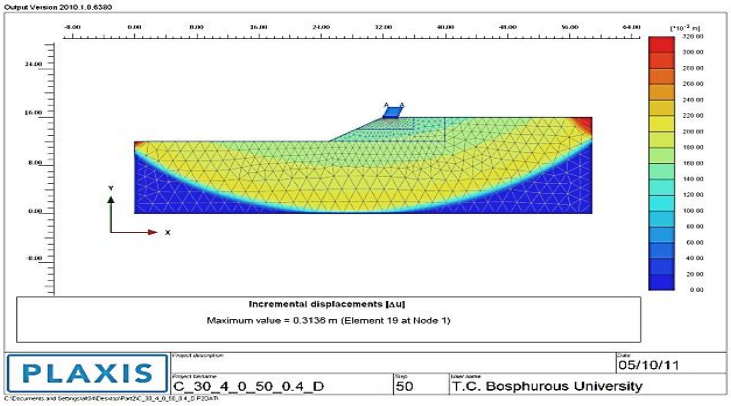


Figure 3.26. Failure mechanism of unstable cohesive slope in seismic condition (β= 30°, H= 4.0 m, c_u= 50 kPa, k_h= 0.4).

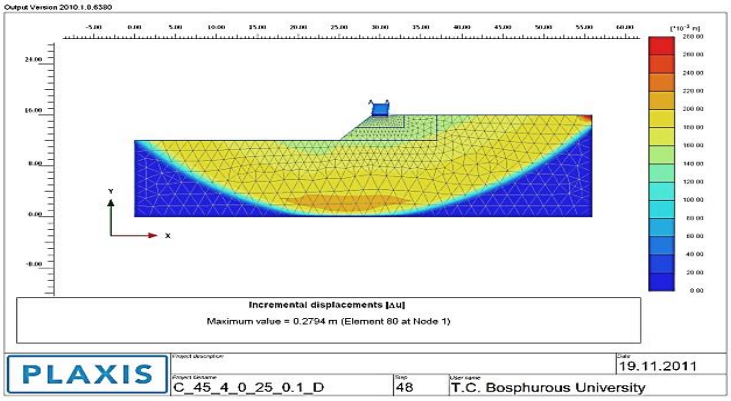


Figure 3.27. Failure mechanism of unstable cohesive slope in seismic condition (β= 45°, H=4.0 m, c_u= 25 kPa, k_h= 0.1).

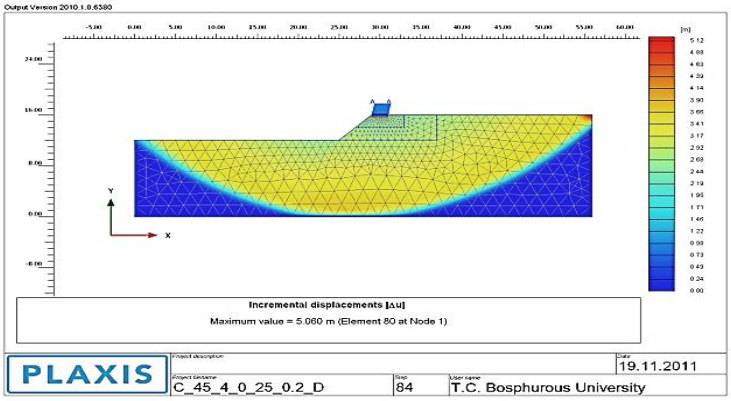


Figure 3.28. Failure mechanism of unstable cohesive slope in seismic condition (β= 45°, H=4.0 m, c_u= 25 kPa, k_h= 0.2).

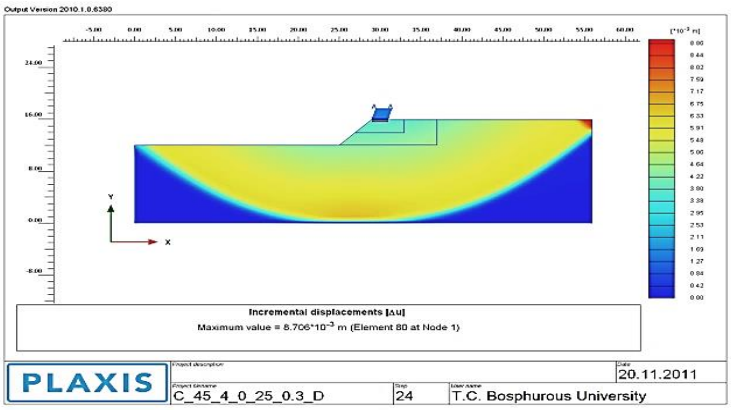


Figure 3.29. Failure mechanism of unstable cohesive slope in seismic condition (β= 45°, H=4.0 m, c_u= 25 kPa, k_h= 0.3).

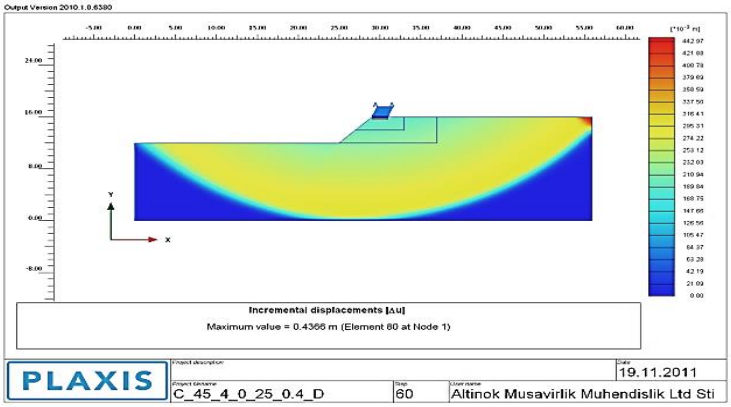


Figure 3.30. Failure mechanism of unstable cohesive slope in seismic condition (β= 45°, H=4.0 m, c_u= 25 kPa, k_h= 0.4).

4. RESULTS AND DISCUSSIONS

In this chapter, results of the parametric study made will be given. In this context, the aim is to clarify the parameters that are influential on seismic bearing capacity factor (N_{cse}) of surficial strip footings located near cohesive slopes. With the evaluations to be made, it would be possible that seismic bearing capacity factor is defined by a specific function of several influential variables. Also, another significant purpose of this chapter is to determine various types of failure mechanisms formed at the ultimate state by the influence of earthquake forces beneath the footing or within the cohesive slope. However, as it will be seen in the following parts of this chapter, it is not limited only with types of failure mechanisms determined at the ultimate state. Beyond that, the variation of type of failure mechanism with the influential parameters on seismic bearing capacity factor will be investigated and prepared diagrams regarding this issue will be presented.

As a result of this parametric study, a simple method that can be used even for routine applications of geotechnical engineering was developed. According to the methodology developed, parameters required to calculate seismic bearing capacity of footings located near cohesive slopes are simply undrained shear strength of cohesive slope soil (c_u) and seismic bearing capacity factor (N_{cse}). Undrained shear strength of cohesive soils can be readily determined using one of the techniques stated in Chapter 3.3. Seismic bearing capacity factor should be determined by design charts presented in the advancing part of this chapter as well. At the same time, these design charts indicate threshold distances at which effect of the slope on seismic bearing capacity disappears.

In the final part of this chapter, different than two issues mentioned above (determination of seismic bearing capacity factor and failure mechanism formed at the ultimate state), other remarkable consequences found will be addressed.

4.1. Determination of Influential Parameters

There are five parameters which influence seismic bearing capacity factor directly or indirectly. These parameters are horizontal seismic acceleration coefficient (k_h), slope angle (β), normalized footing distance from the slope edge (λ), normalized slope height (H/B) and normalized undrained cohesive slope soil strength ($c_u/\gamma B$). When results of parametric study given in tabular form in Appendix C are investigated, aforementioned parameters can be readily found out. The influence of each parameter on seismic bearing capacity factor will be described in detail in the following.

4.1.1. Influence of Horizontal Seismic Acceleration Coefficient

Seismic bearing capacity factor (N_{cse}) decreases dramatically with the increase of horizontal seismic acceleration coefficient (k_h). As shown in the chart presented in Figure 4.1, it is obvious that horizontal seismic acceleration coefficient has a reducing influence on seismic bearing capacity factor for all normalized footing distances considered in this study.

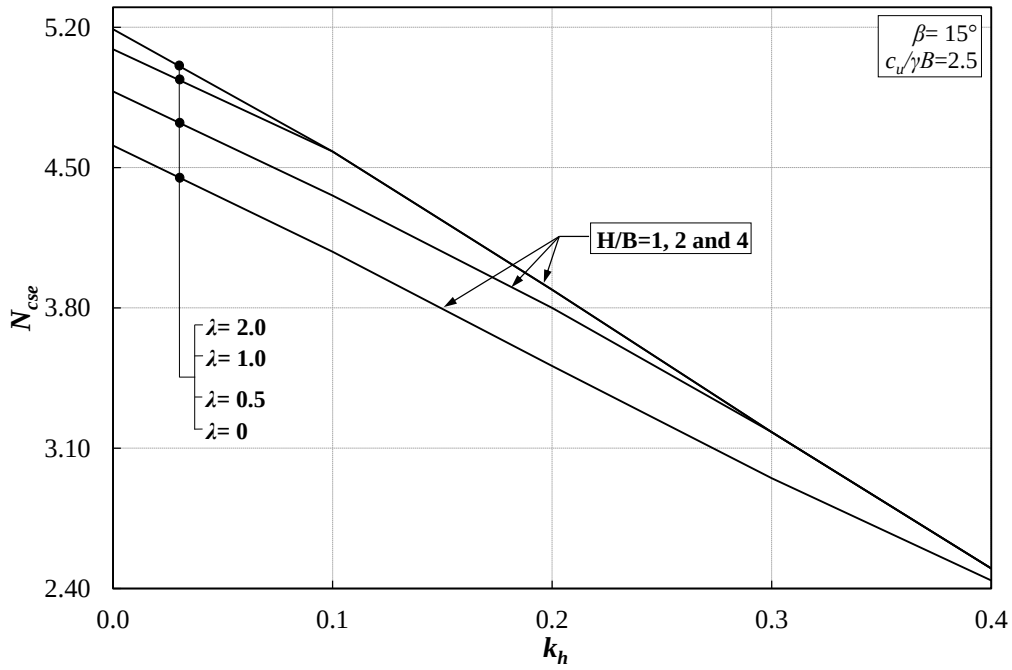


Figure 4.1. Variation of N_{cse} with k_h for all λ values (β= 15°, $c_u/\gamma B$= 2.5).

4.1.2. Influence of Slope Angle

Seismic bearing capacity factor (N_{cse}) decreases with the increase of slope angle (β). But this is only valid under the circumstance in which the footing is closer than threshold distance to the slope edge ($\lambda \leq \lambda_0$) (it should be noted that for each set of parameters, the threshold value of normalized footing distance may vary). For instance, in the chart shown in Figure 4.2, it is seen that seismic bearing capacity factor has no relationship with slope angle for the greatest value of normalized footing distance considered in this study. This case clearly indicates that there is no reducing effect on seismic bearing capacity factor due to the presence of slope, since the footing is placed beyond the threshold distance. Otherwise, for smaller values of the normalized footing distance, it can be said that seismic bearing capacity factor decreases considerably with the increase of slope angle particularly for footings placed on the slope edge ($\lambda = 0$).

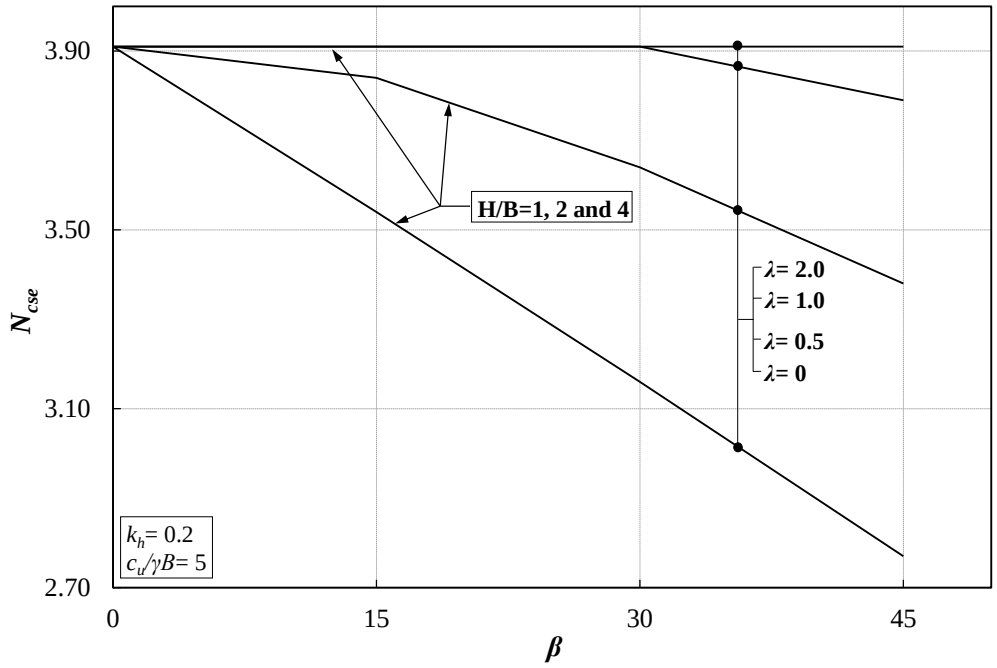


Figure 4.2. Variation of N_{cse} with β for all λ values (k_h= 0.2, $c_u/\gamma B$= 5).

4.1.3. Influence of Normalized Footing Distance

The influence of normalized footing distance (λ) on seismic bearing capacity factor (N_{cse}) can be briefly summarized. As seen in Figure 4.3, seismic bearing capacity factor

increases until reaching the threshold distance, as the footing moves away from the slope edge. For greater values of the normalized footing distance than threshold value, reduction in the seismic bearing capacity factor due to the presence of slope is no longer valid and seismic bearing capacity factor takes nearly the same values. In this case, the inertia force acting on footing and soil mass is the only reason why seismic bearing capacity factor takes lesser values relatively than those calculated in static condition. Another significant conclusion to be drawn from the chart presented in Figure 4.3 is that threshold distance decreases with the increase of horizontal seismic acceleration coefficient. It can be explained by the fact that failure mechanism passes through shallower depths with the increase of horizontal seismic acceleration coefficient.

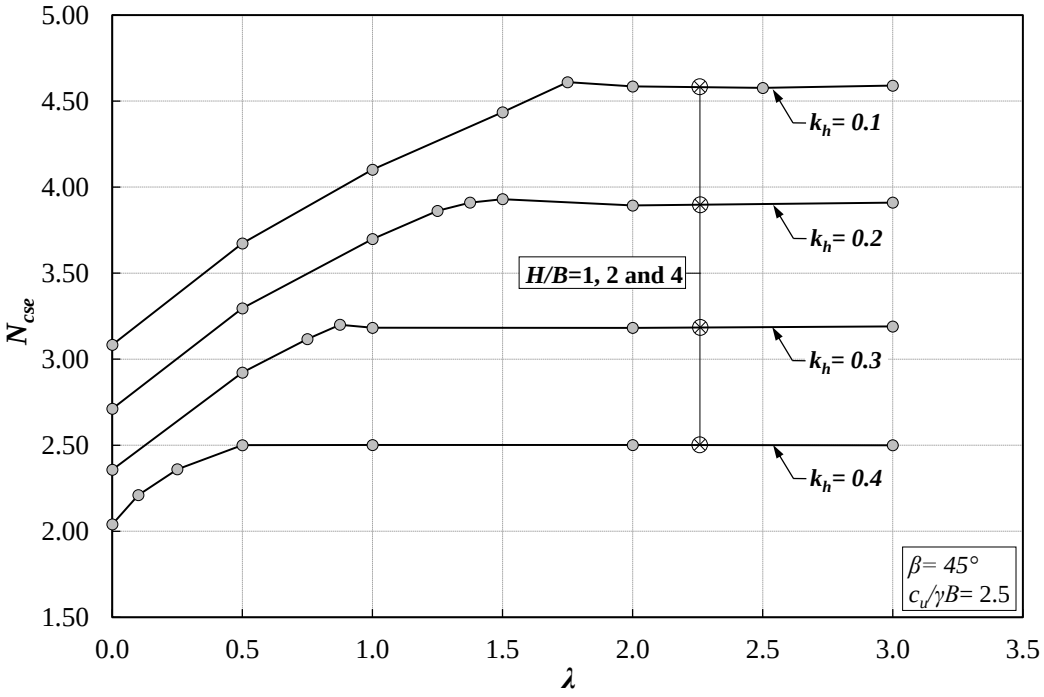


Figure 4.3. Variation of N_{cse} with λ for all k_h values (β= 45°, $c_u/\gamma B$= 2.5).

4.1.4. Influence of Slope Height

Slope height (H) was normalized with footing width (B) and then the influence of the H/B ratio was investigated. Essentially, the influence of normalized slope height on seismic bearing capacity factor is negligible for circumstances in which the footing reaches to its ultimate seismic capacity with "foundation failure" failure mode (a few exceptional cases were also observed). However, for the smaller values of $c_u/\gamma B$ ratio, the failure mode varies

as *H*/*B* ratio increases. Accordingly, as *H*/*B* ratio increases, failure mode transition from "foundation failure" to "base failure due to earthquake" was initially observed. Then, the transition proceeds towards other failure mode called "base failure due to self-weight of slope". Two findings expressed in above can be easily seen in the lists given in Appendix C.

4.1.5. Influence of Slope Soil Strength

It was previously mentioned that due to selected material model and assumptions made, the unique parameter that may affect seismic bearing capacity factor is undrained shear strength of cohesive slope soil (c_u). Likewise, this parameter was also normalized with γB and then the influence of slope soil strength on seismic bearing capacity factor was investigated. As seen in the chart presented in Figure 4.4, seismic bearing capacity factor (N_{cse}) increases with the increase of $c_u/\gamma B$ ratio. However, it is understood from presented chart that the influence of this factor is quite limited for the values greater than 1.25. The reason why lack of some data points for k_h=0.2, 0.3 and 0.4 curves is that the failure mode was determined as "base failure due to earthquake effect" for these sets of parameters (various combinations of geometrical, soil strength and seismic parameters). Like the influence of *H*/*B* ratio, there is a definite transition between various failure modes expressed previously as $c_u/\gamma B$ ratio decreases.

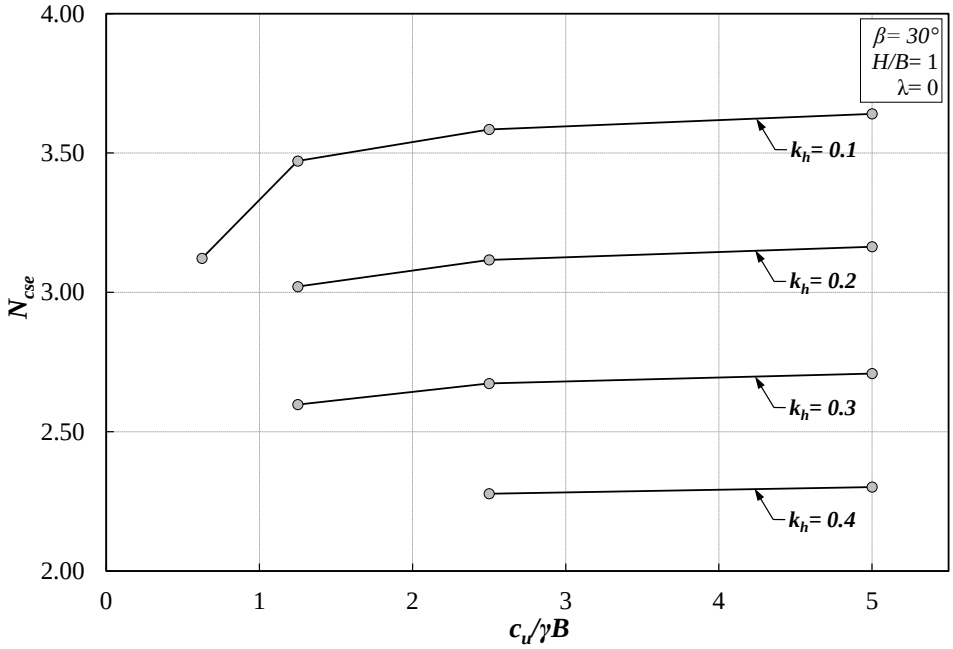


Figure 4.4. Variation of N_{cse} with $c_u/\gamma B$ for all k_h values (β= 30°, *H*/*B*= 1, λ= 0).

4.2. Examination of Failure Mechanisms

In consequence of performed numerical analyses, it was found out that there are three principal failure modes that may occur either beneath the footing or within cohesive slope soil at the ultimate state under seismic conditions. As mentioned previously, while the determination of failure at the end of the first stage means that the cohesive slope cannot maintain its own stability by the influence of even gravity, the determination of failure at the end of the third stage means that the cohesive slope loses its stability by the influence of earthquake inertia force acting on slope. Both failure modes mentioned above are classified as "base failure" in this study. Typical view of each failure mode is shown in Figure 4.5 and Figure 4.6 respectively.

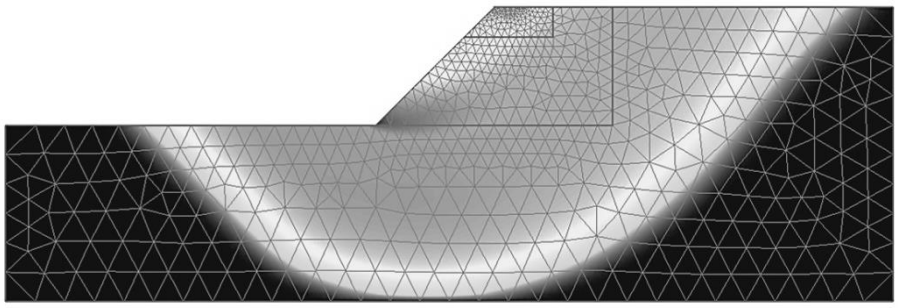


Figure 4.5. Base failure due to self-weight of cohesive slope (β= 45°, H/B= 4, $c_u/\gamma B$= 0.625).

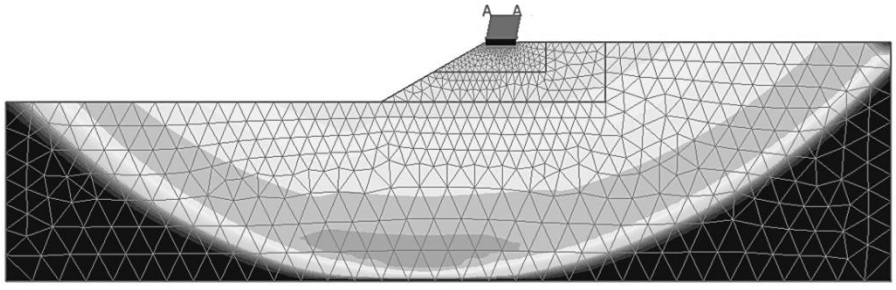


Figure 4.6. Base failure due to earthquake inertia force (β= 30°, H/B= 2, $c_u/\gamma B$= 0.625, k_h= 0.2).

On the other hand, the determination of failure at the end of the fourth stage means that the footing reaches its seismic bearing capacity with a failure mechanism formed beneath the footing. For the failure mode called as "foundation failure" in all lists presented in Appendix C, failure mechanism starts propagation from the footing edge and then intersects with slope line, passes from the slope toe or intersects at any point with upper horizontal line of the slope if the footing is placed far enough from the slope edge. This characterization is quite similar with failure mode classification made by Meyerhof (1957) and Georgiadis (2010). While typical failure modes obtained for the specific case in which the footing is on the slope edge (λ= 0) are shown in Figure 4.7, typical failure modes obtained for cases in which the footing is far away from the slope edge (λ> 0) are shown in Figure 4.8.

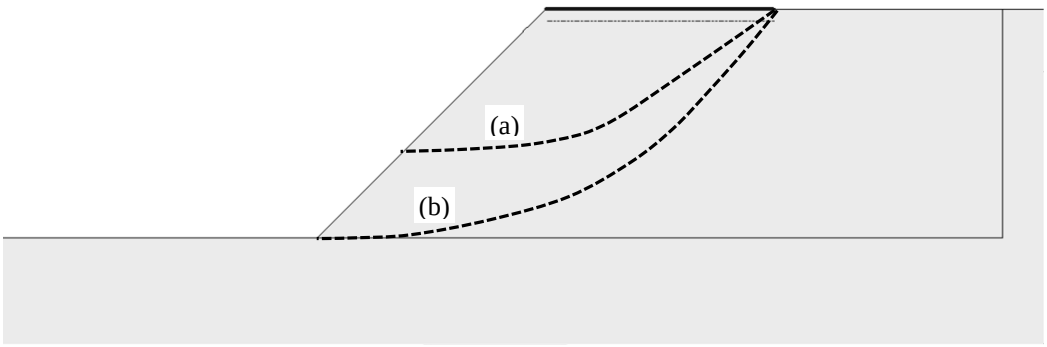


Figure 4.7. Typical “Foundation failure” modes for λ= 0 condition (a) β= 45°, H/B= 1, $c_u/\gamma B$= 1.25, k_h= 0.2; (b) β= 45°, H/B= 1, $c_u/\gamma B$= 0.625, k_h= 0.1.

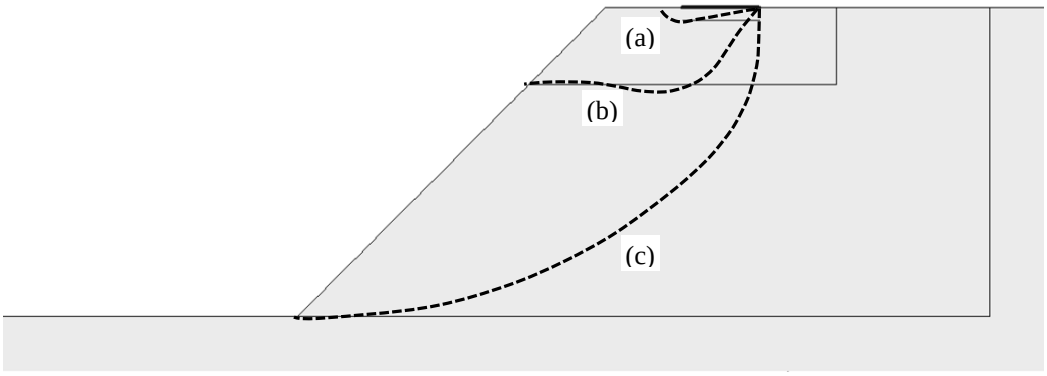


Figure 4.8. Typical “Foundation failure” modes for λ> 0 condition (a) β= 45°, H/B= 4, $c_u/\gamma B$= 2.5, k_h= 0.3; (b) β= 45°, H/B= 4, $c_u/\gamma B$= 2.5, k_h= 0.1; (c) β= 45°, H/B= 4, $c_u/\gamma B$= 1.25, k_h= 0.1.

In addition to the several “foundation failure” mechanisms presented in Figure 4.7 and Figure 4.8, there is one more failure mechanism observed only under specific conditions. Accordingly, for all finite element models in which $\lambda \geq 0.25$ or 0.5 (this value is 0.25 for $\beta = 15°$, 30° and is 0.5 for $\beta = 45°$) and $k_h \geq 0.36$, failure mode was determined as “foundation sliding”. Typical view of this failure mode in which a very shallow failure surface is observed beneath the footing is shown in Figure 4.9.

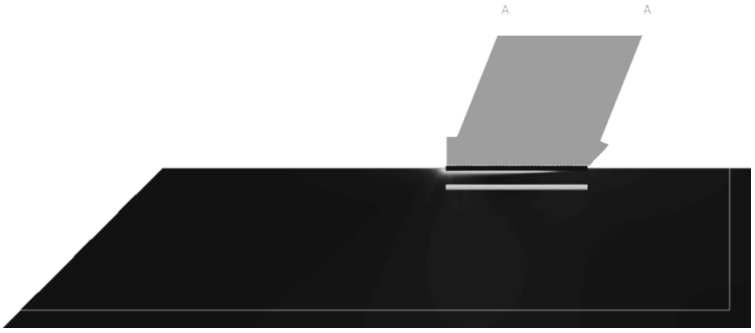


Figure 4.9. Typical view of “Foundation sliding” failure mode ($\beta = 45°$, $H/B = 4$, $\lambda = 2$, $c_u/\gamma B = 2.5$, $k_h = 0.4$).

As mentioned earlier, horizontal seismic acceleration coefficient (k_h) takes the values of 0.1, 0.2, 0.3 and 0.4. Therefore, "foundation sliding" failure mode was observed only in finite element models of which horizontal seismic acceleration coefficient is 0.4. However, this issue was investigated in detail and additional finite element analyses were performed in order to find the threshold value of horizontal seismic acceleration coefficient that leads to create this failure mode. Since the failure surface is very shallow, failure surface cannot extend to the slope surface, thus the slope angle does not affect analysis results. For this reason, as seen in Figure 4.10, the slope angle was taken as zero in additional analyses performed.

According to the formula given in Equation 3.1, seismic bearing capacity (q_f),

$$q_f = c_u \, N_{ce}$$

The magnitude of horizontal component of inclined load (q_{fh}) imposed on the footing,

$$q_f = \frac{q_{fh}}{k_h} \tag{4.1}$$

If Equation 3.1 is rearranged with the formula given in Equation 4.1, then

$$q_{fh} = c_u \, N_{ce} k_h \tag{4.2}$$

If "fully rough" rigid footing is sliding, then

$$q_{fh} = c_u \tag{4.3}$$

Therefore, the product of "$N_{ce}\ k_h$" given in Equation 4.2 should be one. The smallest horizontal acceleration value, also known as "threshold value", which satisfies this condition is 0.36 as seen in Table 4.1. For all values of the horizontal seismic acceleration coefficient which are greater than the threshold value, the product of "$N_{ce}\ k_h$" always takes the value of one. For this failure mode, there is no actual bearing capacity failure mechanism formed beneath the footing and the failure surface becomes completely horizontal.

If $N_{ce}\ k_h < 1$, then the length of failure surface is greater than the footing width. Therefore, the footing is not sliding. As shown in Figure 4.10, the relationship between N_{ce}-k_h can be considered to be linear for $k_h < 0.36$.

Table 4.1. Variation of N_{ce} with k_h ($\beta = 0°$).

k_h	N_{cse}	$k_h\ N_{ce}$
0.00	5.16	0.00
0.10	4.59	0.46
0.20	3.90	0.78
0.30	3.19	0.96
0.33	2.98	0.98
0.35	2.84	0.99
0.36	2.77	**1.00**
0.37	2.71	1.00
0.39	2.57	1.00
0.40	2.50	1.00
0.50	2.00	1.00
0.60	1.66	1.00
0.70	1.43	1.00
0.80	1.25	1.00
0.90	1.11	1.00
1.00	1.00	1.00

The threshold value of horizontal seismic acceleration coefficient determined by following the approach given in above is also valid for footings located near cohesive slopes. By the way, it should be mentioned that this failure mode was never observed for the specific case in which the footing is at the edge of the slope ($\lambda = 0$).

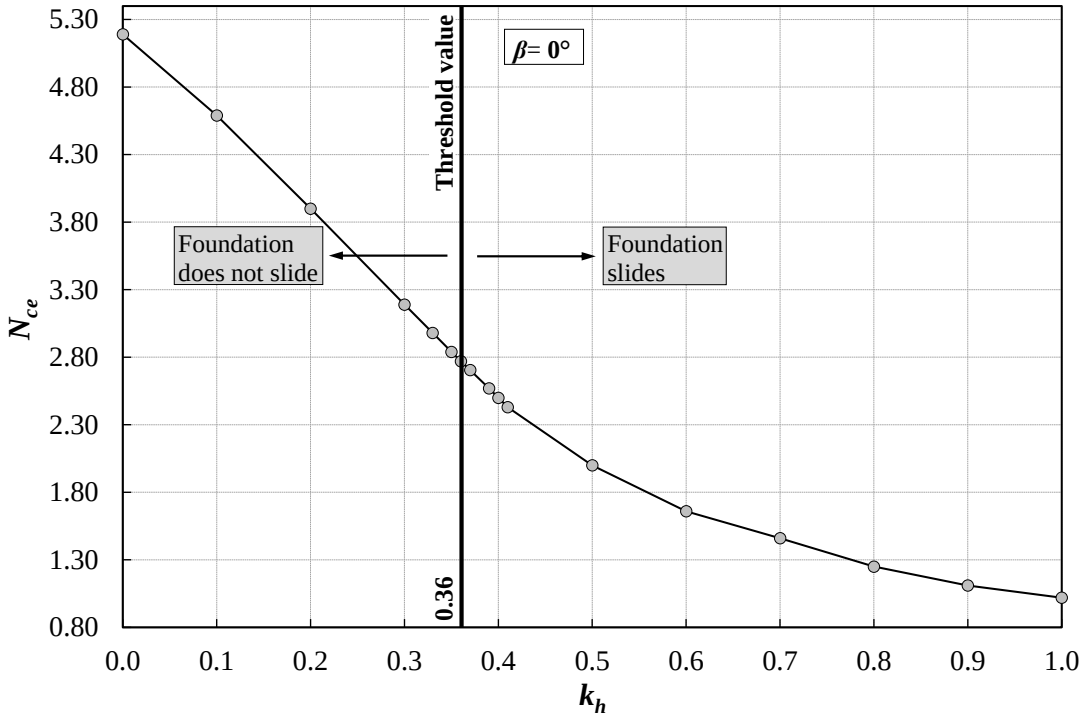


Figure 4.10. Variation of N_{ce} with k_h ($\beta = 0°$).

Finally, variation of four failure modes with the influential parameters of seismic bearing capacity factor was investigated. Consequently, two different charts were prepared for all slope angles considered in this study. While one of those diagrams was prepared for the condition $\lambda < 0.25$ or 0.5 (this value is 0.25 for $\beta = 15°$, 30° and is 0.5 for $\beta = 45°$), the other one is prepared for the condition $\lambda \geq 0.25$ or 0.5. Through presented charts, failure mode of either footing or cohesive slope can be readily estimated depending on set of parameters at hand.

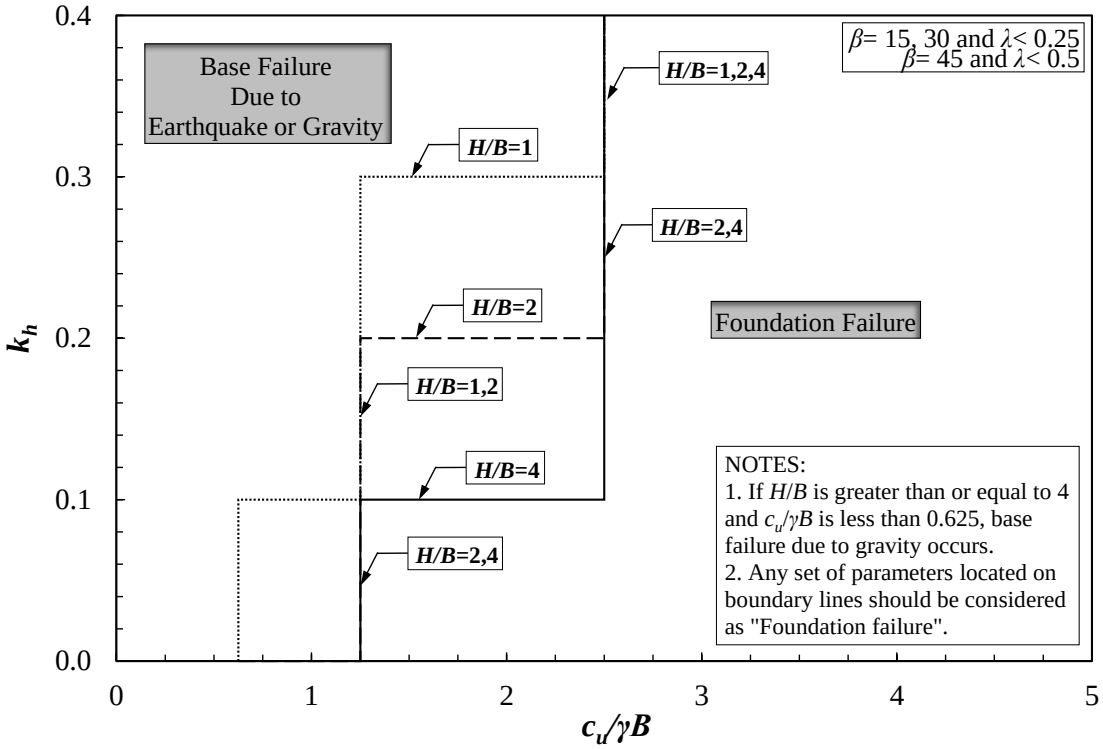


Figure 4.11. Variation of failure modes with influential parameters (λ< 0.25 or 0.5).

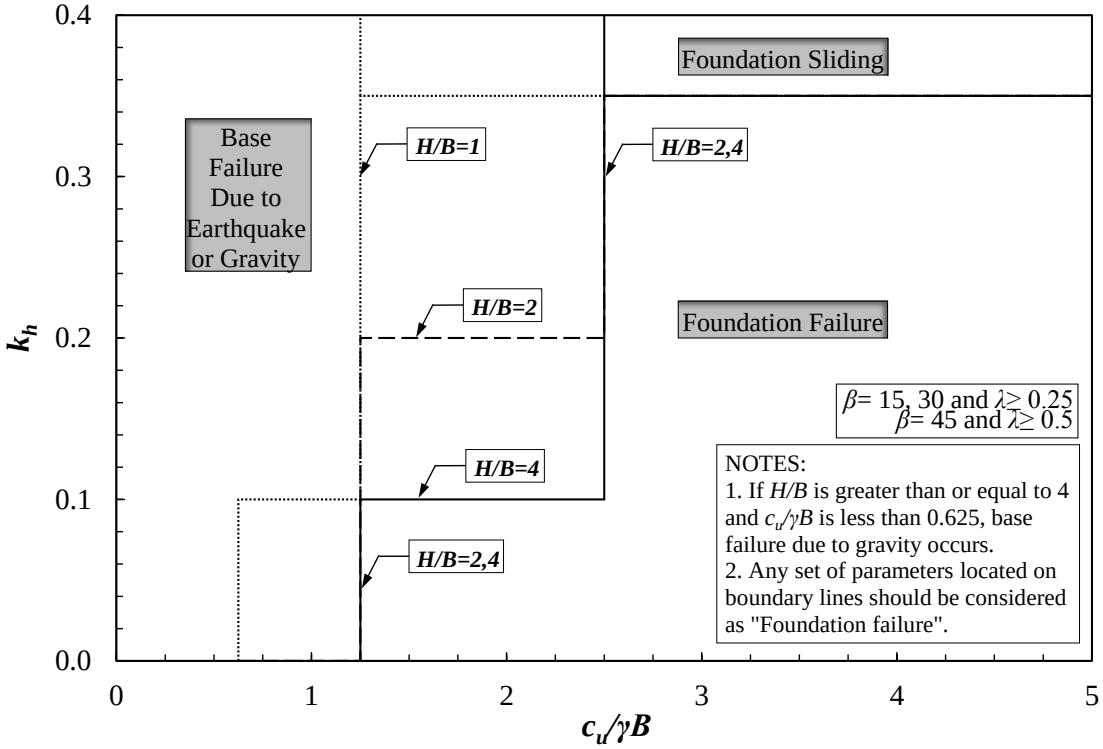


Figure 4.12. Variation of failure modes with influential parameters ($\lambda\geq$ 0.25 or 0.5).

4.3. Design Charts

Seismic bearing capacity of surficial strip footings located near cohesive slopes can be estimated by Equation 3.1. It was clearly demonstrated that seismic bearing capacity factor given in this equation is a function of several independent variables mentioned in Chapter 4.1. With the evaluation of parametric study results, a solution methodology that can be easily applied by geotechnical designers or practitioners was developed. Design charts that are absolutely supplementary items of this solution methodology are presented in between Figure 4.13 and Figure 4.24.

In these design charts, it is seen that the relationship between seismic bearing capacity factor (N_{cse}) and normalized footing distance (λ) is expressed as either linear or second degree polynomial until reaching threshold distance (λ_0). Despite the fact that *H/B* ratio does not affect seismic bearing capacity factor calculated for "foundation failure" failure mode in general, exceptional cases were also observed as slope angle increases and slope soil strength decreases.

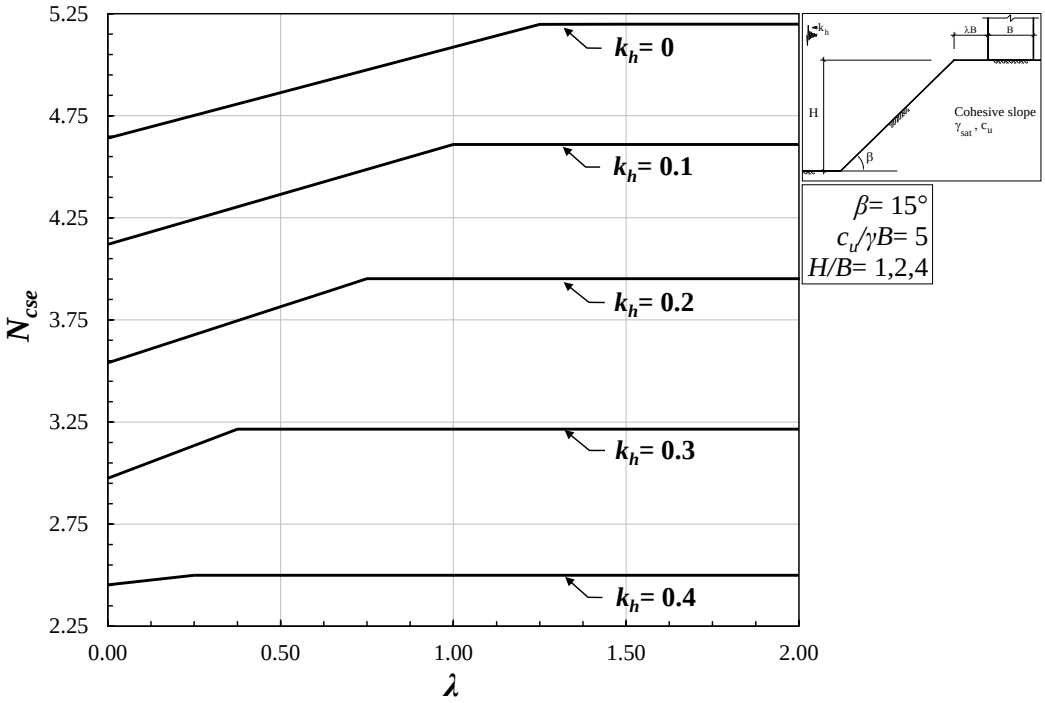


Figure 4.13. Design chart for seismic bearing capacity factor of surficial strip footings near cohesive slopes (β= 15°, $c_u/\gamma B$= 5, H/B= 1, 2, 4).

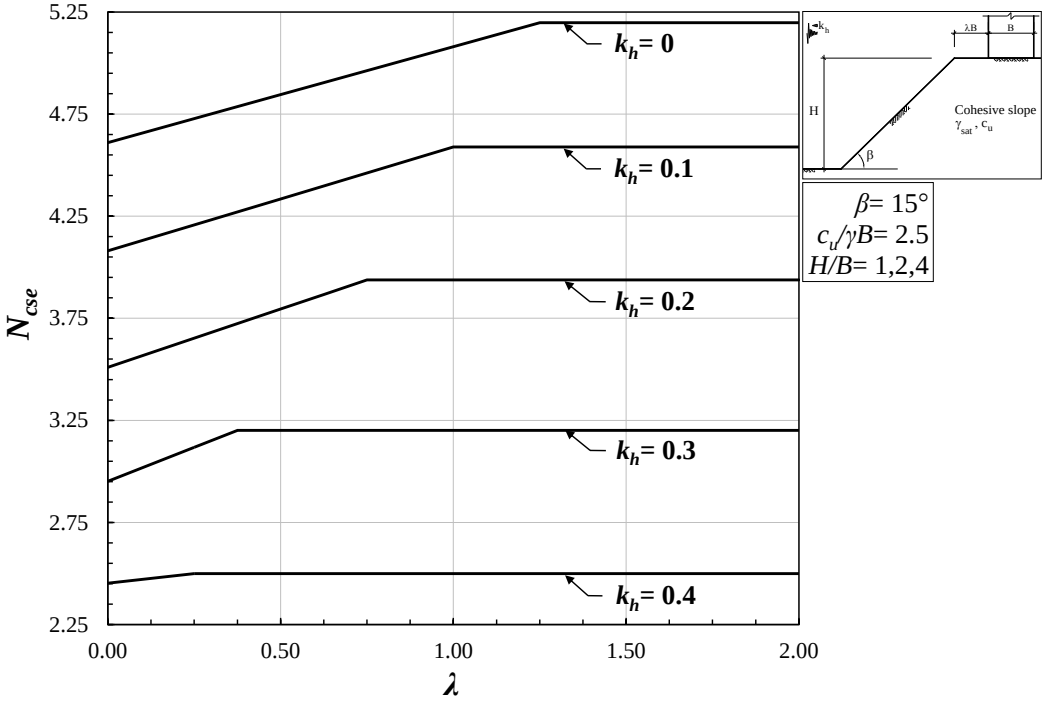


Figure 4.14. Design chart for seismic bearing capacity factor of surficial strip footings near cohesive slopes (β= 15°, $c_u/\gamma B$= 2.5, H/B= 1, 2, 4).

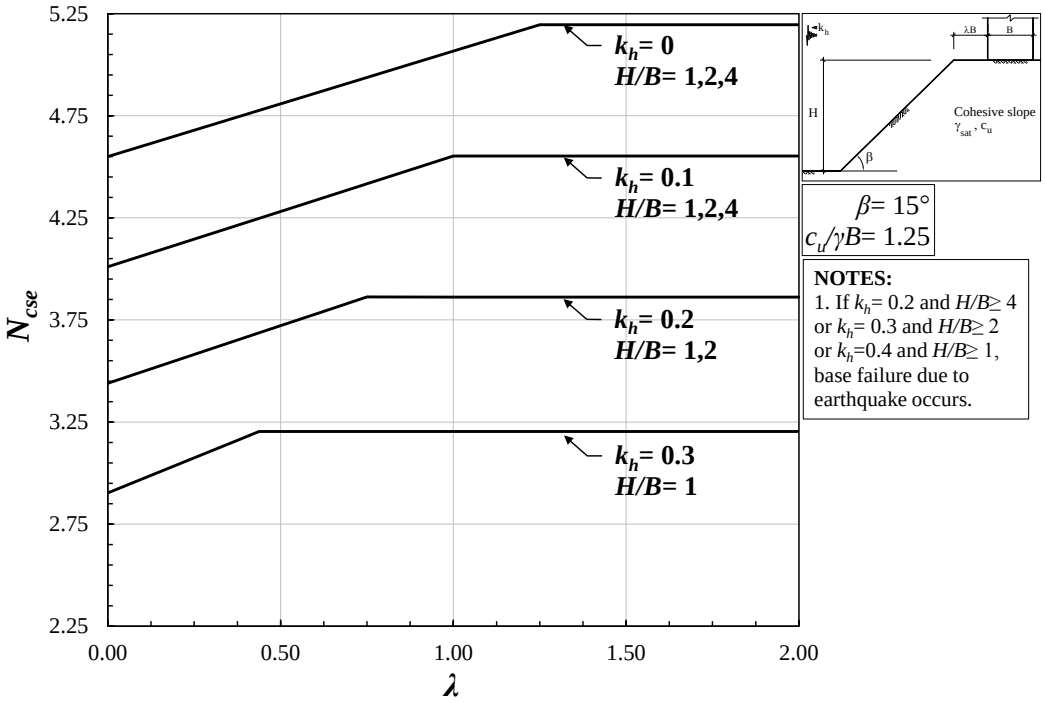


Figure 4.15. Design chart for seismic bearing capacity factor of surficial strip footings near cohesive slopes (β= 15°, $c_u/\gamma B$= 1.25, H/B= 1, 2, 4).

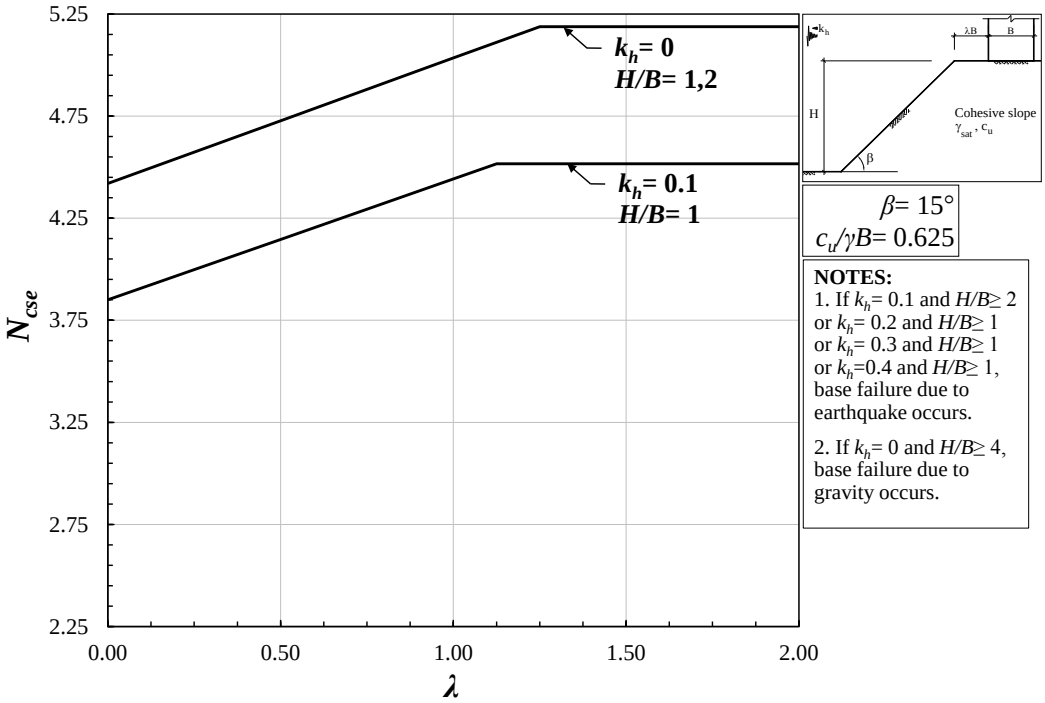


Figure 4.16. Design chart for seismic bearing capacity factor of surficial strip footings near cohesive slopes (β= 15°, $c_u/\gamma B$= 0.625, H/B= 1, 2, 4).

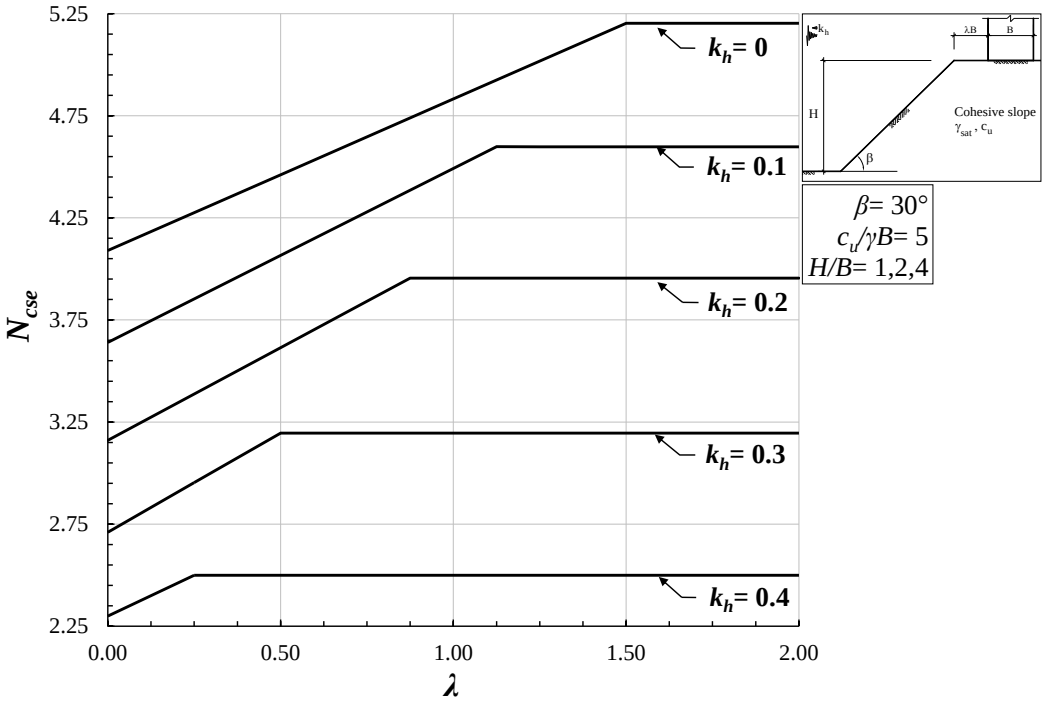


Figure 4.17. Design chart for seismic bearing capacity factor of surficial strip footings near cohesive slopes (β= 30°, $c_u/\gamma B$= 5, H/B= 1, 2, 4).

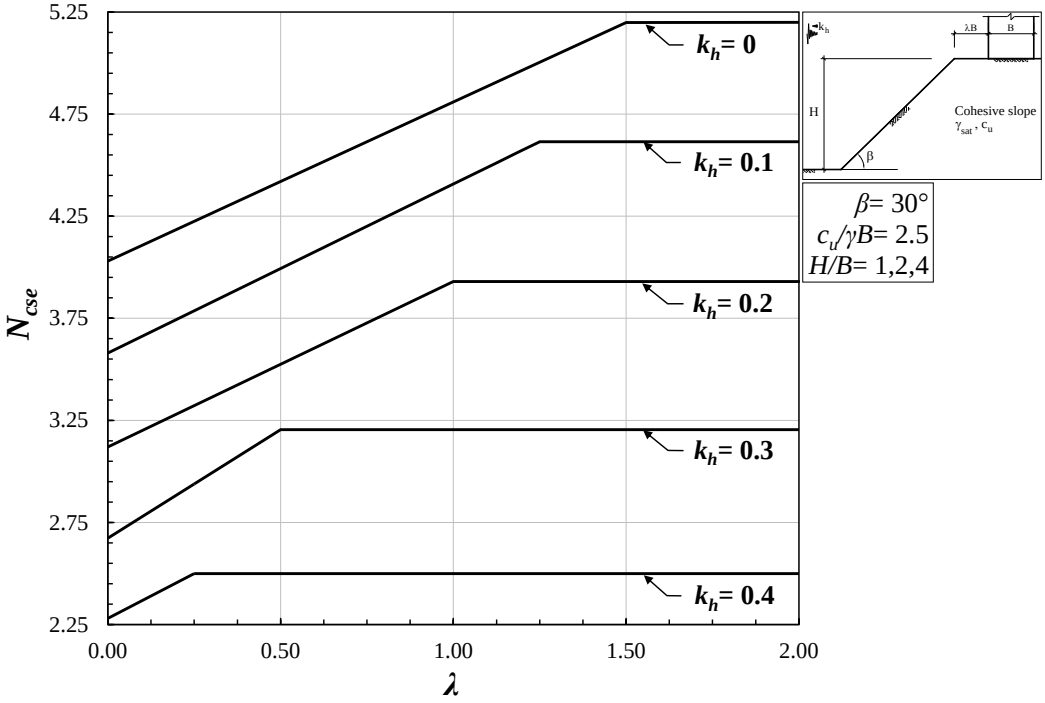


Figure 4.18. Design chart for seismic bearing capacity factor of surficial strip footings near cohesive slopes (β= 30°, $c_u/\gamma B$= 2.5, H/B= 1, 2, 4).

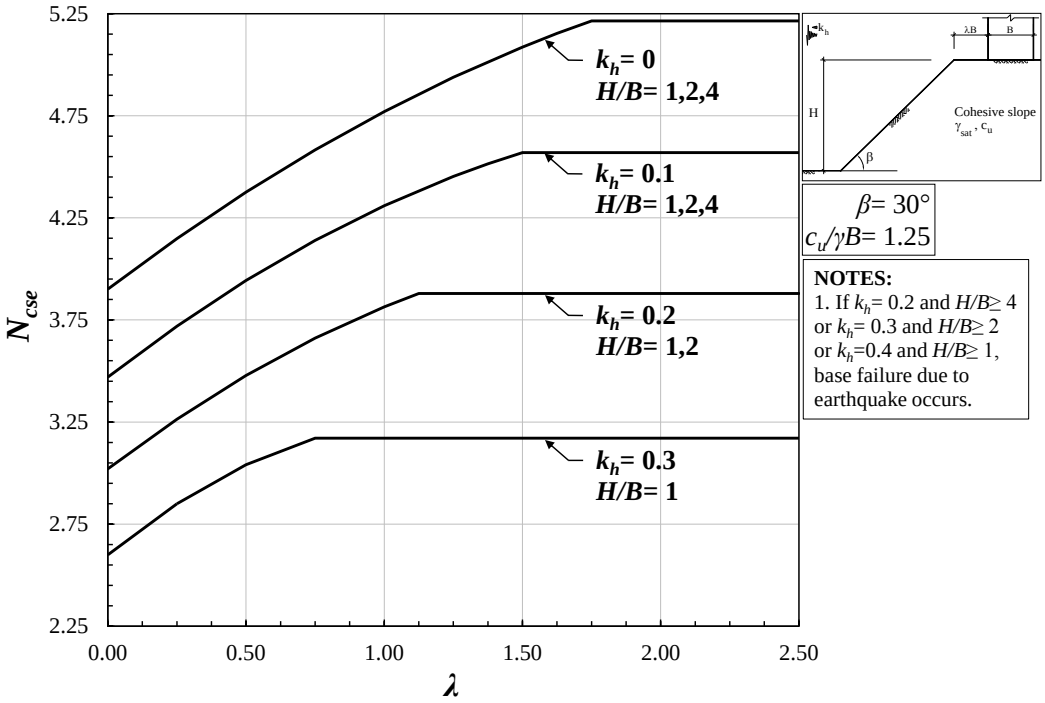


Figure 4.19. Design chart for seismic bearing capacity factor of surficial strip footings near cohesive slopes (β= 30°, $c_u/\gamma B$= 1.25, H/B= 1, 2, 4).

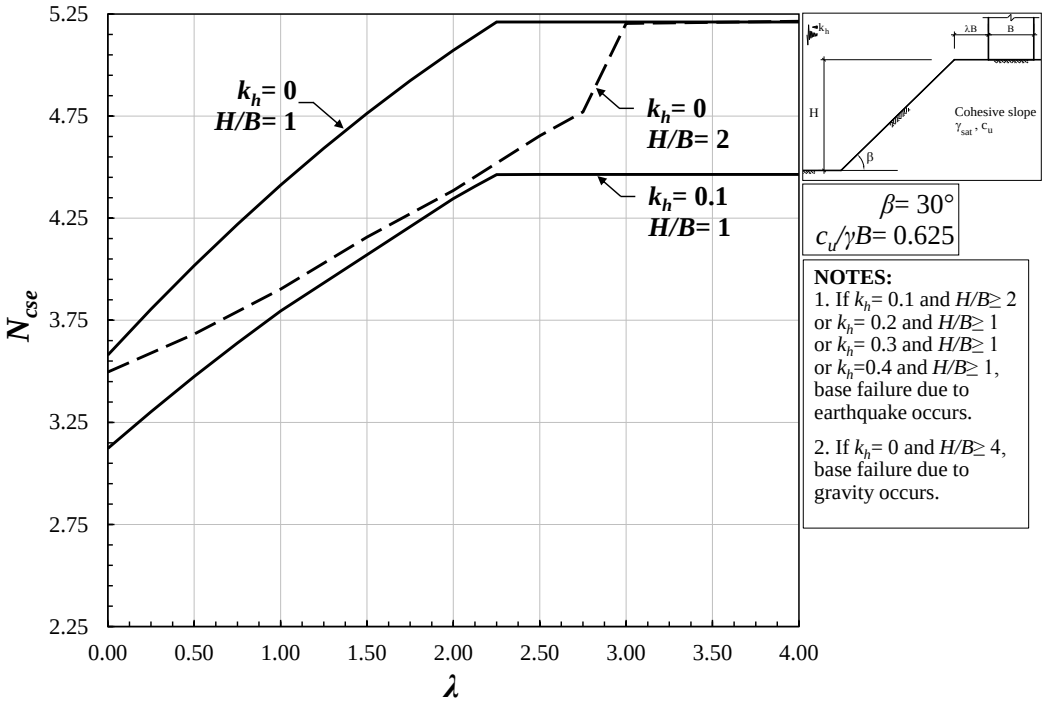


Figure 4.20. Design chart for seismic bearing capacity factor of surficial strip footings near cohesive slopes (β= 30°, $c_u/\gamma B$= 0.625, H/B= 1, 2, 4).

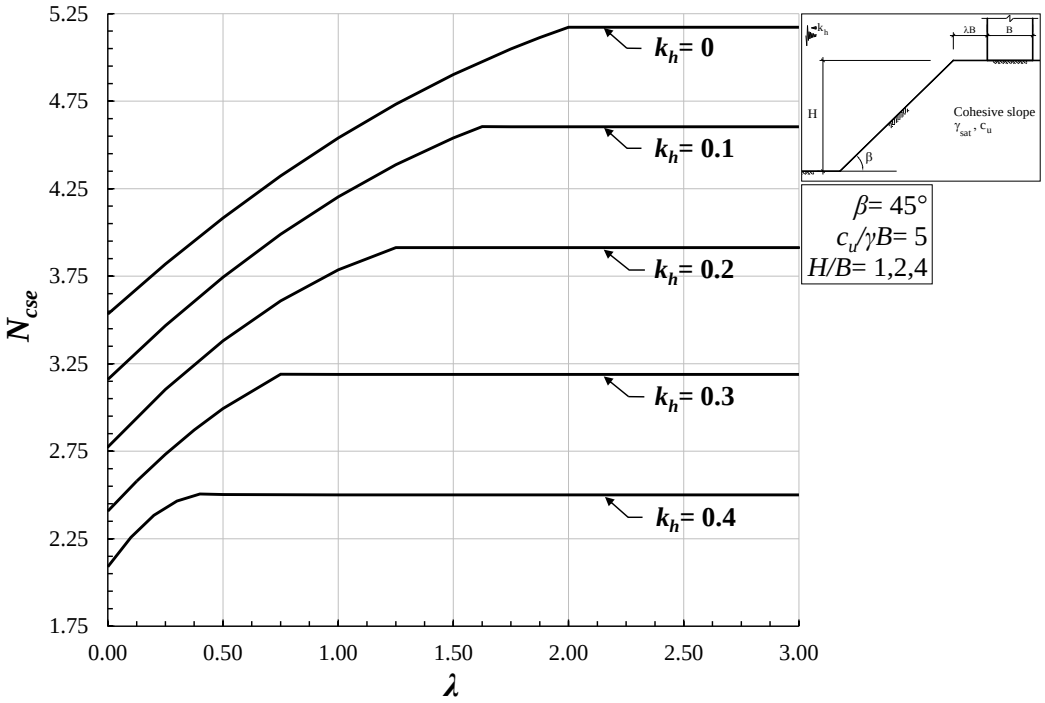


Figure 4.21. Design chart for seismic bearing capacity factor of surficial strip footings near cohesive slopes (β= 45°, $c_u/\gamma B$= 5, H/B= 1, 2, 4).

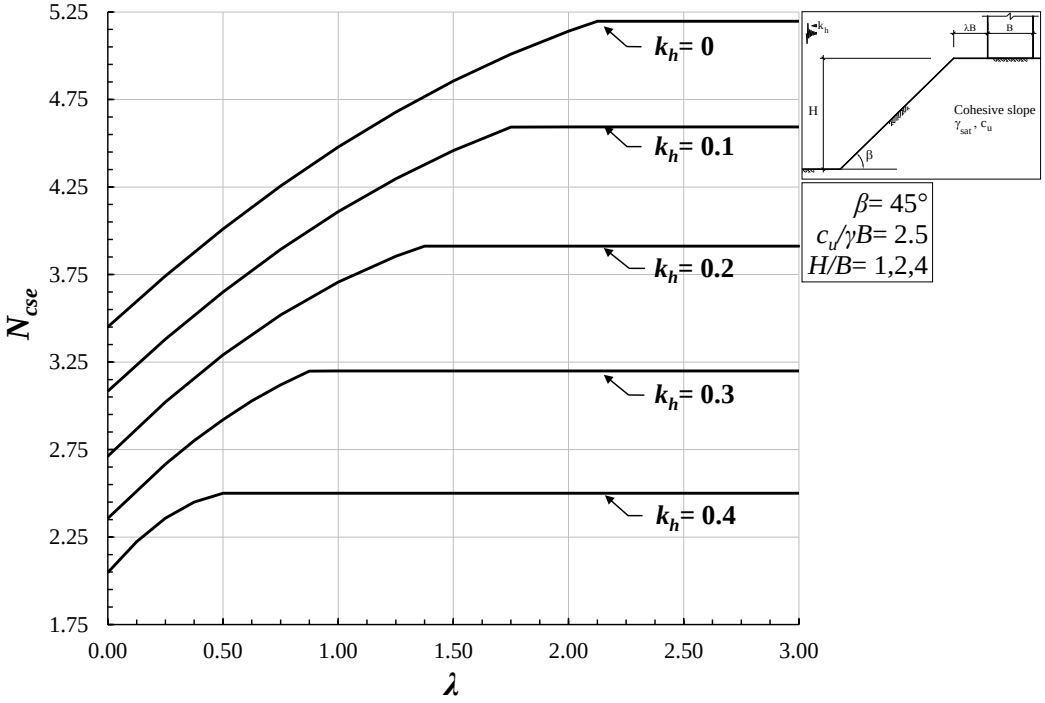


Figure 4.22. Design chart for seismic bearing capacity factor of surficial strip footings near cohesive slopes (β= 45°, $c_u/\gamma B$= 2.5, H/B= 1, 2, 4).

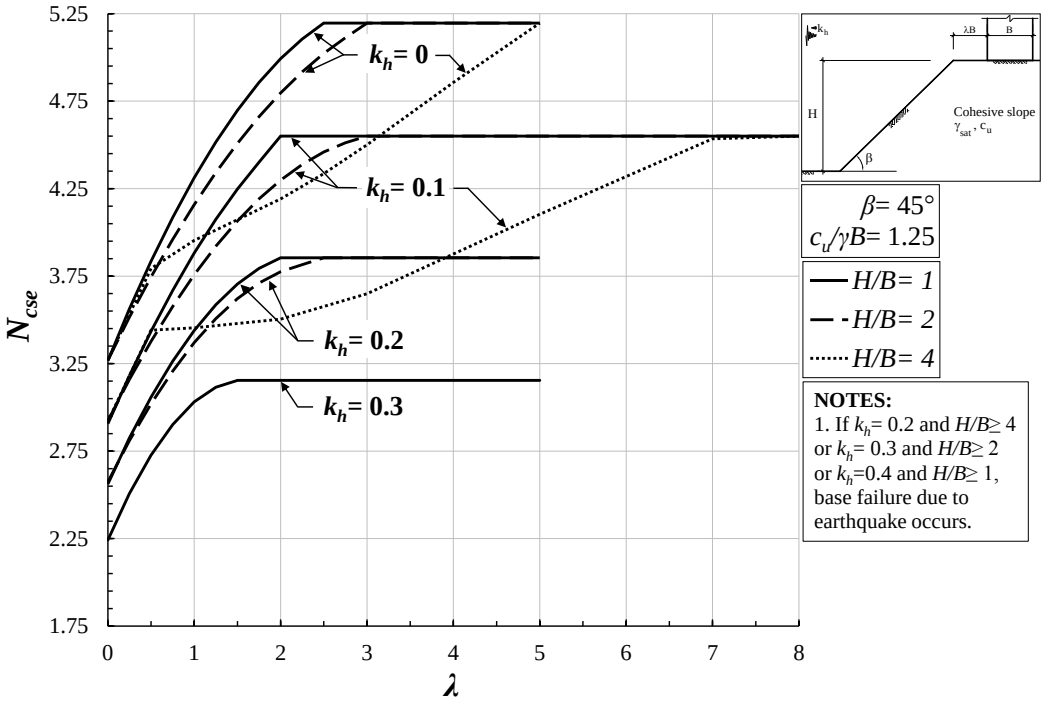


Figure 4.23. Design chart for seismic bearing capacity factor of surficial strip footings near cohesive slopes (β= 45°, $c_u/\gamma B$= 1.25, H/B= 1, 2, 4).

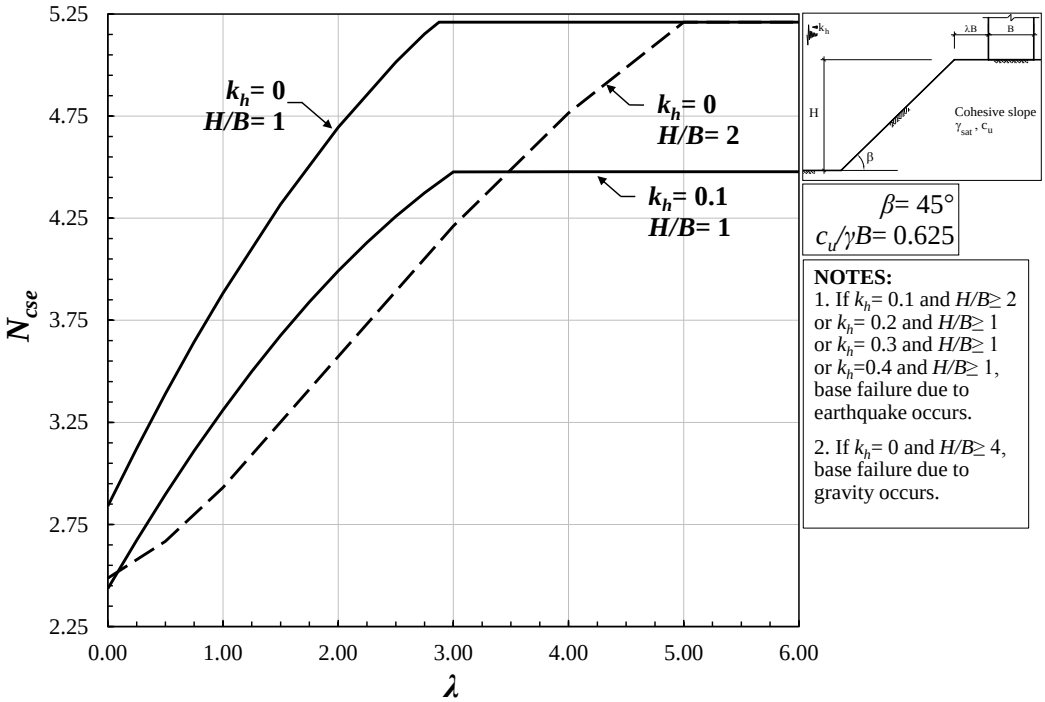


Figure 4.24. Design chart for seismic bearing capacity factor of surficial strip footings near cohesive slopes (β= 45°, $c_u/\gamma B$= 0.625, H/B= 1, 2, 4).

4.4. Other Remarkable Results

While evaluating parametric study results, other remarkable results obtained will be given in this chapter. Accordingly, the variation of the threshold distance (λ_0) with the influential parameters of the seismic bearing capacity problem was investigated. Essentially, there are two factors namely horizontal seismic acceleration coefficient **(k_h)** and slope angle (β) that are influential on the threshold distance. Actually, the influence of horizontal seismic acceleration coefficient on the threshold distance is more obvious and stronger relatively. Therefore, instead of defining a single value for each $\beta - k_h$ couple, variation ranges of the threshold distance are given in Table 3.2 depending on the horizontal seismic acceleration coefficient **(k_h)** owing to the combined effect of these two factors. As shown in Table 4.1, the increase in horizontal seismic acceleration coefficient clearly leads to the reduction of the upper and lower bound values of threshold distance. This fact can be explained by noting that the failure mechanism passes through shallower depth in case of more severe earthquake. Moreover, threshold distance increases with the increase of slope angle ($c_u/\gamma B$ and k_h are constant) in both static and seismic condition.

Table 4.2. Range of threshold distance varied with horizontal seismic acceleration coefficient.

Horizontal seismic acceleration coefficient (k_h)	**Range of threshold distance (λ_0)**
0	1.25-3.00
0.1	1.00-3.00
0.2	0.75-2.50
0.3	0.375-1.50
0.4	0.25-0.50

Secondly, a remarkable finding regarding the geometry of various failure mechanisms obtained at the ultimate state will be discussed. Accordingly, if the footing is closer than threshold distance to the slope edge, also means that the failure mechanism intersects with the slope line, it was determined that the failure surface makes an angle of 45 degrees with the slope line (Refer to Figure 4.25). In the solution proposed by Bowles (1997) for static condition, he expressed that the exit angle of failure surface is (45-Φ/2) since the slope line is essentially a principal plane. When it is considered that all analyses

were performed in undrained condition ($\Phi = \Phi_u = 0°$), the statement given in Bowles (1997) verifies the output obtained by the software.

Finally, it will be discussed that failure surface passes through shallower depths as horizontal seismic acceleration coefficient increases. In the drawing given in Figure 4.25, failure mechanisms obtained for five different horizontal seismic acceleration values are presented. Accordingly, failure mechanism passes through shallower depth as horizontal seismic acceleration coefficient increases. Moreover, it is also seen that shear fan becomes narrow with the increase of horizontal seismic acceleration coefficient. This fact is also valid for cases in which the footing is far away from the slope edge (λ>0).

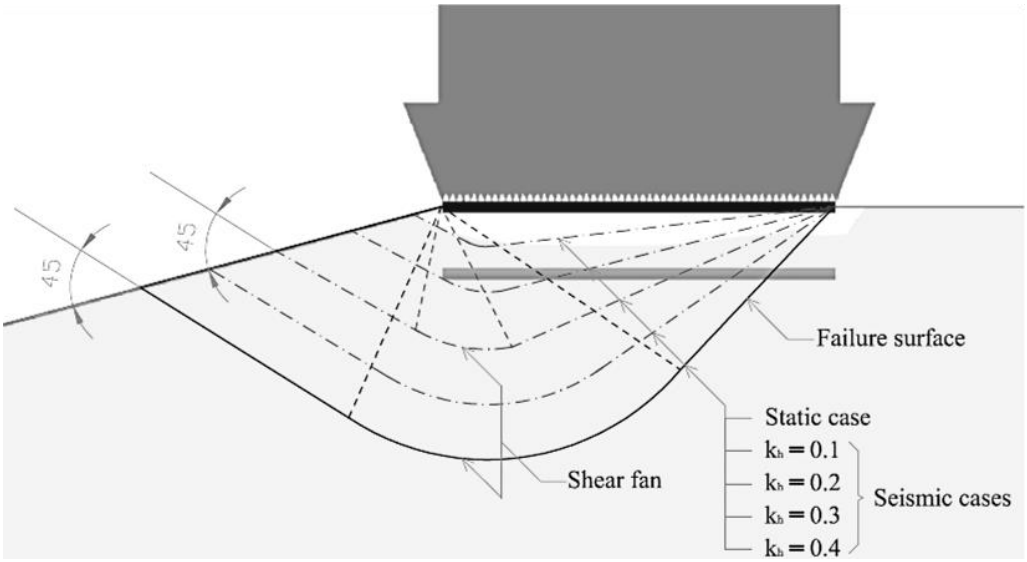


Figure 4.25. Geometry of failure mechanisms obtained at the ultimate state for all k_h values.

4.5. Design Examples

In order to demonstrate the practical usage of design charts presented in this study (including those developed for the estimation of N_{cse} and the expected failure mode formed at the ultimate state), six design examples were chosen and their solutions will be obtained using the methodology suggested in this study. While linear interpolation was done for the estimation of N_{cse} in between design examples 1-3, linear extrapolation was also done in design example 4 to predict the value of N_{cse} for a slope angle that is greater than the

maximum slope angle considered in this study. Additionally, in the design examples 5 and 6, it will also be demonstrated how to estimate the failure mode formed either beneath the footing or within the cohesive slope using the charts presented in Chapter 4.2.

4.5.1. Design Example 1

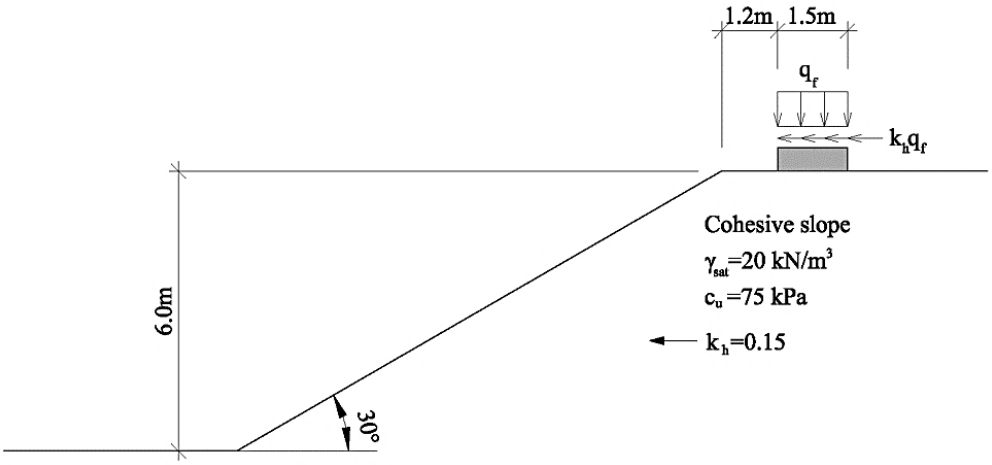


Figure 4.26. Schematic representation of the design example 1.

For the design example presented in Figure 4.26, H/B, λ and $c_u/\gamma B$ are 4, 0.8 and 2.5 respectively. Since β is 30° and λ is greater than 0.25, expected failure mode can be estimated with the design chart presented in Figure 4.12. As shown in Figure 4.27, the cohesive slope is stable under both static and seismic conditions and expected failure mode for the set of parameters given in above is "foundation failure". Since k_h= 0.15 is an intermediate value, the value of N_{cse} is calculated by making linear interpolation between the values obtained through the curves of k_h= 0.1 and k_h= 0.2. Accordingly, N_{cse} are determined as 4.25 and 3.77 respectively by means of k_h= 0.1 and k_h= 0.2 curves (Refer to Figure 4.28)

Seismic bearing capacity factor (N_{cse}) for k_h= 0.15,

$$N_{cse} = 3.77 + (4.25 - 3.77)\frac{0.15 - 0.10}{0.20 - 0.10} = 4.01 \tag{4.4}$$

Thus, seismic bearing capacity (q_f),

$$q_f = c_u N_{cse} = 75 \times 4.01 = 301 \text{ kPa} \tag{4.5}$$

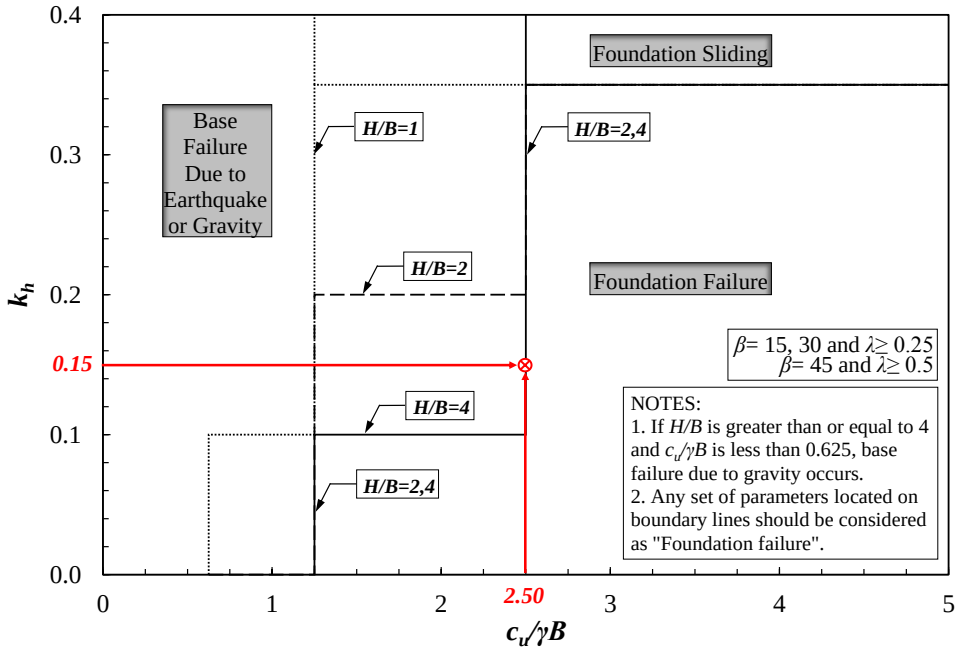


Figure 4.27. Estimation of the failure mode for the design example 1.

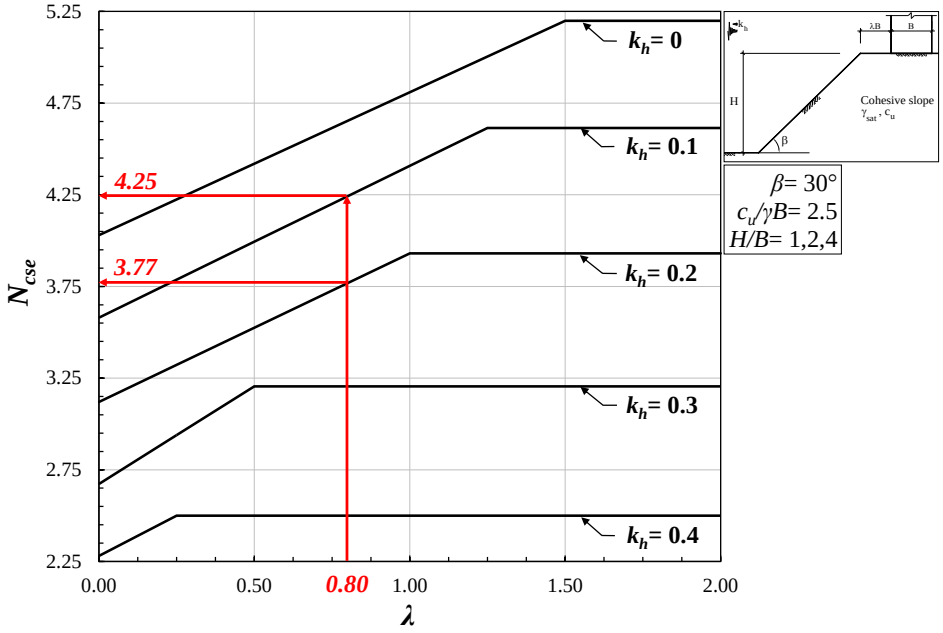


Figure 4.28. N_{cse} values to be used in linear interpolation for the design example 1.

On the other hand, a finite element model was prepared for the same problem. The load multiplier (*Σ-MloadA*) is found as 61.73 at the ultimate state and the seismic bearing capacity obtained by Plaxis 2D is 309 kPa. Estimated seismic bearing capacity value via linear interpolation is on the safe side and the difference between the result of linear interpolation and Plaxis 2D is only %2.6. Also, as shown in Figure 4.29, the failure mode determined by Plaxis 2D is "foundation failure" which is consistent with the estimation of the proposed method.

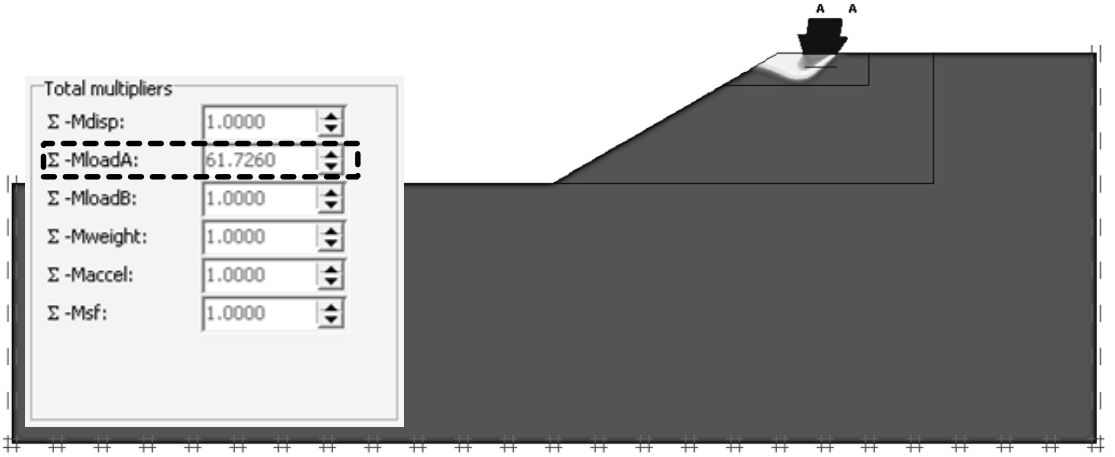


Figure 4.29. Load multiplier (*Σ-MloadA*) and the failure mechanism obtained by Plaxis 2D for the design example 1.

4.5.2. Design Example 2

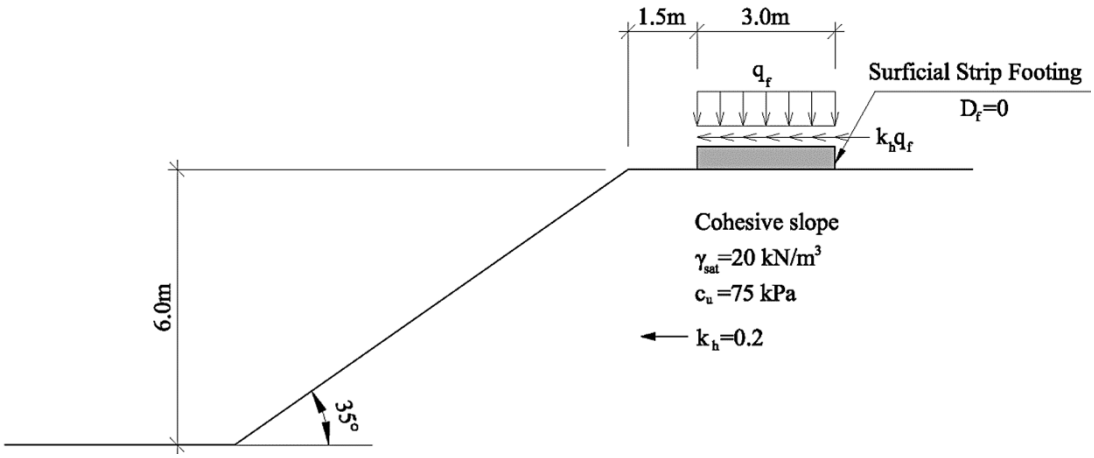


Figure 4.30. Schematic representation of the design example 2.

For the design example presented in Figure 4.30, H/B, λ and $c_u/\gamma B$ are 2, 0.5 and 1.25 respectively. Since β is 35° and λ is greater than 0.25, expected failure mode can be estimated with the design chart presented in Figure 4.12. As shown in Figure 4.31, the cohesive slope is stable under both static and seismic conditions and expected failure mode for the set of parameters given in above is "foundation failure". Since β= 35° is an intermediate value, the value of N_{cse} is calculated by making linear interpolation between the values obtained through the design charts of β = 30° and β = 45°. Accordingly, N_{cse} are determined as 3.48 and 3.02 respectively by means of β = 30° and β = 45°charts (Refer to Figure 4.32 and Figure 4.33)

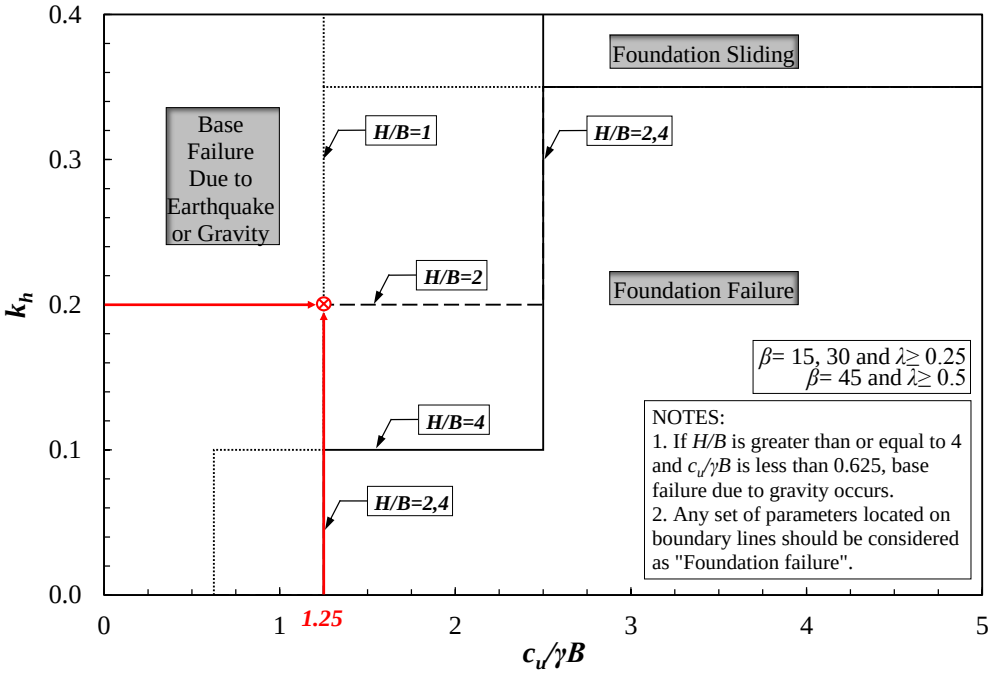


Figure 4.31. Estimation of the failure mode for the design example 2.

Seismic bearing capacity factor (N_{cse}) for β = 35°,

$$N_{cse} = 3.48 + (3.02 - 3.48)\frac{35-30}{45-30} = 3.33 \tag{4.6}$$

Thus, seismic bearing capacity (q_f),

$$q_f = c_u N_{cse} = 75 \times 3.33 = 250 \text{ kPa} \tag{4.7}$$

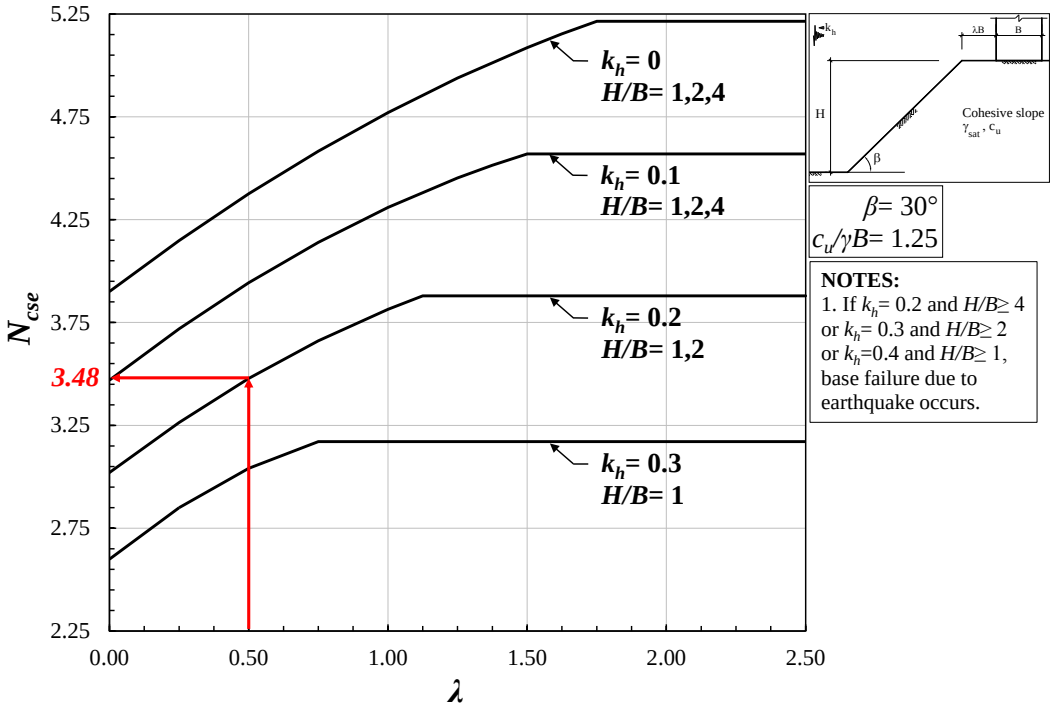


Figure 4.32. The first N_{cse} value to be used in linear interpolation for the design example 2.

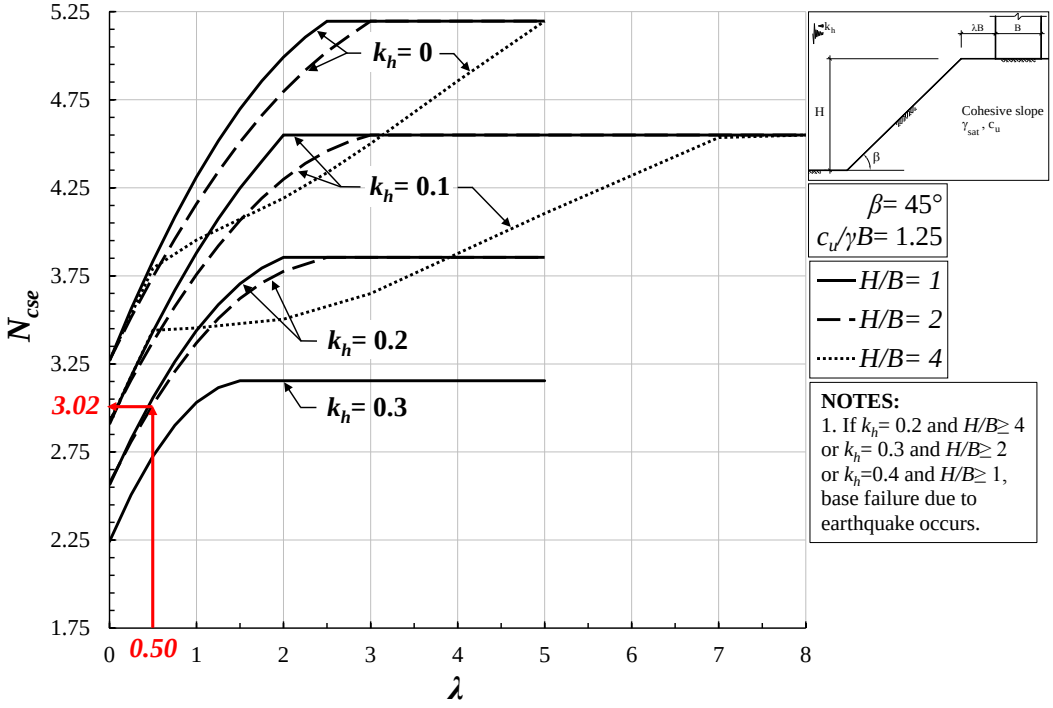


Figure 4.33. The second N_{cse} value to be used in linear interpolation for the design example 2.

On the other hand, a finite element model was prepared for the same problem. The load multiplier (*Σ-MloadA*) is found as 50.48 at the ultimate state and the seismic bearing capacity obtained by Plaxis 2D is 252 kPa. The difference between the result of linear interpolation and Plaxis 2D is less than %1. Also, as shown in Figure 4.34, the failure mode determined by Plaxis 2D is "foundation failure" which is consistent with the estimation of the proposed method.

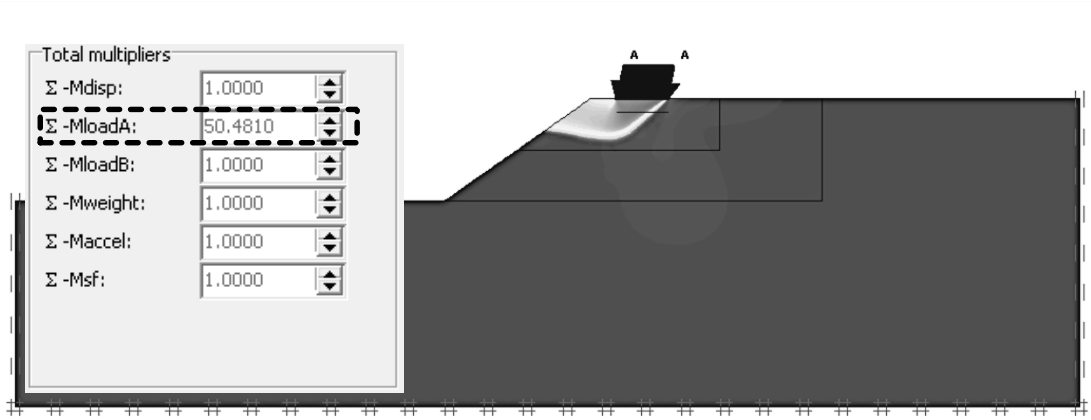


Figure 4.34. Load multiplier (*Σ-MloadA*) and the failure mechanism obtained by Plaxis 2D for the design example 2.

4.5.3. Design Example 3

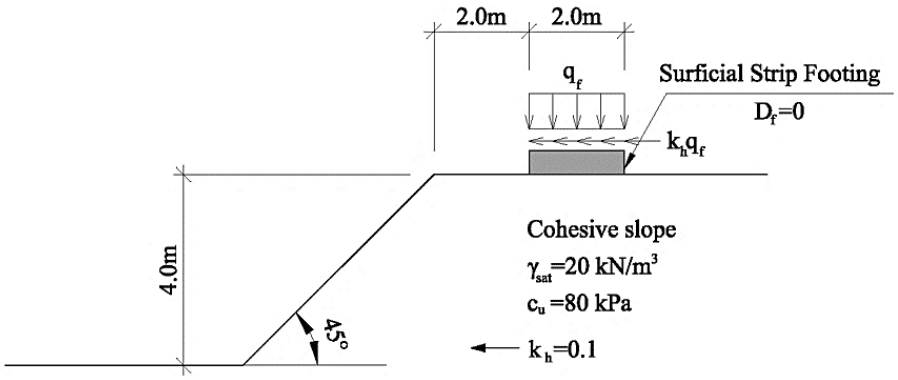


Figure 4.35. Schematic representation of the design example 3.

For the design example presented in Figure 4.35, H/B, λ and $c_u/\gamma B$ are 2, 1 and 2 respectively. Since β is 45° and λ is greater than 0.50, expected failure mode can be estimated with the design chart presented in Figure 4.12. As shown in Figure 4.36, the

cohesive slope is stable under both static and seismic conditions and expected failure mode for the set of parameters given in above is "foundation failure". Since $c_u/\gamma B$= 2 is an intermediate value, the value of N_{cse} is calculated by making linear interpolation between the values obtained through the design charts of $c_u/\gamma B$= 2.5 and $c_u/\gamma B$= 1.25. Accordingly, N_{cse} are determined as 4.11 and 3.75 respectively by means of $c_u/\gamma B$= 2.5 and $c_u/\gamma B$= 1.25 charts (Refer to Figure 4.37 and Figure 4.38)

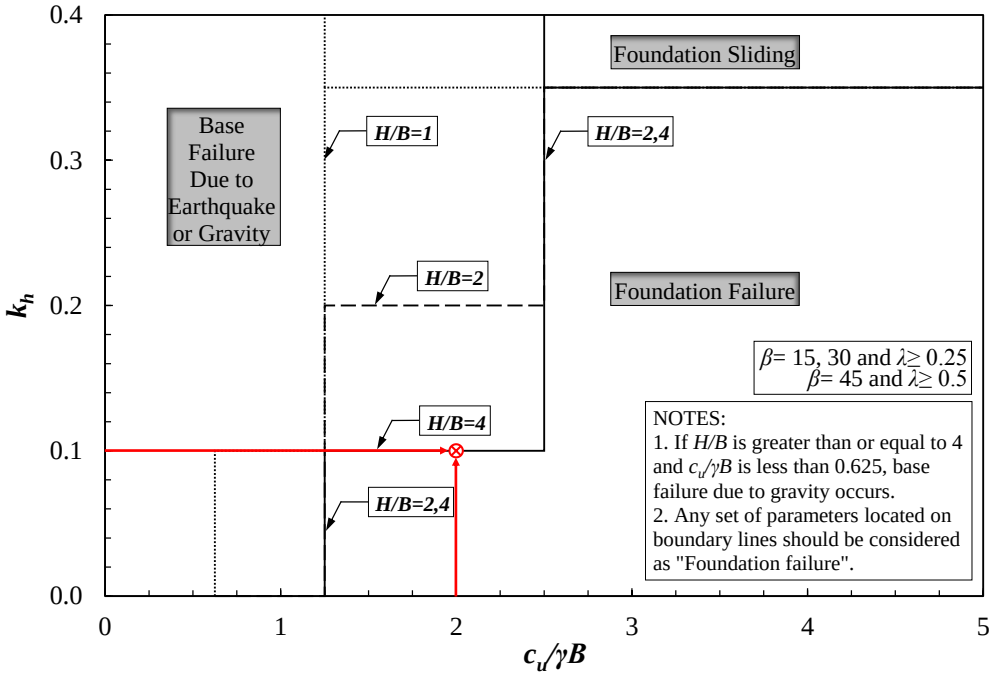


Figure 4.36. Estimation of the failure mode for the design example 3.

Seismic bearing capacity factor (N_{cse}) for $c_u/\gamma B$= 2,

$$N_{cse} = 3.75 + (4.11 - 3.75)\frac{2 - 1.25}{2.5 - 1.25} = 3.97 \tag{4.8}$$

Thus, seismic bearing capacity (q_f),

$$q_f = c_u\, N_{cse} = 80 \times 3.97 = 318 \text{ kPa} \tag{4.9}$$

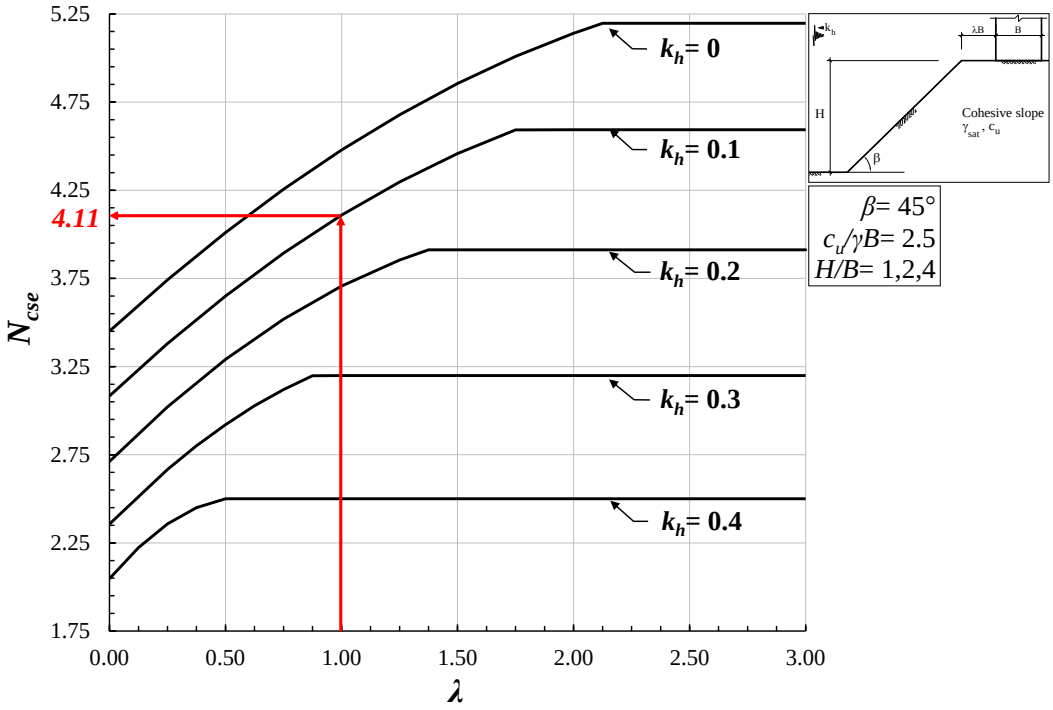


Figure 4.37. The first N_{cse} value to be used in linear interpolation for the design example 3.

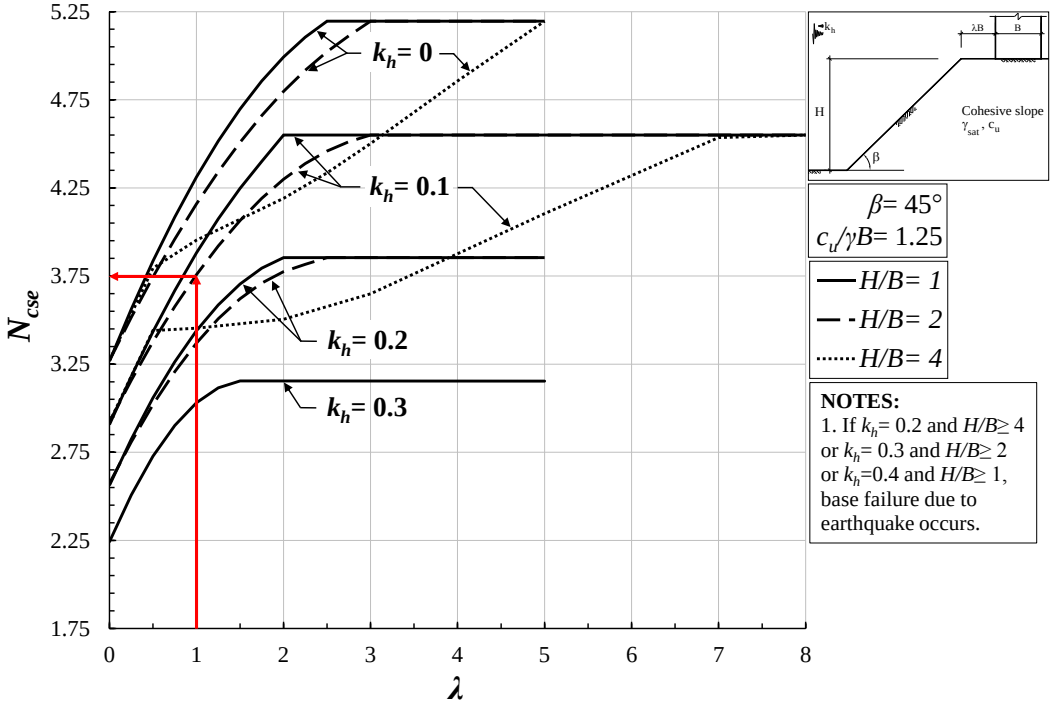


Figure 4.38. The second N_{cse} value to be used in linear interpolation for the design example 3.

On the other hand, a finite element model was prepared for the same problem. The load multiplier (*Σ-MloadA*) is found as 65.15 at the ultimate state and the seismic bearing capacity obtained by Plaxis 2D is 326 kPa. Estimated seismic bearing capacity value via linear interpolation is on the safe side and the difference between the result of linear interpolation and Plaxis 2D is only %2.5. Also, as shown in Figure 4.39, the failure mode determined by Plaxis 2D is "foundation failure" which is consistent with the estimation of the proposed method.

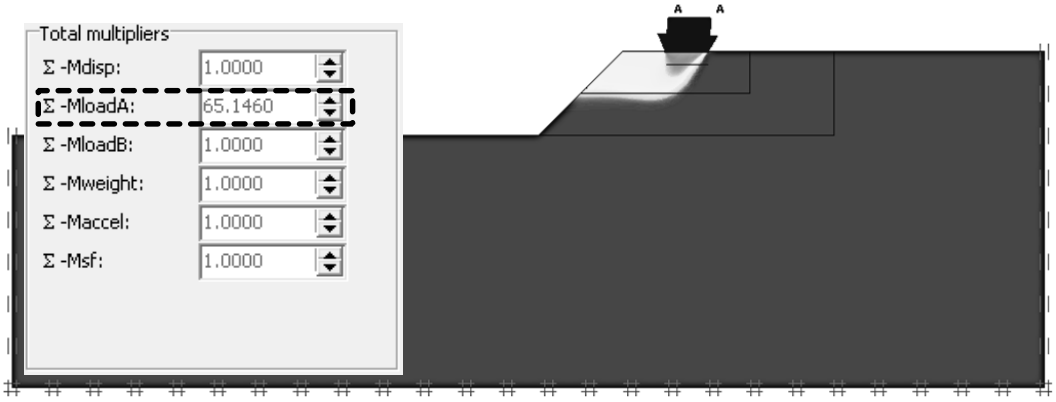


Figure 4.39. Load multiplier (*Σ-MloadA*) and the failure mechanism obtained by Plaxis 2D for the design example 3.

4.5.4. Design Example 4

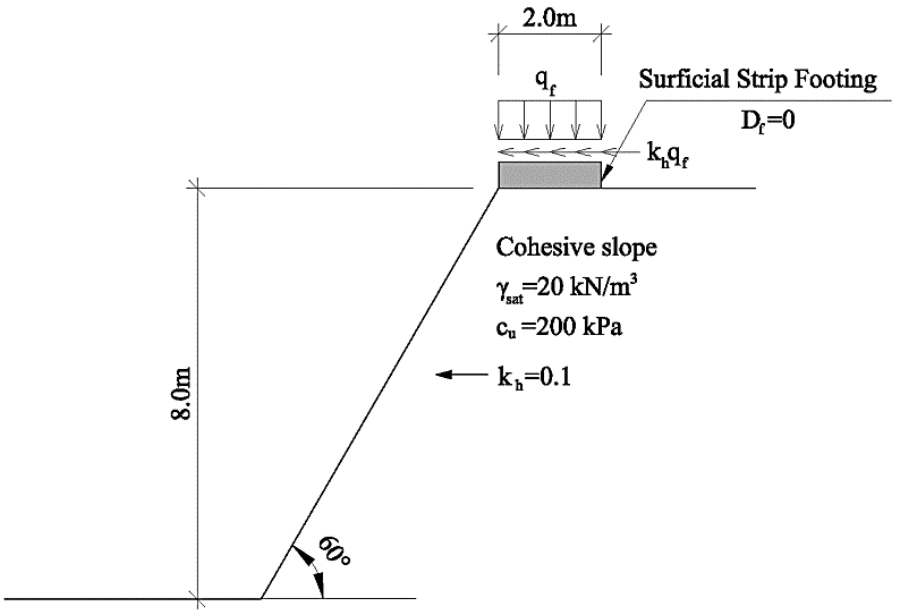


Figure 4.40. Schematic representation of the design example 4.

The slope angle given in this example is greater than the maximum slope angle considered in the parametric study. Therefore, estimation of expected failure mechanism by the charts given in Figure 4.11 and Figure 4.12 is not possible. However, in order to estimate only the value of N_{cse}, firstly, the relationship between slope angle and seismic bearing capacity factor was investigated. As shown in the chart given in Figure 4.41, the relationship between these variables is linear. By using this linear relationship, linear extrapolation can be made for the estimation of N_{cse} corresponding to β= 60°.

Seismic bearing capacity factor (N_{cse}) for β= 60° can be estimated using the formula given in below. Accordingly,

$$N_{cse}= -0.0317\beta+4.59= -0.0317\times60+4.59= 2.69 \quad (4.10)$$

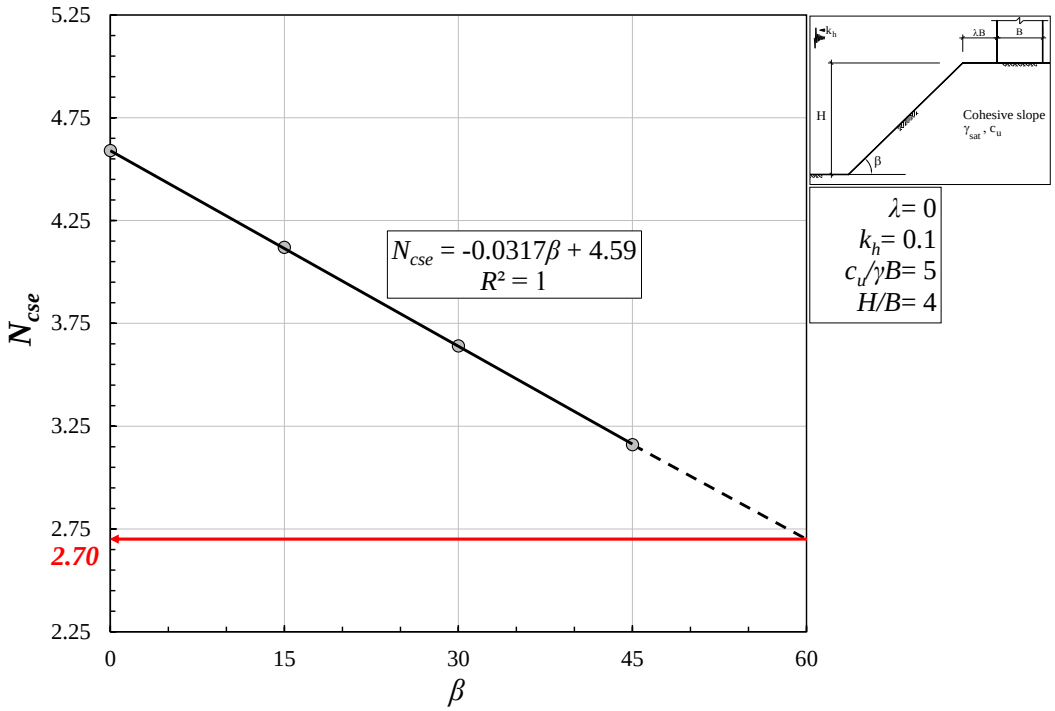


Figure 4.41. Linear relationship between $N_{cse} - \beta$.

Thus, seismic bearing capacity (q_f),

$$q_f = c_u\, N_{cse}= 200\times2.69= 538 \text{ kPa} \quad (4.11)$$

On the other hand, a finite element model was prepared for the same problem. The load multiplier (*Σ-MloadA*) is found as 108.02 at the ultimate state and the seismic bearing capacity obtained by Plaxis 2D is 540 kPa. Estimated seismic bearing capacity value via linear extrapolation is on the safe side and the difference between the result of linear extrapolation and Plaxis 2D is less than %1. As shown in Figure 4.42, the failure mode determined by Plaxis 2D is "foundation failure". Finally, it should be noted that the "extrapolation approach" should be used with caution. When this approach is used, one must verify initially that the cohesive slope is able to maintain its overall stability by the influence of selected design earthquake.

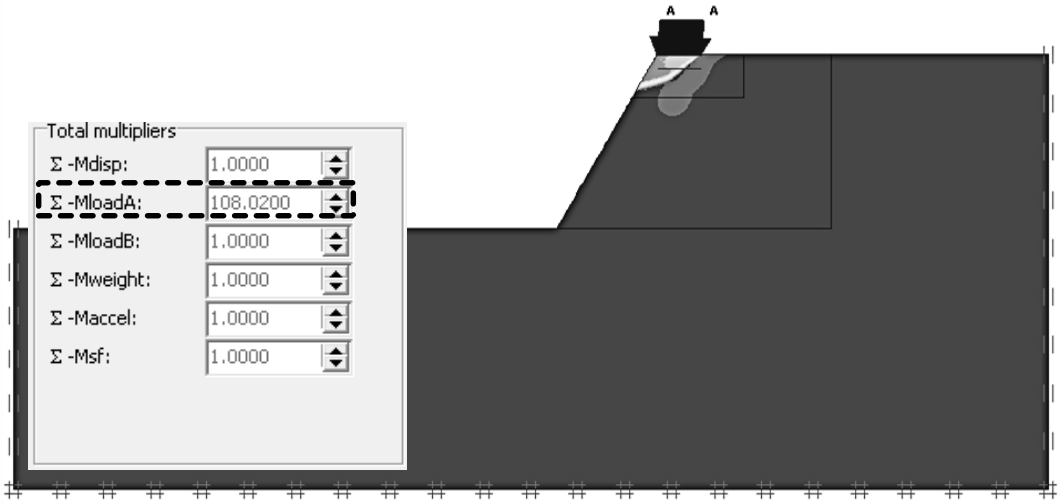


Figure 4.42. Load multiplier (*Σ-MloadA*) and the failure mechanism obtained by Plaxis 2D for the design example 4.

4.5.5. Design Example 5

For the design example presented in Figure 4.43, H/B, λ and $c_u/\gamma B$ are 4, 0 and 1.43 respectively. Since β is 45° and λ is less than 0.50, expected failure mode can be estimated with the design chart presented in Figure 4.11. As shown in Figure 4.44, since the data point corresponding to k_h-$c_u/\gamma B$ couple given in this example remains in the area of "Base failure due to earthquake or gravity", it can be said that the cohesive slope loses its overall stability by the influence of inertia force or purely of the self-weight. At this point, an additional rule is defined in the chart presented in Figure 4.11 to make a distinction

between these two alternatives. Accordingly, since $c_u/\gamma B$= 1.43 is greater than 0.625, base failure due to earthquake is expected to occur.

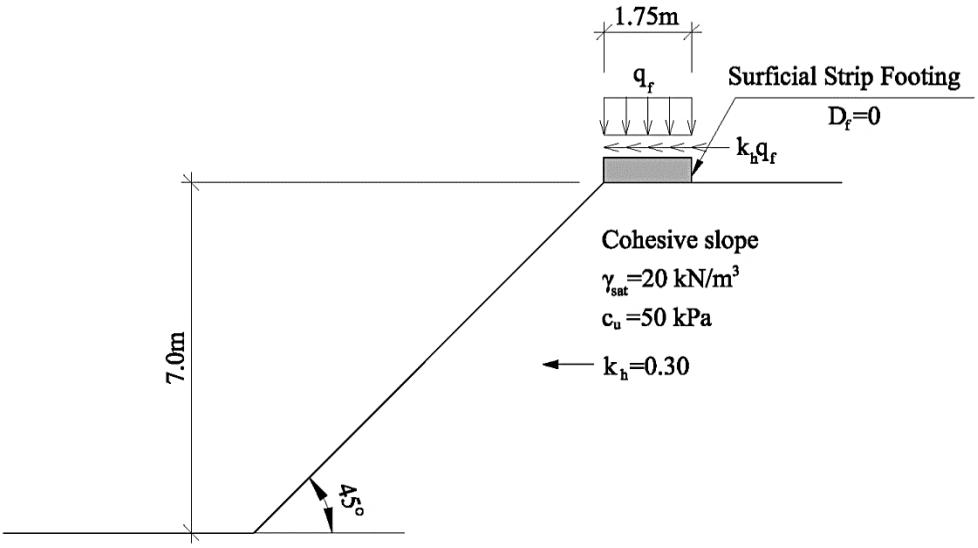


Figure 4.43. Schematic representation of the design example 5.

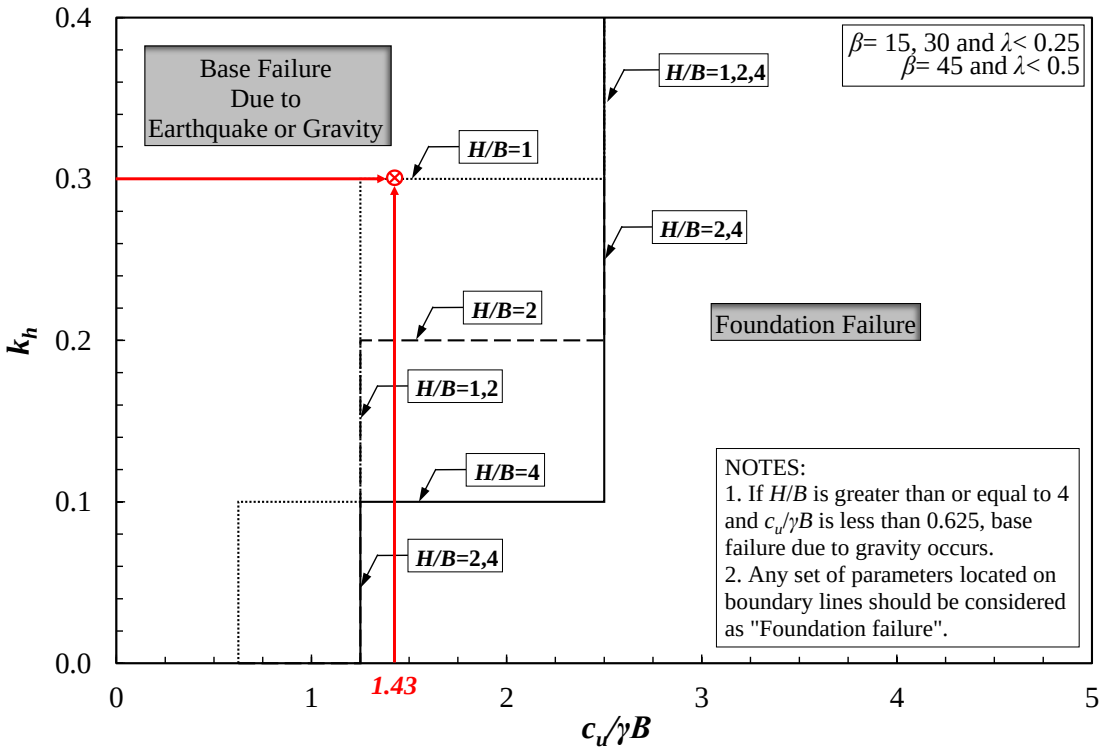


Figure 4.44. Estimation of the failure mode for the design example 5.

On the other hand, a finite element model was prepared for the same problem. As shown in Figure 4.45, failure was observed at the end of the third calculation stage which means that the cohesive slope loses its stability in case of an earthquake. Furthermore, failure mechanism formed within the cohesive slope is presented in Figure 4.46. It is concluded that the failure mode determined by Plaxis 2D is "base failure due to earthquake" which is consistent with the estimation of the proposed method.

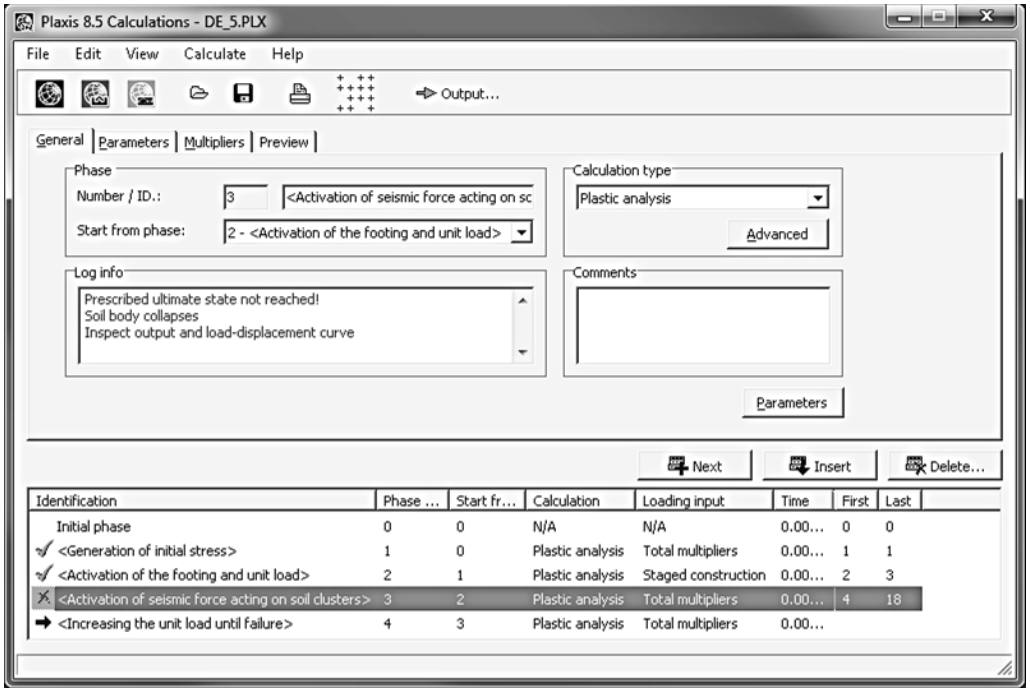


Figure 4.45. View of "Calculations Module" window for the design example 5.

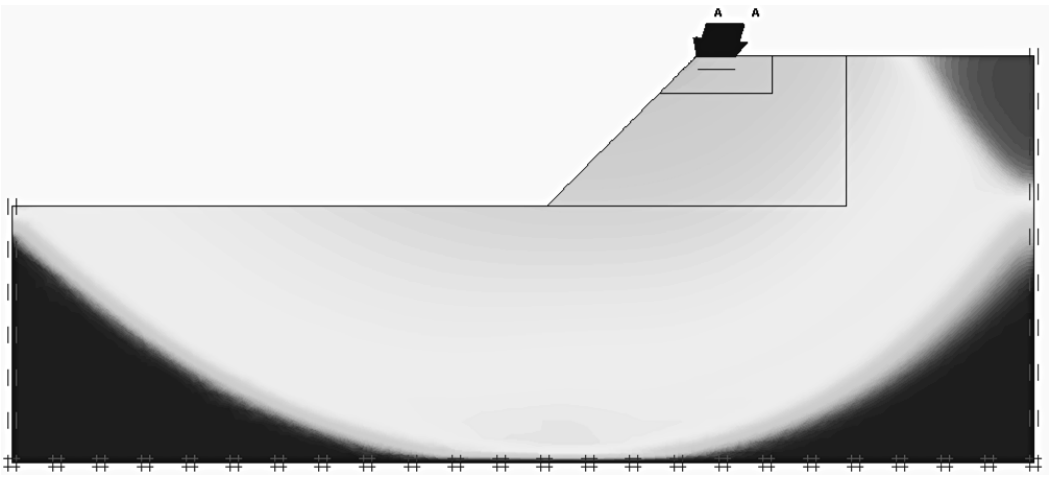


Figure 4.46. Failure mechanism obtained by Plaxis 2D for the design example 5.

4.5.6. Design Example 6

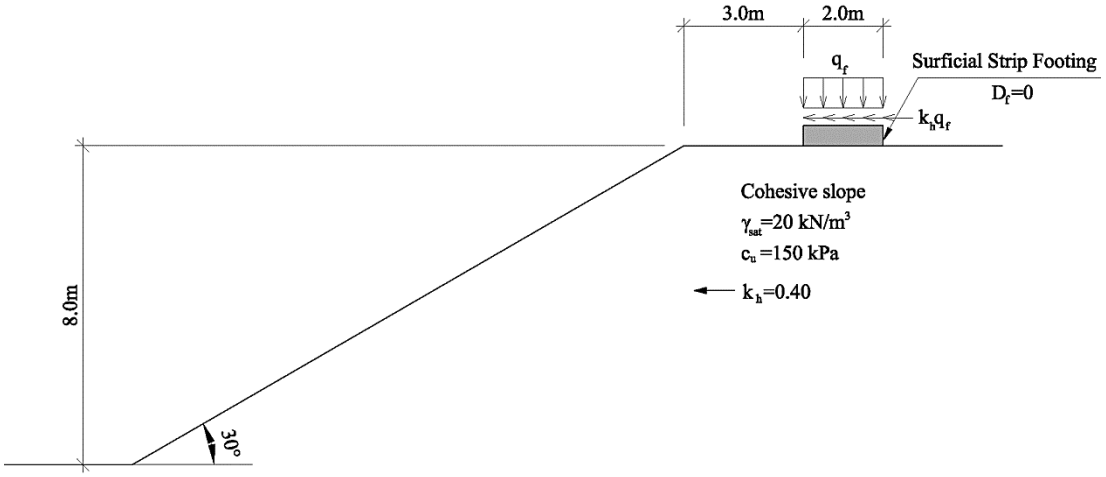


Figure 4.47. Schematic representation of the design example 5

For the design example presented in Figure 4.47, H/B, λ and $c_u/\gamma B$ are 4, 1.5 and 3.75 respectively. Since β is 30° and λ is greater than 0.25, expected failure mode can be estimated with the design chart presented in Figure 4.12. As shown in Figure 4.48, the cohesive slope is stable under both static and seismic conditions. Moreover, expected failure mode for the set of parameters given in above is "foundation sliding" since k_h is greater than 0.36.

As previously mentioned in Chapter 4.2, when "foundation sliding" starts, the product of "$N_{ce}\ k_h$" should be one. Therefore, seismic bearing capacity factor (N_{cse}),

$$N_{cse}=\frac{1}{k_h}=\frac{1}{0.4}=2.50 \tag{4.12}$$

Thus, seismic bearing capacity (q_f),

$$q_f = c_u\ N_{cse} = 150\times 2.50 = 375 \text{ kPa} \tag{4.13}$$

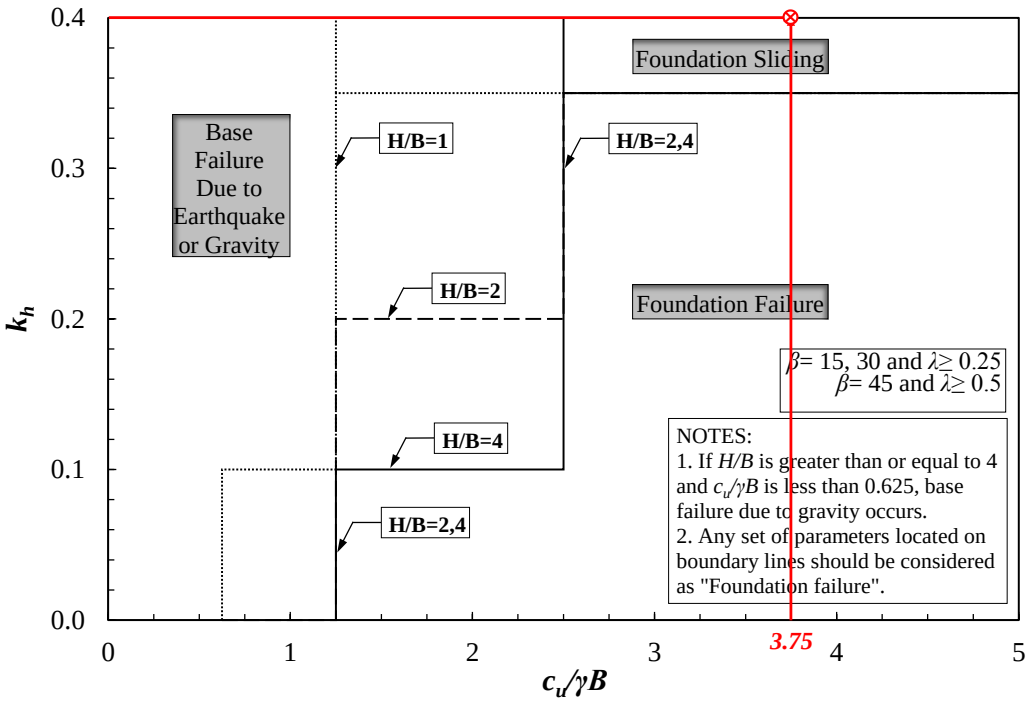


Figure 4.48. Estimation of the failure mode for the design example 6.

On the other hand, a finite element model was prepared for the same problem. The load multiplier (*Σ-MloadA*) is found as 75.15 at the ultimate state and the seismic bearing capacity obtained by Plaxis 2D is 376 kPa. The result of suggested method and Plaxis 2D is nearly the same. Also, as shown in Figure 4.34, the failure mode determined by Plaxis 2D is "foundation sliding" which is consistent with the estimation of the proposed method.

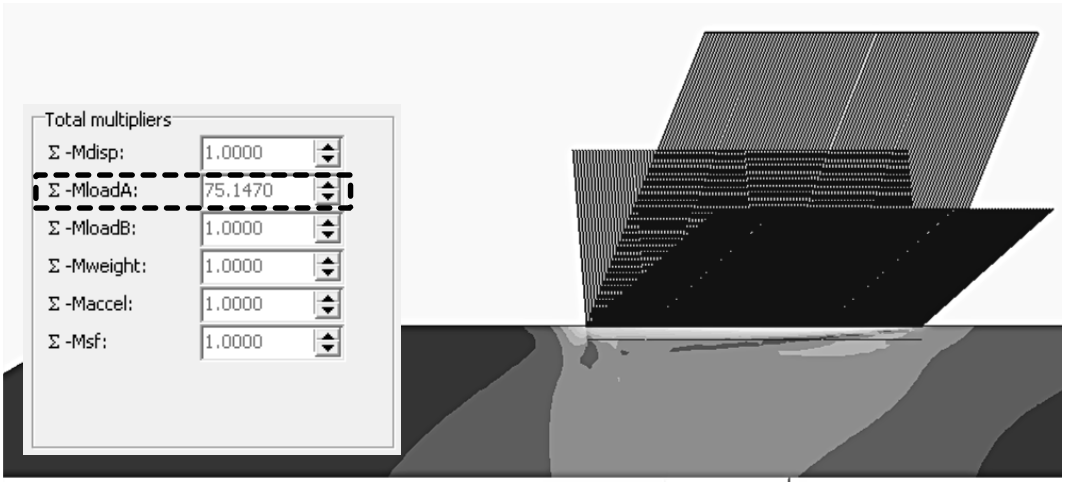


Figure 4.49. Load multiplier (*Σ-MloadA*) and the failure mechanism obtained by Plaxis 2D for the design example 6.

5. CONCLUSIONS

Seismic bearing capacity of surficial strip footings located near cohesive slopes is a problem of geotechnical earthquake engineering for which a few research studies has been made so far. In this study, for the purposes of developing a complete solution technique, a commercial software package, namely Plaxis 2D, based on FEM was used and a great effort was made to establish a methodology by evaluating numerical analysis results in a systematic way.

With the development of user interfaces of commercial software packages based on FEM, users who do not have an extensive knowledge of FEM utilizes these software as a "black box". Essentially, the accuracy of software outputs obtained purely depends on idealization and assumptions made for the solution of the problem and modelling technique. Therefore, suitability of the assumptions and the modelling technique was evaluated initially by comparing results of Plaxis 2D software package with those of previous research studies. As discussed in detail in Chapter 3.8, it can be said that results of this study are quite consistent with those of previous researches made in all cases selected for the comparison. Also, it should be mentioned that differences found in some cases between the results of this study and those of previous researches are as small as that they can be neglected.

In this thesis study, it was shown that seismic bearing capacity of surficial strip footings located near cohesive slopes could be estimated by a simplified formula. One of those two parameters indicated in the formula is undrained shear strength of cohesive slope soil (c_u) and its value can be readily determined by several methods. However, seismic bearing capacity factor (N_{cse}) should be determined by the design charts presented in Chapter 4.3. It should be noted that the design charts are the consequence of the parametric study made in the scope of this study. The parametric study includes the creation of Plaxis 2D input files (the number of finite elements model used is greater than 1000), the analysis of all input files and finally the evaluation of outputs obtained by the software. With the evaluation of analysis results in a systematic way, the results given in following were obtained.

- Seismic bearing capacity factor (N_{cse}) can be expressed by a function of $f\left(k_h, \beta, \lambda, {c_u}/{\gamma B}, {H}/{B}\right)$.

- The increase in horizontal seismic acceleration coefficient (k_h) reduces seismic bearing capacity factor considerably.

- Seismic bearing capacity factor decreases with the increase in the slope angle (β) for footing positions that are closer than the threshold distance to the slope edge ($\lambda \leq \lambda_0$).

- Seismic bearing capacity factor takes the minimum value for the case in which the footing is at the edge of the slope ($\lambda = 0$) $\left(k_h, \beta, {c_u}/{\gamma B}, {H}/{B} \text{ are constant}\right)$. Seismic bearing capacity factor increases with the increase of normalized footing distance (λ) until reaching threshold distance (λ_0). The value of this factor is constant for all footing positions beyond the threshold distance.

- The influence of H/B ratio on seismic bearing capacity factor is negligible for the cases in which "foundation failure" occurs. For smaller values of slope soil strength ($c_u/\gamma B$), the increase in H/B ratio leads to reduce the value of seismic bearing capacity factor or to change the failure mode observed at the ultimate state.

- Normalized slope soil strength ($c_u/\gamma B$) has a minor influence on seismic bearing capacity factor and it increases with the increase of normalized slope soil strength. Also, the failure mode varies as the soil strength decreases $\left(k_h, \beta, \lambda, {H}/{B} \text{ are constant}\right)$.

- Four different failure modes (foundation failure, sliding, base failure due to earthquake and base failure due to gravity) were determined. Variation of failure mode with influential parameters was demonstrated with two graphs presented.

- Design charts were prepared for geotechnical designers and practitioners particularly for the cases in which the use of any geotechnical design software is not possible.

- Normalized threshold distance (λ_0) varies in between 0.25-3.00 depending on horizontal seismic acceleration coefficient.

- For the failure surfaces intersecting with the slope line, the failure surface makes an angle of 45 degrees with the slope line.

- Failure surface passes through shallower depths as horizontal seismic acceleration coefficient increases.

- Seismic bearing capacity factor (N_{cse}) can be estimated by making lineer interpolation for the intermediate values of influential parameters.

- If the cohesive slope is able to maintain its overall stability in case of an earthquake, extrapolation can be made to estimate seismic bearing capacity factor (N_{cse}) for slope angles that are greater than the maximum slope angle considered in this study.

APPENDIX A: STABILITY ASSESMENT of COHESIVE SLOPES in SEISMIC CONDITION by USING KOPPULA'S METHOD (1984).

For all combinations of the slope geometry, the undrained shear strength of cohesive slope soil and the horizontal seismic acceleration coefficient, critical height values (H_{cr}) calculated with Koppula's method (1984) and slope stability assessments are given in Table A.1.

Table A.1. H_{cr} values calculations and stability assessment of cohesive slopes in seismic condition using Koppula's method.

H (m)	D	β (°)	k_h	N_2	γ (kN/m^3)	c_u (kPa)	H_{cr} (m)	Stability Check
2	7	30	0.1	3.24	20	200	32.4	STABLE
2	7	30	0.2	2.11	20	200	21.1	STABLE
2	7	30	0.3	1.49	20	200	14.9	STABLE
2	7	30	0.4	1.08	20	200	10.8	STABLE
4	4	30	0.1	3.24	20	200	32.4	STABLE
4	4	30	0.2	2.11	20	200	21.1	STABLE
4	4	30	0.3	1.49	20	200	14.9	STABLE
4	4	30	0.4	1.08	20	200	10.8	STABLE
8	2.5	30	0.1	4.12	20	200	41.2	STABLE
8	2.5	30	0.2	3.16	20	200	31.6	STABLE
8	2.5	30	0.3	2.59	20	200	25.9	STABLE
8	2.5	30	0.4	2.14	20	200	21.4	STABLE
2	7	30	0.1	3.24	20	100	16.2	STABLE
2	7	30	0.2	2.11	20	100	10.5	STABLE
2	7	30	0.3	1.49	20	100	7.4	STABLE
2	7	30	0.4	1.08	20	100	5.4	STABLE
4	4	30	0.1	3.24	20	100	16.2	STABLE
4	4	30	0.2	2.11	20	100	10.5	STABLE
4	4	30	0.3	1.49	20	100	7.4	STABLE
4	4	30	0.4	1.08	20	100	5.4	STABLE
8	2.5	30	0.1	4.12	20	100	20.6	STABLE
8	2.5	30	0.2	3.16	20	100	15.8	STABLE
8	2.5	30	0.3	2.59	20	100	12.9	STABLE
8	2.5	30	0.4	2.14	20	100	10.7	STABLE
2	7	30	0.1	3.24	20	50	8.1	STABLE
2	7	30	0.2	2.11	20	50	5.3	STABLE
2	7	30	0.3	1.49	20	50	3.7	STABLE
2	7	30	0.4	1.08	20	50	2.7	STABLE
4	4	30	0.1	3.24	20	50	8.1	STABLE
4	4	30	0.2	2.11	20	50	5.3	STABLE
4	4	30	0.3	1.49	20	50	**3.7**	**UNSTABLE**
4	4	30	0.4	1.08	20	50	**2.7**	**UNSTABLE**
8	2.5	30	0.1	4.12	20	50	10.3	STABLE
8	2.5	30	0.2	3.16	20	50	**7.9**	**UNSTABLE**
8	2.5	30	0.3	2.59	20	50	**6.5**	**UNSTABLE**
8	2.5	30	0.4	2.14	20	50	**5.3**	**UNSTABLE**

Table A.1. H_{cr} values calculations and stability assessment of cohesive slopes in seismic condition using Koppula's method (Cont.).

H (m)	D	β (°)	k_h	N_2	γ (kN/m^3)	c_u (kPa)	H_{cr} (m)	Stability Check
2	7	30	0.1	3.24	20	25	4.0	STABLE
2	7	30	0.2	2.11	20	25	2.6	STABLE
2	7	30	0.3	1.49	20	25	**1.9**	**UNSTABLE**
2	7	30	0.4	1.08	20	25	**1.3**	**UNSTABLE**
4	4	30	0.1	3.24	20	25	4.0	STABLE
4	4	30	0.2	2.11	20	25	**2.6**	**UNSTABLE**
4	4	30	0.3	1.49	20	25	**1.9**	**UNSTABLE**
4	4	30	0.4	1.08	20	25	**1.3**	**UNSTABLE**
8	2.5	30	0.1	4.12	20	25	**5.1**	**UNSTABLE**
8	2.5	30	0.2	3.16	20	25	**4.0**	**UNSTABLE**
8	2.5	30	0.3	2.59	20	25	**3.2**	**UNSTABLE**
8	2.5	30	0.4	2.14	20	25	**2.7**	**UNSTABLE**
2	7	45	0.1	2.73	20	200	27.3	STABLE
2	7	45	0.2	1.68	20	200	16.8	STABLE
2	7	45	0.3	1.15	20	200	11.5	STABLE
2	7	45	0.4	0.81	20	200	8.1	STABLE
4	4	45	0.1	2.73	20	200	27.3	STABLE
4	4	45	0.2	1.68	20	200	16.8	STABLE
4	4	45	0.3	1.15	20	200	11.5	STABLE
4	4	45	0.4	0.81	20	200	8.1	STABLE
8	2.5	45	0.1	3.58	20	200	35.8	STABLE
8	2.5	45	0.2	2.51	20	200	25.1	STABLE
8	2.5	45	0.3	1.97	20	200	19.7	STABLE
8	2.5	45	0.4	1.61	20	200	16.1	STABLE
2	7	45	0.1	2.73	20	100	13.7	STABLE
2	7	45	0.2	1.68	20	100	8.4	STABLE
2	7	45	0.3	1.15	20	100	5.8	STABLE
2	7	45	0.4	0.81	20	100	4.0	STABLE
4	4	45	0.1	2.73	20	100	13.7	STABLE
4	4	45	0.2	1.68	20	100	8.4	STABLE
4	4	45	0.3	1.15	20	100	5.8	STABLE
4	4	45	0.4	0.81	20	100	4.0	STABLE
8	2.5	45	0.1	3.58	20	100	17.9	STABLE
8	2.5	45	0.2	2.51	20	100	12.5	STABLE
8	2.5	45	0.3	1.97	20	100	9.9	STABLE
8	2.5	45	0.4	1.61	20	100	8.0	STABLE
2	7	45	0.1	2.73	20	50	6.8	STABLE
2	7	45	0.2	1.68	20	50	4.2	STABLE
2	7	45	0.3	1.15	20	50	2.9	STABLE
2	7	45	0.4	0.81	20	50	2.0	STABLE
4	4	45	0.1	2.73	20	50	6.8	STABLE
4	4	45	0.2	1.68	20	50	4.2	STABLE
4	4	45	0.3	1.15	20	50	**2.9**	**UNSTABLE**
4	4	45	0.4	0.81	20	50	**2.0**	**UNSTABLE**
8	2.5	45	0.1	3.58	20	50	9.0	STABLE
8	2.5	45	0.2	2.51	20	50	**6.3**	**UNSTABLE**
8	2.5	45	0.3	1.97	20	50	**4.9**	**UNSTABLE**
8	2.5	45	0.4	1.61	20	50	**4.0**	**UNSTABLE**
2	7	45	0.1	2.73	20	25	3.4	STABLE
2	7	45	0.2	1.68	20	25	2.1	STABLE

Table A.1. Hcr values calculations and stability assessment of cohesive slopes in seismic condition using Koppula's method (Cont.).

H (m)	D	β (°)	k_h	N_2	γ (kN/m^3)	c_u (kPa)	H_{cr} (m)	Stability Check
2	7	45	0.3	1.15	20	25	**1.4**	**UNSTABLE**
2	7	45	0.4	0.81	20	25	**1.0**	**UNSTABLE**
4	4	45	0.1	2.73	20	25	**3.4**	**UNSTABLE**
4	4	45	0.2	1.68	20	25	**2.1**	**UNSTABLE**
4	4	45	0.3	1.15	20	25	**1.4**	**UNSTABLE**
4	4	45	0.4	0.81	20	25	**1.0**	**UNSTABLE**
8	2.5	45	0.1	3.58	20	25	**4.5**	**UNSTABLE**
8	2.5	45	0.2	2.51	20	25	**3.1**	**UNSTABLE**
8	2.5	45	0.3	1.97	20	25	**2.5**	**UNSTABLE**
8	2.5	45	0.4	1.61	20	25	**2.0**	**UNSTABLE**

APPENDIX B: LIST OF RESULTS OF FINITE ELEMENTS MODELS CREATED FOR STATIC CONDITION.

List of results for finite element models created for static condition is presented in Table B.1.

Table B.1. List of results of finite elements models created for static condition.

	GEOMETRICAL PROPERTIES				SLOPE SOIL PROPERTIES					SEISMIC EFFECT	FILE NAME	ANALYSIS RESULTS FOR STATIC LOADING					
Model No.	β (°)	H (m)	λ	B (m)	γ (kN/m^3)	c_u (kN/m^2)	Φ_u (°)	E_u (MPa)	ν_u	k_h		H/B	β (°)	$C_u/\gamma B$	Load multiplier	q_f (kPa)	N_{cs}	Failure mode
1	15	2	0	2.0	20	25	0	5	0.495	0.0	C_15_2_0_25_S	1	15	0.625	22.1	111	4.42	Foundation failure
2	30	2	0	2.0	20	25	0	5	0.495	0.0	C_30_2_0_25_S	1	30	0.625	17.9	90	3.58	Foundation failure
3	45	2	0	2.0	20	25	0	5	0.495	0.0	C_45_2_0_25_S	1	45	0.625	14.2	71	2.84	Foundation failure
4	15	4	0	2.0	20	25	0	5	0.495	0.0	C_15_4_0_25_S	2	15	0.625	22.2	111	4.44	Foundation failure
5	30	4	0	2.0	20	25	0	5	0.495	0.0	C_30_4_0_25_S	2	30	0.625	17.5	87	3.50	Foundation failure
6	45	4	0	2.0	20	25	0	5	0.495	0.0	C_45_4_0_25_S	2	45	0.625	12.4	62	2.49	Foundation failure
7	15	8	0	2.0	20	25	0	5	0.495	0.0	C_15_8_0_25_S	4	15	0.625	N.F.	N.F.	N.F.	Base failure_GR
8	30	8	0	2.0	20	25	0	5	0.495	0.0	C_30_8_0_25_S	4	30	0.625	N.F.	N.F.	N.F.	Base failure_GR
9	45	8	0	2.0	20	25	0	5	0.495	0.0	C_45_8_0_25_S	4	45	0.625	N.F.	N.F.	N.F.	Base failure_GR
10	15	2	0.5	2.0	20	25	0	5	0.495	0.0	C_15_2_0.5_25_S	1	15	0.625	23.8	119	4.77	Foundation failure
11	30	2	0.5	2.0	20	25	0	5	0.495	0.0	C_30_2_0.5_25_S	1	30	0.625	20.0	100	4.00	Foundation failure
12	45	2	0.5	2.0	20	25	0	5	0.495	0.0	C_45_2_0.5_25_S	1	45	0.625	16.9	85	3.38	Foundation failure
13	15	4	0.5	2.0	20	25	0	5	0.495	0.0	C_15_4_0.5_25_S	2	15	0.625	23.9	120	4.79	Foundation failure
14	30	4	0.5	2.0	20	25	0	5	0.495	0.0	C_30_4_0.5_25_S	2	30	0.625	18.4	92	3.68	Foundation failure
15	45	4	0.5	2.0	20	25	0	5	0.495	0.0	C_45_4_0.5_25_S	2	45	0.625	13.3	67	2.67	Foundation failure
16	15	8	0.5	2.0	20	25	0	5	0.495	0.0	C_15_8_0.5_25_S	4	15	0.625	N.F.	N.F.	N.F.	Base failure_GR
17	30	8	0.5	2.0	20	25	0	5	0.495	0.0	C_30_8_0.5_25_S	4	30	0.625	N.F.	N.F.	N.F.	Base failure_GR
18	45	8	0.5	2.0	20	25	0	5	0.495	0.0	C_45_8_0.5_25_S	4	45	0.625	N.F.	N.F.	N.F.	Base failure_GR
19	15	2	1	2.0	20	25	0	5	0.495	0.0	C_15_2_1_25_S	1	15	0.625	25.3	126	5.05	Foundation failure
20	30	2	1	2.0	20	25	0	5	0.495	0.0	C_30_2_1_25_S	1	30	0.625	22.1	110	4.42	Foundation failure
21	45	2	1	2.0	20	25	0	5	0.495	0.0	C_45_2_1_25_S	1	45	0.625	19.4	97	3.88	Foundation failure
22	15	4	1	2.0	20	25	0	5	0.495	0.0	C_15_4_1_25_S	2	15	0.625	25.3	127	5.06	Foundation failure
23	30	4	1	2.0	20	25	0	5	0.495	0.0	C_30_4_1_25_S	2	30	0.625	19.5	98	3.90	Foundation failure
24	45	4	1	2.0	20	25	0	5	0.495	0.0	C_45_4_1_25_S	2	45	0.625	14.7	73	2.93	Foundation failure
25	15	8	1	2.0	20	25	0	5	0.495	0.0	C_15_8_1_25_S	4	15	0.625	N.F.	N.F.	N.F.	Base failure_GR
26	30	8	1	2.0	20	25	0	5	0.495	0.0	C_30_8_1_25_S	4	30	0.625	N.F.	N.F.	N.F.	Base failure_GR
27	45	8	1	2.0	20	25	0	5	0.495	0.0	C_45_8_1_25_S	4	45	0.625	N.F.	N.F.	N.F.	Base failure_GR
28	15	2	2	2.0	20	25	0	5	0.495	0.0	C_15_2_2_25_S	1	15	0.625	26.0	130	5.19	Foundation failure
29	30	2	2	2.0	20	25	0	5	0.495	0.0	C_30_2_2_25_S	1	30	0.625	25.3	127	5.07	Foundation failure
30	45	2	2	2.0	20	25	0	5	0.495	0.0	C_45_2_2_25_S	1	45	0.625	23.5	118	4.71	Foundation failure
31	15	4	2	2.0	20	25	0	5	0.495	0.0	C_15_4_2_25_S	2	15	0.625	26.0	130	5.20	Foundation failure
32	30	4	2	2.0	20	25	0	5	0.495	0.0	C_30_4_2_25_S	2	30	0.625	21.9	110	4.39	Foundation failure
33	45	4	2	2.0	20	25	0	5	0.495	0.0	C_45_4_2_25_S	2	45	0.625	17.9	89	3.57	Foundation failure
34	15	8	2	2.0	20	25	0	5	0.495	0.0	C_15_8_2_25_S	4	15	0.625	N.F.	N.F.	N.F.	Base failure_GR
35	30	8	2	2.0	20	25	0	5	0.495	0.0	C_30_8_2_25_S	4	30	0.625	N.F.	N.F.	N.F.	Base failure_GR
36	45	8	2	2.0	20	25	0	5	0.495	0.0	C_45_8_2_25_S	4	45	0.625	N.F.	N.F.	N.F.	Base failure_GR

N.F.: Not Found (Corresponds to the case in which base failure is observed under the gravity loading).

Table B.1. List of results of finite elements models created for static condition (Cont.).

	GEOMETRICAL PROPERTIES				SLOPE SOIL PROPERTIES				SEISMIC EFFECT	FILE NAME	ANALYSIS RESULTS FOR STATIC LOADING					
Model No.	β (°)	H (m)	λ	B (m)	γ (kN/m^3)	c_u (kN/m^2)	Φ_u (°)	E_u (MPa)	ν_u	k_h		H/B	β (°)	$C_u/\gamma B$	Load multiplier	q_f (kPa)	N_{cs}	Failure mode
37	15	2	0	2.0	20	50	0	10	0.495	0.0	C_15_2_0_50_S	1	15	1.25	45.5	227	4.55	Foundation failure
38	30	2	0	2.0	20	50	0	10	0.495	0.0	C_30_2_0_50_S	1	30	1.25	39.0	195	3.90	Foundation failure
39	45	2	0	2.0	20	50	0	10	0.495	0.0	C_45_2_0_50_S	1	45	1.25	32.7	163	3.27	Foundation failure
40	15	4	0	2.0	20	50	0	10	0.495	0.0	C_15_4_0_50_S	2	15	1.25	45.6	228	4.56	Foundation failure
41	30	4	0	2.0	20	50	0	10	0.495	0.0	C_30_4_0_50_S	2	30	1.25	39.1	196	3.91	Foundation failure
42	45	4	0	2.0	20	50	0	10	0.495	0.0	C_45_4_0_50_S	2	45	1.25	32.7	163	3.27	Foundation failure
43	15	8	0	2.0	20	50	0	10	0.495	0.0	C_15_8_0_50_S	4	15	1.25	45.7	228	4.57	Foundation failure
44	30	8	0	2.0	20	50	0	10	0.495	0.0	C_30_8_0_50_S	4	30	1.25	39.1	196	3.91	Foundation failure
45	45	8	0	2.0	20	50	0	10	0.495	0.0	C_45_8_0_50_S	4	45	1.25	32.7	164	3.27	Foundation failure
46	15	2	0.5	2.0	20	50	0	10	0.495	0.0	C_15_2_0.5_50_S	1	15	1.25	48.4	242	4.84	Foundation failure
47	30	2	0.5	2.0	20	50	0	10	0.495	0.0	C_30_2_0.5_50_S	1	30	1.25	43.8	219	4.38	Foundation failure
48	45	2	0.5	2.0	20	50	0	10	0.495	0.0	C_45_2_0.5_50_S	1	45	1.25	38.4	192	3.84	Foundation failure
49	15	4	0.5	2.0	20	50	0	10	0.495	0.0	C_15_4_0.5_50_S	2	15	1.25	48.7	243	4.87	Foundation failure
50	30	4	0.5	2.0	20	50	0	10	0.495	0.0	C_30_4_0.5_50_S	2	30	1.25	43.8	219	4.38	Foundation failure
51	45	4	0.5	2.0	20	50	0	10	0.495	0.0	C_45_4_0.5_50_S	2	45	1.25	37.9	190	3.79	Foundation failure
52	15	8	0.5	2.0	20	50	0	10	0.495	0.0	C_15_8_0.5_50_S	4	15	1.25	48.9	244	4.89	Foundation failure
53	30	8	0.5	2.0	20	50	0	10	0.495	0.0	C_30_8_0.5_50_S	4	30	1.25	44.1	220	4.41	Foundation failure
54	45	8	0.5	2.0	20	50	0	10	0.495	0.0	C_45_8_0.5_50_S	4	45	1.25	37.9	190	3.79	Foundation failure
55	15	2	1	2.0	20	50	0	10	0.495	0.0	C_15_2_1_50_S	1	15	1.25	50.8	254	5.08	Foundation failure
56	30	2	1	2.0	20	50	0	10	0.495	0.0	C_30_2_1_50_S	1	30	1.25	47.6	238	4.76	Foundation failure
57	45	2	1	2.0	20	50	0	10	0.495	0.0	C_45_2_1_50_S	1	45	1.25	43.0	215	4.30	Foundation failure
58	15	4	1	2.0	20	50	0	10	0.495	0.0	C_15_4_1_50_S	2	15	1.25	50.9	255	5.09	Foundation failure
59	30	4	1	2.0	20	50	0	10	0.495	0.0	C_30_4_1_50_S	2	30	1.25	47.7	238	4.77	Foundation failure
60	45	4	1	2.0	20	50	0	10	0.495	0.0	C_45_4_1_50_S	2	45	1.25	41.5	208	4.15	Foundation failure
61	15	8	1	2.0	20	50	0	10	0.495	0.0	C_15_8_1_50_S	4	15	1.25	51.1	255	5.11	Foundation failure
62	30	8	1	2.0	20	50	0	10	0.495	0.0	C_30_8_1_50_S	4	30	1.25	47.7	239	4.77	Foundation failure
63	45	8	1	2.0	20	50	0	10	0.495	0.0	C_45_8_1_50_S	4	45	1.25	39.5	198	3.95	Foundation failure
64	15	2	2	2.0	20	50	0	10	0.495	0.0	C_15_2_2_50_S	1	15	1.25	51.9	260	5.19	Foundation failure
65	30	2	2	2.0	20	50	0	10	0.495	0.0	C_30_2_2_50_S	1	30	1.25	51.9	259	5.19	Foundation failure
66	45	2	2	2.0	20	50	0	10	0.495	0.0	C_45_2_2_50_S	1	45	1.25	50.1	251	5.01	Foundation failure
67	15	4	2	2.0	20	50	0	10	0.495	0.0	C_15_4_2_50_S	2	15	1.25	52.0	260	5.20	Foundation failure
68	30	4	2	2.0	20	50	0	10	0.495	0.0	C_30_4_2_50_S	2	30	1.25	52.0	260	5.20	Foundation failure
69	45	4	2	2.0	20	50	0	10	0.495	0.0	C_45_4_2_50_S	2	45	1.25	47.6	238	4.76	Foundation failure
70	15	8	2	2.0	20	50	0	10	0.495	0.0	C_15_8_2_50_S	4	15	1.25	52.2	261	5.22	Foundation failure
71	30	8	2	2.0	20	50	0	10	0.495	0.0	C_30_8_2_50_S	4	30	1.25	52.0	260	5.20	Foundation failure
72	45	8	2	2.0	20	50	0	10	0.495	0.0	C_45_8_2_50_S	4	45	1.25	41.9	210	4.19	Foundation failure

N.F.: Not Found (Corresponds to the case in which base failure is observed under the gravity loading).

Table B.1. List of results of finite elements models created for static condition (Cont.).

	GEOMETRICAL PROPERTIES				SLOPE SOIL PROPERTIES				SEISMIC EFFECT	FILE NAME	ANALYSIS RESULTS FOR STATIC LOADING					
Model No.	β (°)	H (m)	λ	B (m)	γ (kN/m^3)	c_u (kN/m^2)	Φ_u (°)	E_u (MPa)	ν_u	k_h		H/B	β (°)	$C_u/\gamma B$	Load multiplier	q_f (kPa)	N_{cs}	Failure mode
73	15	2	0	2.0	20	100	0	20	0.495	0.0	C_15_2_0_100_S	1	15	2.5	92.2	461	4.61	Foundation failure
74	30	2	0	2.0	20	100	0	20	0.495	0.0	C_30_2_0_100_S	1	30	2.5	80.5	403	4.03	Foundation failure
75	45	2	0	2.0	20	100	0	20	0.495	0.0	C_45_2_0_100_S	1	45	2.5	69.0	345	3.45	Foundation failure
76	15	4	0	2.0	20	100	0	20	0.495	0.0	C_15_4_0_100_S	2	15	2.5	92.6	463	4.63	Foundation failure
77	30	4	0	2.0	20	100	0	20	0.495	0.0	C_30_4_0_100_S	2	30	2.5	80.7	403	4.03	Foundation failure
78	45	4	0	2.0	20	100	0	20	0.495	0.0	C_45_4_0_100_S	2	45	2.5	69.2	346	3.46	Foundation failure
79	15	8	0	2.0	20	100	0	20	0.495	0.0	C_15_8_0_100_S	4	15	2.5	92.5	462	4.62	Foundation failure
80	30	8	0	2.0	20	100	0	20	0.495	0.0	C_30_8_0_100_S	4	30	2.5	81.1	405	4.05	Foundation failure
81	45	8	0	2.0	20	100	0	20	0.495	0.0	C_45_8_0_100_S	4	45	2.5	69.1	346	3.46	Foundation failure
82	15	2	0.5	2.0	20	100	0	20	0.495	0.0	C_15_2_0.5_100_S	1	15	2.5	97.6	488	4.88	Foundation failure
83	30	2	0.5	2.0	20	100	0	20	0.495	0.0	C_30_2_0.5_100_S	1	30	2.5	89.7	449	4.49	Foundation failure
84	45	2	0.5	2.0	20	100	0	20	0.495	0.0	C_45_2_0.5_100_S	1	45	2.5	80.6	403	4.03	Foundation failure
85	15	4	0.5	2.0	20	100	0	20	0.495	0.0	C_15_4_0.5_100_S	2	15	2.5	97.9	490	4.90	Foundation failure
86	30	4	0.5	2.0	20	100	0	20	0.495	0.0	C_30_4_0.5_100_S	2	30	2.5	90.0	450	4.50	Foundation failure
87	45	4	0.5	2.0	20	100	0	20	0.495	0.0	C_45_4_0.5_100_S	2	45	2.5	80.7	403	4.03	Foundation failure
88	15	8	0.5	2.0	20	100	0	20	0.495	0.0	C_15_8_0.5_100_S	4	15	2.5	98.4	492	4.92	Foundation failure
89	30	8	0.5	2.0	20	100	0	20	0.495	0.0	C_30_8_0.5_100_S	4	30	2.5	90.3	451	4.51	Foundation failure
90	45	8	0.5	2.0	20	100	0	20	0.495	0.0	C_45_8_0.5_100_S	4	45	2.5	80.9	405	4.05	Foundation failure
91	15	2	1	2.0	20	100	0	20	0.495	0.0	C_15_2_1_100_S	1	15	2.5	101.8	509	5.09	Foundation failure
92	30	2	1	2.0	20	100	0	20	0.495	0.0	C_30_2_1_100_S	1	30	2.5	96.8	484	4.84	Foundation failure
93	45	2	1	2.0	20	100	0	20	0.495	0.0	C_45_2_1_100_S	1	45	2.5	89.4	447	4.47	Foundation failure
94	15	4	1	2.0	20	100	0	20	0.495	0.0	C_15_4_1_100_S	2	15	2.5	102.1	510	5.10	Foundation failure
95	30	4	1	2.0	20	100	0	20	0.495	0.0	C_30_4_1_100_S	2	30	2.5	96.7	484	4.84	Foundation failure
96	45	4	1	2.0	20	100	0	20	0.495	0.0	C_45_4_1_100_S	2	45	2.5	89.3	447	4.47	Foundation failure
97	15	8	1	2.0	20	100	0	20	0.495	0.0	C_15_8_1_100_S	4	15	2.5	102.4	512	5.12	Foundation failure
98	30	8	1	2.0	20	100	0	20	0.495	0.0	C_30_8_1_100_S	4	30	2.5	97.1	485	4.85	Foundation failure
99	45	8	1	2.0	20	100	0	20	0.495	0.0	C_45_8_1_100_S	4	45	2.5	89.4	447	4.47	Foundation failure
100	15	2	2	2.0	20	100	0	20	0.495	0.0	C_15_2_2_100_S	1	15	2.5	103.9	519	5.19	Foundation failure
101	30	2	2	2.0	20	100	0	20	0.495	0.0	C_30_2_2_100_S	1	30	2.5	103.7	519	5.19	Foundation failure
102	45	2	2	2.0	20	100	0	20	0.495	0.0	C_45_2_2_100_S	1	45	2.5	102.6	513	5.13	Foundation failure
103	15	4	2	2.0	20	100	0	20	0.495	0.0	C_15_4_2_100_S	2	15	2.5	104.1	520	5.20	Foundation failure
104	30	4	2	2.0	20	100	0	20	0.495	0.0	C_30_4_2_100_S	2	30	2.5	104.1	520	5.20	Foundation failure
105	45	4	2	2.0	20	100	0	20	0.495	0.0	C_45_4_2_100_S	2	45	2.5	102.1	511	5.11	Foundation failure
106	15	8	2	2.0	20	100	0	20	0.495	0.0	C_15_8_2_100_S	4	15	2.5	104.4	522	5.22	Foundation failure
107	30	8	2	2.0	20	100	0	20	0.495	0.0	C_30_8_2_100_S	4	30	2.5	104.1	520	5.20	Foundation failure
108	45	8	2	2.0	20	100	0	20	0.495	0.0	C_45_8_2_100_S	4	45	2.5	102.1	511	5.11	Foundation failure

N.F.: Not Found (Corresponds to the case in which base failure is observed under the gravity loading).

Table B.1. List of results of finite elements models created for static condition (Cont.).

	GEOMETRICAL PROPERTIES				SLOPE SOIL PROPERTIES				SEISMIC EFFECT	FILE NAME	ANALYSIS RESULTS FOR STATIC LOADING					
Model No.	β (°)	H (m)	λ	B (m)	γ (kN/m^3)	c_u (kN/m^2)	Φ_u (°)	E_u (MPa)	ν_u	k_h		H/B	β (°)	$C_u/\gamma B$	Load multiplier	q_f (kPa)	N_{cs}	Failure mode
109	15	2	0	2.0	20	200	0	40	0.495	0.0	C_15_2_0_200_S	1	15	5	185.5	927	4.64	Foundation failure
110	30	2	0	2.0	20	200	0	40	0.495	0.0	C_30_2_0_200_S	1	30	5	163.6	818	4.09	Foundation failure
111	45	2	0	2.0	20	200	0	40	0.495	0.0	C_45_2_0_200_S	1	45	5	141.3	707	3.53	Foundation failure
112	15	4	0	2.0	20	200	0	40	0.495	0.0	C_15_4_0_200_S	2	15	5	186.1	931	4.65	Foundation failure
113	30	4	0	2.0	20	200	0	40	0.495	0.0	C_30_4_0_200_S	2	30	5	163.6	818	4.09	Foundation failure
114	45	4	0	2.0	20	200	0	40	0.495	0.0	C_45_4_0_200_S	2	45	5	141.4	707	3.53	Foundation failure
115	15	8	0	2.0	20	200	0	40	0.495	0.0	C_15_8_0_200_S	4	15	5	186.5	932	4.66	Foundation failure
116	30	8	0	2.0	20	200	0	40	0.495	0.0	C_30_8_0_200_S	4	30	5	164.4	822	4.11	Foundation failure
117	45	8	0	2.0	20	200	0	40	0.495	0.0	C_45_8_0_200_S	4	45	5	141.9	710	3.55	Foundation failure
118	15	2	0.5	2.0	20	200	0	40	0.495	0.0	C_15_2_0.5_200_S	1	15	5	195.6	978	4.89	Foundation failure
119	30	2	0.5	2.0	20	200	0	40	0.495	0.0	C_30_2_0.5_200_S	1	30	5	181.2	906	4.53	Foundation failure
120	45	2	0.5	2.0	20	200	0	40	0.495	0.0	C_45_2_0.5_200_S	1	45	5	164.2	821	4.11	Foundation failure
121	15	4	0.5	2.0	20	200	0	40	0.495	0.0	C_15_4_0.5_200_S	2	15	5	196.4	982	4.91	Foundation failure
122	30	4	0.5	2.0	20	200	0	40	0.495	0.0	C_30_4_0.5_200_S	2	30	5	181.7	909	4.54	Foundation failure
123	45	4	0.5	2.0	20	200	0	40	0.495	0.0	C_45_4_0.5_200_S	2	45	5	164.8	824	4.12	Foundation failure
124	15	8	0.5	2.0	20	200	0	40	0.495	0.0	C_15_8_0.5_200_S	4	15	5	197.3	986	4.93	Foundation failure
125	30	8	0.5	2.0	20	200	0	40	0.495	0.0	C_30_8_0.5_200_S	4	30	5	182.3	911	4.56	Foundation failure
126	45	8	0.5	2.0	20	200	0	40	0.495	0.0	C_45_8_0.5_200_S	4	45	5	165.4	827	4.14	Foundation failure
127	15	2	1	2.0	20	200	0	40	0.495	0.0	C_15_2_1_200_S	1	15	5	203.8	1019	5.10	Foundation failure
128	30	2	1	2.0	20	200	0	40	0.495	0.0	C_30_2_1_200_S	1	30	5	194.8	974	4.87	Foundation failure
129	45	2	1	2.0	20	200	0	40	0.495	0.0	C_45_2_1_200_S	1	45	5	182.1	911	4.55	Foundation failure
130	15	4	1	2.0	20	200	0	40	0.495	0.0	C_15_4_1_200_S	2	15	5	204.4	1022	5.11	Foundation failure
131	30	4	1	2.0	20	200	0	40	0.495	0.0	C_30_4_1_200_S	2	30	5	195.1	975	4.88	Foundation failure
132	45	4	1	2.0	20	200	0	40	0.495	0.0	C_45_4_1_200_S	2	45	5	182.1	911	4.55	Foundation failure
133	15	8	1	2.0	20	200	0	40	0.495	0.0	C_15_8_1_200_S	4	15	5	205.0	1025	5.13	Foundation failure
134	30	8	1	2.0	20	200	0	40	0.495	0.0	C_30_8_1_200_S	4	30	5	195.3	977	4.88	Foundation failure
135	45	8	1	2.0	20	200	0	40	0.495	0.0	C_45_8_1_200_S	4	45	5	182.1	910	4.55	Foundation failure
136	15	2	2	2.0	20	200	0	40	0.495	0.0	C_15_2_2_200_S	1	15	5	207.7	1039	5.19	Foundation failure
137	30	2	2	2.0	20	200	0	40	0.495	0.0	C_30_2_2_200_S	1	30	5	207.5	1037	5.19	Foundation failure
138	45	2	2	2.0	20	200	0	40	0.495	0.0	C_45_2_2_200_S	1	45	5	207.2	1036	5.18	Foundation failure
139	15	4	2	2.0	20	200	0	40	0.495	0.0	C_15_4_2_200_S	2	15	5	208.1	1041	5.20	Foundation failure
140	30	4	2	2.0	20	200	0	40	0.495	0.0	C_30_4_2_200_S	2	30	5	207.9	1039	5.20	Foundation failure
141	45	4	2	2.0	20	200	0	40	0.495	0.0	C_45_4_2_200_S	2	45	5	207.0	1035	5.18	Foundation failure
142	15	8	2	2.0	20	200	0	40	0.495	0.0	C_15_8_2_200_S	4	15	5	208.8	1044	5.22	Foundation failure
143	30	8	2	2.0	20	200	0	40	0.495	0.0	C_30_8_2_200_S	4	30	5	208.1	1041	5.20	Foundation failure
144	45	8	2	2.0	20	200	0	40	0.495	0.0	C_45_8_2_200_S	4	45	5	207.2	1036	5.18	Foundation failure

N.F.: Not Found (Corresponds to the case in which base failure is observed under the gravity loading).

APPENDIX C: LIST OF RESULTS OF FINITE ELEMENTS MODELS CREATED FOR SEISMIC CONDITION.

Lists of results for finite element models created for seismic condition are presented in Table C.1, Table C.2 and Table C.3.

Table C.1. List of results of finite elements models created for seismic condition (β= 15°).

	GEOMETRICAL PROPERTIES				SLOPE SOIL PROPERTIES					SEISMIC EFFECT	FILE NAME	ANALYSIS RESULTS FOR SEISMIC LOADING						
Model No.	β (°)	H (m)	λ	B (m)	γ (kN/m^3)	c_u (kN/m^2)	Φ_u (°)	E_u (MPa)	ν_u	k_h		H/B	β (°)	$C_u/\gamma B$	Load multiplier	q_{fs} (kPa)	N_{cse}	Failure mode
1	15	2	0	2.0	20	25	0	5	0.495	0.1	C_15_2_0_25_0.1_D	1	15	0.625	19.3	96	3.85	Foundation failure
2	15	4	0	2.0	20	25	0	5	0.495	0.1	C_15_4_0_25_0.1_D	2	15	0.625	N.F.	N.F.	N.F.	Base failure_EQ
3	15	8	0	2.0	20	25	0	5	0.495	0.1	C_15_8_0_25_0.1_D	4	15	0.625	N.F.	N.F.	N.F.	Base failure_GR
4	15	2	0.5	2.0	20	25	0	5	0.495	0.1	C_15_2_0.5_25_0.1_D	1	15	0.625	20.9	104	4.18	Foundation failure
5	15	4	0.5	2.0	20	25	0	5	0.495	0.1	C_15_4_0.5_25_0.1_D	2	15	0.625	N.F.	N.F.	N.F.	Base failure_EQ
6	15	8	0.5	2.0	20	25	0	5	0.495	0.1	C_15_8_0.5_25_0.1_D	4	15	0.625	N.F.	N.F.	N.F.	Base failure_GR
7	15	2	1	2.0	20	25	0	5	0.495	0.1	C_15_2_1_25_0.1_D	1	15	0.625	22.2	111	4.43	Foundation failure
8	15	4	1	2.0	20	25	0	5	0.495	0.1	C_15_4_1_25_0.1_D	2	15	0.625	N.F.	N.F.	N.F.	Base failure_EQ
9	15	8	1	2.0	20	25	0	5	0.495	0.1	C_15_8_1_25_0.1_D	4	15	0.625	N.F.	N.F.	N.F.	Base failure_GR
10	15	2	2	2.0	20	25	0	5	0.495	0.1	C_15_2_2_25_0.1_D	1	15	0.625	22.5	112	4.50	Foundation failure
11	15	4	2	2.0	20	25	0	5	0.495	0.1	C_15_4_2_25_0.1_D	2	15	0.625	N.F.	N.F.	N.F.	Base failure_EQ
12	15	8	2	2.0	20	25	0	5	0.495	0.1	C_15_8_2_25_0.1_D	4	15	0.625	N.F.	N.F.	N.F.	Base failure_GR
13	15	2	0	2.0	20	50	0	10	0.495	0.1	C_15_2_0_50_0.1_D	1	15	1.25	40.1	201	4.01	Foundation failure
14	15	4	0	2.0	20	50	0	10	0.495	0.1	C_15_4_0_50_0.1_D	2	15	1.25	40.2	201	4.02	Foundation failure
15	15	8	0	2.0	20	50	0	10	0.495	0.1	C_15_8_0_50_0.1_D	4	15	1.25	40.3	202	4.03	Foundation failure
16	15	2	0.5	2.0	20	50	0	10	0.495	0.1	C_15_2_0.5_50_0.1_D	1	15	1.25	43.1	216	4.31	Foundation failure
17	15	4	0.5	2.0	20	50	0	10	0.495	0.1	C_15_4_0.5_50_0.1_D	2	15	1.25	43.2	216	4.32	Foundation failure
18	15	8	0.5	2.0	20	50	0	10	0.495	0.1	C_15_8_0.5_50_0.1_D	4	15	1.25	43.5	218	4.35	Foundation failure
19	15	2	1	2.0	20	50	0	10	0.495	0.1	C_15_2_1_50_0.1_D	1	15	1.25	45.4	227	4.54	Foundation failure
20	15	4	1	2.0	20	50	0	10	0.495	0.1	C_15_4_1_50_0.1_D	2	15	1.25	45.6	228	4.56	Foundation failure
21	15	8	1	2.0	20	50	0	10	0.495	0.1	C_15_8_1_50_0.1_D	4	15	1.25	45.7	229	4.57	Foundation failure
22	15	2	2	2.0	20	50	0	10	0.495	0.1	C_15_2_2_50_0.1_D	1	15	1.25	45.5	228	4.55	Foundation failure
23	15	4	2	2.0	20	50	0	10	0.495	0.1	C_15_4_2_50_0.1_D	2	15	1.25	45.6	228	4.56	Foundation failure
24	15	8	2	2.0	20	50	0	10	0.495	0.1	C_15_8_2_50_0.1_D	4	15	1.25	45.7	228	4.57	Foundation failure
25	15	2	0	2.0	20	100	0	20	0.495	0.1	C_15_2_0_100_0.1_D	1	15	2.5	81.7	408	4.08	Foundation failure
26	15	4	0	2.0	20	100	0	20	0.495	0.1	C_15_4_0_100_0.1_D	2	15	2.5	81.9	410	4.10	Foundation failure
27	15	8	0	2.0	20	100	0	20	0.495	0.1	C_15_8_0_100_0.1_D	4	15	2.5	81.9	410	4.10	Foundation failure
28	15	2	0.5	2.0	20	100	0	20	0.495	0.1	C_15_2_0.5_100_0.1_D	1	15	2.5	87.2	436	4.36	Foundation failure
29	15	4	0.5	2.0	20	100	0	20	0.495	0.1	C_15_4_0.5_100_0.1_D	2	15	2.5	87.7	439	4.39	Foundation failure
30	15	8	0.5	2.0	20	100	0	20	0.495	0.1	C_15_8_0.5_100_0.1_D	4	15	2.5	88.2	441	4.41	Foundation failure
31	15	2	1	2.0	20	100	0	20	0.495	0.1	C_15_2_1_100_0.1_D	1	15	2.5	91.5	458	4.58	Foundation failure
32	15	4	1	2.0	20	100	0	20	0.495	0.1	C_15_4_1_100_0.1_D	2	15	2.5	91.9	460	4.60	Foundation failure
33	15	8	1	2.0	20	100	0	20	0.495	0.1	C_15_8_1_100_0.1_D	4	15	2.5	92.3	461	4.61	Foundation failure
34	15	2	2	2.0	20	100	0	20	0.495	0.1	C_15_2_2_100_0.1_D	1	15	2.5	91.8	459	4.59	Foundation failure
35	15	4	2	2.0	20	100	0	20	0.495	0.1	C_15_4_2_100_0.1_D	2	15	2.5	92.1	460	4.60	Foundation failure
36	15	8	2	2.0	20	100	0	20	0.495	0.1	C_15_8_2_100_0.1_D	4	15	2.5	92.3	462	4.62	Foundation failure

N.F. : Not found.
Base failure_EQ: Failed due to earthquake.
Base failure_GR: Failed due to gravity.

Table C.1. List of results of finite elements models created for seismic condition (β= 15°) (Cont.).

	GEOMETRICAL PROPERTIES				SLOPE SOIL PROPERTIES				SEISMIC EFFECT	FILE NAME	ANALYSIS RESULTS FOR SEISMIC LOADING						
Model No.	β (°)	H (m)	λ	B (m)	γ (kN/m^3)	c_u (kN/m^2)	Φ_u (°)	E_u (MPa)	ν_u	k_h		H/B	β (°)	$C_u/\gamma B$	Load multiplier	q_{fs} (kPa)	N_{cse}	Failure mode
37	15	2	0	2.0	20	200	0	40	0.495	0.1	C_15_2_0_200_0.1_D	1	15	5	164.8	824	4.12	Foundation failure
38	15	4	0	2.0	20	200	0	40	0.495	0.1	C_15_4_0_200_0.1_D	2	15	5	165.2	826	4.13	Foundation failure
39	15	8	0	2.0	20	200	0	40	0.495	0.1	C_15_8_0_200_0.1_D	4	15	5	166.3	831	4.16	Foundation failure
40	15	2	0.5	2.0	20	200	0	40	0.495	0.1	C_15_2_0.5_200_0.1_D	1	15	5	175.6	878	4.39	Foundation failure
41	15	4	0.5	2.0	20	200	0	40	0.495	0.1	C_15_4_0.5_200_0.1_D	2	15	5	176.4	882	4.41	Foundation failure
42	15	8	0.5	2.0	20	200	0	40	0.495	0.1	C_15_8_0.5_200_0.1_D	4	15	5	177.4	887	4.43	Foundation failure
43	15	2	1	2.0	20	200	0	40	0.495	0.1	C_15_2_1_200_0.1_D	1	15	5	183.9	919	4.60	Foundation failure
44	15	4	1	2.0	20	200	0	40	0.495	0.1	C_15_4_1_200_0.1_D	2	15	5	184.4	922	4.61	Foundation failure
45	15	8	1	2.0	20	200	0	40	0.495	0.1	C_15_8_1_200_0.1_D	4	15	5	185.1	926	4.63	Foundation failure
46	15	2	2	2.0	20	200	0	40	0.495	0.1	C_15_2_2_200_0.1_D	1	15	5	184.0	920	4.60	Foundation failure
47	15	4	2	2.0	20	200	0	40	0.495	0.1	C_15_4_2_200_0.1_D	2	15	5	184.6	923	4.61	Foundation failure
48	15	8	2	2.0	20	200	0	40	0.495	0.1	C_15_8_2_200_0.1_D	4	15	5	18.5	926	4.63	Foundation failure
49	15	2	0	2.0	20	25	0	5	0.495	0.2	C_15_2_0_25_0.2_D	1	15	0.625	N.F.	N.F.	N.F.	Base failure_EQ
50	15	4	0	2.0	20	25	0	5	0.495	0.2	C_15_4_0_25_0.2_D	2	15	0.625	N.F.	N.F.	N.F.	Base failure_EQ
51	15	8	0	2.0	20	25	0	5	0.495	0.2	C_15_8_0_25_0.2_D	4	15	0.625	N.F.	N.F.	N.F.	Base failure_GR
52	15	2	0.5	2.0	20	25	0	5	0.495	0.2	C_15_2_0.5_25_0.2_D	1	15	0.625	N.F.	N.F.	N.F.	Base failure_EQ
53	15	4	0.5	2.0	20	25	0	5	0.495	0.2	C_15_4_0.5_25_0.2_D	2	15	0.625	N.F.	N.F.	N.F.	Base failure_EQ
54	15	8	0.5	2.0	20	25	0	5	0.495	0.2	C_15_8_0.5_25_0.2_D	4	15	0.625	N.F.	N.F.	N.F.	Base failure_GR
55	15	2	1	2.0	20	25	0	5	0.495	0.2	C_15_2_1_25_0.2_D	1	15	0.625	N.F.	N.F.	N.F.	Base failure_EQ
56	15	4	1	2.0	20	25	0	5	0.495	0.2	C_15_4_1_25_0.2_D	2	15	0.625	N.F.	N.F.	N.F.	Base failure_EQ
57	15	8	1	2.0	20	25	0	5	0.495	0.2	C_15_8_1_25_0.2_D	4	15	0.625	N.F.	N.F.	N.F.	Base failure_GR
58	15	2	2	2.0	20	25	0	5	0.495	0.2	C_15_2_2_25_0.2_D	1	15	0.625	N.F.	N.F.	N.F.	Base failure_EQ
59	15	4	2	2.0	20	25	0	5	0.495	0.2	C_15_4_2_25_0.2_D	2	15	0.625	N.F.	N.F.	N.F.	Base failure_EQ
60	15	8	2	2.0	20	25	0	5	0.495	0.2	C_15_8_2_25_0.2_D	4	15	0.625	N.F.	N.F.	N.F.	Base failure_GR
61	15	2	0	2.0	20	50	0	10	0.495	0.2	C_15_2_0_50_0.2_D	1	15	1.25	34.4	172	3.44	Foundation failure
62	15	4	0	2.0	20	50	0	10	0.495	0.2	C_15_4_0_50_0.2_D	2	15	1.25	34.6	173	3.46	Foundation failure
63	15	8	0	2.0	20	50	0	10	0.495	0.2	C_15_8_0_50_0.2_D	4	15	1.25	N.F.	N.F.	N.F.	Base failure_EQ
64	15	2	0.5	2.0	20	50	0	10	0.495	0.2	C_15_2_0.5_50_0.2_D	1	15	1.25	37.4	187	3.74	Foundation failure
65	15	4	0.5	2.0	20	50	0	10	0.495	0.2	C_15_4_0.5_50_0.2_D	2	15	1.25	37.5	187	3.75	Foundation failure
66	15	8	0.5	2.0	20	50	0	10	0.495	0.2	C_15_8_0.5_50_0.2_D	4	15	1.25	N.F.	N.F.	N.F.	Base failure_EQ
67	15	2	1	2.0	20	50	0	10	0.495	0.2	C_15_2_1_50_0.2_D	1	15	1.25	38.4	192	3.84	Foundation failure
68	15	4	1	2.0	20	50	0	10	0.495	0.2	C_15_4_1_50_0.2_D	2	15	1.25	38.6	193	3.86	Foundation failure
69	15	8	1	2.0	20	50	0	10	0.495	0.2	C_15_8_1_50_0.2_D	4	15	1.25	N.F.	N.F.	N.F.	Base failure_EQ
70	15	2	2	2.0	20	50	0	10	0.495	0.2	C_15_2_2_50_0.2_D	1	15	1.25	38.5	192	3.85	Foundation failure
71	15	4	2	2.0	20	50	0	10	0.495	0.2	C_15_4_2_50_0.2_D	2	15	1.25	38.6	193	3.86	Foundation failure
72	15	8	2	2.0	20	50	0	10	0.495	0.2	C_15_8_2_50_0.2_D	4	15	1.25	N.F.	N.F.	N.F.	Base failure_EQ

N.F. : Not found.
Base failure_EQ: Failed due to earthquake.
Base failure_GR: Failed due to gravity.

Table C.1. List of results of finite elements models created for seismic condition (β= 15°) (Cont.).

	GEOMETRICAL PROPERTIES				SLOPE SOIL PROPERTIES				SEISMIC EFFECT	FILE NAME	ANALYSIS RESULTS FOR SEISMIC LOADING						
Model No.	β (°)	H (m)	λ	B (m)	γ (kN/m^3)	c_u (kN/m^2)	Φ_u (°)	E_u (MPa)	ν_u	k_h		H/B	β (°)	$C_u/\gamma B$	Load multiplier	q_{fs} (kPa)	N_{cse}	Failure mode
73	15	2	0	2.0	20	100	0	20	0.495	0.2	C_15_2_0_100_0.2_D	1	15	2.5	70.3	351	3.51	Foundation failure
74	15	4	0	2.0	20	100	0	20	0.495	0.2	C_15_4_0_100_0.2_D	2	15	2.5	70.5	352	3.52	Foundation failure
75	15	8	0	2.0	20	100	0	20	0.495	0.2	C_15_8_0_100_0.2_D	4	15	2.5	70.5	352	3.52	Foundation failure
76	15	2	0.5	2.0	20	100	0	20	0.495	0.2	C_15_2_0.5_100_0.2_D	1	15	2.5	76.1	380	3.80	Foundation failure
77	15	4	0.5	2.0	20	100	0	20	0.495	0.2	C_15_4_0.5_100_0.2_D	2	15	2.5	76.4	382	3.82	Foundation failure
78	15	8	0.5	2.0	20	100	0	20	0.495	0.2	C_15_8_0.5_100_0.2_D	4	15	2.5	76.8	384	3.84	Foundation failure
79	15	2	1	2.0	20	100	0	20	0.495	0.2	C_15_2_1_100_0.2_D	1	15	2.5	77.8	389	3.89	Foundation failure
80	15	4	1	2.0	20	100	0	20	0.495	0.2	C_15_4_1_100_0.2_D	2	15	2.5	77.9	390	3.90	Foundation failure
81	15	8	1	2.0	20	100	0	20	0.495	0.2	C_15_8_1_100_0.2_D	4	15	2.5	78.2	391	3.91	Foundation failure
82	15	2	2	2.0	20	100	0	20	0.495	0.2	C_15_2_2_100_0.2_D	1	15	2.5	77.8	389	3.89	Foundation failure
83	15	4	2	2.0	20	100	0	20	0.495	0.2	C_15_4_2_100_0.2_D	2	15	2.5	77.9	390	3.90	Foundation failure
84	15	8	2	2.0	20	100	0	20	0.495	0.2	C_15_8_2_100_0.2_D	4	15	2.5	78.3	392	3.92	Foundation failure
85	15	2	0	2.0	20	200	0	40	0.495	0.2	C_15_2_0_200_0.2_D	1	15	5	141.8	709	3.54	Foundation failure
86	15	4	0	2.0	20	200	0	40	0.495	0.2	C_15_4_0_200_0.2_D	2	15	5	142.6	713	3.57	Foundation failure
87	15	8	0	2.0	20	200	0	40	0.495	0.2	C_15_8_0_200_0.2_D	4	15	5	142.4	712	3.56	Foundation failure
88	15	2	0.5	2.0	20	200	0	40	0.495	0.2	C_15_2_0.5_200_0.2_D	1	15	5	153.5	768	3.84	Foundation failure
89	15	4	0.5	2.0	20	200	0	40	0.495	0.2	C_15_4_0.5_200_0.2_D	2	15	5	154.0	770	3.85	Foundation failure
90	15	8	0.5	2.0	20	200	0	40	0.495	0.2	C_15_8_0.5_200_0.2_D	4	15	5	154.8	774	3.87	Foundation failure
91	15	2	1	2.0	20	200	0	40	0.495	0.2	C_15_2_1_200_0.2_D	1	15	5	156.1	780	3.90	Foundation failure
92	15	4	1	2.0	20	200	0	40	0.495	0.2	C_15_4_1_200_0.2_D	2	15	5	157.0	785	3.93	Foundation failure
93	15	8	1	2.0	20	200	0	40	0.495	0.2	C_15_8_1_200_0.2_D	4	15	5	157.6	788	3.94	Foundation failure
94	15	2	2	2.0	20	200	0	40	0.495	0.2	C_15_2_2_200_0.2_D	1	15	5	156.3	782	3.91	Foundation failure
95	15	4	2	2.0	20	200	0	40	0.495	0.2	C_15_4_2_200_0.2_D	2	15	5	157.1	785	3.93	Foundation failure
96	15	8	2	2.0	20	200	0	40	0.495	0.2	C_15_8_2_200_0.2_D	4	15	5	157.4	787	3.94	Foundation failure
97	15	2	0	2.0	20	25	0	5	0.495	0.3	C_15_2_0_25_0.3_D	1	15	0.625	N.F.	N.F.	N.F.	Base failure_EQ
98	15	4	0	2.0	20	25	0	5	0.495	0.3	C_15_4_0_25_0.3_D	2	15	0.625	N.F.	N.F.	N.F.	Base failure_EQ
99	15	8	0	2.0	20	25	0	5	0.495	0.3	C_15_8_0_25_0.3_D	4	15	0.625	N.F.	N.F.	N.F.	Base failure_GR
100	15	2	0.5	2.0	20	25	0	5	0.495	0.3	C_15_2_0.5_25_0.3_D	1	15	0.625	N.F.	N.F.	N.F.	Base failure_EQ
101	15	4	0.5	2.0	20	25	0	5	0.495	0.3	C_15_4_0.5_25_0.3_D	2	15	0.625	N.F.	N.F.	N.F.	Base failure_EQ
102	15	8	0.5	2.0	20	25	0	5	0.495	0.3	C_15_8_0.5_25_0.3_D	4	15	0.625	N.F.	N.F.	N.F.	Base failure_GR
103	15	2	1	2.0	20	25	0	5	0.495	0.3	C_15_2_1_25_0.3_D	1	15	0.625	N.F.	N.F.	N.F.	Base failure_EQ
104	15	4	1	2.0	20	25	0	5	0.495	0.3	C_15_4_1_25_0.3_D	2	15	0.625	N.F.	N.F.	N.F.	Base failure_EQ
105	15	8	1	2.0	20	25	0	5	0.495	0.3	C_15_8_1_25_0.3_D	4	15	0.625	N.F.	N.F.	N.F.	Base failure_GR
106	15	2	2	2.0	20	25	0	5	0.495	0.3	C_15_2_2_25_0.3_D	1	15	0.625	N.F.	N.F.	N.F.	Base failure_EQ
107	15	4	2	2.0	20	25	0	5	0.495	0.3	C_15_4_2_25_0.3_D	2	15	0.625	N.F.	N.F.	N.F.	Base failure_EQ
108	15	8	2	2.0	20	25	0	5	0.495	0.3	C_15_8_2_25_0.3_D	4	15	0.625	N.F.	N.F.	N.F.	Base failure_GR

N.F. : Not found.
Base failure_EQ: Failed due to earthquake.
Base failure_GR: Failed due to gravity.

Table C.1. List of results of finite elements models created for seismic condition (β= 15°) (Cont.).

	GEOMETRICAL PROPERTIES				SLOPE SOIL PROPERTIES				SEISMIC EFFECT	FILE NAME	ANALYSIS RESULTS FOR SEISMIC LOADING						
Model No.	β (°)	H (m)	λ	B (m)	γ (kN/m^3)	c_u (kN/m^2)	Φ_u (°)	E_u (MPa)	ν_u	k_h		H/B	β (°)	$C_u/\gamma B$	Load multiplier	q_{fs} (kPa)	N_{cse}	Failure mode
109	15	2	0	2.0	20	50	0	10	0.495	0.3	C_15_2_0_50_0.3_D	1	15	1.25	29.0	145	2.90	Foundation failure
110	15	4	0	2.0	20	50	0	10	0.495	0.3	C_15_4_0_50_0.3_D	2	15	1.25	N.F.	N.F.	N.F.	Base failure_EQ
111	15	8	0	2.0	20	50	0	10	0.495	0.3	C_15_8_0_50_0.3_D	4	15	1.25	N.F.	N.F.	N.F.	Base failure_EQ
112	15	2	0.5	2.0	20	50	0	10	0.495	0.3	C_15_2_0.5_50_0.3_D	1	15	1.25	31.6	158	3.16	Foundation failure
113	15	4	0.5	2.0	20	50	0	10	0.495	0.3	C_15_4_0.5_50_0.3_D	2	15	1.25	N.F.	N.F.	N.F.	Base failure_EQ
114	15	8	0.5	2.0	20	50	0	10	0.495	0.3	C_15_8_0.5_50_0.3_D	4	15	1.25	N.F.	N.F.	N.F.	Base failure_EQ
115	15	2	1	2.0	20	50	0	10	0.495	0.3	C_15_2_1_50_0.3_D	1	15	1.25	31.5	158	3.15	Foundation failure
116	15	4	1	2.0	20	50	0	10	0.495	0.3	C_15_4_1_50_0.3_D	2	15	1.25	N.F.	N.F.	N.F.	Base failure_EQ
117	15	8	1	2.0	20	50	0	10	0.495	0.3	C_15_8_1_50_0.3_D	4	15	1.25	N.F.	N.F.	N.F.	Base failure_EQ
118	15	2	2	2.0	20	50	0	10	0.495	0.3	C_15_2_2_50_0.3_D	1	15	1.25	31.5	158	3.15	Foundation failure
119	15	4	2	2.0	20	50	0	10	0.495	0.3	C_15_4_2_50_0.3_D	2	15	1.25	N.F.	N.F.	N.F.	Base failure_EQ
120	15	8	2	2.0	20	50	0	10	0.495	0.3	C_15_8_2_50_0.3_D	4	15	1.25	N.F.	N.F.	N.F.	Base failure_EQ
121	15	2	0	2.0	20	100	0	20	0.495	0.3	C_15_2_0_100_0.3_D	1	15	2.5	59.0	295	2.95	Foundation failure
122	15	4	0	2.0	20	100	0	20	0.495	0.3	C_15_4_0_100_0.3_D	2	15	2.5	59.2	296	2.96	Foundation failure
123	15	8	0	2.0	20	100	0	20	0.495	0.3	C_15_8_0_100_0.3_D	4	15	2.5	59.2	296	2.96	Foundation failure
124	15	2	0.5	2.0	20	100	0	20	0.495	0.3	C_15_2_0.5_100_0.3_D	1	15	2.5	63.7	319	3.19	Foundation failure
125	15	4	0.5	2.0	20	100	0	20	0.495	0.3	C_15_4_0.5_100_0.3_D	2	15	2.5	63.8	319	3.19	Foundation failure
126	15	8	0.5	2.0	20	100	0	20	0.495	0.3	C_15_8_0.5_100_0.3_D	4	15	2.5	64.0	320	3.20	Foundation failure
127	15	2	1	2.0	20	100	0	20	0.495	0.3	C_15_2_1_100_0.3_D	1	15	2.5	63.6	318	3.18	Foundation failure
128	15	4	1	2.0	20	100	0	20	0.495	0.3	C_15_4_1_100_0.3_D	2	15	2.5	63.8	319	3.19	Foundation failure
129	15	8	1	2.0	20	100	0	20	0.495	0.3	C_15_8_1_100_0.3_D	4	15	2.5	63.9	320	3.20	Foundation failure
130	15	2	2	2.0	20	100	0	20	0.495	0.3	C_15_2_2_100_0.3_D	1	15	2.5	63.7	318	3.18	Foundation failure
131	15	4	2	2.0	20	100	0	20	0.495	0.3	C_15_4_2_100_0.3_D	2	15	2.5	63.7	319	3.19	Foundation failure
132	15	8	2	2.0	20	100	0	20	0.495	0.3	C_15_8_2_100_0.3_D	4	15	2.5	63.9	320	3.20	Foundation failure
133	15	2	0	2.0	20	200	0	40	0.495	0.3	C_15_2_0_200_0.3_D	1	15	5	119.0	595	2.98	Foundation failure
134	15	4	0	2.0	20	200	0	40	0.495	0.3	C_15_4_0_200_0.3_D	2	15	5	119.3	596	2.98	Foundation failure
135	15	8	0	2.0	20	200	0	40	0.495	0.3	C_15_8_0_200_0.3_D	4	15	5	119.3	597	2.98	Foundation failure
136	15	2	0.5	2.0	20	200	0	40	0.495	0.3	C_15_2_0.5_200_0.3_D	1	15	5	128.1	641	3.20	Foundation failure
137	15	4	0.5	2.0	20	200	0	40	0.495	0.3	C_15_4_0.5_200_0.3_D	2	15	5	128.2	641	3.20	Foundation failure
138	15	8	0.5	2.0	20	200	0	40	0.495	0.3	C_15_8_0.5_200_0.3_D	4	15	5	128.5	642	3.21	Foundation failure
139	15	2	1	2.0	20	200	0	40	0.495	0.3	C_15_2_1_200_0.3_D	1	15	5	127.8	639	3.19	Foundation failure
140	15	4	1	2.0	20	200	0	40	0.495	0.3	C_15_4_1_200_0.3_D	2	15	5	128.0	640	3.20	Foundation failure
141	15	8	1	2.0	20	200	0	40	0.495	0.3	C_15_8_1_200_0.3_D	4	15	5	128.3	642	3.21	Foundation failure
142	15	2	2	2.0	20	200	0	40	0.495	0.3	C_15_2_2_200_0.3_D	1	15	5	127.8	639	3.19	Foundation failure
143	15	4	2	2.0	20	200	0	40	0.495	0.3	C_15_4_2_200_0.3_D	2	15	5	128.0	640	3.20	Foundation failure
144	15	8	2	2.0	20	200	0	40	0.495	0.3	C_15_8_2_200_0.3_D	4	15	5	128.3	641	3.21	Foundation failure

N.F. : Not found.
Base failure_EQ: Failed due to earthquake.
Base failure_GR: Failed due to gravity.

Table C.1. List of results of finite elements models created for seismic condition (β= 15°) (Cont.).

	GEOMETRICAL PROPERTIES				SLOPE SOIL PROPERTIES					SEISMIC EFFECT	FILE NAME	ANALYSIS RESULTS FOR SEISMIC LOADING						
Model No.	β (°)	H (m)	λ	B (m)	γ (kN/m^3)	c_u (kN/m^2)	Φ_u (°)	E_u (MPa)	ν_u	k_h		H/B	β (°)	$C_u/\gamma B$	Load multiplier	q_{fs} (kPa)	N_{cse}	Failure mode
145	15	2	0	2.0	20	25	0	5	0.495	0.4	C_15_2_0_25_0.4_D	1	15	0.625	N.F.	N.F.	N.F.	Base failure_EQ
146	15	4	0	2.0	20	25	0	5	0.495	0.4	C_15_4_0_25_0.4_D	2	15	0.625	N.F.	N.F.	N.F.	Base failure_EQ
147	15	8	0	2.0	20	25	0	5	0.495	0.4	C_15_8_0_25_0.4_D	4	15	0.625	N.F.	N.F.	N.F.	Base failure_GR
148	15	2	0.5	2.0	20	25	0	5	0.495	0.4	C_15_2_0.5_25_0.4_D	1	15	0.625	N.F.	N.F.	N.F.	Base failure_EQ
149	15	4	0.5	2.0	20	25	0	5	0.495	0.4	C_15_4_0.5_25_0.4_D	2	15	0.625	N.F.	N.F.	N.F.	Base failure_EQ
150	15	8	0.5	2.0	20	25	0	5	0.495	0.4	C_15_8_0.5_25_0.4_D	4	15	0.625	N.F.	N.F.	N.F.	Base failure_GR
151	15	2	1	2.0	20	25	0	5	0.495	0.4	C_15_2_1_25_0.4_D	1	15	0.625	N.F.	N.F.	N.F.	Base failure_EQ
152	15	4	1	2.0	20	25	0	5	0.495	0.4	C_15_4_1_25_0.4_D	2	15	0.625	N.F.	N.F.	N.F.	Base failure_EQ
153	15	8	1	2.0	20	25	0	5	0.495	0.4	C_15_8_1_25_0.4_D	4	15	0.625	N.F.	N.F.	N.F.	Base failure_GR
154	15	2	2	2.0	20	25	0	5	0.495	0.4	C_15_2_2_25_0.4_D	1	15	0.625	N.F.	N.F.	N.F.	Base failure_EQ
155	15	4	2	2.0	20	25	0	5	0.495	0.4	C_15_4_2_25_0.4_D	2	15	0.625	N.F.	N.F.	N.F.	Base failure_EQ
156	15	8	2	2.0	20	25	0	5	0.495	0.4	C_15_8_2_25_0.4_D	4	15	0.625	N.F.	N.F.	N.F.	Base failure_GR
157	15	2	0	2.0	20	50	0	10	0.495	0.4	C_15_2_0_50_0.4_D	1	15	1.25	N.F.	N.F.	N.F.	Base failure_EQ
158	15	4	0	2.0	20	50	0	10	0.495	0.4	C_15_4_0_50_0.4_D	2	15	1.25	N.F.	N.F.	N.F.	Base failure_EQ
159	15	8	0	2.0	20	50	0	10	0.495	0.4	C_15_8_0_50_0.4_D	4	15	1.25	N.F.	N.F.	N.F.	Base failure_EQ
160	15	2	0.5	2.0	20	50	0	10	0.495	0.4	C_15_2_0.5_50_0.4_D	1	15	1.25	N.F.	N.F.	N.F.	Base failure_EQ
161	15	4	0.5	2.0	20	50	0	10	0.495	0.4	C_15_4_0.5_50_0.4_D	2	15	1.25	N.F.	N.F.	N.F.	Base failure_EQ
162	15	8	0.5	2.0	20	50	0	10	0.495	0.4	C_15_8_0.5_50_0.4_D	4	15	1.25	N.F.	N.F.	N.F.	Base failure_EQ
163	15	2	1	2.0	20	50	0	10	0.495	0.4	C_15_2_1_50_0.4_D	1	15	1.25	N.F.	N.F.	N.F.	Base failure_EQ
164	15	4	1	2.0	20	50	0	10	0.495	0.4	C_15_4_1_50_0.4_D	2	15	1.25	N.F.	N.F.	N.F.	Base failure_EQ
165	15	8	1	2.0	20	50	0	10	0.495	0.4	C_15_8_1_50_0.4_D	4	15	1.25	N.F.	N.F.	N.F.	Base failure_EQ
166	15	2	2	2.0	20	50	0	10	0.495	0.4	C_15_2_2_50_0.4_D	1	15	1.25	N.F.	N.F.	N.F.	Base failure_EQ
167	15	4	2	2.0	20	50	0	10	0.495	0.4	C_15_4_2_50_0.4_D	2	15	1.25	N.F.	N.F.	N.F.	Base failure_EQ
168	15	8	2	2.0	20	50	0	10	0.495	0.4	C_15_8_2_50_0.4_D	4	15	1.25	N.F.	N.F.	N.F.	Base failure_EQ
169	15	2	0	2.0	20	100	0	20	0.495	0.4	C_15_2_0_100_0.4_D	1	15	2.5	48.8	244	2.44	Foundation failure
170	15	4	0	2.0	20	100	0	20	0.495	0.4	C_15_4_0_100_0.4_D	2	15	2.5	48.8	244	2.44	Foundation failure
171	15	8	0	2.0	20	100	0	20	0.495	0.4	C_15_8_0_100_0.4_D	4	15	2.5	48.9	245	2.45	Foundation failure
172	15	2	0.5	2.0	20	100	0	20	0.495	0.4	C_15_2_0.5_100_0.4_D	1	15	2.5	50.0	250	2.50	Sliding
173	15	4	0.5	2.0	20	100	0	20	0.495	0.4	C_15_4_0.5_100_0.4_D	2	15	2.5	50.0	250	2.50	Sliding
174	15	8	0.5	2.0	20	100	0	20	0.495	0.4	C_15_8_0.5_100_0.4_D	4	15	2.5	50.1	250	2.50	Sliding
175	15	2	1	2.0	20	100	0	20	0.495	0.4	C_15_2_1_100_0.4_D	1	15	2.5	50.0	250	2.50	Sliding
176	15	4	1	2.0	20	100	0	20	0.495	0.4	C_15_4_1_100_0.4_D	2	15	2.5	50.0	250	2.50	Sliding
177	15	8	1	2.0	20	100	0	20	0.495	0.4	C_15_8_1_100_0.4_D	4	15	2.5	50.0	250	2.50	Sliding
178	15	2	2	2.0	20	100	0	20	0.495	0.4	C_15_2_2_100_0.4_D	1	15	2.5	49.9	250	2.50	Sliding
179	15	4	2	2.0	20	100	0	20	0.495	0.4	C_15_4_2_100_0.4_D	2	15	2.5	50.0	250	2.50	Sliding
180	15	8	2	2.0	20	100	0	20	0.495	0.4	C_15_8_2_100_0.4_D	4	15	2.5	50.0	250	2.50	Sliding

N.F. : Not found.
Base failure_EQ: Failed due to earthquake.
Base failure_GR: Failed due to gravity.

Table C.1. List of results of finite elements models created for seismic condition (β= 15°) (Cont.).

	GEOMETRICAL PROPERTIES				SLOPE SOIL PROPERTIES				SEISMIC EFFECT	FILE NAME	ANALYSIS RESULTS FOR SEISMIC LOADING					
Model No.	β (°)	H (m)	λ	B (m)	γ (kN/m^3)	c_u (kN/m^2)	Φ_u (°)	E_u (MPa)	v_u	k_h		H/B	β (°)	$C_u/\gamma B$	Load multiplier	q_{fs} (kPa)	N_{cse}	Failure mode
181	15	2	0	2.0	20	200	0	40	0.495	0.4	C_15_2_0_200_0.4_D	1	15	5	98.1	491	2.45	Foundation failure
182	15	4	0	2.0	20	200	0	40	0.495	0.4	C_15_4_0_200_0.4_D	2	15	5	97.9	490	2.45	Foundation failure
183	15	8	0	2.0	20	200	0	40	0.495	0.4	C_15_8_0_200_0.4_D	4	15	5	98.1	491	2.45	Foundation failure
184	15	2	0.5	2.0	20	200	0	40	0.495	0.4	C_15_2_0.5_200_0.4_D	1	15	5	99.9	499	2.50	Sliding
185	15	4	0.5	2.0	20	200	0	40	0.495	0.4	C_15_4_0.5_200_0.4_D	2	15	5	100.0	500	2.50	Sliding
186	15	8	0.5	2.0	20	200	0	40	0.495	0.4	C_15_8_0.5_200_0.4_D	4	15	5	100.0	500	2.50	Sliding
187	15	2	1	2.0	20	200	0	40	0.495	0.4	C_15_2_1_200_0.4_D	1	15	5	100.0	500	2.50	Sliding
188	15	4	1	2.0	20	200	0	40	0.495	0.4	C_15_4_1_200_0.4_D	2	15	5	100.0	500	2.50	Sliding
189	15	8	1	2.0	20	200	0	40	0.495	0.4	C_15_8_1_200_0.4_D	4	15	5	99.9	500	2.50	Sliding
190	15	2	2	2.0	20	200	0	40	0.495	0.4	C_15_2_2_200_0.4_D	1	15	5	100.0	500	2.50	Sliding
191	15	4	2	2.0	20	200	0	40	0.495	0.4	C_15_4_2_200_0.4_D	2	15	5	100.0	500	2.50	Sliding
192	15	8	2	2.0	20	200	0	40	0.495	0.4	C_15_8_2_200_0.4_D	4	15	5	99.9	500	2.50	Sliding

N.F. : Not found.

Base failre_EQ: Failed due to earthquake.

Base failre_GR: Failed due to gravity.

Table C.2. List of results of finite elements models created for seismic condition (β= 30°).

	GEOMETRICAL PROPERTIES				SLOPE SOIL PROPERTIES					SEISMIC EFFECT	FILE NAME	ANALYSIS RESULTS FOR SEISMIC LOADING						
Model No.	β (°)	H (m)	λ	B (m)	γ (kN/m^3)	c_u (kN/m^2)	Φ_u (°)	E_u (MPa)	ν_u	k_h		H/B	β (°)	$C_u/\gamma B$	Load multiplier	q_{fs} (kPa)	N_{cse}	Failure mode
1	30	2	0	2.0	20	25	0	5	0.495	0.1	C_30_2_0_25_0.1_D	1	30	0.625	15.6	78	3.12	Foundation failure
2	30	4	0	2.0	20	25	0	5	0.495	0.1	C_30_4_0_25_0.1_D	2	30	0.625	N.F.	N.F.	N.F.	Base failure_EQ
3	30	8	0	2.0	20	25	0	5	0.495	0.1	C_30_8_0_25_0.1_D	4	30	0.625	N.F.	N.F.	N.F.	Base failure_GR
4	30	2	0.5	2.0	20	25	0	5	0.495	0.1	C_30_2_0.5_25_0.1_D	1	30	0.625	17.4	87	3.47	Foundation failure
5	30	4	0.5	2.0	20	25	0	5	0.495	0.1	C_30_4_0.5_25_0.1_D	2	30	0.625	N.F.	N.F.	N.F.	Base failure_EQ
6	30	8	0.5	2.0	20	25	0	5	0.495	0.1	C_30_8_0.5_25_0.1_D	4	30	0.625	N.F.	N.F.	N.F.	Base failure_GR
7	30	2	1	2.0	20	25	0	5	0.495	0.1	C_30_2_1_25_0.1_D	1	30	0.625	19.0	95	3.80	Foundation failure
8	30	4	1	2.0	20	25	0	5	0.495	0.1	C_30_4_1_25_0.1_D	2	30	0.625	N.F.	N.F.	N.F.	Base failure_EQ
9	30	8	1	2.0	20	25	0	5	0.495	0.1	C_30_8_1_25_0.1_D	4	30	0.625	N.F.	N.F.	N.F.	Base failure_GR
10	30	2	2	2.0	20	25	0	5	0.495	0.1	C_30_2_2_25_0.1_D	1	30	0.625	21.7	108	4.33	Foundation failure
11	30	4	2	2.0	20	25	0	5	0.495	0.1	C_30_4_2_25_0.1_D	2	30	0.625	N.F.	N.F.	N.F.	Base failure_EQ
12	30	8	2	2.0	20	25	0	5	0.495	0.1	C_30_8_2_25_0.1_D	4	30	0.625	N.F.	N.F.	N.F.	Base failure_GR
13	30	2	0	2.0	20	50	0	10	0.495	0.1	C_30_2_0_50_0.1_D	1	30	1.25	34.7	174	3.47	Foundation failure
14	30	4	0	2.0	20	50	0	10	0.495	0.1	C_30_4_0_50_0.1_D	2	30	1.25	34.7	173	3.47	Foundation failure
15	30	8	0	2.0	20	50	0	10	0.495	0.1	C_30_8_0_50_0.1_D	4	30	1.25	34.9	174	3.49	Foundation failure
16	30	2	0.5	2.0	20	50	0	10	0.495	0.1	C_30_2_0.5_50_0.1_D	1	30	1.25	39.4	197	3.94	Foundation failure
17	30	4	0.5	2.0	20	50	0	10	0.495	0.1	C_30_4_0.5_50_0.1_D	2	30	1.25	39.5	197	3.95	Foundation failure
18	30	8	0.5	2.0	20	50	0	10	0.495	0.1	C_30_8_0.5_50_0.1_D	4	30	1.25	39.6	198	3.96	Foundation failure
19	30	2	1	2.0	20	50	0	10	0.495	0.1	C_30_2_1_50_0.1_D	1	30	1.25	43.0	215	4.30	Foundation failure
20	30	4	1	2.0	20	50	0	10	0.495	0.1	C_30_4_1_50_0.1_D	2	30	1.25	43.1	215	4.31	Foundation failure
21	30	8	1	2.0	20	50	0	10	0.495	0.1	C_30_8_1_50_0.1_D	4	30	1.25	43.1	216	4.31	Foundation failure
22	30	2	2	2.0	20	50	0	10	0.495	0.1	C_30_2_2_50_0.1_D	1	30	1.25	45.5	227	4.55	Foundation failure
23	30	4	2	2.0	20	50	0	10	0.495	0.1	C_30_4_2_50_0.1_D	2	30	1.25	45.7	229	4.57	Foundation failure
24	30	8	2	2.0	20	50	0	10	0.495	0.1	C_30_8_2_50_0.1_D	4	30	1.25	45.7	229	4.57	Foundation failure
25	30	2	0	2.0	20	100	0	20	0.495	0.1	C_30_2_0_100_0.1_D	1	30	2.5	71.7	358	3.58	Foundation failure
26	30	4	0	2.0	20	100	0	20	0.495	0.1	C_30_4_0_100_0.1_D	2	30	2.5	71.6	358	3.58	Foundation failure
27	30	8	0	2.0	20	100	0	20	0.495	0.1	C_30_8_0_100_0.1_D	4	30	2.5	71.9	359	3.59	Foundation failure
28	30	2	0.5	2.0	20	100	0	20	0.495	0.1	C_30_2_0.5_100_0.1_D	1	30	2.5	81.0	405	4.05	Foundation failure
29	30	4	0.5	2.0	20	100	0	20	0.495	0.1	C_30_4_0.5_100_0.1_D	2	30	2.5	81.4	407	4.07	Foundation failure
30	30	8	0.5	2.0	20	100	0	20	0.495	0.1	C_30_8_0.5_100_0.1_D	4	30	2.5	81.6	408	4.08	Foundation failure
31	30	2	1	2.0	20	100	0	20	0.495	0.1	C_30_2_1_100_0.1_D	1	30	2.5	88.2	441	4.41	Foundation failure
32	30	4	1	2.0	20	100	0	20	0.495	0.1	C_30_4_1_100_0.1_D	2	30	2.5	88.3	442	4.42	Foundation failure
33	30	8	1	2.0	20	100	0	20	0.495	0.1	C_30_8_1_100_0.1_D	4	30	2.5	88.5	442	4.42	Foundation failure
34	30	2	2	2.0	20	100	0	20	0.495	0.1	C_30_2_2_100_0.1_D	1	30	2.5	91.6	458	4.58	Foundation failure
35	30	4	2	2.0	20	100	0	20	0.495	0.1	C_30_4_2_100_0.1_D	2	30	2.5	92.0	460	4.60	Foundation failure
36	30	8	2	2.0	20	100	0	20	0.495	0.1	C_30_8_2_100_0.1_D	4	30	2.5	92.0	460	4.60	Foundation failure

N.F. : Not found.

Base failure_EQ: Failed due to earthquake.

Base failure_GR: Failed due to gravity.

Table C.2. List of results of finite elements models created for seismic condition (β= 30°) (Cont.).

	GEOMETRICAL PROPERTIES				SLOPE SOIL PROPERTIES				SEISMIC EFFECT	FILE NAME	ANALYSIS RESULTS FOR SEISMIC LOADING						
Model No.	β (°)	H (m)	λ	B (m)	γ (kN/m^3)	c_u (kN/m^2)	Φ_u (°)	E_u (MPa)	v_u	k_h		H/B	β (°)	$C_u/\gamma B$	Load multiplier	q_{fs} (kPa)	N_{cse}	Failure mode
37	30	2	0	2.0	20	200	0	40	0.495	0.1	C_30_2_0_200_0.1_D	1	30	5	145.6	728	3.64	Foundation failure
38	30	4	0	2.0	20	200	0	40	0.495	0.1	C_30_4_0_200_0.1_D	2	30	5	145.9	730	3.65	Foundation failure
39	30	8	0	2.0	20	200	0	40	0.495	0.1	C_30_8_0_200_0.1_D	4	30	5	146.6	733	3.66	Foundation failure
40	30	2	0.5	2.0	20	200	0	40	0.495	0.1	C_30_2_0.5_200_0.1_D	1	30	5	163.9	820	4.10	Foundation failure
41	30	4	0.5	2.0	20	200	0	40	0.495	0.1	C_30_4_0.5_200_0.1_D	2	30	5	164.8	824	4.12	Foundation failure
42	30	8	0.5	2.0	20	200	0	40	0.495	0.1	C_30_8_0.5_200_0.1_D	4	30	5	165.3	827	4.13	Foundation failure
43	30	2	1	2.0	20	200	0	40	0.495	0.1	C_30_2_1_200_0.1_D	1	30	5	178.1	890	4.45	Foundation failure
44	30	4	1	2.0	20	200	0	40	0.495	0.1	C_30_4_1_200_0.1_D	2	30	5	178.4	892	4.46	Foundation failure
45	30	8	1	2.0	20	200	0	40	0.495	0.1	C_30_8_1_200_0.1_D	4	30	5	178.6	893	4.47	Foundation failure
46	30	2	2	2.0	20	200	0	40	0.495	0.1	C_30_2_2_200_0.1_D	1	30	5	183.8	919	4.59	Foundation failure
47	30	4	2	2.0	20	200	0	40	0.495	0.1	C_30_4_2_200_0.1_D	2	30	5	184.5	923	4.61	Foundation failure
48	30	8	2	2.0	20	200	0	40	0.495	0.1	C_30_8_2_200_0.1_D	4	30	5	184.6	923	4.62	Foundation failure
49	30	2	0	2.0	20	25	0	5	0.495	0.2	C_30_2_0_25_0.2_D	1	30	0.625	N.F.	N.F.	N.F.	Base failure_EQ
50	30	4	0	2.0	20	25	0	5	0.495	0.2	C_30_4_0_25_0.2_D	2	30	0.625	N.F.	N.F.	N.F.	Base failure_EQ
51	30	8	0	2.0	20	25	0	5	0.495	0.2	C_30_8_0_25_0.2_D	4	30	0.625	N.F.	N.F.	N.F.	Base failure_GR
52	30	2	0.5	2.0	20	25	0	5	0.495	0.2	C_30_2_0.5_25_0.2_D	1	30	0.625	N.F.	N.F.	N.F.	Base failure_EQ
53	30	4	0.5	2.0	20	25	0	5	0.495	0.2	C_30_4_0.5_25_0.2_D	2	30	0.625	N.F.	N.F.	N.F.	Base failure_EQ
54	30	8	0.5	2.0	20	25	0	5	0.495	0.2	C_30_8_0.5_25_0.2_D	4	30	0.625	N.F.	N.F.	N.F.	Base failure_GR
55	30	2	1	2.0	20	25	0	5	0.495	0.2	C_30_2_1_25_0.2_D	1	30	0.625	N.F.	N.F.	N.F.	Base failure_EQ
56	30	4	1	2.0	20	25	0	5	0.495	0.2	C_30_4_1_25_0.2_D	2	30	0.625	N.F.	N.F.	N.F.	Base failure_EQ
57	30	8	1	2.0	20	25	0	5	0.495	0.2	C_30_8_1_25_0.2_D	4	30	0.625	N.F.	N.F.	N.F.	Base failure_GR
58	30	2	2	2.0	20	25	0	5	0.495	0.2	C_30_2_2_25_0.2_D	1	30	0.625	N.F.	N.F.	N.F.	Base failure_EQ
59	30	4	2	2.0	20	25	0	5	0.495	0.2	C_30_4_2_25_0.2_D	2	30	0.625	N.F.	N.F.	N.F.	Base failure_EQ
60	30	8	2	2.0	20	25	0	5	0.495	0.2	C_30_8_2_25_0.2_D	4	30	0.625	N.F.	N.F.	N.F.	Base failure_GR
61	30	2	0	2.0	20	50	0	10	0.495	0.2	C_30_2_0_50_0.2_D	1	30	1.25	30.2	151	3.02	Foundation failure
62	30	4	0	2.0	20	50	0	10	0.495	0.2	C_30_4_0_50_0.2_D	2	30	1.25	30.3	151	3.03	Foundation failure
63	30	8	0	2.0	20	50	0	10	0.495	0.2	C_30_8_0_50_0.2_D	4	30	1.25	N.F.	N.F.	N.F.	Base failure_EQ
64	30	2	0.5	2.0	20	50	0	10	0.495	0.2	C_30_2_0.5_50_0.2_D	1	30	1.25	34.8	174	3.48	Foundation failure
65	30	4	0.5	2.0	20	50	0	10	0.495	0.2	C_30_4_0.5_50_0.2_D	2	30	1.25	34.9	174	3.49	Foundation failure
66	30	8	0.5	2.0	20	50	0	10	0.495	0.2	C_30_8_0.5_50_0.2_D	4	30	1.25	N.F.	N.F.	N.F.	Base failure_EQ
67	30	2	1	2.0	20	50	0	10	0.495	0.2	C_30_2_1_50_0.2_D	1	30	1.25	38.1	191	3.81	Foundation failure
68	30	4	1	2.0	20	50	0	10	0.495	0.2	C_30_4_1_50_0.2_D	2	30	1.25	38.2	191	3.82	Foundation failure
69	30	8	1	2.0	20	50	0	10	0.495	0.2	C_30_8_1_50_0.2_D	4	30	1.25	N.F.	N.F.	N.F.	Base failure_EQ
70	30	2	2	2.0	20	50	0	10	0.495	0.2	C_30_2_2_50_0.2_D	1	30	1.25	38.4	192	3.84	Foundation failure
71	30	4	2	2.0	20	50	0	10	0.495	0.2	C_30_4_2_50_0.2_D	2	30	1.25	38.6	193	3.86	Foundation failure
72	30	8	2	2.0	20	50	0	10	0.495	0.2	C_30_8_2_50_0.2_D	4	30	1.25	N.F.	N.F.	N.F.	Base failure_EQ

N.F. : Not found.
Base failure_EQ: Failed due to earthquake.
Base failure_GR: Failed due to gravity.

Table C.2. List of results of finite elements models created for seismic condition (β= 30°) (Cont.).

	GEOMETRICAL PROPERTIES				SLOPE SOIL PROPERTIES				SEISMIC EFFECT	FILE NAME	ANALYSIS RESULTS FOR SEISMIC LOADING						
Model No.	β (°)	H (m)	λ	B (m)	γ (kN/m^3)	c_u (kN/m^2)	Φ_u (°)	E_u (MPa)	ν_u	k_h		H/B	β (°)	$C_u/\gamma B$	Load multiplier	q_{fs} (kPa)	N_{cse}	Failure mode
73	30	2	0	2.0	20	100	0	20	0.495	0.2	C_30_2_0_100_0.2_D	1	30	2.5	62.3	312	3.12	Foundation failure
74	30	4	0	2.0	20	100	0	20	0.495	0.2	C_30_4_0_100_0.2_D	2	30	2.5	62.8	314	3.14	Foundation failure
75	30	8	0	2.0	20	100	0	20	0.495	0.2	C_30_8_0_100_0.2_D	4	30	2.5	62.6	313	3.13	Foundation failure
76	30	2	0.5	2.0	20	100	0	20	0.495	0.2	C_30_2_0.5_100_0.2_D	1	30	2.5	71.9	359	3.59	Foundation failure
77	30	4	0.5	2.0	20	100	0	20	0.495	0.2	C_30_4_0.5_100_0.2_D	2	30	2.5	72.1	360	3.60	Foundation failure
78	30	8	0.5	2.0	20	100	0	20	0.495	0.2	C_30_8_0.5_100_0.2_D	4	30	2.5	72.3	361	3.61	Foundation failure
79	30	2	1	2.0	20	100	0	20	0.495	0.2	C_30_2_1_100_0.2_D	1	30	2.5	77.9	390	3.90	Foundation failure
80	30	4	1	2.0	20	100	0	20	0.495	0.2	C_30_4_1_100_0.2_D	2	30	2.5	78.0	390	3.90	Foundation failure
81	30	8	1	2.0	20	100	0	20	0.495	0.2	C_30_8_1_100_0.2_D	4	30	2.5	78.2	391	3.91	Foundation failure
82	30	2	2	2.0	20	100	0	20	0.495	0.2	C_30_2_2_100_0.2_D	1	30	2.5	77.7	389	3.89	Foundation failure
83	30	4	2	2.0	20	100	0	20	0.495	0.2	C_30_4_2_100_0.2_D	2	30	2.5	77.9	390	3.90	Foundation failure
84	30	8	2	2.0	20	100	0	20	0.495	0.2	C_30_8_2_100_0.2_D	4	30	2.5	77.8	389	3.89	Foundation failure
85	30	2	0	2.0	20	200	0	40	0.495	0.2	C_30_2_0_200_0.2_D	1	30	5	126.6	633	3.16	Foundation failure
86	30	4	0	2.0	20	200	0	40	0.495	0.2	C_30_4_0_200_0.2_D	2	30	5	126.8	634	3.17	Foundation failure
87	30	8	0	2.0	20	200	0	40	0.495	0.2	C_30_8_0_200_0.2_D	4	30	5	127.0	635	3.18	Foundation failure
88	30	2	0.5	2.0	20	200	0	40	0.495	0.2	C_30_2_0.5_200_0.2_D	1	30	5	145.8	729	3.64	Foundation failure
89	30	4	0.5	2.0	20	200	0	40	0.495	0.2	C_30_4_0.5_200_0.2_D	2	30	5	146.1	731	3.65	Foundation failure
90	30	8	0.5	2.0	20	200	0	40	0.495	0.2	C_30_8_0.5_200_0.2_D	4	30	5	146.6	733	3.66	Foundation failure
91	30	2	1	2.0	20	200	0	40	0.495	0.2	C_30_2_1_200_0.2_D	1	30	5	156.5	783	3.91	Foundation failure
92	30	4	1	2.0	20	200	0	40	0.495	0.2	C_30_4_1_200_0.2_D	2	30	5	156.8	784	3.92	Foundation failure
93	30	8	1	2.0	20	200	0	40	0.495	0.2	C_30_8_1_200_0.2_D	4	30	5	157.1	785	3.93	Foundation failure
94	30	2	2	2.0	20	200	0	40	0.495	0.2	C_30_2_2_200_0.2_D	1	30	5	156.2	781	3.91	Foundation failure
95	30	4	2	2.0	20	200	0	40	0.495	0.2	C_30_4_2_200_0.2_D	2	30	5	156.7	784	3.92	Foundation failure
96	30	8	2	2.0	20	200	0	40	0.495	0.2	C_30_8_2_200_0.2_D	4	30	5	156.5	782	3.91	Foundation failure
97	30	2	0	2.0	20	25	0	5	0.495	0.3	C_30_2_0_25_0.3_D	1	30	0.625	N.F.	N.F.	N.F.	Base failure_EQ
98	30	4	0	2.0	20	25	0	5	0.495	0.3	C_30_4_0_25_0.3_D	2	30	0.625	N.F.	N.F.	N.F.	Base failure_EQ
99	30	8	0	2.0	20	25	0	5	0.495	0.3	C_30_8_0_25_0.3_D	4	30	0.625	N.F.	N.F.	N.F.	Base failure_GR
100	30	2	0.5	2.0	20	25	0	5	0.495	0.3	C_30_2_0.5_25_0.3_D	1	30	0.625	N.F.	N.F.	N.F.	Base failure_EQ
101	30	4	0.5	2.0	20	25	0	5	0.495	0.3	C_30_4_0.5_25_0.3_D	2	30	0.625	N.F.	N.F.	N.F.	Base failure_EQ
102	30	8	0.5	2.0	20	25	0	5	0.495	0.3	C_30_8_0.5_25_0.3_D	4	30	0.625	N.F.	N.F.	N.F.	Base failure_GR
103	30	2	1	2.0	20	25	0	5	0.495	0.3	C_30_2_1_25_0.3_D	1	30	0.625	N.F.	N.F.	N.F.	Base failure_EQ
104	30	4	1	2.0	20	25	0	5	0.495	0.3	C_30_4_1_25_0.3_D	2	30	0.625	N.F.	N.F.	N.F.	Base failure_EQ
105	30	8	1	2.0	20	25	0	5	0.495	0.3	C_30_8_1_25_0.3_D	4	30	0.625	N.F.	N.F.	N.F.	Base failure_GR
106	30	2	2	2.0	20	25	0	5	0.495	0.3	C_30_2_2_25_0.3_D	1	30	0.625	N.F.	N.F.	N.F.	Base failure_EQ
107	30	4	2	2.0	20	25	0	5	0.495	0.3	C_30_4_2_25_0.3_D	2	30	0.625	N.F.	N.F.	N.F.	Base failure_EQ
108	30	8	2	2.0	20	25	0	5	0.495	0.3	C_30_8_2_25_0.3_D	4	30	0.625	N.F.	N.F.	N.F.	Base failure_GR

N.F. : Not found.
Base failure_EQ: Failed due to earthquake.
Base failure_GR: Failed due to gravity.

Table C.2. List of results of finite elements models created for seismic condition (β= 30°) (Cont.).

	GEOMETRICAL PROPERTIES				SLOPE SOIL PROPERTIES				SEISMIC EFFECT	FILE NAME	ANALYSIS RESULTS FOR SEISMIC LOADING						
Model No.	β (°)	H (m)	λ	B (m)	γ (kN/m^3)	c_u (kN/m^2)	Φ_u (°)	E_u (MPa)	v_u	k_h		H/B	β (°)	$C_u/\gamma B$	Load multiplier	q_{fs} (kPa)	N_{cse}	Failure mode
109	30	2	0	2.0	20	50	0	10	0.495	0.3	C_30_2_0_50_0.3_D	1	30	1.25	26.0	130	2.60	Foundation failure
110	30	4	0	2.0	20	50	0	10	0.495	0.3	C_30_4_0_50_0.3_D	2	30	1.25	N.F.	N.F.	N.F.	Base failure_EQ
111	30	8	0	2.0	20	50	0	10	0.495	0.3	C_30_8_0_50_0.3_D	4	30	1.25	N.F.	N.F.	N.F.	Base failure_EQ
112	30	2	0.5	2.0	20	50	0	10	0.495	0.3	C_30_2_0.5_50_0.3_D	1	30	1.25	30.3	152	3.03	Foundation failure
113	30	4	0.5	2.0	20	50	0	10	0.495	0.3	C_30_4_0.5_50_0.3_D	2	30	1.25	N.F.	N.F.	N.F.	Base failure_EQ
114	30	8	0.5	2.0	20	50	0	10	0.495	0.3	C_30_8_0.5_50_0.3_D	4	30	1.25	N.F.	N.F.	N.F.	Base failure_EQ
115	30	2	1	2.0	20	50	0	10	0.495	0.3	C_30_2_1_50_0.3_D	1	30	1.25	31.5	158	3.15	Foundation failure
116	30	4	1	2.0	20	50	0	10	0.495	0.3	C_30_4_1_50_0.3_D	2	30	1.25	N.F.	N.F.	N.F.	Base failure_EQ
117	30	8	1	2.0	20	50	0	10	0.495	0.3	C_30_8_1_50_0.3_D	4	30	1.25	N.F.	N.F.	N.F.	Base failure_EQ
118	30	2	2	2.0	20	50	0	10	0.495	0.3	C_30_2_2_50_0.3_D	1	30	1.25	31.6	158	3.16	Foundation failure
119	30	4	2	2.0	20	50	0	10	0.495	0.3	C_30_4_2_50_0.3_D	2	30	1.25	N.F.	N.F.	N.F.	Base failure_EQ
120	30	8	2	2.0	20	50	0	10	0.495	0.3	C_30_8_2_50_0.3_D	4	30	1.25	N.F.	N.F.	N.F.	Base failure_EQ
121	30	2	0	2.0	20	100	0	20	0.495	0.3	C_30_2_0_100_0.3_D	1	30	2.5	53.5	267	2.67	Foundation failure
122	30	4	0	2.0	20	100	0	20	0.495	0.3	C_30_4_0_100_0.3_D	2	30	2.5	53.8	269	2.69	Foundation failure
123	30	8	0	2.0	20	100	0	20	0.495	0.3	C_30_8_0_100_0.3_D	4	30	2.5	53.6	268	2.68	Foundation failure
124	30	2	0.5	2.0	20	100	0	20	0.495	0.3	C_30_2_0.5_100_0.3_D	1	30	2.5	62.6	313	3.13	Foundation failure
125	30	4	0.5	2.0	20	100	0	20	0.495	0.3	C_30_4_0.5_100_0.3_D	2	30	2.5	62.8	314	3.14	Foundation failure
126	30	8	0.5	2.0	20	100	0	20	0.495	0.3	C_30_8_0.5_100_0.3_D	4	30	2.5	63.0	315	3.15	Foundation failure
127	30	2	1	2.0	20	100	0	20	0.495	0.3	C_30_2_1_100_0.3_D	1	30	2.5	63.6	318	3.18	Foundation failure
128	30	4	1	2.0	20	100	0	20	0.495	0.3	C_30_4_1_100_0.3_D	2	30	2.5	63.7	319	3.19	Foundation failure
129	30	8	1	2.0	20	100	0	20	0.495	0.3	C_30_8_1_100_0.3_D	4	30	2.5	63.8	319	3.19	Foundation failure
130	30	2	2	2.0	20	100	0	20	0.495	0.3	C_30_2_2_100_0.3_D	1	30	2.5	63.9	320	3.20	Foundation failure
131	30	4	2	2.0	20	100	0	20	0.495	0.3	C_30_4_2_100_0.3_D	2	30	2.5	63.7	319	3.19	Foundation failure
132	30	8	2	2.0	20	100	0	20	0.495	0.3	C_30_8_2_100_0.3_D	4	30	2.5	63.7	318	3.18	Foundation failure
133	30	2	0	2.0	20	200	0	40	0.495	0.3	C_30_2_0_200_0.3_D	1	30	5	108.4	542	2.71	Foundation failure
134	30	4	0	2.0	20	200	0	40	0.495	0.3	C_30_4_0_200_0.3_D	2	30	5	108.5	543	2.71	Foundation failure
135	30	8	0	2.0	20	200	0	40	0.495	0.3	C_30_8_0_200_0.3_D	4	30	5	108.8	544	2.72	Foundation failure
136	30	2	0.5	2.0	20	200	0	40	0.495	0.3	C_30_2_0.5_200_0.3_D	1	30	5	126.9	635	3.17	Foundation failure
137	30	4	0.5	2.0	20	200	0	40	0.495	0.3	C_30_4_0.5_200_0.3_D	2	30	5	127.2	636	3.18	Foundation failure
138	30	8	0.5	2.0	20	200	0	40	0.495	0.3	C_30_8_0.5_200_0.3_D	4	30	5	127.6	638	3.19	Foundation failure
139	30	2	1	2.0	20	200	0	40	0.495	0.3	C_30_2_1_200_0.3_D	1	30	5	127.8	639	3.20	Foundation failure
140	30	4	1	2.0	20	200	0	40	0.495	0.3	C_30_4_1_200_0.3_D	2	30	5	127.9	640	3.20	Foundation failure
141	30	8	1	2.0	20	200	0	40	0.495	0.3	C_30_8_1_200_0.3_D	4	30	5	128.0	640	3.20	Foundation failure
142	30	2	2	2.0	20	200	0	40	0.495	0.3	C_30_2_2_200_0.3_D	1	30	5	127.7	639	3.19	Foundation failure
143	30	4	2	2.0	20	200	0	40	0.495	0.3	C_30_4_2_200_0.3_D	2	30	5	128.0	640	3.20	Foundation failure
144	30	8	2	2.0	20	200	0	40	0.495	0.3	C_30_8_2_200_0.3_D	4	30	5	128.0	640	3.20	Foundation failure

N.F. : Not found.
Base failure_EQ: Failed due to earthquake.
Base failure_GR: Failed due to gravity.

Table C.2. List of results of finite elements models created for seismic condition (β= 30°) (Cont.).

	GEOMETRICAL PROPERTIES				SLOPE SOIL PROPERTIES				SEISMIC EFFECT	FILE NAME	ANALYSIS RESULTS FOR SEISMIC LOADING						
Model No.	β (°)	H (m)	λ	B (m)	γ (kN/m^3)	c_u (kN/m^2)	Φ_u (°)	E_u (MPa)	ν_u	k_h		H/B	β (°)	$C_u/\gamma B$	Load multiplier	q_{fs} (kPa)	N_{cse}	Failure mode
145	30	2	0	2.0	20	25	0	5	0.495	0.4	C_30_2_0_25_0.4_D	1	30	0.625	N.F.	N.F.	N.F.	Base failure_EQ
146	30	4	0	2.0	20	25	0	5	0.495	0.4	C_30_4_0_25_0.4_D	2	30	0.625	N.F.	N.F.	N.F.	Base failure_EQ
147	30	8	0	2.0	20	25	0	5	0.495	0.4	C_30_8_0_25_0.4_D	4	30	0.625	N.F.	N.F.	N.F.	Base failure_GR
148	30	2	0.5	2.0	20	25	0	5	0.495	0.4	C_30_2_0.5_25_0.4_D	1	30	0.625	N.F.	N.F.	N.F.	Base failure_EQ
149	30	4	0.5	2.0	20	25	0	5	0.495	0.4	C_30_4_0.5_25_0.4_D	2	30	0.625	N.F.	N.F.	N.F.	Base failure_EQ
150	30	8	0.5	2.0	20	25	0	5	0.495	0.4	C_30_8_0.5_25_0.4_D	4	30	0.625	N.F.	N.F.	N.F.	Base failure_GR
151	30	2	1	2.0	20	25	0	5	0.495	0.4	C_30_2_1_25_0.4_D	1	30	0.625	N.F.	N.F.	N.F.	Base failure_EQ
152	30	4	1	2.0	20	25	0	5	0.495	0.4	C_30_4_1_25_0.4_D	2	30	0.625	N.F.	N.F.	N.F.	Base failure_EQ
153	30	8	1	2.0	20	25	0	5	0.495	0.4	C_30_8_1_25_0.4_D	4	30	0.625	N.F.	N.F.	N.F.	Base failure_GR
154	30	2	2	2.0	20	25	0	5	0.495	0.4	C_30_2_2_25_0.4_D	1	30	0.625	N.F.	N.F.	N.F.	Base failure_EQ
155	30	4	2	2.0	20	25	0	5	0.495	0.4	C_30_4_2_25_0.4_D	2	30	0.625	N.F.	N.F.	N.F.	Base failure_EQ
156	30	8	2	2.0	20	25	0	5	0.495	0.4	C_30_8_2_25_0.4_D	4	30	0.625	N.F.	N.F.	N.F.	Base failure_GR
157	30	2	0	2.0	20	50	0	10	0.495	0.4	C_30_2_0_50_0.4_D	1	30	1.25	N.F.	N.F.	N.F.	Base failure_EQ
158	30	4	0	2.0	20	50	0	10	0.495	0.4	C_30_4_0_50_0.4_D	2	30	1.25	N.F.	N.F.	N.F.	Base failure_EQ
159	30	8	0	2.0	20	50	0	10	0.495	0.4	C_30_8_0_50_0.4_D	4	30	1.25	N.F.	N.F.	N.F.	Base failure_EQ
160	30	2	0.5	2.0	20	50	0	10	0.495	0.4	C_30_2_0.5_50_0.4_D	1	30	1.25	N.F.	N.F.	N.F.	Base failure_EQ
161	30	4	0.5	2.0	20	50	0	10	0.495	0.4	C_30_4_0.5_50_0.4_D	2	30	1.25	N.F.	N.F.	N.F.	Base failure_EQ
162	30	8	0.5	2.0	20	50	0	10	0.495	0.4	C_30_8_0.5_50_0.4_D	4	30	1.25	N.F.	N.F.	N.F.	Base failure_EQ
163	30	2	1	2.0	20	50	0	10	0.495	0.4	C_30_2_1_50_0.4_D	1	30	1.25	N.F.	N.F.	N.F.	Base failure_EQ
164	30	4	1	2.0	20	50	0	10	0.495	0.4	C_30_4_1_50_0.4_D	2	30	1.25	N.F.	N.F.	N.F.	Base failure_EQ
165	30	8	1	2.0	20	50	0	10	0.495	0.4	C_30_8_1_50_0.4_D	4	30	1.25	N.F.	N.F.	N.F.	Base failure_EQ
166	30	2	2	2.0	20	50	0	10	0.495	0.4	C_30_2_2_50_0.4_D	1	30	1.25	N.F.	N.F.	N.F.	Base failure_EQ
167	30	4	2	2.0	20	50	0	10	0.495	0.4	C_30_4_2_50_0.4_D	2	30	1.25	N.F.	N.F.	N.F.	Base failure_EQ
168	30	8	2	2.0	20	50	0	10	0.495	0.4	C_30_8_2_50_0.4_D	4	30	1.25	N.F.	N.F.	N.F.	Base failure_EQ
169	30	2	0	2.0	20	100	0	20	0.495	0.4	C_30_2_0_100_0.4_D	1	30	2.5	45.6	228	2.28	Foundation failure
170	30	4	0	2.0	20	100	0	20	0.495	0.4	C_30_4_0_100_0.4_D	2	30	2.5	45.7	229	2.29	Foundation failure
171	30	8	0	2.0	20	100	0	20	0.495	0.4	C_30_8_0_100_0.4_D	4	30	2.5	45.6	228	2.28	Foundation failure
172	30	2	0.5	2.0	20	100	0	20	0.495	0.4	C_30_2_0.5_100_0.4_D	1	30	2.5	50.0	250	2.50	Sliding
173	30	4	0.5	2.0	20	100	0	20	0.495	0.4	C_30_4_0.5_100_0.4_D	2	30	2.5	50.0	250	2.50	Sliding
174	30	8	0.5	2.0	20	100	0	20	0.495	0.4	C_30_8_0.5_100_0.4_D	4	30	2.5	50.0	250	2.50	Sliding
175	30	2	1	2.0	20	100	0	20	0.495	0.4	C_30_2_1_100_0.4_D	1	30	2.5	50.0	250	2.50	Sliding
176	30	4	1	2.0	20	100	0	20	0.495	0.4	C_30_4_1_100_0.4_D	2	30	2.5	50.2	251	2.51	Sliding
177	30	8	1	2.0	20	100	0	20	0.495	0.4	C_30_8_1_100_0.4_D	4	30	2.5	50.2	251	2.51	Sliding
178	30	2	2	2.0	20	100	0	20	0.495	0.4	C_30_2_2_100_0.4_D	1	30	2.5	50.1	251	2.51	Sliding
179	30	4	2	2.0	20	100	0	20	0.495	0.4	C_30_4_2_100_0.4_D	2	30	2.5	50.3	251	2.51	Sliding
180	30	8	2	2.0	20	100	0	20	0.495	0.4	C_30_8_2_100_0.4_D	4	30	2.5	50.1	251	2.51	Sliding

N.F. : Not found.
Base failure_EQ: Failed due to earthquake.
Base failure_GR: Failed due to gravity.

Table C.2. List of results of finite elements models created for seismic condition (β= 30°) (Cont.).

	GEOMETRICAL PROPERTIES				SLOPE SOIL PROPERTIES					SEISMIC EFFECT	FILE NAME	ANALYSIS RESULTS FOR SEISMIC LOADING						
Model No.	β (°)	H (m)	λ	B (m)	γ (kN/m^3)	c_u (kN/m^2)	Φ_u (°)	E_u (MPa)	ν_u	k_h		H/B	β (°)	$C_u/\gamma B$	Load multiplier	q_{fs} (kPa)	N_{cse}	Failure mode
181	30	2	0	2.0	20	200	0	40	0.495	0.4	C_30_2_0_200_0.4_D	1	30	5	92.1	460	2.30	Foundation failure
182	30	4	0	2.0	20	200	0	40	0.495	0.4	C_30_4_0_200_0.4_D	2	30	5	92.0	460	2.30	Foundation failure
183	30	8	0	2.0	20	200	0	40	0.495	0.4	C_30_8_0_200_0.4_D	4	30	5	92.2	461	2.31	Foundation failure
184	30	2	0.5	2.0	20	200	0	40	0.495	0.4	C_30_2_0.5_200_0.4_D	1	30	5	100.5	503	2.51	Sliding
185	30	4	0.5	2.0	20	200	0	40	0.495	0.4	C_30_4_0.5_200_0.4_D	2	30	5	100.3	502	2.51	Sliding
186	30	8	0.5	2.0	20	200	0	40	0.495	0.4	C_30_8_0.5_200_0.4_D	4	30	5	100.2	501	2.51	Sliding
187	30	2	1	2.0	20	200	0	40	0.495	0.4	C_30_2_1_200_0.4_D	1	30	5	100.1	501	2.50	Sliding
188	30	4	1	2.0	20	200	0	40	0.495	0.4	C_30_4_1_200_0.4_D	2	30	5	100.4	502	2.51	Sliding
189	30	8	1	2.0	20	200	0	40	0.495	0.4	C_30_8_1_200_0.4_D	4	30	5	100.1	501	2.50	Sliding
190	30	2	2	2.0	20	200	0	40	0.495	0.4	C_30_2_2_200_0.4_D	1	30	5	100.2	501	2.50	Sliding
191	30	4	2	2.0	20	200	0	40	0.495	0.4	C_30_4_2_200_0.4_D	2	30	5	100.1	500	2.50	Sliding
192	30	8	2	2.0	20	200	0	40	0.495	0.4	C_30_8_2_200_0.4_D	4	30	5	100.5	503	2.51	Sliding

N.F. : Not found.
Base failre_EQ: Failed due to earthquake.
Base failre_GR: Failed due to gravity.

Table C.3. List of results of finite elements models created for seismic condition (β= 45°).

	GEOMETRICAL PROPERTIES				SLOPE SOIL PROPERTIES					SEISMIC EFFECT	FILE NAME	ANALYSIS RESULTS FOR SEISMIC LOADING						
Model No.	β (°)	H (m)	λ	B (m)	γ (kN/m^3)	c_u (kN/m^2)	Φ_u (°)	E_u (MPa)	ν_u	k_h		H/B	β (°)	$C_u/\gamma B$	Load multiplier	q_{fs} (kPa)	N_{cse}	Failure mode
1	45	2	0	2.0	20	25	0	5	0.495	0.1	C_45_2_0_25_0.1_D	1	45	0.625	12.2	61	2.44	Foundation failure
2	45	4	0	2.0	20	25	0	5	0.495	0.1	C_45_4_0_25_0.1_D	2	45	0.625	N.F.	N.F.	N.F.	Base failure_EQ
3	45	8	0	2.0	20	25	0	5	0.495	0.1	C_45_8_0_25_0.1_D	4	45	0.625	N.F.	N.F.	N.F.	Base failure_GR
4	45	2	0.5	2.0	20	25	0	5	0.495	0.1	C_45_2_0.5_25_0.1_D	1	45	0.625	14.5	72	2.90	Foundation failure
5	45	4	0.5	2.0	20	25	0	5	0.495	0.1	C_45_4_0.5_25_0.1_D	2	45	0.625	N.F.	N.F.	N.F.	Base failure_EQ
6	45	8	0.5	2.0	20	25	0	5	0.495	0.1	C_45_8_0.5_25_0.1_D	4	45	0.625	N.F.	N.F.	N.F.	Base failure_GR
7	45	2	1	2.0	20	25	0	5	0.495	0.1	C_45_2_1_25_0.1_D	1	45	0.625	16.5	83	3.30	Foundation failure
8	45	4	1	2.0	20	25	0	5	0.495	0.1	C_45_4_1_25_0.1_D	2	45	0.625	N.F.	N.F.	N.F.	Base failure_EQ
9	45	8	1	2.0	20	25	0	5	0.495	0.1	C_45_8_1_25_0.1_D	4	45	0.625	N.F.	N.F.	N.F.	Base failure_GR
10	45	2	2	2.0	20	25	0	5	0.495	0.1	C_45_2_2_25_0.1_D	1	45	0.625	20.0	100	4.01	Foundation failure
11	45	4	2	2.0	20	25	0	5	0.495	0.1	C_45_4_2_25_0.1_D	2	45	0.625	N.F.	N.F.	N.F.	Base failure_EQ
12	45	8	2	2.0	20	25	0	5	0.495	0.1	C_45_8_2_25_0.1_D	4	45	0.625	N.F.	N.F.	N.F.	Base failure_GR
13	45	2	0	2.0	20	50	0	10	0.495	0.1	C_45_2_0_50_0.1_D	1	45	1.25	29.1	145	2.91	Foundation failure
14	45	4	0	2.0	20	50	0	10	0.495	0.1	C_45_4_0_50_0.1_D	2	45	1.25	29.2	146	2.92	Foundation failure
15	45	8	0	2.0	20	50	0	10	0.495	0.1	C_45_8_0_50_0.1_D	4	45	1.25	29.2	146	2.92	Foundation failure
16	45	2	0.5	2.0	20	50	0	10	0.495	0.1	C_45_2_0.5_50_0.1_D	1	45	1.25	34.5	172	3.45	Foundation failure
17	45	4	0.5	2.0	20	50	0	10	0.495	0.1	C_45_4_0.5_50_0.1_D	2	45	1.25	34.3	171	3.43	Foundation failure
18	45	8	0.5	2.0	20	50	0	10	0.495	0.1	C_45_8_0.5_50_0.1_D	4	45	1.25	34.4	172	3.44	Foundation failure
19	45	2	1	2.0	20	50	0	10	0.495	0.1	C_45_2_1_50_0.1_D	1	45	1.25	38.7	194	3.87	Foundation failure
20	45	4	1	2.0	20	50	0	10	0.495	0.1	C_45_4_1_50_0.1_D	2	45	1.25	37.6	188	3.76	Foundation failure
21	45	8	1	2.0	20	50	0	10	0.495	0.1	C_45_8_1_50_0.1_D	4	45	1.25	34.5	173	3.45	Foundation failure
22	45	2	2	2.0	20	50	0	10	0.495	0.1	C_45_2_2_50_0.1_D	1	45	1.25	45.3	227	4.53	Foundation failure
23	45	4	2	2.0	20	50	0	10	0.495	0.1	C_45_4_2_50_0.1_D	2	45	1.25	42.7	213	4.27	Foundation failure
24	45	8	2	2.0	20	50	0	10	0.495	0.1	C_45_8_2_50_0.1_D	4	45	1.25	35.0	175	3.50	Foundation failure
25	45	2	0	2.0	20	100	0	20	0.495	0.1	C_45_2_0_100_0.1_D	1	45	2.5	61.7	308	3.08	Foundation failure
26	45	4	0	2.0	20	100	0	20	0.495	0.1	C_45_4_0_100_0.1_D	2	45	2.5	61.7	308	3.08	Foundation failure
27	45	8	0	2.0	20	100	0	20	0.495	0.1	C_45_8_0_100_0.1_D	4	45	2.5	61.8	309	3.09	Foundation failure
28	45	2	0.5	2.0	20	100	0	20	0.495	0.1	C_45_2_0.5_100_0.1_D	1	45	2.5	73.5	367	3.67	Foundation failure
29	45	4	0.5	2.0	20	100	0	20	0.495	0.1	C_45_4_0.5_100_0.1_D	2	45	2.5	73.5	368	3.68	Foundation failure
30	45	8	0.5	2.0	20	100	0	20	0.495	0.1	C_45_8_0.5_100_0.1_D	4	45	2.5	73.8	369	3.69	Foundation failure
31	45	2	1	2.0	20	100	0	20	0.495	0.1	C_45_2_1_100_0.1_D	1	45	2.5	82.0	410	4.10	Foundation failure
32	45	4	1	2.0	20	100	0	20	0.495	0.1	C_45_4_1_100_0.1_D	2	45	2.5	82.1	410	4.10	Foundation failure
33	45	8	1	2.0	20	100	0	20	0.495	0.1	C_45_8_1_100_0.1_D	4	45	2.5	82.1	411	4.11	Foundation failure
34	45	2	2	2.0	20	100	0	20	0.495	0.1	C_45_2_2_100_0.1_D	1	45	2.5	91.7	459	4.59	Foundation failure
35	45	4	2	2.0	20	100	0	20	0.495	0.1	C_45_4_2_100_0.1_D	2	45	2.5	91.9	460	4.60	Foundation failure
36	45	8	2	2.0	20	100	0	20	0.495	0.1	C_45_8_2_100_0.1_D	4	45	2.5	92.0	460	4.60	Foundation failure

N.F. : Not found.

Base failure_EQ: Failed due to earthquake.

Base failure_GR: Failed due to gravity.

Table C.3. List of results of finite elements models created for seismic condition (β= 45°) (Cont.).

	GEOMETRICAL PROPERTIES				SLOPE SOIL PROPERTIES				SEISMIC EFFECT	FILE NAME	ANALYSIS RESULTS FOR SEISMIC LOADING						
Model No.	β (°)	H (m)	λ	B (m)	γ (kN/m^3)	c_u (kN/m^2)	Φ_u (°)	E_u (MPa)	ν_u	k_h		H/B	β (°)	$C_u/\gamma B$	Load multiplier	q_{fs} (kPa)	N_{cse}	Failure mode
37	45	2	0	2.0	20	200	0	40	0.495	0.1	C_45_2_0_200_0.1_D	1	45	5	126.4	632	3.16	Foundation failure
38	45	4	0	2.0	20	200	0	40	0.495	0.1	C_45_4_0_200_0.1_D	2	45	5	126.6	633	3.17	Foundation failure
39	45	8	0	2.0	20	200	0	40	0.495	0.1	C_45_8_0_200_0.1_D	4	45	5	126.7	633	3.17	Foundation failure
40	45	2	0.5	2.0	20	200	0	40	0.495	0.1	C_45_2_0.5_200_0.1_D	1	45	5	150.5	753	3.76	Foundation failure
41	45	4	0.5	2.0	20	200	0	40	0.495	0.1	C_45_4_0.5_200_0.1_D	2	45	5	150.6	753	3.77	Foundation failure
42	45	8	0.5	2.0	20	200	0	40	0.495	0.1	C_45_8_0.5_200_0.1_D	4	45	5	151.2	756	3.78	Foundation failure
43	45	2	1	2.0	20	200	0	40	0.495	0.1	C_45_2_1_200_0.1_D	1	45	5	168.4	842	4.21	Foundation failure
44	45	4	1	2.0	20	200	0	40	0.495	0.1	C_45_4_1_200_0.1_D	2	45	5	167.9	840	4.20	Foundation failure
45	45	8	1	2.0	20	200	0	40	0.495	0.1	C_45_8_1_200_0.1_D	4	45	5	167.9	840	4.20	Foundation failure
46	45	2	2	2.0	20	200	0	40	0.495	0.1	C_45_2_2_200_0.1_D	1	45	5	184.0	920	4.60	Foundation failure
47	45	4	2	2.0	20	200	0	40	0.495	0.1	C_45_4_2_200_0.1_D	2	45	5	184.3	922	4.61	Foundation failure
48	45	8	2	2.0	20	200	0	40	0.495	0.1	C_45_8_2_200_0.1_D	4	45	5	184.6	923	4.62	Foundation failure
49	45	2	0	2.0	20	25	0	5	0.495	0.2	C_45_2_0_25_0.2_D	1	45	0.625	N.F.	N.F.	N.F.	Base failure_EQ
50	45	4	0	2.0	20	25	0	5	0.495	0.2	C_45_4_0_25_0.2_D	2	45	0.625	N.F.	N.F.	N.F.	Base failure_EQ
51	45	8	0	2.0	20	25	0	5	0.495	0.2	C_45_8_0_25_0.2_D	4	45	0.625	N.F.	N.F.	N.F.	Base failure_GR
52	45	2	0.5	2.0	20	25	0	5	0.495	0.2	C_45_2_0.5_25_0.2_D	1	45	0.625	N.F.	N.F.	N.F.	Base failure_EQ
53	45	4	0.5	2.0	20	25	0	5	0.495	0.2	C_45_4_0.5_25_0.2_D	2	45	0.625	N.F.	N.F.	N.F.	Base failure_EQ
54	45	8	0.5	2.0	20	25	0	5	0.495	0.2	C_45_8_0.5_25_0.2_D	4	45	0.625	N.F.	N.F.	N.F.	Base failure_GR
55	45	2	1	2.0	20	25	0	5	0.495	0.2	C_45_2_1_25_0.2_D	1	45	0.625	N.F.	N.F.	N.F.	Base failure_EQ
56	45	4	1	2.0	20	25	0	5	0.495	0.2	C_45_4_1_25_0.2_D	2	45	0.625	N.F.	N.F.	N.F.	Base failure_EQ
57	45	8	1	2.0	20	25	0	5	0.495	0.2	C_45_8_1_25_0.2_D	4	45	0.625	N.F.	N.F.	N.F.	Base failure_GR
58	45	2	2	2.0	20	25	0	5	0.495	0.2	C_45_2_2_25_0.2_D	1	45	0.625	N.F.	N.F.	N.F.	Base failure_EQ
59	45	4	2	2.0	20	25	0	5	0.495	0.2	C_45_4_2_25_0.2_D	2	45	0.625	N.F.	N.F.	N.F.	Base failure_EQ
60	45	8	2	2.0	20	25	0	5	0.495	0.2	C_45_8_2_25_0.2_D	4	45	0.625	N.F.	N.F.	N.F.	Base failure_GR
61	45	2	0	2.0	20	50	0	10	0.495	0.2	C_45_2_0_50_0.2_D	1	45	1.25	25.6	128	2.56	Foundation failure
62	45	4	0	2.0	20	50	0	10	0.495	0.2	C_45_4_0_50_0.2_D	2	45	1.25	25.7	129	2.57	Foundation failure
63	45	8	0	2.0	20	50	0	10	0.495	0.2	C_45_8_0_50_0.2_D	4	45	1.25	N.F.	N.F.	N.F.	Base failure_EQ
64	45	2	0.5	2.0	20	50	0	10	0.495	0.2	C_45_2_0.5_50_0.2_D	1	45	1.25	30.6	153	3.06	Foundation failure
65	45	4	0.5	2.0	20	50	0	10	0.495	0.2	C_45_4_0.5_50_0.2_D	2	45	1.25	30.6	153	3.06	Foundation failure
66	45	8	0.5	2.0	20	50	0	10	0.495	0.2	C_45_8_0.5_50_0.2_D	4	45	1.25	N.F.	N.F.	N.F.	Base failure_EQ
67	45	2	1	2.0	20	50	0	10	0.495	0.2	C_45_2_1_50_0.2_D	1	45	1.25	34.4	172	3.44	Foundation failure
68	45	4	1	2.0	20	50	0	10	0.495	0.2	C_45_4_1_50_0.2_D	2	45	1.25	33.5	168	3.35	Foundation failure
69	45	8	1	2.0	20	50	0	10	0.495	0.2	C_45_8_1_50_0.2_D	4	45	1.25	N.F.	N.F.	N.F.	Base failure_EQ
70	45	2	2	2.0	20	50	0	10	0.495	0.2	C_45_2_2_50_0.2_D	1	45	1.25	38.6	193	3.86	Foundation failure
71	45	4	2	2.0	20	50	0	10	0.495	0.2	C_45_4_2_50_0.2_D	2	45	1.25	37.6	188	3.76	Foundation failure
72	45	8	2	2.0	20	50	0	10	0.495	0.2	C_45_8_2_50_0.2_D	4	45	1.25	N.F.	N.F.	N.F.	Base failure_EQ

N.F. : Not found.
Base failure_EQ: Failed due to earthquake.
Base failure_GR: Failed due to gravity.

Table C.3. List of results of finite elements models created for seismic condition (β= 45°) (Cont.).

	GEOMETRICAL PROPERTIES				SLOPE SOIL PROPERTIES				SEISMIC EFFECT	FILE NAME	ANALYSIS RESULTS FOR SEISMIC LOADING						
Model No.	β (°)	H (m)	λ	B (m)	γ (kN/m^3)	c_u (kN/m^2)	Φ_u (°)	E_u (MPa)	ν_u	k_h		H/B	β (°)	$C_u/\gamma B$	Load multiplier	q_{fs} (kPa)	N_{cse}	Failure mode
73	45	2	0	2.0	20	100	0	20	0.495	0.2	C_45_2_0_100_0.2_D	1	45	2.5	54.2	271	2.71	Foundation failure
74	45	4	0	2.0	20	100	0	20	0.495	0.2	C_45_4_0_100_0.2_D	2	45	2.5	54.3	271	2.71	Foundation failure
75	45	8	0	2.0	20	100	0	20	0.495	0.2	C_45_8_0_100_0.2_D	4	45	2.5	54.5	273	2.73	Foundation failure
76	45	2	0.5	2.0	20	100	0	20	0.495	0.2	C_45_2_0.5_100_0.2_D	1	45	2.5	65.9	330	3.30	Foundation failure
77	45	4	0.5	2.0	20	100	0	20	0.495	0.2	C_45_4_0.5_100_0.2_D	2	45	2.5	65.9	330	3.30	Foundation failure
78	45	8	0.5	2.0	20	100	0	20	0.495	0.2	C_45_8_0.5_100_0.2_D	4	45	2.5	66.2	331	3.31	Foundation failure
79	45	2	1	2.0	20	100	0	20	0.495	0.2	C_45_2_1_100_0.2_D	1	45	2.5	74.0	370	3.70	Foundation failure
80	45	4	1	2.0	20	100	0	20	0.495	0.2	C_45_4_1_100_0.2_D	2	45	2.5	74.1	371	3.71	Foundation failure
81	45	8	1	2.0	20	100	0	20	0.495	0.2	C_45_8_1_100_0.2_D	4	45	2.5	74.1	371	3.71	Foundation failure
82	45	2	2	2.0	20	100	0	20	0.495	0.2	C_45_2_2_100_0.2_D	1	45	2.5	77.9	389	3.89	Foundation failure
83	45	4	2	2.0	20	100	0	20	0.495	0.2	C_45_4_2_100_0.2_D	2	45	2.5	77.7	389	3.89	Foundation failure
84	45	8	2	2.0	20	100	0	20	0.495	0.2	C_45_8_2_100_0.2_D	4	45	2.5	78.1	391	3.91	Foundation failure
85	45	2	0	2.0	20	200	0	40	0.495	0.2	C_45_2_0_200_0.2_D	1	45	5	110.9	555	2.77	Foundation failure
86	45	4	0	2.0	20	200	0	40	0.495	0.2	C_45_4_0_200_0.2_D	2	45	5	111.0	555	2.77	Foundation failure
87	45	8	0	2.0	20	200	0	40	0.495	0.2	C_45_8_0_200_0.2_D	4	45	5	111.2	556	2.78	Foundation failure
88	45	2	0.5	2.0	20	200	0	40	0.495	0.2	C_45_2_0.5_200_0.2_D	1	45	5	135.1	676	3.38	Foundation failure
89	45	4	0.5	2.0	20	200	0	40	0.495	0.2	C_45_4_0.5_200_0.2_D	2	45	5	135.2	676	3.38	Foundation failure
90	45	8	0.5	2.0	20	200	0	40	0.495	0.2	C_45_8_0.5_200_0.2_D	4	45	5	135.7	678	3.39	Foundation failure
91	45	2	1	2.0	20	200	0	40	0.495	0.2	C_45_2_1_200_0.2_D	1	45	5	151.6	758	3.79	Foundation failure
92	45	4	1	2.0	20	200	0	40	0.495	0.2	C_45_4_1_200_0.2_D	2	45	5	151.8	759	3.80	Foundation failure
93	45	8	1	2.0	20	200	0	40	0.495	0.2	C_45_8_1_200_0.2_D	4	45	5	151.9	759	3.80	Foundation failure
94	45	2	2	2.0	20	200	0	40	0.495	0.2	C_45_2_2_200_0.2_D	1	45	5	156.5	782	3.91	Foundation failure
95	45	4	2	2.0	20	200	0	40	0.495	0.2	C_45_4_2_200_0.2_D	2	45	5	156.5	782	3.91	Foundation failure
96	45	8	2	2.0	20	200	0	40	0.495	0.2	C_45_8_2_200_0.2_D	4	45	5	157.1	785	3.93	Foundation failure
97	45	2	0	2.0	20	25	0	5	0.495	0.3	C_45_2_0_25_0.3_D	1	45	0.625	N.F.	N.F.	N.F.	Base failure_EQ
98	45	4	0	2.0	20	25	0	5	0.495	0.3	C_45_4_0_25_0.3_D	2	45	0.625	N.F.	N.F.	N.F.	Base failure_EQ
99	45	8	0	2.0	20	25	0	5	0.495	0.3	C_45_8_0_25_0.3_D	4	45	0.625	N.F.	N.F.	N.F.	Base failure_GR
100	45	2	0.5	2.0	20	25	0	5	0.495	0.3	C_45_2_0.5_25_0.3_D	1	45	0.625	N.F.	N.F.	N.F.	Base failure_EQ
101	45	4	0.5	2.0	20	25	0	5	0.495	0.3	C_45_4_0.5_25_0.3_D	2	45	0.625	N.F.	N.F.	N.F.	Base failure_EQ
102	45	8	0.5	2.0	20	25	0	5	0.495	0.3	C_45_8_0.5_25_0.3_D	4	45	0.625	N.F.	N.F.	N.F.	Base failure_GR
103	45	2	1	2.0	20	25	0	5	0.495	0.3	C_45_2_1_25_0.3_D	1	45	0.625	N.F.	N.F.	N.F.	Base failure_EQ
104	45	4	1	2.0	20	25	0	5	0.495	0.3	C_45_4_1_25_0.3_D	2	45	0.625	N.F.	N.F.	N.F.	Base failure_EQ
105	45	8	1	2.0	20	25	0	5	0.495	0.3	C_45_8_1_25_0.3_D	4	45	0.625	N.F.	N.F.	N.F.	Base failure_GR
106	45	2	2	2.0	20	25	0	5	0.495	0.3	C_45_2_2_25_0.3_D	1	45	0.625	N.F.	N.F.	N.F.	Base failure_EQ
107	45	4	2	2.0	20	25	0	5	0.495	0.3	C_45_4_2_25_0.3_D	2	45	0.625	N.F.	N.F.	N.F.	Base failure_EQ
108	45	8	2	2.0	20	25	0	5	0.495	0.3	C_45_8_2_25_0.3_D	4	45	0.625	N.F.	N.F.	N.F.	Base failure_GR

N.F. : Not found.
Base failure_EQ: Failed due to earthquake.
Base failure_GR: Failed due to gravity.

Table C.3. List of results of finite elements models created for seismic condition (β= 45°) (Cont.).

	GEOMETRICAL PROPERTIES				SLOPE SOIL PROPERTIES				SEISMIC EFFECT	FILE NAME	ANALYSIS RESULTS FOR SEISMIC LOADING						
Model No.	β (°)	H (m)	λ	B (m)	γ (kN/m^3)	c_u (kN/m^2)	Φ_u (°)	E_u (MPa)	v_u	k_h		H/B	β (°)	$C_u/\gamma B$	Load multiplier	q_{fs} (kPa)	N_{cse}	Failure mode
109	45	2	0	2.0	20	50	0	10	0.495	0.3	C_45_2_0_50_0.3_D	1	45	1.25	22.4	112	2.24	Foundation failure
110	45	4	0	2.0	20	50	0	10	0.495	0.3	C_45_4_0_50_0.3_D	2	45	1.25	N.F.	N.F.	N.F.	Base failure_EQ
111	45	8	0	2.0	20	50	0	10	0.495	0.3	C_45_8_0_50_0.3_D	4	45	1.25	N.F.	N.F.	N.F.	Base failure_EQ
112	45	2	0.5	2.0	20	50	0	10	0.495	0.3	C_45_2_0.5_50_0.3_D	1	45	1.25	27.2	136	2.72	Foundation failure
113	45	4	0.5	2.0	20	50	0	10	0.495	0.3	C_45_4_0.5_50_0.3_D	2	45	1.25	N.F.	N.F.	N.F.	Base failure_EQ
114	45	8	0.5	2.0	20	50	0	10	0.495	0.3	C_45_8_0.5_50_0.3_D	4	45	1.25	N.F.	N.F.	N.F.	Base failure_EQ
115	45	2	1	2.0	20	50	0	10	0.495	0.3	C_45_2_1_50_0.3_D	1	45	1.25	30.4	152	3.04	Foundation failure
116	45	4	1	2.0	20	50	0	10	0.495	0.3	C_45_4_1_50_0.3_D	2	45	1.25	N.F.	N.F.	N.F.	Base failure_EQ
117	45	8	1	2.0	20	50	0	10	0.495	0.3	C_45_8_1_50_0.3_D	4	45	1.25	N.F.	N.F.	N.F.	Base failure_EQ
118	45	2	2	2.0	20	50	0	10	0.495	0.3	C_45_2_2_50_0.3_D	1	45	1.25	31.5	158	3.15	Foundation failure
119	45	4	2	2.0	20	50	0	10	0.495	0.3	C_45_4_2_50_0.3_D	2	45	1.25	N.F.	N.F.	N.F.	Base failure_EQ
120	45	8	2	2.0	20	50	0	10	0.495	0.3	C_45_8_2_50_0.3_D	4	45	1.25	N.F.	N.F.	N.F.	Base failure_EQ
121	45	2	0	2.0	20	100	0	20	0.495	0.3	C_45_2_0_100_0.3_D	1	45	2.5	47.1	236	2.36	Foundation failure
122	45	4	0	2.0	20	100	0	20	0.495	0.3	C_45_4_0_100_0.3_D	2	45	2.5	47.2	236	2.36	Foundation failure
123	45	8	0	2.0	20	100	0	20	0.495	0.3	C_45_8_0_100_0.3_D	4	45	2.5	47.4	237	2.37	Foundation failure
124	45	2	0.5	2.0	20	100	0	20	0.495	0.3	C_45_2_0.5_100_0.3_D	1	45	2.5	58.4	292	2.92	Foundation failure
125	45	4	0.5	2.0	20	100	0	20	0.495	0.3	C_45_4_0.5_100_0.3_D	2	45	2.5	58.5	292	2.92	Foundation failure
126	45	8	0.5	2.0	20	100	0	20	0.495	0.3	C_45_8_0.5_100_0.3_D	4	45	2.5	58.7	293	2.93	Foundation failure
127	45	2	1	2.0	20	100	0	20	0.495	0.3	C_45_2_1_100_0.3_D	1	45	2.5	63.6	318	3.18	Foundation failure
128	45	4	1	2.0	20	100	0	20	0.495	0.3	C_45_4_1_100_0.3_D	2	45	2.5	63.7	319	3.19	Foundation failure
129	45	8	1	2.0	20	100	0	20	0.495	0.3	C_45_8_1_100_0.3_D	4	45	2.5	63.7	319	3.19	Foundation failure
130	45	2	2	2.0	20	100	0	20	0.495	0.3	C_45_2_2_100_0.3_D	1	45	2.5	63.6	318	3.18	Foundation failure
131	45	4	2	2.0	20	100	0	20	0.495	0.3	C_45_4_2_100_0.3_D	2	45	2.5	63.7	319	3.19	Foundation failure
132	45	8	2	2.0	20	100	0	20	0.495	0.3	C_45_8_2_100_0.3_D	4	45	2.5	63.8	319	3.19	Foundation failure
133	45	2	0	2.0	20	200	0	40	0.495	0.3	C_45_2_0_200_0.3_D	1	45	5	96.3	482	2.41	Foundation failure
134	45	4	0	2.0	20	200	0	40	0.495	0.3	C_45_4_0_200_0.3_D	2	45	5	96.4	482	2.41	Foundation failure
135	45	8	0	2.0	20	200	0	40	0.495	0.3	C_45_8_0_200_0.3_D	4	45	5	96.8	484	2.42	Foundation failure
136	45	2	0.5	2.0	20	200	0	40	0.495	0.3	C_45_2_0.5_200_0.3_D	1	45	5	119.7	599	2.99	Foundation failure
137	45	4	0.5	2.0	20	200	0	40	0.495	0.3	C_45_4_0.5_200_0.3_D	2	45	5	119.8	599	3.00	Foundation failure
138	45	8	0.5	2.0	20	200	0	40	0.495	0.3	C_45_8_0.5_200_0.3_D	4	45	5	120.2	601	3.00	Foundation failure
139	45	2	1	2.0	20	200	0	40	0.495	0.3	C_45_2_1_200_0.3_D	1	45	5	127.8	639	3.20	Foundation failure
140	45	4	1	2.0	20	200	0	40	0.495	0.3	C_45_4_1_200_0.3_D	2	45	5	127.9	640	3.20	Foundation failure
141	45	8	1	2.0	20	200	0	40	0.495	0.3	C_45_8_1_200_0.3_D	4	45	5	128.0	640	3.20	Foundation failure
142	45	2	2	2.0	20	200	0	40	0.495	0.3	C_45_2_2_200_0.3_D	1	45	5	127.8	639	3.19	Foundation failure
143	45	4	2	2.0	20	200	0	40	0.495	0.3	C_45_4_2_200_0.3_D	2	45	5	127.9	640	3.20	Foundation failure
144	45	8	2	2.0	20	200	0	40	0.495	0.3	C_45_8_2_200_0.3_D	4	45	5	128.1	640	3.20	Foundation failure

N.F. : Not found.
Base failure_EQ: Failed due to earthquake.
Base failure_GR: Failed due to gravity.

Table C.3. List of results of finite elements models created for seismic condition (β= 45°) (Cont.).

	GEOMETRICAL PROPERTIES				SLOPE SOIL PROPERTIES				SEISMIC EFFECT	FILE NAME	ANALYSIS RESULTS FOR SEISMIC LOADING						
Model No.	β (°)	H (m)	λ	B (m)	γ (kN/m^3)	c_u (kN/m^2)	Φ_u (°)	E_u (MPa)	ν_u	k_h		H/B	β (°)	$C_u/\gamma B$	Load multiplier	q_{fs} (kPa)	N_{cse}	Failure mode
145	45	2	0	2.0	20	25	0	5	0.495	0.4	C_45_2_0_25_0.4_D	1	45	0.625	N.F.	N.F.	N.F.	Base failure_EQ
146	45	4	0	2.0	20	25	0	5	0.495	0.4	C_45_4_0_25_0.4_D	2	45	0.625	N.F.	N.F.	N.F.	Base failure_EQ
147	45	8	0	2.0	20	25	0	5	0.495	0.4	C_45_8_0_25_0.4_D	4	45	0.625	N.F.	N.F.	N.F.	Base failure_GR
148	45	2	0.5	2.0	20	25	0	5	0.495	0.4	C_45_2_0.5_25_0.4_D	1	45	0.625	N.F.	N.F.	N.F.	Base failure_EQ
149	45	4	0.5	2.0	20	25	0	5	0.495	0.4	C_45_4_0.5_25_0.4_D	2	45	0.625	N.F.	N.F.	N.F.	Base failure_EQ
150	45	8	0.5	2.0	20	25	0	5	0.495	0.4	C_45_8_0.5_25_0.4_D	4	45	0.625	N.F.	N.F.	N.F.	Base failure_GR
151	45	2	1	2.0	20	25	0	5	0.495	0.4	C_45_2_1_25_0.4_D	1	45	0.625	N.F.	N.F.	N.F.	Base failure_EQ
152	45	4	1	2.0	20	25	0	5	0.495	0.4	C_45_4_1_25_0.4_D	2	45	0.625	N.F.	N.F.	N.F.	Base failure_EQ
153	45	8	1	2.0	20	25	0	5	0.495	0.4	C_45_8_1_25_0.4_D	4	45	0.625	N.F.	N.F.	N.F.	Base failure_GR
154	45	2	2	2.0	20	25	0	5	0.495	0.4	C_45_2_2_25_0.4_D	1	45	0.625	N.F.	N.F.	N.F.	Base failure_EQ
155	45	4	2	2.0	20	25	0	5	0.495	0.4	C_45_4_2_25_0.4_D	2	45	0.625	N.F.	N.F.	N.F.	Base failure_EQ
156	45	8	2	2.0	20	25	0	5	0.495	0.4	C_45_8_2_25_0.4_D	4	45	0.625	N.F.	N.F.	N.F.	Base failure_GR
157	45	2	0	2.0	20	50	0	10	0.495	0.4	C_45_2_0_50_0.4_D	1	45	1.25	N.F.	N.F.	N.F.	Base failure_EQ
158	45	4	0	2.0	20	50	0	10	0.495	0.4	C_45_4_0_50_0.4_D	2	45	1.25	N.F.	N.F.	N.F.	Base failure_EQ
159	45	8	0	2.0	20	50	0	10	0.495	0.4	C_45_8_0_50_0.4_D	4	45	1.25	N.F.	N.F.	N.F.	Base failure_EQ
160	45	2	0.5	2.0	20	50	0	10	0.495	0.4	C_45_2_0.5_50_0.4_D	1	45	1.25	N.F.	N.F.	N.F.	Base failure_EQ
161	45	4	0.5	2.0	20	50	0	10	0.495	0.4	C_45_4_0.5_50_0.4_D	2	45	1.25	N.F.	N.F.	N.F.	Base failure_EQ
162	45	8	0.5	2.0	20	50	0	10	0.495	0.4	C_45_8_0.5_50_0.4_D	4	45	1.25	N.F.	N.F.	N.F.	Base failure_EQ
163	45	2	1	2.0	20	50	0	10	0.495	0.4	C_45_2_1_50_0.4_D	1	45	1.25	N.F.	N.F.	N.F.	Base failure_EQ
164	45	4	1	2.0	20	50	0	10	0.495	0.4	C_45_4_1_50_0.4_D	2	45	1.25	N.F.	N.F.	N.F.	Base failure_EQ
165	45	8	1	2.0	20	50	0	10	0.495	0.4	C_45_8_1_50_0.4_D	4	45	1.25	N.F.	N.F.	N.F.	Base failure_EQ
166	45	2	2	2.0	20	50	0	10	0.495	0.4	C_45_2_2_50_0.4_D	1	45	1.25	N.F.	N.F.	N.F.	Base failure_EQ
167	45	4	2	2.0	20	50	0	10	0.495	0.4	C_45_4_2_50_0.4_D	2	45	1.25	N.F.	N.F.	N.F.	Base failure_EQ
168	45	8	2	2.0	20	50	0	10	0.495	0.4	C_45_8_2_50_0.4_D	4	45	1.25	N.F.	N.F.	N.F.	Base failure_EQ
169	45	2	0	2.0	20	100	0	20	0.495	0.4	C_45_2_0_100_0.4_D	1	45	2.5	40.9	205	2.05	Foundation failure
170	45	4	0	2.0	20	100	0	20	0.495	0.4	C_45_4_0_100_0.4_D	2	45	2.5	40.9	204	2.04	Foundation failure
171	45	8	0	2.0	20	100	0	20	0.495	0.4	C_45_8_0_100_0.4_D	4	45	2.5	41.0	205	2.05	Foundation failure
172	45	2	0.5	2.0	20	100	0	20	0.495	0.4	C_45_2_0.5_100_0.4_D	1	45	2.5	50.0	250	2.50	Sliding
173	45	4	0.5	2.0	20	100	0	20	0.495	0.4	C_45_4_0.5_100_0.4_D	2	45	2.5	50.0	250	2.50	Sliding
174	45	8	0.5	2.0	20	100	0	20	0.495	0.4	C_45_8_0.5_100_0.4_D	4	45	2.5	50.0	250	2.50	Sliding
175	45	2	1	2.0	20	100	0	20	0.495	0.4	C_45_2_1_100_0.4_D	1	45	2.5	50.0	250	2.50	Sliding
176	45	4	1	2.0	20	100	0	20	0.495	0.4	C_45_4_1_100_0.4_D	2	45	2.5	50.0	250	2.50	Sliding
177	45	8	1	2.0	20	100	0	20	0.495	0.4	C_45_8_1_100_0.4_D	4	45	2.5	50.0	250	2.50	Sliding
178	45	2	2	2.0	20	100	0	20	0.495	0.4	C_45_2_2_100_0.4_D	1	45	2.5	50.0	250	2.50	Sliding
179	45	4	2	2.0	20	100	0	20	0.495	0.4	C_45_4_2_100_0.4_D	2	45	2.5	50.0	250	2.50	Sliding
180	45	8	2	2.0	20	100	0	20	0.495	0.4	C_45_8_2_100_0.4_D	4	45	2.5	50.0	250	2.50	Sliding

N.F. : Not found.
Base failure_EQ: Failed due to earthquake.
Base failure_GR: Failed due to gravity.

Table C.3. List of results of finite elements models created for seismic condition (β= 45°) (Cont.).

	GEOMETRICAL PROPERTIES				SLOPE SOIL PROPERTIES				SEISMIC EFFECT	FILE NAME	ANALYSIS RESULTS FOR SEISMIC LOADING						
Model No.	β (°)	H (m)	λ	B (m)	γ (kN/m^3)	c_u (kN/m^2)	Φ_u (°)	E_u (MPa)	v_u	k_h		H/B	β (°)	$C_u/\gamma B$	Load multiplier	q_{fs} (kPa)	N_{cse}	Failure mode
181	45	2	0	2.0	20	200	0	40	0.495	0.4	C_45_2_0_200_0.4_D	1	45	5	83.4	417	2.09	Foundation failure
182	45	4	0	2.0	20	200	0	40	0.495	0.4	C_45_4_0_200_0.4_D	2	45	5	83.3	417	2.08	Foundation failure
183	45	8	0	2.0	20	200	0	40	0.495	0.4	C_45_8_0_200_0.4_D	4	45	5	83.6	418	2.09	Foundation failure
184	45	2	0.5	2.0	20	200	0	40	0.495	0.4	C_45_2_0.5_200_0.4_D	1	45	5	100.0	500	2.50	Sliding
185	45	4	0.5	2.0	20	200	0	40	0.495	0.4	C_45_4_0.5_200_0.4_D	2	45	5	100.0	500	2.50	Sliding
186	45	8	0.5	2.0	20	200	0	40	0.495	0.4	C_45_8_0.5_200_0.4_D	4	45	5	100.1	500	2.50	Sliding
187	45	2	1	2.0	20	200	0	40	0.495	0.4	C_45_2_1_200_0.4_D	1	45	5	99.9	500	2.50	Sliding
188	45	4	1	2.0	20	200	0	40	0.495	0.4	C_45_4_1_200_0.4_D	2	45	5	100.0	500	2.50	Sliding
189	45	8	1	2.0	20	200	0	40	0.495	0.4	C_45_8_1_200_0.4_D	4	45	5	100.0	500	2.50	Sliding
190	45	2	2	2.0	20	200	0	40	0.495	0.4	C_45_2_2_200_0.4_D	1	45	5	99.9	500	2.50	Sliding
191	45	4	2	2.0	20	200	0	40	0.495	0.4	C_45_4_2_200_0.4_D	2	45	5	99.9	499	2.50	Sliding
192	45	8	2	2.0	20	200	0	40	0.495	0.4	C_45_8_2_200_0.4_D	4	45	5	100.0	500	2.50	Sliding

N.F. : Not found.

Base failure_EQ: Failed due to earthquake.

Base failure_GR: Failed due to gravity.

REFERENCES

AASHTO, 1996, *Standard Specifications for Highway Bridges*, American Association of State Highway and Transportation Officials, USA.

Askari, F., and O. Farzaneh, 2003, "Upper Bound Solution for Seismic Bearing Capacity of Shallow Foundations near Slopes", *Geotechnique*, Vol. 53, No.8, pp. 697-702.

Bowles, J. E., 1996, *Foundation Analysis and Design*, McGraw - Hill, New York, USA.

Brinkgreve, R. B. J., W. Broere, and D. Waterman, 2006, *Plaxis User's Manual*, Plaxis B. V., Delft, Netherlands.

Castelli, F., and E. Motta, 2010, "Bearing Capacity of Strip Footings Near Slopes", *Geotech Geol Eng.*, Vol. 28, pp. 187-198.

Das, B. M., 2010, *Principles of Geotechnical Engineering*, Cengage Learning, Stamford, 7th Edition.

Das, B. M., and G. V. Ramana, 2011, *Principles of Soil Dynamics*, Cengage Learning, Stamford, 2nd Edition.

Day, R. W., 2002, *Geotechnical Earthquake Engineering Handbook*, McGraw Hill Professional, New York, USA.

Erkli, A., and Ö. Çinicioğlu, 2012, "Kohezyonlu Şevlerin Üzerindeki Yüzeysel Şerit Temellerin Sismik Taşıma Gücü", *Zemin Mekaniği ve Temel Mühendisliği 14. Ulusal Kongresi*, Isparta.

Farzaneh, O., J. Mofidi, and F. Askari, 2013, "Seismic Bearing Capacity of Strip Footings near Cohesive Slopes Using Lower Bound Limit Analysis", *Proceedings of the 18th*

International Conference on Soil Mechanics and Geotechnical Engineering, Paris, pp. 1467-1470.

Georgiadis, K., 2010, "Undrained Bearing Capacity of Strip Footings on Slopes", *Journal of Geotechnical and Geoenviromental Engineering*, Vol. 136, No. 5, pp. 677-685.

Hansen, J. B., 1961, "A General Formula for Bearing Capacity", *Danish Geotechnical Institute*, Bulletin 11, Copenhagen, Denmark, pp. 38–46.

Koppula, S. D., 1984, "On Stability of Slopes on Clays with Linearly Increasing Strength", *Canadian Geotechnical Journal*, Vol. 21, No. 3, pp. 557-581.

Kramer, S. L., 1996, *Geotechnical Earthquake Engineering*, Prentice Hall, New Jersey.

Kumar, J., and M. Rao, 2003, "Seismic Bearing Capacity of Foundations on Slopes", *Geotechnique*, Vol. 53, No.3, pp. 347-361.

Kusakabe, O., T. Kimura, and H. Yamaguchi, 1981, "Bearing Capacity of Slopes under Strip Loads on the Top Surfaces", *Soils and Foundations*, Vol. 21, No. 4, pp. 29–40.

Merlos, J., and M. P. Romo, 2006, "Fluctuant bearing capacity of shallow foundations during earthquakes", *Soil Dynamics and Earthquake Engineering*, Vol. 26, pp. 103-114.

Meyerhof, G. G., 1957, "The Ultimate Bearing Capacity of Foundation on Slopes", *Proceedings of the Fourth International Conference on Soil Mechanics*, London, pp. 384-386.

Potts, D. M., and L. Zdravkovic, 1999, *Finite Element Analysis in Geotechnical Engineering: Theory*, Thomas Telford, London.

Potts, D. M., and L. Zdravkovic, 2001, *Finite Element Analysis in Geotechnical Engineering: Application*, Thomas Telford, London.

Potts, D. M., K. Axelsson, L. Grande, H. Scheweiger, and M. Long, 2002, *Guidelines for the Use of Advanced Numerical Analysis*, Thomas Telford, London.

Prandtl, L., 1920, "Uber die Harte Plastischer Korper", *Nachrichten von der Koniglichen Gesellschaft der Wissenschaften*, Gottingen, Math. Phys., Klasse, pp. 74-85.

Sarma, S.K., and I. Iossifelis, 1990, "Seismic Bearing Capacity Factors of Shallow Strip Footings", *Geotechnique*, Vol. 40, No.2, pp. 265-273.

Sarma, S. K., and Y. C. Chen, 1996, "Bearing Capacity of Strip Footings near Sloping Ground During Earthquakes", *Eleventh World Conference on Earthquake Engineering*, Paper No. 2078.

Sawada, T., G. N. Sumio, and W. F. Chen, 1994, "Seismic Bearing Capacity of a Mounded Foundation near a Down-Hill Slope by Pseudo-Static Analysis", *Soils and Foundations*, Vol. 34, No. 1, pp. 11-17.

Shiau, J., A. Lyamin, and S. Sloan, 2006, "Application of Pseudo-Static Limit Analysis in Geotechnical Earthquake Design", *Numerical Methods in Geotechnical Engineering – Schweiger (ed.)*, Taylor & Francis Group, LLC., London.

Skempton, A. W., 1951, "The Bearing Capacity of Clays", *Building Research Congress*, London, pp. 180-189.

Sloan, S. W., 1988, "Lower Bound Limit Analysis Using Finite Elements and Linear Programming", *International Journal for Numerical and Analytical Methods in Geomechanics*, Vol. 12, pp. 61–67.

Taiebat, H. A., and J. P. Carter, 2008, "Flow Rule Effects in the Tresca Model", *Computers and Geotechnics*, Vol. 35, pp. 500-503.

Taylor, D. W., 1937, "Stability of Earth Slopes", *Journal of the Boston Society of Civil Engineers*, Vol. 24, pp. 197-246.

Terzaghi, K., 1943, *Theoretical Soil Mechanics*, John Wiley & Sons, Inc., New York, USA.

U.S. Army Corps of Engineers, 1995, *Engineering and Design: Geotechnical Analysis by the Finite Element Method*, Washington, DC.

Vesic, A. S., 1975, *Foundation Engineering Handbook*, H. F. Winterkorn and H. Y. Fang, eds., Van Nostrand Reinhold, New York, USA.

Washington State Department of Transportation, 2005, *Geotechnical Design Manual*, Washington, DC.

Yamamoto, K., 2010, "Seismic Bearing Capacity of Shallow Foundations near Slopes Using the Upper-Bound Method", *International Journal of Geotechnical Engineering*, Vol. 4, No. 2, pp. 255-267.